MONASH University

Development of novel inorganic nanocrystals for delivery of pDNA and siRNA to breast cancer cells

Athirah Bakhtiar

Bachelor of pharmacy (Honours)

A thesis submitted for the degree of *Doctor of Philosophy* at
Monash University in 2016

Jeffrey Cheah School of Medicine & Health Sciences

To my sons, Anas Irsyad and Anas Isyraf who have inspired me

Copyright notice

Declaration

This thesis contains no material which has been accepted for the award of any other degree or diploma at any university or equivalent institution and that, to the best of my knowledge and belief, this thesis contains no material previously published or written by another person, except where due reference is made in the text of the thesis.

Acknowledgement

In the name of Allah, the most merciful, the most compassionate.

Firstly and foremost, I would like to express my deepest gratitude to my principal supervisor, Associate Professor Dr. Ezharul Hoque Chowdhury for his endless support of my doctorate program. His motivation, patience, and guidance have helped me along the course of my research study and writing of this thesis. I could not have asked for a better teacher and mentor for my doctorate journey. My appreciation also goes to my co-supervisors, Professor Dr. Iekhsan Othman and Professor Dato' Dr. Anuar Zaini for their excellent encouragements, advices and supports throughout my years in Monash University Malaysia. Their work ethics and professionalism has inspired me to become a better researcher and critical thinker.

Special credit goes to Dr. Snigdha Tiash and Ms. Tahereh Fatemian for their excellent advices and thoughtfulness as my senior. To my buddy and lab partner, Ms. Nur Izyani Kamaruzaman, thank you so much for your profound assistance and joyfulness over the years. I would also like to thank all my colleagues in School of Medicine and Health Sciences, for their tremendous help and support throughout the years. I am obliged to Mr. Andrew Leong and Mr. Zulkhaili Zainal Abidin from the Animal Facility Unit for inspiring me with their outstanding work ethics, 'ready to help' attitude and excellent training. Special thanks to laboratory technicians, especially Mr. Rashid Masran and Ms. Adillah Akhsan, who I often seek for consultations and pleasant chats. And to my great friends who have made my research life more colorful and pleasurable, I thank you. My appreciation to all the administrative staffs from School of Medicine and Health Sciences, including Ms. Lee Ching Teng, for their excellent work

in ensuring the smoothness of my Ph.D. journey. Deepest gratitude to School of Engineering, for allowing me to utilize the facilities, with exclusive thanks to technical officers, Mr. Azarudin Ahmad, and Ms. Lithnes K. Palniandy, who were willing to share their expertise despite their tight schedules.

I am largely indebted to my dear parents, Mr. Bakhtiar Kendut and Mrs. Khasniyati Salehuddin for showering me with their prayers, supports, encouragement and unconditional love. I am able to grasp my dreams because of your continuous sacrificial and relentless assistance, which I could never repay. I hope, with this, I have made you both proud in many ways. And to my brothers, Muhammad Irfan, Muhammad Izhar, Muhammad Imran and Muhammad Irham, thank you so much for being such amazing brothers. Deepest thoughts to my grandparents and relatives who consistently expressed their encouragements throughout my career pursuit.

To my cherished husband and best friend, Dr. Muhammad Hafizi Shuhaimi Fauzi, your love and support have made my life more meaningful and worthwhile. Thank you for standing together in every step, all the way, hence empowering me to complete this long journey. My deepest adoration to my twin boys, my babies, my shining stars; Anas Irsyad Muhammad Hafizi and Anas Isyraf Muhammad Hafizi. You both have given me the uttermost inspiration and joyfulness as your mother, and I am profoundly grateful for such blessing. I am truly sorry for taking a little time of your childhood to conclude this journey, but I will do my best to compensate the lost times.

Last but not the least, I would like to thank everyone, who knowingly or otherwise, has provided advices, encouragements, and assistances along the way.

Abstract

Genetic manipulation of human cells through the delivery of functional genes such as plasmid DNA (pDNA) and short-interfering RNA (siRNA) is an attractive approach to treat many critical diseases with single or multiple gene defects, including carcinoma; precisely and efficiently. Despite their potential effect, naked therapeutic genes are rapidly degraded by nucleases, non-specific to the target cells; in addition to exhibiting low cellular uptake, and poor transfection efficiency. Hence, the development of safe and efficient gene carriers is undeniably crucial for the success of gene therapy.

Recent studies have been focused on developing smart nanoparticles for excellent delivery of transgenes and siRNAs into cancerous cells of an animal model through active and passive targeting. The precipitation reaction is one of the facile and convenient ways to synthesize nanoparticles, which an insoluble salt is formed upon the mixture of two water-soluble salts. In this study, we aim to develop the potential salt crystals with nano-size diameters having the capacity of adsorbing negatively charged plasmid DNA and siRNA, effectively carrying them across the plasma membrane and finally leading to efficient gene expression and silencing of the target (reporter as well as endogenous) gene(s), respectively, in mammary carcinoma of mammalian cells.

The generated insoluble salts have been subjected to a rigorous screening process based on observation of particle morphology under optical microscope, determination of growth kinetics, particle diameters and electrostatic affinity towards the negatively charged pDNA/siRNA, qualitative and quantitative estimation of cellular endocytosis rate and finally assessment of transfection efficacy in case of transgene expression and knockdown by target siRNAs. Among the screened precipitates,

strontium sulfite, strontium fluoride, and magnesium sulfite have shown the best potency in aiding cellular delivery of reporter gene/siRNA, in addition to proficient transgene expression and silencing effect into both mice and human mammary carcinoma cells.

Our *in vivo* discoveries revealed efficiency of nanocrystals with the ability to efficiently transport pDNA as well as siRNA into 4T1-induced tumor model through biodistribution assays and tumor regression activities. Strontium sulfite, strontium fluoride, and magnesium sulfite improve the genetic material delivery, demonstrated through regression of tumor growth activity. Protein coating enhances the nanocarrier activity through the involvement of active targeting via ligand-receptor interactions. It is hoped that the potential nanoparticles can be applied for conceivable nano-vector application in the clinical setting for cancer treatment in the future.

Table of Contents

List of tables

List of figures

List of abbreviation

AF 488	Alexa Fluor® 488
$BaCl_2$	Barium chloride
$BaCO_3$	Barium carbonate
BaF_2	Barium fluoride
BALB/c mice	Albino, laboratory-inbred strain of house mice
$Ba_3(PO_4)_2$	Barium phosphate
$BaSO_4$	Barium sulfate
$BaSO_3$	Barium sulfite
BBB	Blood brain barrier
$CaCl_2$	Calcium chloride
$CaCO_3$	Calcium carbonate
CaF_2	Calcium fluoride
$Ca_3(PO_4)_2$	Calcium phosphate
$CaSO_3$	Calcium sulfite
CO_3 AP	Carbonate apatite
DMEM	Dulbecco's modified eagle's medium
DMSO	Dimethyl sulfoxide
EDTA	Ethylenediaminetetraacetic acid
EPR	Enhance permeability and retention
FBS	Fetal bovine serum
$FeCl_2$	Ferrous (II) chloride
$FeCO_3$	Ferrous carbonate
$Fe_3(PO_4)_2$	Ferrous phosphate
FE-SEM	Field emission scanning electron microscope
$FeSO_3$	Ferrous sulfite
HCl	Hydrochloric acid
HEPES	4-(2-hydroxyethyl)-1-piperazineethanesulfonic acid
MAPK	Mitogen-activated protein kinase
MCF-7	Michigan cancer foundation-7 / Human mammary carcinoma cells
$MgCl_2$	Magnesium chloride
$MgCO_3$	Magnesium carbonate

MgF_2	Magnesium fluoride
$Mg_3(PO_4)_2$	Magnesium phosphate
$MgSO_3$	Magnesium sulfite
MPS	Mononuclear phagocyte system
mRNA	Messenger RNA
MTT	3-(4,5-dimethylthiazol-2-yl)-2,5-diphenyltetrazolium bromide
Na_2CO_3	Sodium bicarbonate
NaH_2PO_4	Sodium dihydrogen phosphate
NaF	Sodium fluoride
Na_2SO_4	Sodium sulfate
Na_2SO_3	Sodium sulfite
OD	Optical density
PBS	Phosphate-buffered saline
pDNA	Plasmid DNA
pGFP	Green fluorescence protein plasmid
pGL3	Luciferase reporter plasmid
PI	Propidium iodide
p53	Tumour protein p53
PVDF	Polyvinylidene fluoride
RES	Reticulo-endothelial system
RISC	RNA-induced silencing complex
RNAi	RNA interference
SD	Standard deviation
SDS-PAGE	Sodium dodecyl sulfate polyacrylamide gel electrophoresis
SEM	Scanning electron microscope
siRNA	Small interfering RNA
$SrCl_2$	Strontium chloride
$SrCO_3$	Strontium carbonate
SrF_2	Strontium fluoride
$SrSO_4$	Strontium sulfate
$SrSO_3$	Strontium sulfite
RLU	Relative luminescence unit
4T1	BALB/c mice mammary carcinoma cells

Chapter 1

General introduction

1.1 Introduction

The use of genes for the therapeutic applications has increased vastly due to its tremendous potential as a future strategy for clinical applications. Gene therapy involves delivery of a therapeutic gene within a vector, enabling it to transcribe and translate into a therapeutic protein of interest within a particular cell. Genetic manipulation of human cells through delivery of functional genes such as plasmid DNA (pDNA) and short-interfering RNA (siRNA) is an attractive approach to treat cancers and many critical diseases with single or multiple gene defects (including cystic fibrosis, Alzheimer's disease, and carcinoma) precisely and efficiently. Strategies of gene therapy involve substitution of non-functional or mutated genes including p53, RB1 and BRCA-1 genes and down-regulation of over-expressed proto-oncogenes and anti-apoptotic genes through introduction of target siRNAs (MAPK, ROS1 and Bcl-2 siRNA). The establishment of genetic modification on carcinoma tissues of breast demonstrated a comparable reduction in tumor growth both *in vitro* and *in vivo* (1).

Despite their potential outcome, naked therapeutic genes are rapidly degraded by nucleases, non-specific to the target cells, exhibit low cellular uptake, and poor transfection efficacy. Hence, the development of safe and efficient gene carriers is utterly fundamental to the success of gene therapy. Recent studies are focusing on efficient gene carrier for cancer treatment by incorporating the means of active and passive targeting. Active targeting is achieved through conjugation of nanoparticles to ligands that are highly tumor specific. Passive tissue targeting is accomplished by utilizing the distinctive biochemical and physiological characteristics of the tumor microenvironment. At the size lower than 500 nm, nanoparticles can easily penetrate

through the ‘leaky' capillary system of malignant tissues without permeating the intact endothelium of the normal tissues, a phenomenon known as enhance permeability and retention (EPR) effect. Additionally, morphological changes in the lymphatic system of malignant tissues resulted in inadequate lymphatic drainage, extending the retention time of genetic materials within the tumor tissue surrounding (2).

Nanoparticles have emerged as one of the novel gene delivery systems for delivery in targeted manner. The most significant advantage of the nanoparticles is providing specified gene delivery to the intended area, increasing the effectiveness of gene therapy while at the same time, reducing the side effects of non-specific delivery. Precipitation reaction is one of the facile and convenient ways to synthesize nanoparticles, in which an insoluble salt is formed after mixing two water-soluble salts (3). Such reaction is represented schematically below, where A and B are two different cations, while X and Y are two different anions:

AX (soluble) + BY (soluble) à AY (solid) + BX (soluble)

The reaction proceeds to the right by a driving force derived from precipitation of a product (AY). The formation of a precipitate is illustrated with an example in equation form below:

$BaCl_2$ (soluble) + Na_2SO_4 (soluble) à $BaSO_4$ (solid) + 2NaCl (soluble)

The advantages in comparison with other methods include requiring only simple equipment, ability to prepare and control particle size and composition at near ambient temperature and pressure. Recent development has shown favorable transfection activities using the nanoparticles prepared from precipitation method including $CaCO_3$,

$Fe3O_4$, and $BaSO_4$. The approach would pave a new way for efficient, low toxicity and large-scale synthesis of inorganic nanoparticles with well-controlled dimensions and properties (3).

1.2 Research objectives

To develop potential salt crystals with nano-size diameters having the attributes of:

1. Adsorbing negatively charged pDNA and siRNA;
2. Carrying them across the plasma membrane;
3. Leading to efficient transgene expression and silencing of the target (reporter as well as apoptotic) gene(s), in breast cancer cells both *in vitro* and *in vivo*.

1.3 Research hypotheses

Nanoparticles fabricated based on precipitation reaction of the potential salt crystals will have strong affinity towards pDNA and small interfering RNA (siRNA). pDNA- or siRNA-bound nanocrystals can be transported efficiently to cancer cells both *in vitro* and *in vivo*, with subsequent therapeutic efficacy.

References:

1. Das SK, Menezes ME, Bhatia S, Wang X-Y, Emdad L, Sarkar D, et al. Gene Therapies for Cancer: Strategies, Challenges and Successes. J Cell Physiol [Internet]. 2015 Feb [cited 2016 Mar 4];230(2):259–71. Available from: http://doi.wiley.com/10.1002/jcp.24791
2. Kudera S, Maus L, Zanella M, Pelaz B, Zhang Q, Parak WJ, et al. Inorganic Core–Shell Nanoparticles. In: Reference Module in Materials Science and Materials Engineering. 2016.
3. Noguera C, Fritz B, Cl??ment A. Precipitation mechanism of amorphous silica nanoparticles: A simulation approach. J Colloid Interface Sci. 2015;448:553–63.

Chapter 2

Literature review

2.1 Overview of breast cancer

Cancer is a group of diseases, characterized by uncontrollable cell growth, local tissue invasion and distance metastases (1). It was estimated that in the year 2012, 14.1 million new cases of cancer were diagnosed, 8.2 million of people died due to cancer, and 32 million people were living with cancer globally (2). In Malaysia, cancer is the third leading cause of death, after septicemia and cardiovascular diseases. National Cancer Registry (NCR) in 2006 reported that cancer incidence rate for males was 128 cases per 100 000 people while incidence rate for females was 135 cases per 100 000 people. Most common carcinomas among Malaysian populations were breast, colorectal, lung, cervix, and nasopharynx with cancer incidence in Malaysia augmented from 32,000 to 37,400 new cases from the year 2008 to 2012, and cancer-related mortality stood at 21,700 deaths in 2012 from 20,100 deaths in 2008 (3).

Breast cancer is the disease of uncontrolled cell division in the mammary tissues. It is the leading cause of cancer affecting women worldwide and is also associated with the primary causes of cancer-related deaths among women. In the year 2012 alone, there were about 1.67 million women diagnosed with breast cancer annually, and more than 522 000 died due to cancer. Breast cancer ranks the fifth cause of mortality from cancer worldwide, with a higher frequency of death recorded in women of less developed nations (4). In Malaysia, carcinoma of the breast is the most commonly diagnosed cancer in women, with the national pattern of age-standardize incidence rate (ASR) being 39.3 per 100,000 populations. The rate was higher among Chinese, having 46.4 cases per 100 000 people, followed by Indian and Malay with respective 38.1 and 30 cases per 100 000 populations.

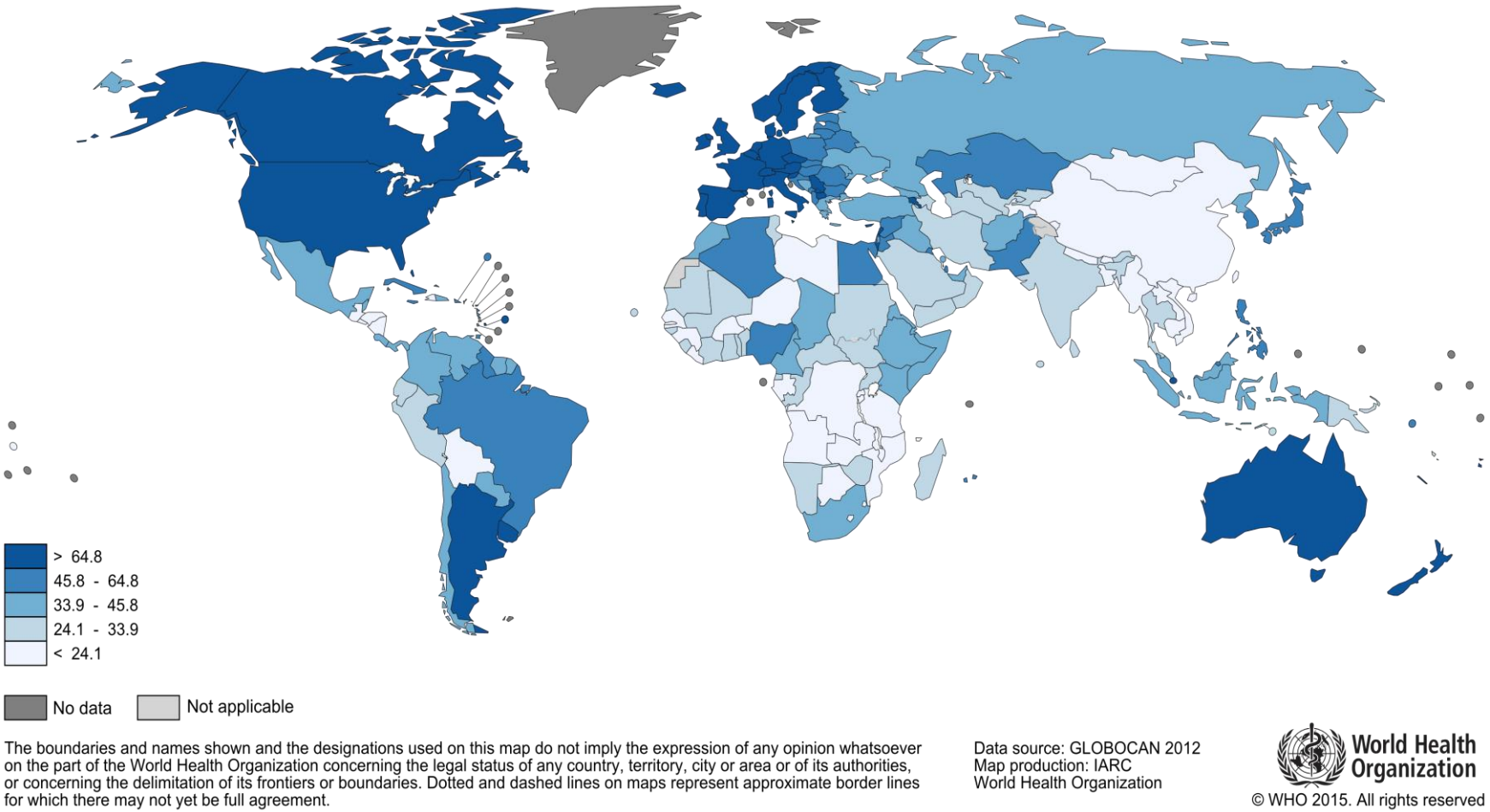

Figure 2.1: Trends in incidence of female breast cancer worldwide. Adapted from: Ferlay J, Soerjomataram I, ervik M, *et al*. GLOBOCAN 2012 V01, Cancer Incidence and Mortality Worldwide: IARC CancerBase. 2013; 11.

The incidence of cancer was also the highest in the female age group of 50-59 (5).

Risk factors for breast cancer include female gender, alcohol consumption, obesity, increasing age, environmental (radiation exposure), endocrine (early menarche, nulliparity, late age at first childbirth and estrogen therapy) and genetic factors (family history and mutations of genes including BRCA1, BRCA2 and p53) (6). Breast cancers that are detected early by physical examination, mammography and ultrasound often have a higher percentage of curability than the later stages (5).

2.2 Current management of breast cancer

Treatment of choice for breast cancer depends on the stages and the types of cancers, which often comprises of surgery and radiotherapy, endocrine therapy and chemotherapy. Surgical treatment for breast cancer remains one of the ideal therapies with high curative rate especially for solid breast tumors, particularly in situ and early stages with minimal invasion towards surrounding tissues. The invasive procedure of mastectomy of the breast (defined by the removal of breast tissues) may be preferred for advanced disease presentation with aggression towards the lymph nodes and metastasized regions (7). Radiotherapy utilizes high-energy x-rays and other radiations to kill cancer cells through external and internal radiation, involving respective radiation energy emitted by machine and radioactive substances in needles or wires. Radiotherapy is often used as an adjuvant treatment following breast–conserving surgery to minimize the reoccurrence of cancer in the mammary tissues, in addition to the conditions when invasive procedure bears the disability and disfigurement consequences (1). Hormone receptor-positive breast cancer represents the majority of

the breast cancer cases, with approximately 65% cases involving estrogen receptor positive (EGF+) and progesterone receptor positive carcinoma. The endocrinal therapy often acts as an adjuvant and neoadjuvant between various treatment such as pre-and post-surgery that increases the curability rate through selective estrogen receptor modulator drug, tamoxifen and aromatase inhibitors, including anastrozole (8). Chemotherapy utilizes chemical agents, known as cytotoxic drugs, which are associated with cellular apoptosis through induction of DNA damage or interference with DNA synthesis or other crucial steps in cell division. The cytotoxic agents are usually used as an adjuvant therapy in the earlier stages of cancer upon surgery, and quite often as a maintenance therapy and palliative therapy for the later stages. Chemotherapy is offered as a single or more commonly, combined treatment of platinum groups, anthracycline antibiotics, and taxanes (9).

2.3 Mutation in breast cancer

Extensive research on the genetic basis of human diseases with complete sequencing of the human genome revealed many vital genes as possible targets in gene therapy programs. Cancer is the result of an accumulation of single or multiple gene defects, from down-regulation of tumor suppressor genes to up-regulation of proto-oncogenes and anti-apoptotic genes, hence promoting uncontrollable cell replication. Tumor suppressor genes are divided into two groups: promoters and caretakers. p53, an example of promoter tumor suppressors is involved in inhibition of cell proliferation, whereas caretaker genes, including BRCA1 and BRCA2, ensure the integrity of the genome, especially in DNA repair (10). MLH1 and MSH2 are frequently studied caretaker genes, involved in mismatching DNA bases during DNA repair that was mis-

incorporated during DNA replication. The mutation is hence associated with a dramatic increase in the rate of point mutations (11). It is believed that more than 50% of mutated or missing occurs in patients with cancer (12). The up-regulation of proto-oncogenes and anti-apoptotic genes is linked with greater cell replication whereby oncogenes, mutated and cancer-causing forms of proto-oncogenes typically increase the activity of encoded protein, hence driving the activity of cell growth or loss in the regulatory process to initiate proliferation genes such as MAP kinase and Ras (13). The up-regulated anti-apoptotic genes (including Bcl-2 and Fas) enhance the survivability of the cells overexpressing such genes, hence increase the opportunity to acquire the cellular mutation that eventually leads to cancer (14).

Types of genes	Genes	Main functions
Tumor suppressor genes	**p53**	Initiate transcription of Cdk inhibitor p21 and GADD45 that blocks cell cycle progress by acting as a general inhibitor of Cdk/cyclin complexes. Apoptosis is facilitated through activation of many genes including BAX and NOXA, destabilizing mitochondrial membrane to assist cytochrome C release and thus triggering the apoptotic cascade of caspase activation. p53 transcriptional target genes, p53R2, encodes ribonucleotide reductase, essential for both DNA replication and repair.
	BRCA1, BRCA2	BRCA 1 controls G2/M DNA damage-induced checkpoints via activation of Chk1 kinase, thus inducing signaling downstream of Chk1. BRCA2 controls G2/M by acting with novel protein, BRCA-associated factor 35 (BRAF35), binding to branched DNA structure.
	Rb	Blocks the passage through restriction point at G_1 by preventing transcription genes associated with DNA synthesis and cell cycle progression.
	PTEN	Dephosphorylates PIP at 3 position of inositol to yield PIP_2. Countering the action of PI3-kinase and Akt (related to cell survival).
	INK4	Encodes Cdk inhibitor p16 (controls passage through G2 restriction point) that inhibits Cdk4/cyclin D activity that

		inactivates Rb via phosphorylation.
	WT1	Inhibit transcription of growth factor-inducing genes, such as the gene that encodes insulin-like growth factor II, activates autocrine growth factor.
	MADR2	Encode SMAD transcription factors which are activated by TGF-β signaling, causing inhibition of cell proliferation.
	APC	Binds to β-catenin, which has functions in cell adhesion and signal transducer shuttling to the nucleus with response to Wnt signaling, essential for tumorigenesis. Attachment of APC to microtubules interacts with cytoskeletal architecture.
Proto-oncogenes	**HER2**	Type 1 transmembrane growth factor receptor associated with activation of intracellular signaling pathways via extracellular signals by dimerization and transphosphorylation domains to form phosphorylated tyrosine residues.
	EGFR	Phosphorylated EGFR induces receptor dimerization, leading to cell proliferation via kinase-activating autophosphorylation or trans-phosphorylation sites.
	VEGF	Phosphorylated VEGF initiates receptor dimerization and activation of tyrosine kinase, in addition to induction of cellular process associated with the growth-factor receptor, including cell proliferation, survival, and migration.
	BCR-ABL	Activates signal transduction pathways including RAS/MAPK, PI-3 kinase, JAK-STAT, and Src pathway. Ras, Jun-kinase, and PI-3 kinase are commonly associated with cell proliferation.
	MAP kinase	Phosphorylation causes activation of RAS-RAF-MEK-ERK pathway, involved in cell proliferation.
Apoptotic genes	**Bcl-2**	Encodes integral outer mitochondrial membrane protein, which regulates cell death by controlling mitochondrial permeability. Inhibits caspase activity by either blocking release of cytochrome c from mitochondria or apoptosis-activating factor (APAF-1).

Table 2.1: Examples of genes associated with carcinoma cell survival (15) (16) (17) (18)(19) (20)(21)(22) (23)

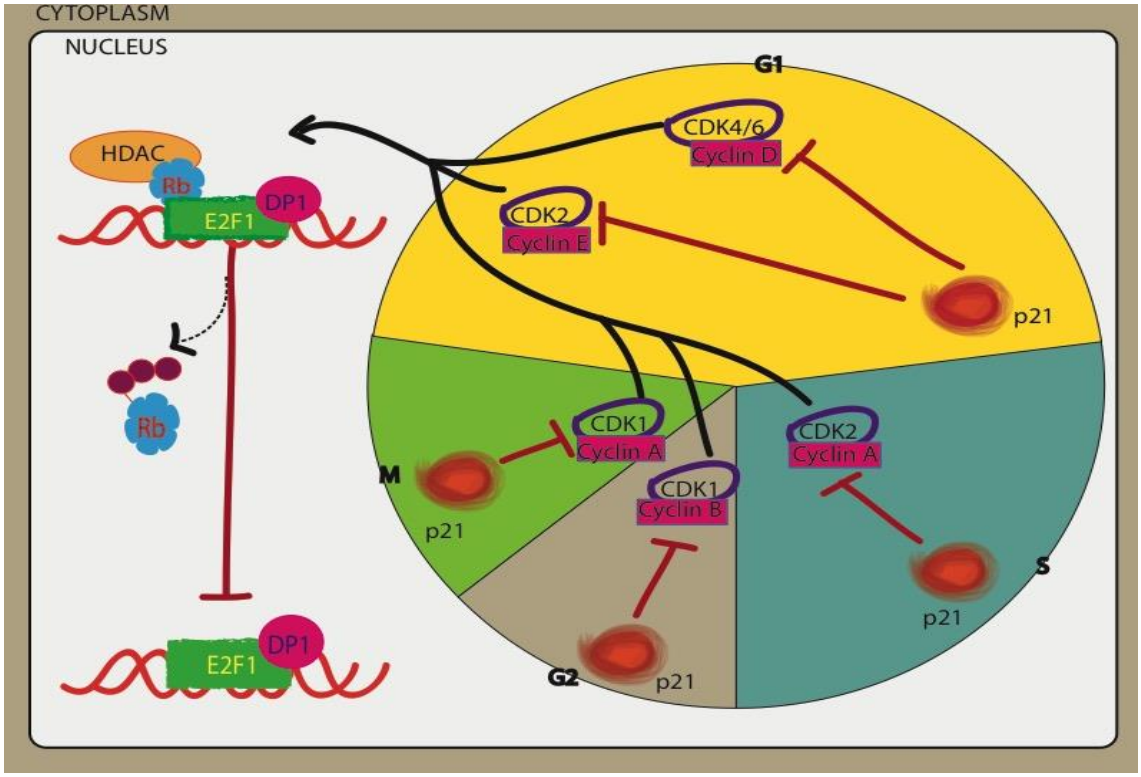

Figure 2.2: Different Cyclin-CDK complexes involved in regulating different cell cycle transitions: Cyclin-D/CDK4 or CDK6 for G1 progression, Cyclin-E/CDK2 for the G1-S transition, Cyclin-A/CDK2 for S-phase progression, Cyclin-B/CDK1 for G2 progression and Cyclin-A/CDK1 for entry into M phase. Cyclins associate with CDKs to regulate their activity and the progression of the cell cycle. CDK/Cyclin and the transcription complex that includes Rb and E2F are pivotal in controlling cell cycle checkpoint. The Rb-HDAC repressor complex binds to the E2F-DP1 transcription factors, inhibiting the downstream transcription. E2F activity consists of a heterodimeric complex of an E2F polypeptide and a DP1 protein. Phosphorylation of Rb by CDK dissociates the Rb-repressor complex, permitting transcription of phase genes encoding for proteins that amplify phase switch, required for replication. Under non-stressed conditions, p21 is expressed at low levels, thus enabling cell cycle progression. Under stress condition, p21 expression is increased through p53 dependent and independent pathways. Increased p21 binds and inactivates Cyclin/CDK activity, thus halting cell cycle activity (16).

2.4 Gene therapy in breast cancer

Gene therapy is designed to modify cancer cells at the molecular level, in which many gene therapy strategies are being assessed through replacement of down-regulated genes associated with missing/non-functional gene activity, or down-regulation of the over-expressed genes, as previously discussed. The involvement of genes as part of therapeutic regimen could be harnessed in potential treatment approaches particularly over chemotherapy, which is often associated with low selectivity and high cytotoxicity (24).

In the normal circumstances, DNA breakdown, UV, stress signal and oncogenes activate p53, forming phosphorylated tetrameric p53. The phosphorylated p53 can bind the transcriptional factor and enable the RNA polymerase activity transcribing a number of genes involved in inducing growth arrest (p21, GADD45), DNA repair (p53R2) and apoptosis (FAS, NOXA, BAX) via different mechanisms (25). Regulation of p53 is performed by MDM2 by ubiquitylation of p53 to initiate proteasome-dependent p53 degradation. The “loss of function” p53 causes the inability to initiate such response, hence growth of the tumor (26). Mutation in tumor suppressor genes, including p53 protein, resulted in missing or loss of function that interferes the ability of mutated cells to undergo apoptosis. Therefore the wild genotype, normal p53 genes is directly introduced into the cancer cells to provide a gene replacement for the non-functional ones (27).

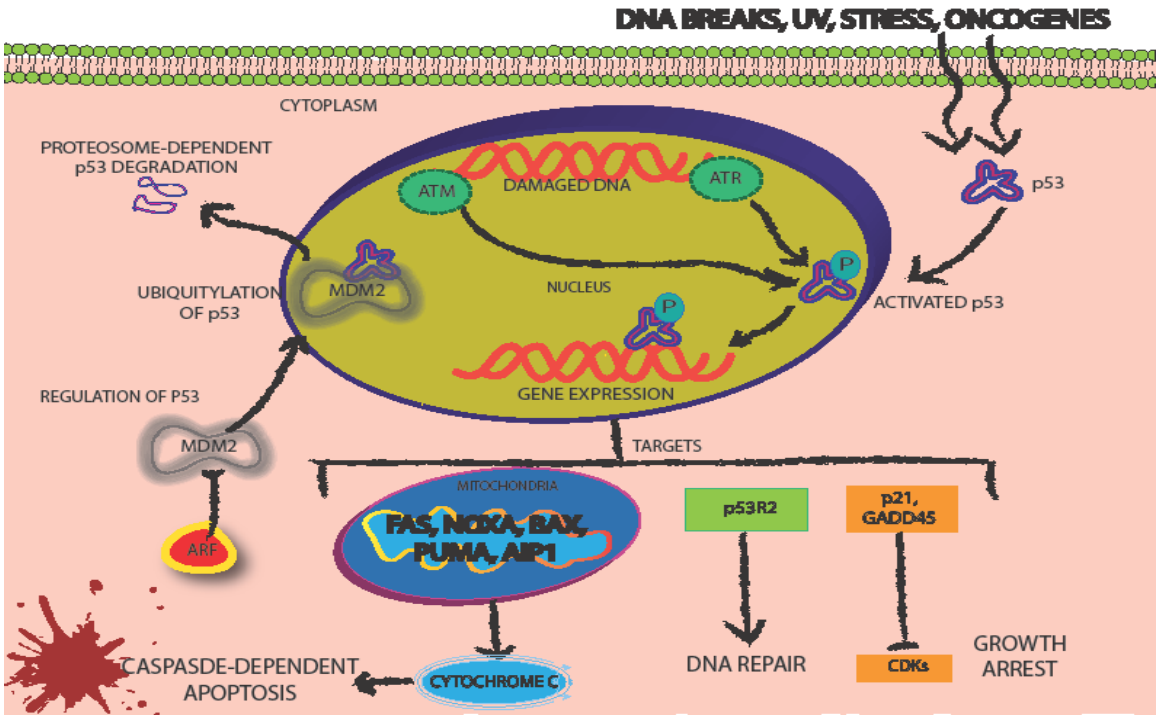

Figure 2.3: p53 pathway upon activation signals. The expression of p53 is controlled by rapid ubiquitin/proteasome-dependent degradation, mainly caused by MDM2, often over-expressed in many cancers. Adapted from Bakhtiar A, Sayyad M, Rosli R, Maruyama A, Chowdhury EH. Intracellular delivery of potential therapeutic genes: prospects in cancer gene therapy. Curr Gene Ther. 2014; 14(4):247-57.

Down-regulation of proto-oncogenes and anti-apoptotic genes is induced by gene silencing activity to inhibit expression of specific genes that are involved in cell growth and proliferation, through the incorporation of endogenous small interfering RNAs (siRNAs) that modulate RNA interference process (RNAi), a post-transcriptional gene regulatory mechanism (24). siRNA is a 21-25 base pairs RNA strand, which upon cellular internalization, unwinds and incorporates into RNA-induced silencing complex (RISC), a stable protein-RNA complex. siRNA is subsequently directed to target mRNA resulting in mRNA degradation and interruption of protein synthesis of the targeted gene (28). Long dsRNAs are cleaved by endoribonuclease Dicer into short dsRNA duplex, also known as siRNA. RISC contains Argonaute 2 (Ago-2) that cleaves and releases one strand of dsRNA to form activated RISC with single strand RNA (guide siRNA). The complex will next direct the target mRNA recognition via

complementary base pairing, followed by cleavage of mRNA between bases 10 and 11 by Ago-2 to induce mRNA degradation and silencing of the gene (29) (30).

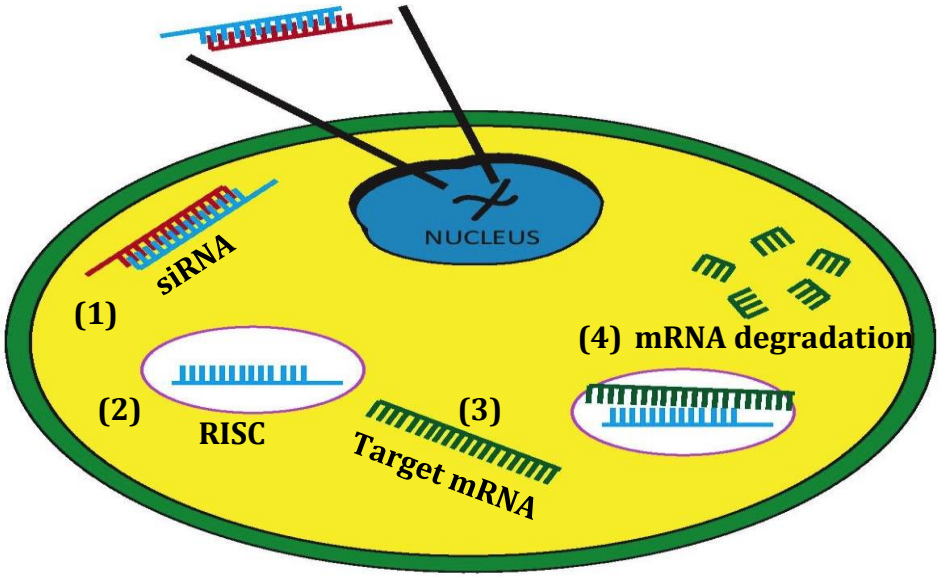

Figure 2.4: Diagram of RNAi pathway upon exposure of siRNA in a numerical manner. (1) Endogenous targeted siRNA enters the cell and (2) is incorporated into RISC. (3) Formed complex is directed to target mRNA, causing (4) mRNA to degrade, hence interrupting protein synthesis. Adapted from: Bakhtiar A, Othman I, Zaini A & Chowdhury EH. Development of novel barium inorganic nanoparticles for delivery of plasmid DNA and siRNA to breast cancer cells. Nano Today Conference, UAE. 2015.

2.5 Vectors for gene therapy

As discussed earlier, the manifestation of wild-type tumor suppressor genes and siRNAs shows promising treatment option in cancer therapeutics with direct targeting approach. Nonetheless, many barriers are existing in the biological structures that impede the proposed gene activities involving extracellular barriers such as endo- and exonuclease attack resulting in the short half-life of DNA/siRNA in the circulatory system, ranging from 1.2 to 21 minutes upon parenteral delivery of naked genetic loads (31). Genes are non-specific to the targeted site and have low cellular uptake, deemed by their negatively-charged forms. Non-specific plasma protein interactions will also

bring in premature degradation of genes, in addition to reticuloendothelial system (RES) entrapment, in which upon intravenous delivery, naked genes are often phagocytosed by mononuclear phagocyte system (examples include Kupffer cells and macrophages) (32). The eliminatory process mediated by blood component interactions results in greater particle accumulation in RES organs, liver, and kidney. The negative surface charge of naked genomic structures increases the clearance activity from the system in comparison to neutral and positively charged particles (30).

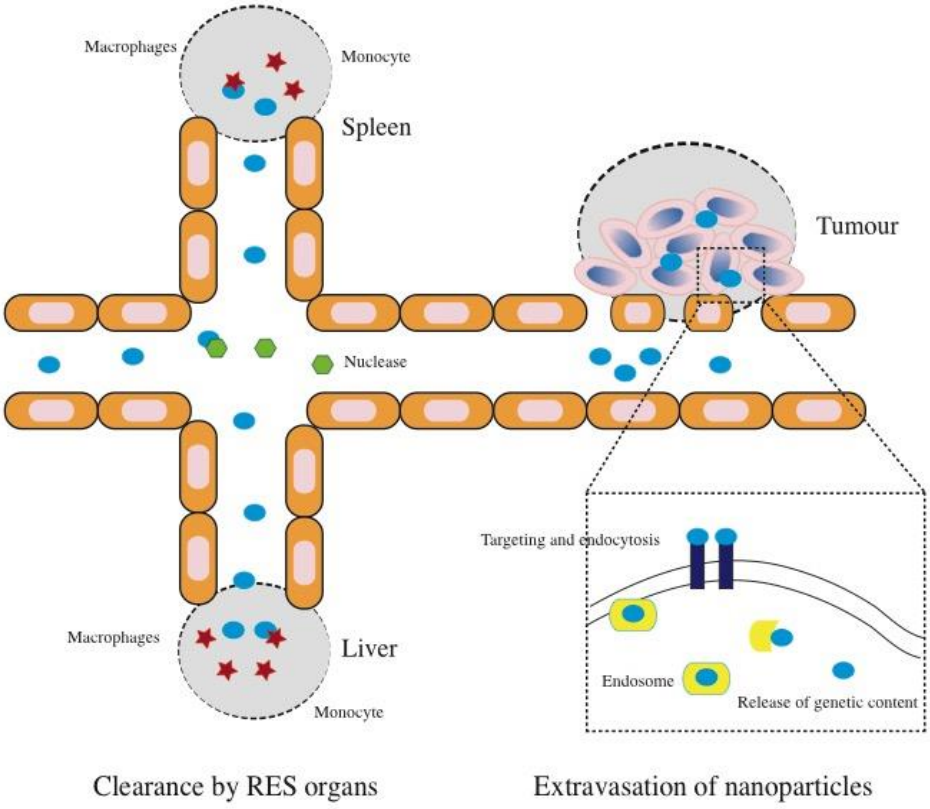

Figure 2.5: Extracellular and intracellular barriers faced by gene vectors. Among the extracellular hurdles including nuclease are associated with premature degradation of vectors while circulating macrophages, and monocyte induce RES elimination. Intracellular barriers include difficulties in internalization of gene-vector via endocytosis and release of the gene from the endosomal cavity. Adapter from: Mitragotri S, *et al*. Overcoming the challenges in administering biopharmaceuticals: formulation and delivery strategies. Nature Reviews Drug Discovery. 2014, 13: 665-672.

Subsequent target genes must further overcome intracellular barriers involving inefficient cellular binding for internalization to form endosomes, followed by endosomal escape and for transcription/ translation activity inside the cytosol or nuclear cavity (33). Hence, developing efficient delivery structure is vital as part of defense mechanism for genetic materials and to ensure a targeted delivery approach. The ideal vectors should be able to transport "object of interest" to the desired area, improving the protection against premature degradation, ensuring the specific organ targeting and helping endosomal escape while simultaneously minimizing the side effects (33,34).

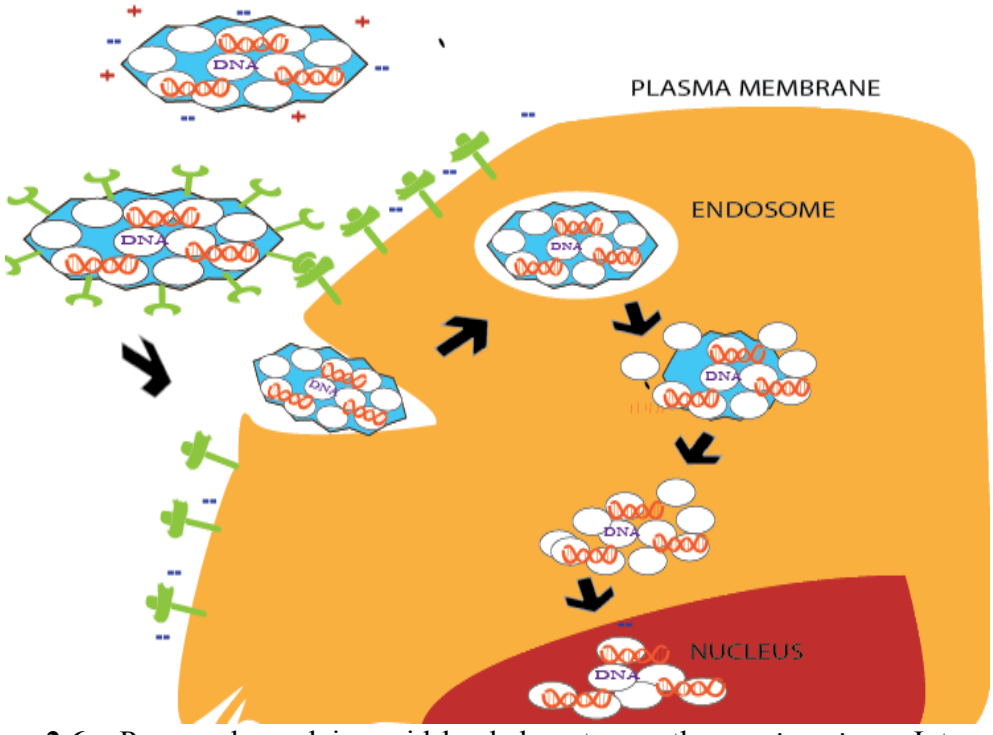

Figure 2.6: Proposed nucleic acid-loaded-vector pathway *in vitro*. Internalised complexes via active or passive extracellular transportation form endosome containing the bound genetic materials (shown as DNA). Endosomal escape of the complexes should release the genetic content which will enter the nuclear cavity to instigate transcription process. Adapted from Kylie M. Wagstaff, David A. Jans. Nucleocytoplasmic transport of DNA: enhancing non-viral gene transfer. Biochemical Journal 2007, 406 (2): 185-202.

Types of viral delivery	Functions
Adenovirus	The viral has the ability to transfect both dividing and non-dividing cells with little host specificity hence can be delivered to various tissues. It can transport large DNA, up to 38kb, although cannot integrate into the host genome, hence, gene expression is temporary. The virus triggers natural immunologic responses, causing serious side effects including death, associated with adenovirus, limit the clinical application to localized gene therapy.
Adeno-associated virus (AAV)	The viral carrier has similar features like adenovirus but with the lack of replication and pathogenicity, hence safer than adenovirus. Integration of AAV into the specific site on chromosome 19 was noticeable with long-term expression *in vivo*. The vector production, however, is complicated with limited gene carrier capacity.
Retrovirus	The vector has the ability to transfect dividing cells as they can pass through nuclear pores in mitotic cells. It is useful for *ex vivo* transfection of somatic cells based on ability to integrate linearly into host cell genome. Additionally, the removal of viral genes will create approximately 8kb space for gene incorporation.
Herpes simplex virus (HSV)	The vector is known as a disabled infectious single copy (DISC) virus as when propagated into complementing cells, viral particles can infect subsequent cells to replicate permanently their own genome without producing infectious particles. The virus can transport up to 150kb DNA with potential as gene carrier especially for the nervous system based on their neuronotropic characteristic.
Lentivirus	The virus has the ability to integrate both dividing and non-dividing cells, with the long-term stable expression of the transgene, low immunogenicity and accommodate large genes, up to 8kb.
Pox virus	The vector has the ability to transport larger capacity of DNA (>25kb). Used for high-level cytoplasmic expression of transgene, which utilizes homologous recombination. Safety features of the virus are still largely unknown due to their complex structures.
Epstein-Barr virus	A type of herpes virus that can be used for large DNA transportation into target cells. It is suitable for long-term retention in cells forming extrachromosomal circular plasmid in the latent state of host nucleus.

Table 2.2: Most common viral delivery systems for gene therapy (35)(36)(37)(38)(39)(40)(41)

Intensive research in the last three decades led to the development of many carriers which are classified into two distinctive groups: viral and non-viral vectors. Viral systems are by far the most efficient means of DNA/RNA delivery to mammalian cells, which comprise of available successful gene delivery systems, such as retrovirus, adenovirus, adeno-associated virus and lentivirus (42). The effectiveness of a viral particle is the result of its highly evolved and specialized structure composed of a protein coat surrounding a nucleic acid core. Such a highly organized structure can prevent viral particles from unwanted interactions with serum components while promoting subsequent internalization by cells, escape from endosomes, and release of genetic material from the viral load either before or after entering the nucleus (43).

Modification of viral vector was performed by deleting the parts of the genome to cause derangement of their replication, allowing them to be much safer (44). Nonetheless, their marked immunogenicity causes the activation of the inflammatory response, leading to degeneration of transduced tissues, in addition to viral toxin production, insertional mutagenesis and limited DNA carrying capacity. Additional production and packaging problem, along with high recombinant cost, limit their successful applications in laboratory and clinical research (34,42). Limitation in cell mitosis for the retrovirus, contamination with adenovirus and packaging constraint of AAV further lessen the appeal for a potent viral application (45). Therefore, the ideal vector incorporating the safety and efficacy aspects is still lacking. Development of a non-viral approach devouring the beneficial virus-like properties and lacking the disadvantageous aspects would emerge as the most attractive one for implementation in research laboratories and gene therapy. Non-viral vectors, generated from various biocompatible materials, utilize innovative fabrication approaches to safely deliver the

gene cargo (46). Ideally, negatively charged pDNA/siRNA molecules should be condensed with cationic reagents of non-viral structures to allow the formation of the complexes carrying net positive charges. The resulting composite thus interacts electrostatically with anionic heparan sulfate proteoglycans (syndecans) on the cell surface and reach the cytoplasmic side in the form of endosomes through endocytosis (33)(47). The extremely low pH and enzymes within the late endosomes usually bring about the degradation of entrapped pDNA/siRNA and associated complexes. Finally, pDNA or siRNA that survives both endocytic processing and cytoplasmic nucleases must dissociate from the condensed complexes either before or after nuclear translocation through the nuclear pore or during cell division (48).

Despite articulation of low transfection efficacy in comparison to viral carriers, their cost-effectiveness, low immunogenicity, an unlimited size of transgenic DNA to of viral vectors have made them highly promising for gene delivery (34)(33). The system, which comprises of all physical-chemical system without viral presence are often divided into three categories, physical methods, synthetic or natural biocompatible particles and inorganic particles. The physical method introduces a physical force to overcome the cytoplasmic membrane and facilitate in intracellular gene transfer by directly introducing the genes into the cells, such as ballistic DNA injection, electroporation, sonoporation, hydroporation and magnetofection (49)(50). The internalized genetic materials via physical methods can only be utilized for local delivery; hence, a more diverged gene transportation may fulfill the broader requirement (51).

Types of non-viral delivery	Functions
Liposome	-Membrane-like surface with encapsulated nucleic acids inside lipid structure. There are three types of liposome: cationic, anionic and neutral. Cationic liposome/lipoplexes are commonly used based on high affinity with the cell membrane, nonpathogenic and non-immunogenic characteristics. -e.g. Lipofectamine, SilentFect, DharmaFECT -Short half-life (several hours) associated with non-specific binding to serum proteins. Neutral or anionic liposomes are used to prevent instability related to interaction of plasma protein. Conjugation of hydrophilic PEG may increase the stability of liposome, up to 72 hours.
Polymers	-The approach of polymer-based delivery utilizes polyethyleneimine (PEI), poly (lactide-co-glycolide) (PLGA), poly (amidoamine) (PAMAMs) dendrimers or cell-penetrating peptide (CP-peptides). -Polymers are associated with low toxicity to cells, with low transfection efficiency. -Most polymers are poorly biodegradable, including PEI. Hydrophobic nature of PLGA decreases the effectiveness in gene delivery. PAMAMs are positively charged; hence improve the transfection efficiency of the genetic material. -PAMAM dendrimers, however, have the tendency to accumulate in the liver, associated with RES activity. -The natural-derived polymer of CP-peptides is non-toxic but prone to premature degradation.
Inorganic particles	-Include gold nanoparticles (AuNPs), Fe_3O_4 NPs, and silica-based NPs. Inorganic carriers have high stability in the circulatory system with low interaction with microbes. -However, they are associated with little nucleic acid binding, reducing transfection activity in gene therapy.

Table 2.3: Examples of non-viral delivery system for gene therapy (52)(53)(34)

Synthetic or natural biodegradable particles consist of cationic polymers, cationic lipids or peptides. The low toxicity of many polymers leads to non-toxic waste and avoidance of accumulation of intracellular polymer (54)(55). Cationic polymers, most standard nano-scale transportation system, prevent degradation of genetic materials through condensation process into polyplexes, either entrapped inside the polymeric matrix or conjugated onto the particles surfaces. Examples of cationic polymers include Poly(Lactic-co-Glycolic Acid)(PLGA), Polylactic acid (PLA),

chitosan, dendrimers and polyethyleneimine (PEI) (56). Cationic lipid, in the form of lipoplex upon complexation of lipid and nucleic acid, often formed by partial condensation of nucleic acid with ordered substructure and irregular morphology, to form cationic liposomes, lipid nanoemulsion, and solid lipid nanoemulsion (57). Cationic peptides contain residues including lysine and arginine, which can condense DNA and siRNA into compacted structure (58). The ability for lysing the endosomal cavity derived from the peptide sequence from protein transduction domains. Nuclear localization signals may be further improved by short peptide sequence obtained from viral proteins (53). Polyplexes exposure with serum protein may induce aggregation, severely limiting the ability to reach the targeted site for endocytosis process, in addition to the robustly stabilized structure of polyplexes prevents an efficient release of genetic load (59). Highly unstable lipoplex structure often prematurely disintegrate before reaching the tumor site, therefore reducing the amount available for cellular expression (60).

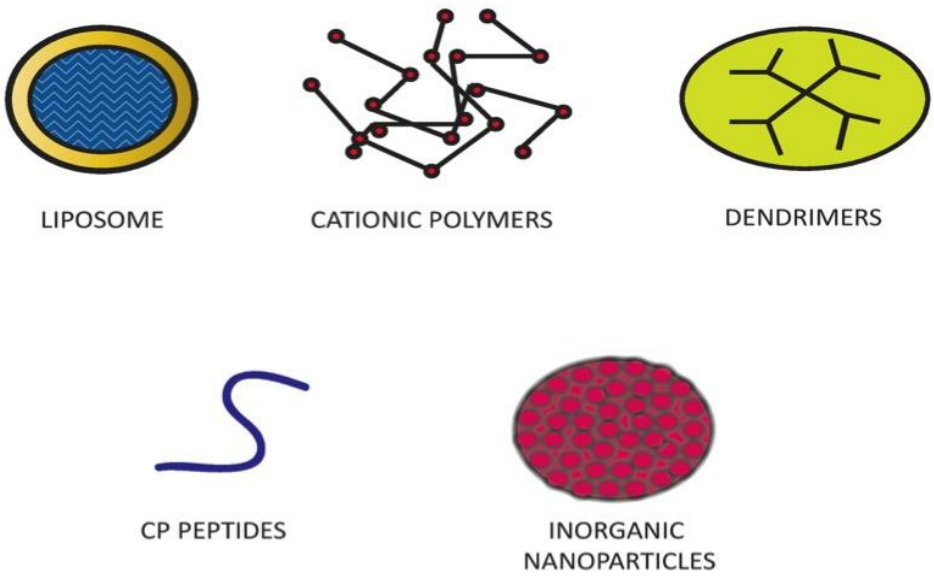

Figure 2.7: Examples of non-viral carriers utilised for gene therapy. Adapted from Xing Y, Zhao J, Conti PS, Chen K. Radiolabeled Nanoparticles for Multimodality Tumour Imaging. *Theranostics* 2014; 4(3): 290-306.

Nanoparticles have emerged as one of the novel gene delivery systems for delivery in targeted manner. Nanoparticles defined as solid carriers having the size of 1-1000 nm are receiving considerable interest due to numerous advantages over many other carriers. The most significant advantage of the nanoparticles is providing specified delivery to the specified area, increasing the effectiveness of gene therapy while concurrently reducing the side effects of non-specific delivery (61). Nanoparticles with sizes up to several hundred nanometers can enter the cells via membrane-bound vesicles through endocytosis process. Steps of endocytosis comprise of three main phases: formation of membrane vesicles with particle load, endosomal delivery of the cargo into the cell and distribution to intracytoplasmic organelles (62). Inorganic nanoparticles, an engineered structure varying in size, shape and porosity able to protect entrapped molecular content from degradation, examples include calcium phosphate, silica, gold and iron oxide. Inorganic particles are conveniently prepared and display low toxicity, with the ability to be surface-functionalized (63)(64). Additionally, high genetic material loads of inorganic particles are associated with high porosity and size of materials. However, many inorganic particles are non-biodegradable, namely gold and iron oxide, hence unable to efficiently disintegrate intracellularly to release genetic content (65).

Carbonate apatite (CO_3 AP) nanoparticles emerge as one of the most recently studied inorganic nanoparticles, with biodegradable properties and similarity to hard body tissue components (66). The high efficiency of apatite particles in transporting genetic materials and drugs both *in vitro* and *in vivo* is attributed to on its responsiveness to pH changes, disintegrating the structure upon exposure to acidic pH (67). The derivation of hydroxyapatite particles showed enhanced transgene expression

in both cancer and primary cells (68). The factors influencing the formation of CO_3 AP include modifying the 'supersaturation' in the bicarbonate-buffered medium of calcium, phosphate and DNA content (69). However, CO_3 AP nanoparticles still less efficient comparatively to viral delivery, in addition to stability issues which is associated with the release of CO_2 by the interaction of carbonate ions (70).

2.6 Active and passive tumor targeting

Current techniques for cytotoxic therapy with nanoparticles are based on active and passive tumor targeting. Active targeting builds on the nanoparticles conjugated to tumor biomarker ligands, which are specific for tumor extracellular carbohydrates and receptors, such as peptides and antibodies. The coated nanocarriers will recognize and bind to the targeted cells through ligand-receptor interaction, followed by subsequent internalization of targeted conjugates by receptor-mediated endocytosis (71)(72). Protein coating is associated with improvement in the pharmacokinetics of the particles, preventing the complexes from RES uptake for subsequent elimination process (73).

Passive tissue targeting is achieved by taking the advantage of the biochemical and physiological properties of the tumor microenvironment, which differs from the normal tissues (74). At the size of approximately 100 nm, nanoparticles can easily penetrate through the 'leaky' capillary system of malignant tissues without passing through the intact endothelium to the normal tissues, due to a phenomenon known as Enhance Permeability and Retention (EPR) effect (75). Furthermore, the morphological changes in the lymphatic system of malignant tissues will result in inadequate lymphatic

drainage, causing more retention time of the drugs within the tumor microenvironment (76).

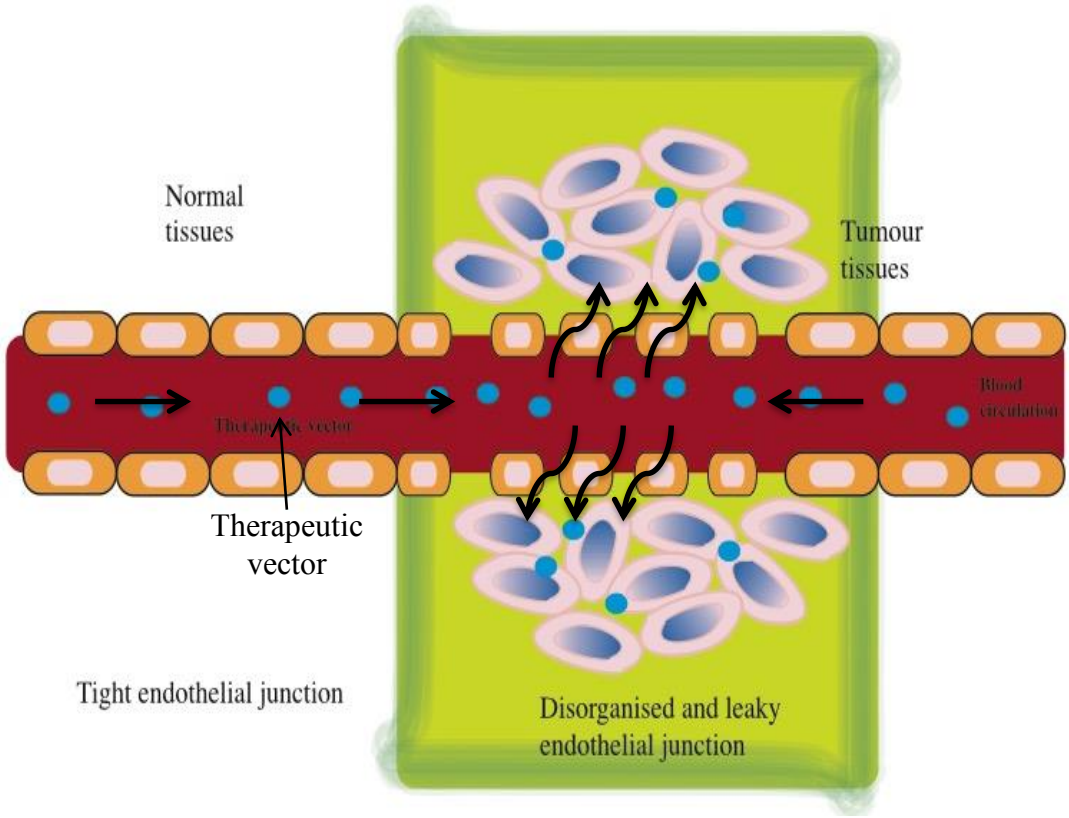

Figure 2.8: Passive Tissue Targeting achieved by EPR effect

2.7 Fabrication of nanoparticles via precipitation reaction

Precipitation reaction has emerged as one of the most recent approaches in synthesizing nanoscale materials, which exhibit many unique and exciting physical and chemical properties. It involves the reaction of chemical reactants with other reactants in an aqueous solution forming insoluble ionic products (77). The desired chemicals react and self-assemble to produce a supersaturated solution, resulting in particle nucleation and ultimately into nanosized particles (78). Crystalline solids, the products

of precipitation reaction may be suspended throughout the liquid or sedimented at the bottom of the solution (79).

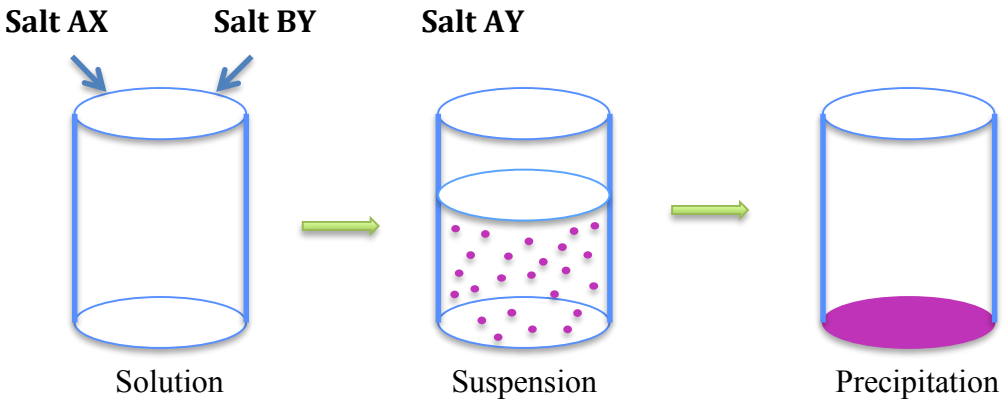

Figure 2.9: Generation of salt crystals through precipitation reaction

The formation of particles is accompanied by growth and aggregation of the particles, causing large-sized crystals (80). Thus, optimization in pH, the concentration of reactants, time and temperature or incubation is vital in fabricating ideal nanoparticles. Particle formation is accelerated as the concentration of reactants escalates, acting as a driving force for the chemical reaction. The increment in pH, temperature and incubation time shifts the ionization equilibrium towards the forward direction, and the rate of reaction is therefore enhanced. Besides, incorporation of magnesium salt causes a decrement in the size of the particles, suggesting apparently that incorporation of various salts decelerated particles growth to a significant extends (81)(82).

Binding of inorganic crystals to DNA or siRNA suggests the involvement of ionic interactions between salt crystals and DNA or siRNA (83). Studies have reported the high amount of non-thiol-mediated (nonspecific) binding of both single- and

double-stranded DNA to nanoparticles, suggested by the mechanism of ion-induced dipole dispersive interactions, which negative charge of DNA represented by phosphate group induces dipoles in the highly polarizable particle (84)(85). The vicinity of NPs is influenced by local ions and protein ligands (86)(87). As many proteins are charged, electrostatic interactions between them and NP may occur, in addition to local hydrophilic and hydrophobic patterns existing on the particle surface, resulting in protein adsorption called, namely protein corona (88)(89). Adsorbed proteins, therefore, alter the parameters of NPs, including hydrodynamic diameter and colloidal stability (90).

Cellular uptake is highly dependent on NPs size, charge and ligand binding. It was found that the adsorption efficacy and concentration of saturated particles differ with particle sizes, with optimal efficiency achieved with less than 100nm. Additionally, spherical particles of similar size were internalized 500% more compared to rod-shaped particles, possibly due to the greater time required for membrane wrapping for elongated particles (91). Manipulation of particles to produce nanosized compounds confers many benefits over microparticles. Nanoparticles have in general relatively higher intracellular uptake compared to microparticles. Tests were done on the rat intestinal model, where the formulation of nano- and microparticles were compared. There were 15 to 250 greater folds of uptake of 100 nm size particles in comparison with 1 and 10 µm microparticles. Also, the penetration of nanoparticles was found across the submucosal layers while larger size microparticles were mostly localized in the epithelial lining (92).

Ideally, neutral charged NPs are necessary to prevent unwanted particle-biological interactions, namely non-specific adsorption of serum protein onto the surface of particles, leading to aggregation and elimination from RES, subsequently reduced genetic material transportation to the targeted site, in addition to inefficient tagging and detection of NPs (93). Studies by Verma *et al.* showed that neutral and negatively charged nanoparticles adsorbed less on the negatively charged cell membrane surface and consequently displayed lower levels of internalization in comparison with positively charged particles (94).

2.8 Barium salt as potential vector

Barium compounds have been associated with many applications in the medical field. The insoluble component of this alkaline earth metal is non-toxic, allowing many types barium salts being used in clinical and cosmeceutical areas (95). Barium sulfate ($BaSO_4$) has low toxicity and high opacity for x-ray imaging, thus being used as a radiocontrast agent for digestive tract (96). Studies by Dempsey *et al.* proved that barium titanate nanoparticles exhibited promising future in biological imaging due to properties such as nontoxic, non-bleach and having narrow, multi-directional signal spectrum. Barium crystals complex also has a significant cell association and uptake of DNA, although it is often associated with low cellular uptake upon internalization, hence requires concomitant ligand coating such as cationic polymer PEI, resulting in an 8-fold increment of cellular uptake by modification of zeta potential of barium particles (97)(98).

2.9 Strontium salt as potential vector

Strontium compound, also an alkaline earth metal has recently been found to be beneficial for patients with osteoporosis and fractures, often act as calcium substitution for hydroxyapatite particles (99). Strontium inhibits bone resorption while simultaneously stimulating bone growth, six times more efficient than placebo. Strontium ranelate, a combination of strontium with ranelic acid, was found to be aiding bone growth, increasing bone density, and lessen vertebral, peripheral and hip fractures (100). Studies by Ravi *et al.* found that incorporation of strontium into bone cement *in vivo,* improved bone formation and decreased bone resorption (99). Strontium is also used for superficial radiotherapy for bone cancer treatment due to beta emission and long half-life. The beta particles are accountable for its therapeutic effect penetrating within 3 to 4 mm in bone and 6 to 7mm in soft tissues (101). Qian *et al.* showed in their study on the effectiveness of strontium carbonate as the carrier for the drug (etoposide). Etoposide-strontium carbonate complexes displayed high loading ability and encapsulation efficiency (102). The release of etoposide from its carrier was showed highest at pH 3.0, therefore potentially being pH-sensitive. The healthy kidney eliminates the majority of absorbed element; hence patients with renal insufficiency are at risk of accumulating this metals. High strontium is associated with accumulation of strontium in bone and presence of osteomalacia, with uptake is shown to be dose dependent with distribution is often in newly formed bone (103).

2.10 Calcium salt as potential vector

Calcium salt is the most abundant compound in human due to its vital importance in signaling many cellular pathways and mineralization of bone, teeth. Medically, the alkaline metal compounds are frequently used in an antacid as calcium carbonate, whereas other calcium salts such as calcium lactate and calcium gluconate are widely used as calcium supplements for hypocalcemic patients, pediatric patients and pregnant patients (104). Sokolova *et al.* proved that calcium phosphate nanoparticles are efficient as non-toxic carriers to transport compounds of interest across the cell membrane due to their dissolution behaviors under an acidic condition in the lysosome after internalization by the cell. As calcium phosphate concentration increases, more particles are internalized by the cells, providing more release of particle load (64)(105,106).

2.11 Magnesium as potential vector

Magnesium, an alkaline earth metal is vital for many essential metabolic reactions, including energy productions, nucleic acid and enzyme synthesis, ion transport across the cell membrane and cell signaling. Pharmaceutically, magnesium compounds are used as antacids, laxatives, treatment of eclampsia and asthma. Magnesium carbonate and magnesium phosphate are used widely for magnesium supplementary in patients with hypomagnesemia (107). Lellouche *et al.* reported antimicrobial and antibiofilm activities on Escherichia coli and Staphylococcus aureus bacteria by nano-sized magnesium fluoride, whose actions are influenced by nanoparticles sizes (108). Magnesium phosphate with sizes of approximately 100nm

showed efficient in vitro DNA transfection in HeLa cells and dissolved in mild acidic pH of 5 therefore indicated possible release of pDNA in the endosome (109).

2.12 Iron as potential vector

Iron is the key component in oxygen transportation and storage due to the formation of complexes with molecular oxygen in hemoglobin and myoglobin. Iron is also used for electron transport and energy metabolism as a component of cytochrome (a heme-containing compound). Some heme-containing enzymes are also beneficial as antioxidants, protecting cells from free radicals (110). Ferrous oxide nanoparticles were reported by Dresco et al. to increase the sensitivity of daunorubicin against cancer cells and initiate apoptosis through caspase 8-poly(ADP-ribose) polymerase (PARP) pathway. In vivo studies showed significant inhibition of tumor growth in mice (111).

2.13 HEPES as inert buffer media

HEPES buffer, also known as N-2-hydroxyethylpiperazine-N-2-ethane sulfonic acid) is a zwitterionic organic buffering agent frequently used in cell culture media. Supplementing 10-25mM HEPES improves buffering competency of cell culture with limited effect on biochemical reaction, being stable chemically and enzymatically and expressed low visible and ultraviolet (UV) light absorbance (112) (113). HEPES buffer has low metal binding constant and is therefore suited to investigate metal-dependent interactions. Various nanostructures, including zinc oxide, were readily synthesized in HEPES buffer solution. HEPES contains two free nitrogen atoms (piperazine group) and terminal hydroxyl groups, playing a crucial role as a reactant and surfactant to prevent the transition metal oxide nanoparticles from aggregation (114) (115).

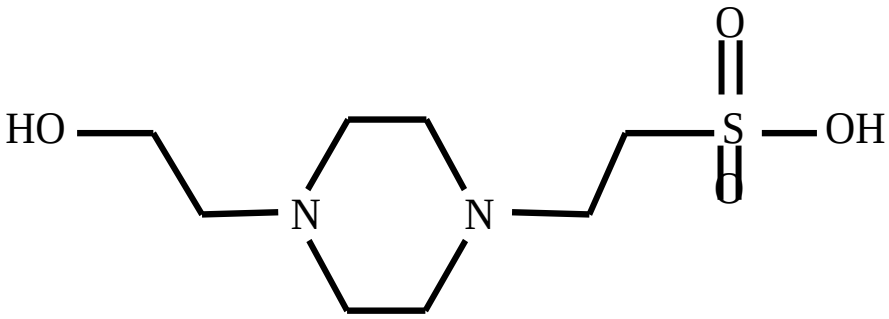

Figure 2.10: Chemical structure of HEPES

2.14 References

1. Brian K. Alldredge, Corelli RL, Ernst ME. Koda-Kimble and Young's applied therapeutics : the clinical use of drugs 10 th Edition. Lippincott Williams and Wilkins, a Wolter Kluwer bussines. 2013.
2. Ferlay J, Soerjomataram I, Ervik M, Dikshit R, Eser S, Mathers C, et al. GLOBOCAN 2012 v1.0, Cancer Incidence and Mortality Worldwide: IARC CancerBase. No. 11 [Internet]. Lyon, France: International Agency for Research on Cancer. 2013. p. http://globocan.iarc.f.
3. National Cancer Registry. Malaysia cancer statistics data and figure Peninsular Malaysia. 2006;1–137.
4. GLOBOCAN 2012: Estimated Cancer Incidence.
5. Moh. Edition. Das Totenb des Mainzer Dominikanerklosters [Internet]. 2010; Available from: http://www.degruyter.com/view/books/9783050047348/9783050047348.123/9783050047348.123.xml
6. Washbrook E. Risk factors and epidemiology of breast cancer. Women's Heal Med [Internet]. 2006;3(1):8–14. Available from: http://www.sciencedirect.com/science/article/pii/S174418700600117X
7. Mediterranean P. EMRO Technical Publications Series 31 Guidelines for management of breast cancer WHO Library Cataloguing in Publication Data Guidelines for management of breast cancer/by WHO Regional Office for the Eastern. Breast neoplasms – Ther Breast – Cancer. 3(4).
8. Burstein HJ, Temin S, Anderson H, Buchholz T a, Davidson NE, Gelmon KE, et al. Adjuvant endocrine therapy for women with hormone receptor-positive breast cancer: american society of clinical oncology clinical practice guideline focused update. J Clin Oncol [Internet]. 2014;32(21):2255–69. Available from: http://www.ncbi.nlm.nih.gov/pubmed/24868023
9. Rang, H.P., Ritter, J.M., Flower, R.J., Henderson G. Rang & Dale's Pharmacology, 8th Edition | Humphrey Rang, James Ritter, Rod Flower, Graeme Henderson | ISBN 9780702053627 [Internet]. Pharmacology. 2016. p. 776.

Available from: http://store.elsevier.com/Rang-and-Dales-Pharmacology/Humphrey-Rang/isbn-9780702053627/
10. Alberts. Tumor Suppressor Genes and Oncogenes : Genes that Prevent and Cause Cancer. Mol Biol Cell; 5th Ed Garl Sci. 2008;Chapter 20; Cancer, pp.1230–56.
11. Deininger P. Genetic instability in cancer: caretaker and gatekeeper genes. Ochsner J [Internet]. 1999 Oct [cited 2016 Apr 3];1(4):206–9. Available from: http://www.ncbi.nlm.nih.gov/pubmed/21845140
12. Rivlin N, Brosh R, Oren M, Rotter V. Mutations in the p53 Tumor Suppressor Gene: Important Milestones at the Various Steps of Tumorigenesis. Genes Cancer [Internet]. 2011;2(4):466–74. Available from: papers3://publication/doi/10.1177/1947601911408889
13. Chial BH, Write PD, Right S, Education N. Proto-oncogenes to Oncogenes to Cancer. Nature Education. 2008. p. 1–5.
14. Lodish HF, Berk A, Zipursky SL, Matsudaira P, Baltimore D, James D. Molecular Cell Biology [Internet]. Book. 2008. 801-846 p. Available from: http://www.amazon.com/Molecular-Cell-Biology-Harvey-Lodish/dp/0716743663
15. Yoshida K, Miki Y. Role of BRCA1 and BRCA2 as regulators of DNA repair, transcription, and cell cycle in response to DNA damage. Cancer Science. 2004. p. 866–71.
16. Bakhtiar A, Sayyad M, Rosli R, Maruyama A, Chowdhury EH. Intracellular delivery of potential therapeutic genes: prospects in cancer gene therapy. Curr Gene Ther [Internet]. 2014 [cited 2016 Mar 6];14(4):247–57. Available from: http://www.ncbi.nlm.nih.gov/pubmed/25039616
17. Cooper GM. Tumor Suppressor Genes. Sinauer Associates; 2000.
18. Aoki K, Taketo MM. Adenomatous polyposis coli (APC): a multi-functional tumor suppressor gene. J Cell Sci [Internet]. The Company of Biologists Ltd; 2007 Oct 1 [cited 2016 Apr 4];120(19):3327–35. Available from: http://jcs.biologists.org/cgi/doi/10.1242/jcs.03485
19. Moasser MM. The oncogene HER2: its signaling and transforming functions and its role in human cancer pathogenesis. Oncogene [Internet]. 2007 Oct 4 [cited 2016 Apr 4];26(45):6469–87. Available from: http://www.ncbi.nlm.nih.gov/pubmed/17471238
20. Sato K ichi. Cellular functions regulated by phosphorylation of EGFR on TYR845. International Journal of Molecular Sciences. 2013. p. 10761–90.
21. Olsson A-K, Dimberg A, Kreuger J, Claesson-Welsh L. VEGF receptor signalling - in control of vascular function. Nat Rev Mol Cell Biol [Internet]. 2006;7(5):359–71. Available from: http://dx.doi.org/10.1038/nrm1911
22. Pearson G, Robinson F, Beers Gibson T, Xu B, Karandikar M, Berman K, et al. Mitogen-Activated Protein (MAP) Kinase Pathways: Regulation and Physiological Functions [1]. Endocr Rev [Internet]. 2001 Apr [cited 2016 Apr 4];22(2):153–83. Available from: http://press.endocrine.org/doi/abs/10.1210/edrv.22.2.0428
23. Yip KW, Reed JC. Bcl-2 family proteins and cancer. Oncogene. 2008;27(50):6398–406.
24. Das SK, Menezes ME, Bhatia S, Wang X-Y, Emdad L, Sarkar D, et al. Gene Therapies for Cancer: Strategies, Challenges and Successes. J Cell Physiol [Internet]. 2015 Feb [cited 2016 Mar 4];230(2):259–71. Available from: http://doi.wiley.com/10.1002/jcp.24791
25. Caspari T. Checkpoints: How to activate p53. Curr Biol. 2000;10(8):R315–7.

26. Bakhtiar A, Sayyad M, Rosli R, Maruyama A, Chowdhury E. Intracellular Delivery of Potential Therapeutic Genes: Prospects in Cancer Gene Therapy. Curr Gene Ther [Internet]. 2014 Sep 3 [cited 2016 Mar 5];14(4):247–57. Available from: http://www.eurekaselect.com/openurl/content.php?genre=article&issn=1566-5232&volume=14&issue=4&spage=247
27. Muller PAJ, Vousden KH. p53 mutations in cancer. Nat Cell Biol [Internet]. 2013 Jan [cited 2016 Mar 4];15(1):2–8. Available from: http://www.nature.com/doifinder/10.1038/ncb2641
28. Jeong EH, Kim H, Jang B, Cho H, Ryu J, Kim B, et al. Technological development of structural DNA/RNA-based RNAi systems and their applications. Adv Drug Deliv Rev. 2015;
29. Ghildiyal M, Zamore PD. Small silencing RNAs: an expanding universe. Nat Rev Genet [Internet]. 2009;10(2):94–108. Available from: http://www.ncbi.nlm.nih.gov/pubmed/19148191
30. Wang J, Lu Z, Wientjes MG, Au JL-S. Delivery of siRNA Therapeutics: Barriers and Carriers. AAPS J [Internet]. 2010 Dec 11 [cited 2016 Mar 5];12(4):492–503. Available from: http://www.springerlink.com/index/10.1208/s12248-010-9210-4
31. F. L, A. D. Extracellular and Intracellular Barriers to Non-Viral Gene Transfer. In: Novel Gene Therapy Approaches [Internet]. InTech; 2013 [cited 2016 Mar 5]. Available from: http://www.intechopen.com/books/novel-gene-therapy-approaches/extracellular-and-intracellular-barriers-to-non-viral-gene-transfer
32. Lee Goldman and AIS. Goldman's Cecil Medicine, Twenty-Fourth Edition, EXPERT CONSULT PREMIUM EDITION -- ENHANCED ONLINE FEATURES AND PRINT, TWO VOLUME SET. In: 5. 2012. p. 17–20.
33. Yin H, Kanasty RL, Eltoukhy A a, Vegas AJ, Dorkin JR, Anderson DG. Non-viral vectors for gene-based therapy. Nat Rev Genet [Internet]. 2014;15(8):541–55. Available from: http://dx.doi.org/10.1038/nrg3763\nhttp://www.ncbi.nlm.nih.gov/pubmed/25022906
34. Nayerossadat N, Ali P, Maedeh T. Viral and nonviral delivery systems for gene delivery. Adv Biomed Res [Internet]. 2012 [cited 2016 Mar 5];1(1):27. Available from: http://www.advbiores.net/text.asp?2012/1/1/27/98152
35. Bushman FD. Retroviral integration and human gene therapy. Journal of Clinical Investigation. 2007. p. 2083–6.
36. Vorburger SA, Hunt KK. Adenoviral Gene Therapy. Oncologist [Internet]. 2002;7(1):46–59. Available from: http://theoncologist.alphamedpress.org/content/7/1/46\nhttp://theoncologist.alphamedpress.org/content/7/1/46.full.pdf\nhttp://theoncologist.alphamedpress.org/content/7/1/46.long\nhttp://www.ncbi.nlm.nih.gov/pubmed/11854546
37. Lai CM, Lai YKY, Rakoczy PE. Adenovirus and adeno-associated virus vectors. DNA Cell Biol. 2002;21(12):895–913.
38. Burton E a, Wechuck JB, Wendell SK, Goins WF, Fink DJ, Glorioso JC. Multiple applications for replication-defective herpes simplex virus vectors. Stem Cells [Internet]. 2001;19(5):358–77. Available from: http://www.ncbi.nlm.nih.gov/pubmed/11553845
39. Vigna E, Naldini L. Lentiviral vectors: excellent tools for experimental gene transfer and promising candidates for gene therapy. J Gene Med. 2000;2(5):308–16.
40. Moroziewicz D, Kaufman HL. Gene therapy with poxvirus vectors. Curr Opin

Mol Ther. 2005;7(4):317–25.
41. Hodin TL, Najrana T, Yates JL. Efficient replication of Epstein-Barr virus-derived plasmids requires tethering by EBNA1 to host chromosomes. J Virol [Internet]. 2013;87(23):13020–8. Available from: http://www.ncbi.nlm.nih.gov/pubmed/24067969
42. Huang Y, Liu X, Dong L, Liu Z, He X, Liu W. Development of viral vectors for gene therapy for chronic pain. Pain Research and Treatment. 2011.
43. Stone D, David A, Bolognani F, Lowenstein PR, Castro MG. REVIEW Viral vectors for gene delivery and gene therapy within the endocrine system. J Endocrinol. 2000;164:103–18.
44. Thomas CE, Ehrhardt A, Kay MA. Progress and problems with the use of viral vectors for gene therapy. Nat Rev Genet [Internet]. 2003 May [cited 2016 Mar 5];4(5):346–58. Available from: http://www.nature.com/doifinder/10.1038/nrg1066
45. Ferrari M, Lee AP, Lee LJ, editors. BioMEMS and Biomedical Nanotechnology [Internet]. Boston, MA: Springer US; 2006 [cited 2016 Mar 6]. Available from: http://link.springer.com/10.1007/b136237
46. Zhang Y, Satterlee A, Huang L. In Vivo Gene Delivery by Nonviral Vectors: Overcoming Hurdles? Mol Ther [Internet]. 2012;20(7):1298–304. Available from: http://dx.doi.org/10.1038/mt.2012.79/nature06264
47. Philip H, Marlene R. Transplantation Immunology [Internet]. New Jersey: Humana Press; 2006 [cited 2016 Mar 6]. Available from: http://link.springer.com/10.1385/1597450499
48. Kay M a. State-of-the-art gene-based therapies: the road ahead. Nat Rev Genet [Internet]. 2011;12(5):316–28. Available from: http://dx.doi.org/10.1038/nrg2971
49. Kamimura K, Suda T, Zhang G, Liu D. Advances in Gene Delivery Systems. Pharm Med [Internet]. 2011;25(5):293–306. Available from: http://www.ncbi.nlm.nih.gov/pubmed/22200988
50. Niidome T, Huang L. Gene Therapy Progress and Prospects: Nonviral vectors. Gene Ther [Internet]. 2002 Nov 29 [cited 2016 Mar 6];9(24):1647–52. Available from: http://www.nature.com/doifinder/10.1038/sj.gt.3301923
51. Jafari M, Soltani M, Naahidi S, N. Karunaratne D, Chen P. Nonviral Approach for Targeted Nucleic Acid Delivery. Curr Med Chem. 2012;19(2):197–208.
52. Wu Y, Crawford M, Mao Y, Lee RJ, Davis IC, Elton TS, et al. Therapeutic Delivery of MicroRNA-29b by Cationic Lipoplexes for Lung Cancer. Mol Ther Nucleic Acids [Internet]. 2013;2(April):e84. Available from: http://www.pubmedcentral.nih.gov/articlerender.fcgi?artid=3650246&tool=pmcentrez&rendertype=abstract
53. Martin ME, Rice KG. Peptide-guided gene delivery. AAPS J. 2007;9(1):E18–29.
54. Rodriguez A, del A, Angeles M. Non-Viral Delivery Systems in Gene Therapy. In: Gene Therapy - Tools and Potential Applications [Internet]. InTech; 2013 [cited 2016 Mar 6]. Available from: http://www.intechopen.com/books/gene-therapy-tools-and-potential-applications/non-viral-delivery-systems-in-gene-therapy
55. Nie H, Khew ST, Lee LY, Poh KL, Tong YW, Wang CH. Lysine-based peptide-functionalized PLGA foams for controlled DNA delivery. J Control Release. 2009;138(1):64–70.
56. Luten J, van Nostrum CF, De Smedt SC, Hennink WE. Biodegradable polymers as non-viral carriers for plasmid DNA delivery. Journal of Controlled Release.

2008. p. 97–110.
57. Gascon AR, Pedraz JL. Cationic lipids as gene transfer agents: a patent review. Expert Opin Ther PATENTS;18 515-524 MAY 2008 [Internet]. 2008;18. Available from: http://www.thomsoninnovation.com/tip-innovation/recordView.do?datasource=WOK&category=LIT&selRecord=1&totalRecords=1&databaseIds=WOS&idType=uid/recordid&recordKeys=000257083500001/171553697\nhttp://www.thomsoninnovation.com/tip-innovation/
58. McKenzie DL, Kwok KY, Rice KG. A potent new class of reductively activated peptide gene delivery agents. J Biol Chem. 2000;275(14):9970–7.
59. Maeda H, Bharate GY, Daruwalla J. Polymeric drugs for efficient tumor-targeted drug delivery based on EPR-effect. European Journal of Pharmaceutics and Biopharmaceutics. 2009. p. 409–19.
60. Al-Dosari MS, Gao X. Nonviral gene delivery: principle, limitations, and recent progress. AAPS J. 2009;11(4):671–81.
61. Auffan M, Rose J, Bottero J-Y, Lowry G V, Jolivet J-P, Wiesner MR. Towards a definition of inorganic nanoparticles from an environmental, health and safety perspective. Nat Nanotechnol [Internet]. 2009;4(10):634–41. Available from: http://dx.doi.org/10.1038/nnano.2009.242
62. Kudera S, Maus L, Zanella M, Pelaz B, Zhang Q, Parak WJ, et al. Inorganic Core–Shell Nanoparticles. In: Reference Module in Materials Science and Materials Engineering. 2016.
63. Guo X, Huang L. Recent advances in nonviral vectors for gene delivery. Acc Chem Res. 2012;45(7):971–9.
64. Sokolova V, Epple M. Inorganic nanoparticles as carriers of nucleic acids into cells. Angewandte Chemie - International Edition. 2008. p. 1382–95.
65. Zhao L, Seth A, Wibowo N, Zhao CX, Mitter N, Yu C, et al. Nanoparticle vaccines. Vaccine. 2014. p. 327–37.
66. Chowdhury EH, Maruyama A, Kano A, Nagaoka M, Kotaka M, Hirose S, et al. pH-sensing nano-crystals of carbonate apatite: Effects on intracellular delivery and release of DNA for efficient expression into mammalian cells. Gene. 2006;376(1-2):87–94.
67. Chowdhury EH, Akaike T. A bio-recognition device developed onto nano-crystals of carbonate apatite for cell-targeted gene delivery. Biotechnol Bioeng. 2005;90(4):414–21.
68. Chowdhury EH. Self-assembly of DNA and cell-adhesive proteins onto pH-sensitive inorganic crystals for precise and efficient transgene delivery. Curr Pharm Des [Internet]. 2008;14(22):2212–28. Available from: http://www.ncbi.nlm.nih.gov/pubmed/18781973
69. Chowdhury EH. pH-responsive magnesium- and carbonate-substituted apatite nano-crystals for efficient and cell-targeted delivery of transgenes. Open J Genet [Internet]. 2013;03(02):38–44. Available from: http://www.scirp.org/journal/PaperDownload.aspx?DOI=10.4236/ojgen.2013.32A1005
70. Co-investigator N. Hydroxyapatite and related materials. Journal of Chemical Information and Modeling. 2013. 1689-1699 p.
71. Torchilin VP. Passive and active drug targeting: Drug delivery to tumors as an example. Handbook of Experimental Pharmacology. 2010. p. 3–53.
72. Danhier F, Feron O, Pr??at V. To exploit the tumor microenvironment: Passive and active tumor targeting of nanocarriers for anti-cancer drug delivery. Journal of Controlled Release. 2010. p. 135–46.

73. Schiffelers RM, de Wolf HK, van Rooy I, Storm G. Synthetic delivery systems for intravenous administration of nucleic acids. Nanomedicine (Lond) [Internet]. 2007;2(2):169–81. Available from: http://www.ncbi.nlm.nih.gov/pubmed/17716119
74. Hirsjärvi S, Passirani C, Benoit J-P. Passive and active tumour targeting with nanocarriers. Curr Drug Discov Technol [Internet]. 2011;8(3):188–96. Available from: http://www.ncbi.nlm.nih.gov/pubmed/21513482
75. Khawar IA, Kim JH, Kuh HJ. Improving drug delivery to solid tumors: Priming the tumor microenvironment. Journal of Controlled Release. 2015. p. 78–89.
76. Maruyama K. Intracellular targeting delivery of liposomal drugs to solid tumors based on EPR effects. Advanced Drug Delivery Reviews. 2011. p. 161–9.
77. Niemeyer CM. NANOTECHNOLOGY: Tools for the Biomolecular Engineer. Science (80-) [Internet]. 2002;297(5578):62–3. Available from: http://www.sciencemag.org
78. Noguera C, Fritz B, Cl??ment A. Precipitation mechanism of amorphous silica nanoparticles: A simulation approach. J Colloid Interface Sci. 2015;448:553–63.
79. Naidoo S, Naidoo Q, Musil E, Linkov V, Vaivars G. Precipitation and calcination synthesis methods forming nano-sized platinum catalytic particles for methanol and hydrogen oxidation. Adv Nat Sci Nanosci Nanotechnol [Internet]. 2013 Feb 7 [cited 2016 Mar 8];4(1):015014. Available from: http://stacks.iop.org/2043-6262/4/i=1/a=015014?key=crossref.c10cb63807b9497746bc5ec9a09cd782
80. Walliser RM, Boudoire F, Orosz E, T??th R, Braun A, Constable EC, et al. Growth of nanoparticles and microparticles by controlled reaction-diffusion processes. Langmuir. 2015;31(5):1828–34.
81. Tobler DJ, Shaw S, Benning LG. Quantification of initial steps of nucleation and growth of silica nanoparticles: An in-situ SAXS and DLS study. Geochim Cosmochim Acta. 2009;73(18):5377–93.
82. Fouilloux S, Taché O, Spalla O, Thill A. Nucleation of silica nanoparticles measured in situ during controlled supersaturation increase. Restructuring toward a monodisperse nonspherical shape. Langmuir. 2011;27(20):12304–11.
83. Tassa C, Duffner JL, Lewis TA, Weissleder R, Schreiber SL, Koehler AN, et al. Binding affinity and kinetic analysis of targeted small molecule-modified nanoparticles. Bioconjug Chem. 2010;21(1):14–9.
84. Cárdenas M, Barauskas J, Schillén K, Brennan JL, Brust M, Nylander T. Thiol-Specific and Nonspecific Interactions between DNA and Gold Nanoparticles. Langmuir [Internet]. 2006 Mar [cited 2016 Mar 9];22(7):3294–9. Available from: http://pubs.acs.org/doi/abs/10.1021/la0530438
85. Sandström P, Boncheva M, Åkerman B. Nonspecific and thiol-specific binding of DNA to gold nanoparticles. Langmuir. 2003;19(18):7537–43.
86. Pfeiffer C, Rehbock C, Hühn D, Carrillo-Carrion C, de Aberasturi DJ, Merk V, et al. Interaction of colloidal nanoparticles with their local environment: the (ionic) nanoenvironment around nanoparticles is different from bulk and determines the physico-chemical properties of the nanoparticles. J R Soc Interface [Internet]. 2014;11(96):20130931. Available from: http://www.pubmedcentral.nih.gov/articlerender.fcgi?artid=4032524&tool=pmcentrez&rendertype=abstract
87. Hung A, Mwenifumbo S, Mager M, Kuna JJ, Stellacci F, Yarovsky I, et al. Ordering surfaces on the nanoscale: Implications for protein adsorption. J Am Chem Soc. 2011;133(5):1438–50.

88. Cedervall T, Lynch I, Lindman S, Berggård T, Thulin E, Nilsson H, et al. Understanding the nanoparticle-protein corona using methods to quantify exchange rates and affinities of proteins for nanoparticles. Proc Natl Acad Sci U S A. 2007;104(7):2050–5.
89. Kittler S, Greulich C, Gebauer JS, Diendorf J, Treuel L, Ruiz L, et al. The influence of proteins on the dispersability and cell-biological activity of silver nanoparticles. J Mater Chem. 2010;20(3):512.
90. Jiang W, Kim BYS, Rutka JT, Chan WCW. Nanoparticle-mediated cellular response is size-dependent. Nat Nanotechnol [Internet]. 2008;3(3):145–50. Available from: http://dx.doi.org/10.1038/nnano.2008.30
91. Kohane DS. Microparticles and nanoparticles for drug delivery. Biotechnology and Bioengineering. 2007. p. 203–9.
92. Xie J, Xu C, Kohler N, Hou Y, Sun S. Controlled PEGylation of monodisperse Fe3O4 nanoparticles for reduced non-specific uptake by macrophage cells. Adv Mater. 2007;19(20):3163–6.
93. Verma A, Stellacci F. Effect of surface properties on nanoparticle-cell interactions. Small. 2010. p. 12–21.
94. Ramaswamy V, Vimalathithan RM, Ponnusamy V. Synthesis of monodispersed barium sulphate nanoparticles using water-benzene mixed solvent. Adv Mat Lett [Internet]. 2012 [cited 2016 Mar 9];3(31):29–33. Available from: www.vbripress.com
95. Meagher MJ, Leone B, Turnbull TL, Ross RD, Zhang Z, Roeder RK. Dextran-encapsulated barium sulfate nanoparticles prepared for aqueous dispersion as an X-ray contrast agent. J Nanoparticle Res. 2013;15(12).
96. Ĉulić-Viskota J, Dempsey WP, Fraser SE, Pantazis P, J. Culic-Viskota, W. P. Dempsey, et al. Surface functionalization of barium titanate SHG nanoprobes for in vivo imaging in zebrafish. Nat Protoc [Internet]. 2012;7(9):1618–33. Available from: <Go to ISI>://WOS:000308526300005
97. Dempsey C, Lee I, Cowan KR, Suh J. Coating barium titanate nanoparticles with polyethylenimine improves cellular uptake and allows for coupled imaging and gene delivery. Colloids Surfaces B Biointerfaces. 2013;112:108–12.
98. Ravi ND, Balu R, Sampath Kumar TS. Strontium-substituted calcium deficient hydroxyapatite nanoparticles: Synthesis, characterization, and antibacterial properties. In: Journal of the American Ceramic Society. 2012. p. 2700–8.
99. Zhou H, Nedley M, Bhaduri SB. The impacts of Mg2+ on strontium phosphate: A preliminary study. Mater Lett. 2013;113:63–6.
100. Wang Y, Tao H, Yu X, Wang Z, Wang M. Clinical significance of zoledronic acid and strontium-89 in patients with asymptomatic bone metastases from non-small-cell lung cancer. Clin Lung Cancer. 2013;14(3):254–60.
101. Qian WY, Sun DM, Zhu RR, Du XL, Liu H, Wang SL. pH-sensitive strontium carbonate nanoparticles as new anticancer vehicles for controlled etoposide release. Int J Nanomedicine. 2012;7:5781–92.
102. Cohen-Solal M. Strontium overload and toxicity: impact on renal osteodystrophy. Nephrol Dial Transplant [Internet]. 2002;17 Suppl 2:30–4. Available from: http://www.ncbi.nlm.nih.gov/pubmed/11904356
103. Emkey RD, Emkey GR. Calcium Metabolism and Correcting Calcium Deficiencies. Endocrinology and Metabolism Clinics of North America. 2012. p. 527–56.
104. Hou S, Ma H, Ji Y, Hou W, Jia N. A calcium phosphate nanoparticle-based

biocarrier for efficient cellular delivery of antisense oligodeoxynucleotides. ACS Appl Mater Interfaces. 2013;5(3):1131–6.
105. Liu Y, Wang T, He F, Liu Q, Zhang D, Xiang S, et al. An efficient calcium phosphate nanoparticle-based nonviral vector for gene delivery. Int J Nanomedicine. 2011;6:721–7.
106. de Baaij JHF, Hoenderop JGJ, Bindels RJM. Magnesium in Man: Implications for Health and Disease. Physiol Rev [Internet]. 2015;95(1):1–46. Available from: http://www.ncbi.nlm.nih.gov/pubmed/25540137
107. Lellouche J, Kahana E, Elias S, Gedanken A, Banin E. Antibiofilm activity of nanosized magnesium fluoride. Biomaterials. 2009;30(30):5969–78.
108. Bhakta G, Nurcombe V, Maitra A, Shrivastava A. DNA-encapsulated magnesium phosphate nanoparticles elicit both humoral and cellular immune responses in mice. Results Immunol. 2014;4(1):46–53.
109. Sangani RG, Ghio AJ. Iron, human growth, and the global epidemic of obesity. Nutrients. 2013. p. 4231–49.
110. Dresco PA, Zaitsev VS, Gambino RJ, Chu B. Preparation and properties of magnetite and polymer magnetite nanoparticles. Langmuir. 1999;15(6):1945–51.
111. Huang Z, Huang J, Chen N, Huang J. The syntheses, characterization and properties of some metallophthalocyanine complexes substituted by (N-(2-hydroxyethyl)piperazine)-N′-2-ethane sulfonic acid (HEPES). Dye Pigment. 2008;77(3):584–9.
112. Soko??owska M, Bal W. Cu(II) complexation by “non-coordinating” N-2-hydroxyethylpiperazine-N???-2-ethanesulfonic acid (HEPES buffer). J Inorg Biochem. 2005;99(8):1653–60.
113. Good NE, Winget GD, Winter W, Connolly TN, Izawa S, Sing RMM. Hydrogen ion buffers for bifological Research. Biochemistry. 1966;5(2):467–77.
114. Burgess RR. Methods in Enzymology Volume 463. Methods [Internet]. 2009;463(09):331–42. Available from: http://dx.doi.org/10.1016/S0076-6879(09)63020-2
115. Bai J, Wang T, Wang Y, Jiang X. Effects of nanoparticle surface ligands on protein adsorption and subsequent cytotoxicity. Biomater Sci [Internet]. 2014;(2). Available from: www.rsc.org/biomaterialsscience

Chapter 3

Salt selection and optimization

3.1 Introduction

Non-viral vectors have been intensively explored in the recent years due to their excellent safety features, ease of production, low cost, and unlimited carrying capacity, in contrast to the viral counterparts. Nonetheless, their lack of efficiency leads to an extensive search for alternative strategies for synthesizing novel nanoparticles that would overcome the hurdles to achieve an ideal genetic material delivery.

Inorganic nanoparticles have emerged as potential non-viral vector candidates based on numerous cellular and animal studies with the current focus being on constructing particles with biodegradable properties. The readily available inorganic nanoparticles (NP), including gold, silver and iron oxide particles are not efficiently degraded in the biological systems, in addition to extensive structural sizes due to aggregation, which is associated with low gene transportation activity into the targeted areas. Recent experimental studies have explored the potential activity of inorganic NPs of carbonate apatite (CO_3 AP) with excellent biodegradable properties and comparatively small in size (±300nm), involving modest fabrication methods. Its responsiveness to pH changes allows the transportation process with the ability to disintegrate upon exposure to the acidic environment inside the endosomal cavity. Although pH-sensitive CO_3 AP is a very efficient non-viral vector, it is still less efficient than viral vectors. Hence, it is of our interest to explore the other types of biodegradable inorganic nanoparticles with vast delivery improvement, but similarly excellent safety and productivity features of CO_3 AP.

Alkaline earth metals are often elaborated in the fields of electrical and medical industries based on their ability for controllable synthesis to form different morphological configuration with scalable production. The metals, including barium, strontium, calcium and magnesium, however, have yet to be extensively elaborated in the areas of gene delivery, hence inspiring us to design the project. The fabrication of NPs was performed based on proposed chemical reaction of two soluble components within an inert environment, also including the salts from non-metal groups comprising sulfate, sulfite, fluoride, carbonate and phosphate. Additionally, the efficient production of iron NPs for the current biomedical experimental design was also explored through analogous precipitation reaction.

In the initial stage of the project, salts were screened following fabrication of salt particles based on precipitation reactions, through microscopic observation and spectrophotometric analysis. Subsequent size and charge evaluation of the precipitated crystals was performed by Zetasizer and scanning electron microscopy (SEM), which showed various sizes and shapes of the particles formed, with variation in sizes and shapes also seen with different salts incorporated. The size characterization of salt crystals was influenced by various physical factors including pH, temperature, and time of incubation, on top of variation in concentration of soluble salts. High temperature and pH, prolonged incubation time and concentrated salts are associated with shifting of ionization equilibrium to the forward, hence generating more particles and subsequently larger forms of aggregates. Ferrous salt crystals create bigger particle sizes and increased numbers based on the qualitative and quantitative analysis, escalating at 60^{o}C, 60 minutes incubation, basic pH of 9, and 10mM salt concentration. Magnesium salts form smaller crystals numbers, with lowest values seen at the temperature of 4^{o}C, zero

incubation period, acidic pH of 4 and 2mM salt concentrations. Spectrophotometric analysis of barium and strontium salts were comparable to CO_3 AP particles, defining the probability of a similar range of particle sizes, established further through interpretation via Zetasizer. The absorbance of >0.4 is likely to have the size of more than 500nm, which may reflect in low efficiency in vitro and in vivo experimentation.

Efficiency in adsorption of negatively charged pDNA and siRNA towards fabricated NPs was >80% for most of the barium and strontium salts despite being negatively charged, owing to the proposed electrostatic interactions between the genetic materials and the cationic regions of salt particles. Barium, strontium, and magnesium salts are likely to be successful in vitro based on their ideal sizes and high binding affinity.

Attachment of ligands, e.g. fibronectin or transferrin on the surface of NPs reveals size reduction of the salt crystals with less negative charges, endorsing a potential improvement of particles in cellular internalization through active and passive targeting. Salt combinations, however, magnifies the sizes of complex particles with more negative charges. Salt combinations are unlikely to influence adjunctive effect on intracellular transfection, associated with repulsion with the negatively-charged cellular surface.

3.2 Methods and materials

3.2.1 Fabrication of NPs based on precipitation reaction

Each type of NPs was prepared by incorporating 5µl of 1M of cation-providing salts: barium chloride ($BaCl_2$) (Sigma-Aldrich, USA), strontium chloride ($SrCl_2$) (Sigma-Aldrich, USA), calcium chloride ($CaCl_2$) (Sigma-Aldrich, USA), magnesium chloride ($MgCl_2$) (Sigma Aldrich, USA) or iron (II) chloride ($FeCl_2$) (Sigma-Aldrich, USA) into 10µl HEPES-buffered media (pH adjusted to 7.5) (Sigma-Aldrich, USA) and mixing 5µl of 1M of anion-providing salts: sodium sulfate (Na_2SO_4) (Sigma-Aldrich, USA), sodium sulfite (Na_2SO_3) (Sigma-Aldrich, USA), sodium fluoride (NaF) (Sigma-Aldrich, USA), sodium carbonate (Na_2CO_3) (Sigma-Aldrich, USA) or sodium phosphate (Na_2PO_4) (Sigma-Aldrich, USA). The mixing process was followed by subsequent 30 minutes incubation at 37^{o}C and addition of FBS-supplemented DMEM media (Sigma-Aldrich, USA) to obtain the final volume of 1ml particle suspension. Absorbance at 320nm wavelength was measured for all fabricated NPs spectrophotometrically (UV 1800 Spectrophotometer, Shimadzu, Japan) upon generation of NPs, with concern to CO_3 AP. Preparation of CO_3 AP particles involves dissolving 44mM of sodium bicarbonate with DMEM powder in miliQ water, adjusted to pH 7.4 upon mixing of 5mM exogenous $CaCl_2$ to form 1ml particle suspension, at same incubation time and temperature. Following 30 minutes incubation of CO_3 AP, 10% FBS was introduced to the generated CO_3 AP particles to prevent further aggregation. Microscopic visualization and spectrophotometric analysis were acquired using the optical microscope (Olympus, Japan) and microplate reader (Biorad, USA) to visualize the presentation of particle formation.

The spectrophotometric determination was done in triplicates and plotted into a graph with mean±SD.

Salts	$BaCl_2$	$SrCl_2$	$CaCl_2$	$MgCl_2$	$FeCl_2$
Na_2SO_4	Barium sulfate ($BaSO_4$)	Strontium sulfate ($SrSO_4$)			
Na_2SO_3	Barium sulfite ($BaSO_3$)	Strontium sulfite ($SrSO_3$)	Calcium sulfite ($CaSO_3$)	Magnesium sufite ($MgSO_3$)	Ferrous sulfite ($FeSO_3$)
NaF	Barium fluoride (BaF_2)	Strontium fluoride (SrF_2)	Calcium fluoride (CaF_2)	Magnesium fluoride (MgF_2)	
Na_2CO_3	Barium carbonate ($BaCO_3$)	Strontium carbonate ($SrCO_3$)	Calcium carbonate ($CaCO_3$)	Magnesium carbonate ($MgCO_3$)	Ferrous carbonate ($FeCO_3$)
Na_3PO_4	Barium phosphate ($Ba_3(PO_4)_2$)	Strontium phosphate ($Sr_3PO_4)_2$)	Calcium phosphate ($Ca_3PO_4)_2$)	Magnesium phosphate ($Mg_3PO_4)_2$)	Ferrous phosphate ($Fe_3PO_4)_2$)

Table 3.1: Inorganic salt crystals generated from proposed precipitation reaction. The mixing of soluble salts was performed in HEPES-buffered media, projecting various types of precipitates.

3.2.2 Assessment of NPs growth via spectrophotometric analysis

Manipulation of concentration of reacting salts on NP generation effect was performed through addition of $BaCl_2$, $SrCl_2$, $CaCl_2$, $MgCl_2$ or $FeCl_2$ ranging from 2µl to 10µl of 1M into HEPES media with subsequent mixing of fixed 5µl of 1M Na_2SO_4, Na_2SO_3, NaF, Na_2CO_3 or Na_2PO_4. Consequently, the experiment on particle growth involving fixed 5µl of 1M $BaCl_2$, $SrCl_2$, $CaCl_2$, $MgCl_2$ or $FeCl_2$ versus 2µl to 10µl of 1M Na_2SO_4, Na_2SO_3, NaF, Na_2CO_3 or Na_2PO_4, was executed prior to incubation for 30 minutes at 37°C.

Time-dependent analysis was performed by addition of 5µl of 1M $BaCl_2$, $SrCl_2$, $CaCl_2$, $MgCl_2$ or $FeCl_2$ to 10µl HEPES-buffered media (pH 7.5) and mixing with 2µl of 1M Na_2SO_4, Na_2SO_3, NaF, Na_2CO_3 or Na_2PO_4, followed incubation at 37°C for 0, 30, and 60 minutes and subsequent mixing of serum-supplemented DMEM. pH-dependent experiment was initiated by preparation of HEPES-buffered media with various pHs of 4, 5, 6, 7, 8 and 9 upon introduction of 5µl of 1M $BaCl_2$, $SrCl_2$, $CaCl_2$, $MgCl_2$ or $FeCl_2$ and 2µl of 1M Na_2SO_4, Na_2SO_3, NaF, Na_2CO_3 or Na_2PO_4, and incubation at 37°C for 30 minutes. Experimental studies on the influence of temperature changes involve incubation of generated salt crystals at various temperatures, 4°C, 37°C and 70°C following mixing of 5µl of 1M $BaCl_2$, $SrCl_2$, $CaCl_2$, $MgCl_2$ or $FeCl_2$ and 2µl of 1M Na_2SO_4, Na_2SO_3, NaF, Na_2CO_3 or Na_2PO_4, at fixed pH and incubation time. CO_3 AP was included individually in each experiment as a positive control. Experimental studies were completed in triplicates and analysis was carried out as graphs with mean±SD.

3.2.3 Size estimation and zeta potential measurement of NPs

Size and zeta potential measurement of fabricated NPs utilizing Zeta Sizer (Malvern, Nano ZS, UK) were executed following 30 minutes incubation to form the crystal precipitates. A preliminary study involving the formation of NPs was performed by mixing of 5µl of 1M $BaCl_2$, $SrCl_2$, $CaCl_2$, $MgCl_2$ or $FeCl_2$ and 2µl to 10µl of 1M Na_2SO_4, Na_2SO_3, NaF, Na_2CO_3 or Na_2PO_4 in HEPES media, followed by incubation at 37°C for 30 minutes. The generated salt crystals were maintained on ice prior to observation under Zetasizer. A refractive index (RI) ratio of 1.325 (measured in DMEM media by refractometer) was used to calculate particle sizes and zeta potential. Analysis of data was done using Zetasizer software 6.20 and all salt samples were

measured in duplicate and shown as mean±SD. The size and morphology of selected nanocrystal samples were visualized through Field Emission scanning electron microscopic (Hitachi S-4700 FE-SEM, Japan) observation. NPs were centrifuged at 15,000 RPM for 10 seconds, followed by removal of supernatant and resuspension with milli-Q water. Salt particle suspensions were maintained under ice before microscopic observation. 1µl of each sample was placed onto carbon tape on the sample holder to dry (at room temperature), followed by platinum sputtering of the dried samples for 30 seconds. Microscopic observation of sputtered NPs was done using FE-SEM, with optimal image achieved at 10-15kV.

3.2.4 Binding affinity of pDNA and siRNA towards NPs

A study involving binding affinity of genetic materials, pDNA and siRNA towards NPs includes qualitative and quantitative measurement of fluorescence-labeled pDNA and siRNA. 1µg pGFP, green fluorescence protein pDNA was labeled non-covalently with propidium iodide (PI) at 1:1 ratio, added to 5µl of 1M $BaCl_2$, $SrCl_2$, $CaCl_2$, $MgCl_2$ or $FeCl_2$, followed by incorporation of 2µl of 1M Na_2SO_4, Na_2SO_3, NaF, Na_2CO_3 or Na_2PO_4 in 10µl HEPES-buffered media to generate respective salt precipitates. The chemical reactions were maintained at 37^oC for 30 minutes, followed by mixing of DMEM media to form the final volume of 1ml salt suspension. CO_3 AP was kept as the positive control for the study, incorporating pGFP: PI of the similar ratio. Microscopic visualization was achieved by the addition of fabricated salt crystals to 24-well plate (Nunc, Denmark), and observed under fluorescence microscope (Olympus, Japan) through PI filter. Quantitative measurement of NPs-bound pDNA involved multi-label plate reading of supernatant representing the bound fraction of

DNA (Victor X5, Perkin Elmer) following centrifugation of fabricated NPs at 15,000 RPM for 5 minutes. The 100µl supernatant was aspirated and transferred into 96-well plate (Nunc, Denmark), prior to fluorescence intensity measurement. 1µg/ml ethidium bromide, EtBr (Sigma-Aldrich, USA) was added in 100µl to each well of pDNA loaded with differentially formulated particle preparation medium. Experiments involving binding affinity of siRNA-NPs were established throughout introduction of 100nM AF 488 negative siRNA (fluorescence siRNA, Qiagen, Germany) into 5µl of 1M $BaCl_2$, $SrCl_2$, $CaCl_2$, $MgCl_2$ or $FeCl_2$ upon mixing of 2µl of 1M Na_2SO_4, Na_2SO_3, NaF, Na_2CO_3 or Na_2PO_4 in 10µl HEPES-buffered media with same incubation time and temperature. Each experiment was done in triplicates and analyzed with mean±SD.

3.2.5 Influence of ligand coating on morphology and size of NPs

The impact of ligand coating on structural changes of selected NPs was demonstrated by glazing fibronectin protein (rat plasma, Sigma-Aldrich, USA) onto the fabricated particles. 1µg fibronectin was introduced after mixing 5µl of 1M $BaCl_2$, $SrCl_2$ or $MgCl_2$ with 2µl of 1M Na_2SO_4, Na_2SO_3 and NaF in 10µl HEPES-buffered media before additional 10 minutes incubation to coat the NPs, followed by the brief mixture of DMEM media to form the final volume of 1ml suspension (Table 3.2). The analysis was performed through size measurement and zeta potential using Zeta Sizer. Electron microscopic visualization through FE-SEM was conducted on selected NPs after centrifugation of the particles solution at 15,000 RPM for 5 minutes and upon resuspension of supernatant to 1ml of miliQ water. Resuspended particles were kept on ice prior to microscopic observation at 10-15kV to prevent further formation aggregation.

Salt	Regimen for analysis
$BaSO_3$	5µl of 1M $BaCl_2$, 2µl of 1M Na_2SO_3, in 10µl HEPES media, followed by addition of DMEM to achieve 1ml
	5µl of 1M $BaCl_2$, 2µl of 1M Na_2SO_3, in 10µl HEPES media, followed by 1µg fibronectin and addition of DMEM to achieve 1ml
	5µl of 1M $BaCl_2$, 2µl of 1M Na_2SO_3, in 10µl HEPES media, followed by 1µg transferrin and addition of DMEM to achieve 1ml
BaF_2	5µl of 1M $BaCl_2$, 2µl of 1M NaF, in 10µl HEPES media, followed by addition of DMEM to achieve 1ml
	5µl of 1M $BaCl_2$, 2µl of 1M NaF, in 10µl HEPES media, followed by 1µg fibronectin and addition of DMEM to achieve 1ml
	5µl of 1M $BaCl_2$, 2µl of 1M NaF, in 10µl HEPES media, followed by 1µg transferrin and addition of DMEM to achieve 1ml
$SrSO_4$	5µl of 1M $SrCl_2$, 2µl of 1M Na_2SO_4, in 10µl HEPES media, followed by addition of DMEM to achieve 1ml
	5µl of 1M $SrCl_2$, 2µl of 1M Na_2SO_4, in 10µl HEPES media, followed by 1µg fibronectin and addition of DMEM to achieve 1ml
	5mM $SrCl_2$, 2µl of 1M Na_2SO_4, in 10µl HEPES media, followed by 1µg transferrin and addition of DMEM to achieve 1ml
$SrSO_3$	5µl of 1M $SrCl_2$, 2µl of 1M Na_2SO_3, in 10µl HEPES media, followed by addition of DMEM to achieve 1ml
	5mM $SrCl_2$, 2µl of 1M Na_2SO_3, in 10µl HEPES media, followed by 1µg fibronectin and addition of DMEM to achieve 1ml
	5µl of 1M $SrCl_2$, 2µl of 1M Na_2SO_3, in 10µl HEPES media, followed by 1µg transferrin and addition of DMEM to achieve 1ml
SrF_2	5µl of 1M $SrCl_2$, 2µl of 1M NaF, in 10µl HEPES media, followed by addition of DMEM to achieve 1ml
	5µl of 1M $SrCl_2$, 2µl of 1M NaF, in 10µl HEPES media, followed by 1µg fibronectin and addition of DMEM to achieve 1ml
	5µl of 1M $SrCl_2$, 2µl of 1M NaF, in 10µl HEPES media, followed by 1µg transferrin and addition of DMEM to achieve 1ml
$MgSO_3$	5µl of 1M $MgCl_2$, 2µl of 1M Na_2SO_3, in 10µl HEPES media, followed by addition of DMEM to achieve 1ml
	5µl of 1M $MgCl_2$, 2µl of 1M Na_2SO_3 in 10µl HEPES media, followed by 1µg fibronectin and addition of DMEM to achieve 1ml
	5µl of 1M $MgCl_2$, 2µl of 1M Na_2SO_3, in 10µl HEPES media, followed by 1µg transferrin and addition of DMEM to achieve 1ml
CO_3 AP	44mM Na_2CO_3, 5mM $CaCl_2$, added to DMEM media, final volume of 1ml
	44mM Na_2CO_3, 5mM $CaCl_2$, added to DMEM media, followed by 1µg fibronectin, final volume of 1ml
	44mM Na_2CO_3, 5mM $CaCl_2$, added to DMEM media, followed by 1µg transferrin, final volume of 1ml

Table 3.2: Generation of ligand-coated NPs via transferrin or fibronectin

3.2.6 Effect of salt combination on morphology and size of NPs

Manipulation of the NPs exploiting combination of two inorganic salts was performed by allowing the mixing of two individual salt crystals, to carry out quantitative experimental studies of salt combinations. Two selected insoluble salts individually formulated (Table 3.3), were mixed in HEPES-buffered media, before additional incubation at 37°C for 30 minutes. DMEM medium was subsequently introduced into the particles to form the final volume of 1ml suspension, with analysis performed to obtain size estimation and zeta charge of the hybridized particles.

Group	Combination regimen
$BaSO_3$+ $SrSO_3$	[5µl of 1M $BaCl_2$ + 2µl of 1M Na_2SO_3 and 5µl of 1M $SrCl_2$ + 2µl of 1M of Na_2SO_3] in 10µl HEPES buffered media, with the final volume of DMEM adjusted to 1ml
$SrSO_3$ + SrF_2	[5µl of 1M $SrCl_2$+ 2µl of 1M of Na_2SO_3 and 5µl of 1M $SrCl_2$ + 2µl of 1M NaF] in 10µl HEPES buffered media, with the final volume of DMEM adjusted to 1ml
$SrSO_3$ + $MgSO_3$	[5µl of 1M $SrCl_2$ + 2µl of 1M Na_2SO_3 and 5µl of 1M $MgCl_2$ + 2µl of 1M Na_2SO_3] in 10µl HEPES buffered media, with the final volume of DMEM adjusted to 1ml
SrF_2 + BaF_2	[5µl of 1M $SrCl_2$ + 2µl of 1M NaF and 5µl of 1M $BaCl_2$ + 2µl of 1M NaF] in 10µl HEPES buffered media, with the final volume of DMEM adjusted to 1ml
$BaSO_3$ + $MgSO_3$	[5µl of 1M $BaCl_2$ + 2µl of 1M Na_2SO_3 and 5µl of 1M $MgCl_2$ + 2µl of 1M Na_2SO_3] in 10µl HEPES buffered media, with the final volume of DMEM adjusted to 1ml

Table 3.3: Combination salt regimen through mixing of two salt precipitates. Mixing of two insoluble salts was performed following 30 minutes incubation, and the mixture was further incubated for 10 minutes upon addition of DMEM medium.

Visional observation of above salt combination in comparison with single salts crystals using FE-SEM was also made following resuspension of salts with 1ml miliQ water after centrifugation at 15,000 RPM for 5 minutes, and maintained at 4^{o}C.

3.3 Results

3.3.1 Fabrication of NPs based on precipitation reactions

Experimental studies on the fabrication of NPs were performed to observe the formation of salt particles. Spectrophotometric measurement demonstrated absorbance ranging from 0.3 to 2.1 at 320nm wavelength upon generation of salt precipitates (Figure 3.1). High absorbance intensity was observed for fabricated ferrous crystals, with the highest value seen with $FeSO_3$ and $Fe_3(PO_4)_2$ salt particles upon 30 minutes incubation. Barium salts are also associated with high absorbance volume, varying from 0.5 to 1.0, followed by strontium salts at the range of 0.4 to 0.8. Small crystals sizes were seen with $CaCO_3$ and MgF_2, comparable to those of CO_3 AP, showing the absorbance of approximately 0.3. Calcium and magnesium salts showed low overall intensity, with detection ranges from 0.3 to 0.6. Na_2SO_4 and Na_2PO_4 are similar with respect to larger particle sizes and number, referring to high absorbance data in comparison with other anion-providing salts. Based on the figure, NaF and Na_2CO_3 are linked with the modest formation of particles. CO_3 AP particles are more likely to be smaller in particle numbers and sizes, determined by lower absorbance intensity at the similar wavelength in comparison to other generated salts crystals.

Visualization of each type of fabricated NPs was determined using optical microscope, revealing the generation of salt particles varying in size and numbers (Figure 3.2). Microscopic observation of all NPs represents similarities with spectrophotometric evaluation at 320nm of earlier experiments. Barium and strontium salt crystals are associated with an immense number of particles. Generated ferrous salts demonstrated enormous particle sizes up to 10µm. Comparative studies on size and number estimation of NPs further showed that the particles incorporated with calcium and magnesium salts were generally smaller in sizes and fewer in numbers, as similarly interpreted by spectrophotometric analysis. Concentrated salt particles visualized under the images also established the involvement of Na_2SO_4 and Na_2PO_4 in leading to the high number and sizes of particles formed.

The actual sizes of each particle were determined in the subsequent experiment involving Zeta Sizer.

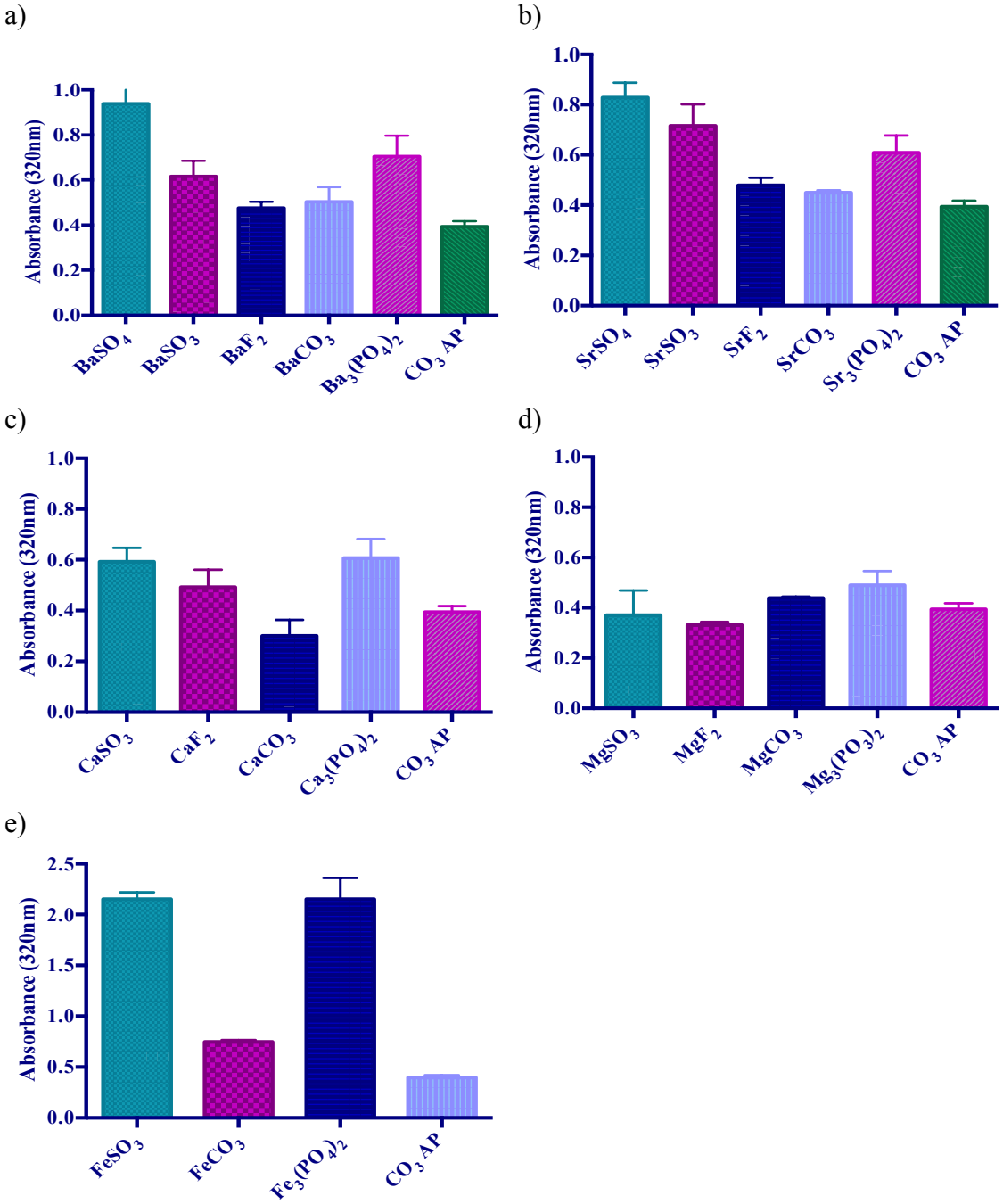

Figure 3.1: Absorbance intensity of NPs formed by precipitation reaction. Addition of 5µl of 1M (a) $BaCl_2$, (b) $SrCl_2$, (c) $CaCl_2$, (d) $MgCl_2$) or (e) $FeCl_2$ into 10µl HEPES buffered media (pH adjusted to 7.5) followed by mixing of 5µl of 1M Na_2SO_4, Na_2SO_3, NaF, Na_2CO_3 or Na_3PO_4, generated various salt crystals upon 30 minutes incubation at 37°C. Subsequently, serum-supplemented DMEM media was added to achieve 1ml particle suspension. Absorbance at 320nm wavelength was measured for all fabricated NPs using spectrophotometer with reference to CO_3 AP.

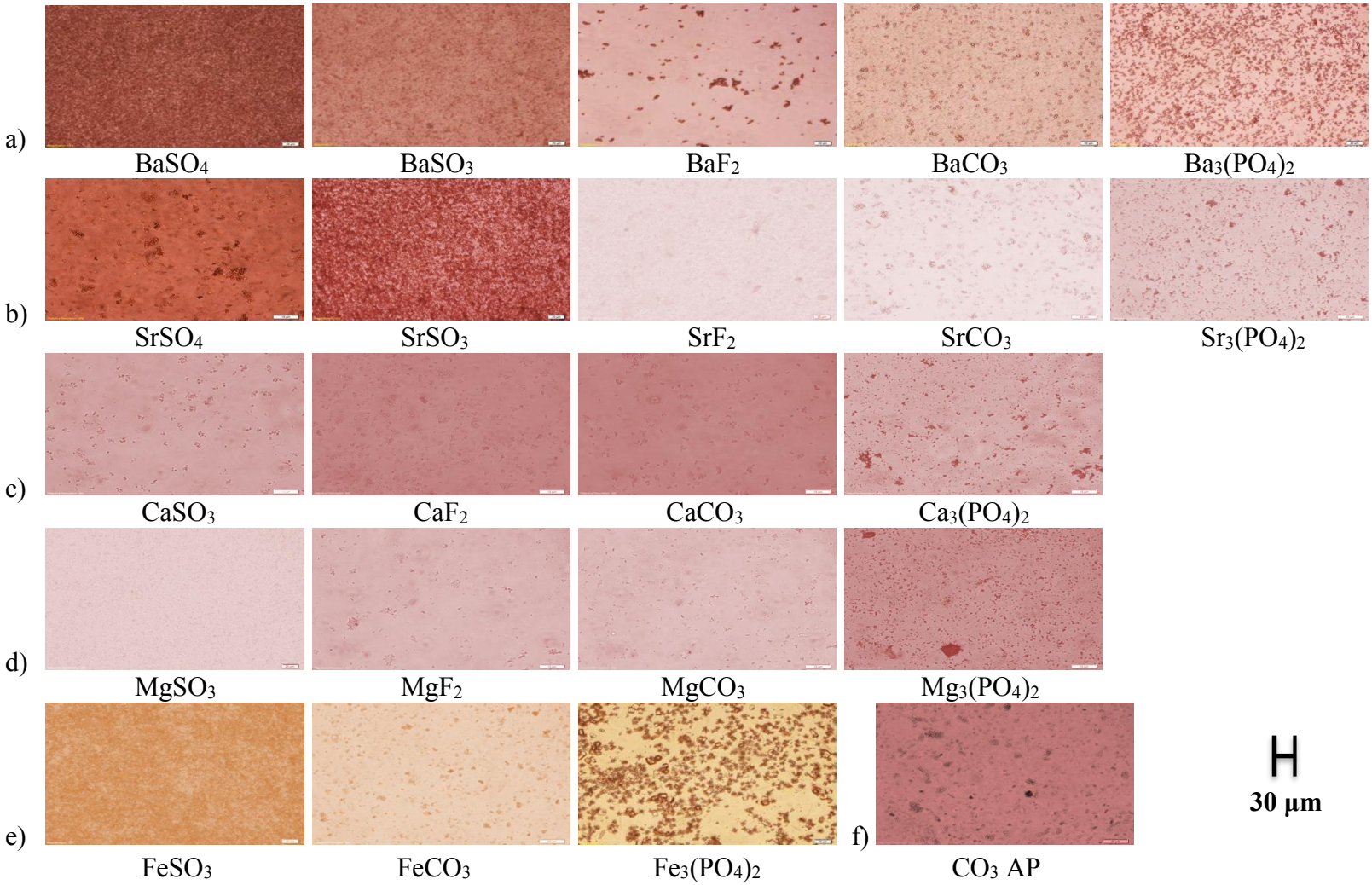

Figure 3.2: Microscopic observation of NPs formed by precipitation reaction. 5µl of 1M (a) $BaCl_2$, (b) $SrCl_2$, (c) $CaCl_2$, (d) $MgCl_2$) or (e) $FeCl_2$ was introduced into 10µl HEPES buffered media, followed by mixing of 5µl of 1M Na_2SO_4, Na_2SO_3, NaF, Na_2CO_3 or Na_3PO_4, generating various salt crystals upon 30 minutes incubation at 37°C. Subsequently, FBS-containing DMEM media was added to achieve 1ml particle suspension. Image was captured at 10X resolution, with reference to (f) CO_3 AP.

3.3.2 Assessment of NPs growth via spectrophotometric analyses

Concentration-dependent analysis was initially performed following adjustment of $BaCl_2$, $SrCl_2$, $CaCl_2$, $MgCl_2$ or $FeCl_2$ concentration from 2µl to 10µl of 1M with fixed 5µl of 1M of anion-providing salts consisted of Na_2SO_4, NA_2SO_3, NaF, Na_2CO_3 or Na_2PO_4 within HEPES-buffered media (pH 7.5), prior to incubation for 30 minutes at 37^oC and addition of DMEM medium to achieve final volume of 1ml suspension. Determination of absorbance intensity was performed at 320nm wavelength. At 2mM, relative absorbance values amongst all NPs studied showed low intensity, specifically with salts containing fluoride and carbonate ions. Superior intensity was seen with a gradual escalation in salt concentration, particularly at 10mM, reaching a maximum level of 2.4 with Fe_2SO_3 and $Fe_3(PO_4)_2$ salts. Higher cation-providing salt concentrations induced greater particle sizes and numbers, especially with barium and strontium salts.

The second phase of the concentration-dependent study was to investigate the influence of anion-providing salt concentration on NPs formation, which was also determined spectrophotometrically. Similarly, the absorbance intensity was augmented as the concentration of Na_2SO_4, Na_2SO_3, NaF, Na_2CO_3 or Na_2PO_4 was increased, as seen in Figure 3.3. At 10mM, absorbance intensity was generally more than 0.5, with exception to magnesium NPs, with an average of 0.3. High cation-providing salt concentration escalated absorbance level especially with Na_2SO_3 salts, in comparison with other anion-providing salts. Comparative studies with CO_3 AP revealed that 2mM of anion-providing salt concentrations mimicked the absorbance data articulated by the CO_3 AP particles with no adjustment on CO_3 AP-forming salt concentration.

To obtain the ideal absorbance ranging from 0.3 to 0.4, in reference to CO_3 AP, the optimal concentration for cation-providing salts ranges from 2 to 5mM. Large salt sizes and numbers were seen with ferrous NPs, with Fe_2SO_3 and $Fe_3(PO_4)_2$ giving intensities of more than 2.0 from 2mM onwards. Incorporation of Na_2SO_4 and Na_2SO_3 into the particle structures was associated with greater absorbance intensity, particularly with ferrous, strontium and barium salts.

Based on both experimental designs determining the ideal concentrations of both cation- and anion-providing salts, it is projected that the ranges of salts concentrations should be of 2 to 5mM. However, we have proposed to maximize the cation-providing salt concentration for subsequent experiments to increase the probability for more electrostatic interactions between the negatively charged pDNA and siRNA. Additionally, anion-providing salts will remain at the minimal concentration of 2mM to maintain the overall crystals sizes of <500nm.

Spectrophotometric reading of NPs suspension was done to assess their growth in the different arrangement of external variations to optimize the formation of salt particles. The time-dependent analysis was initially executed through maneuvering of crystal's incubation time, with fixed salt concentration and pH condition. Following mixing of 2 soluble salts, various incubation intervals were introduced, from 4 to 60 minutes upon absorbance measurement at 320nm wavelength. Based on Figure 3.5, each salt demonstrated higher absorbance intensity with increasing of incubation interval. Low crystals formation was seen at 4 minutes, portrayed by low absorbance reading. As incubation time was extended, the level was intensified for all 21 salts.

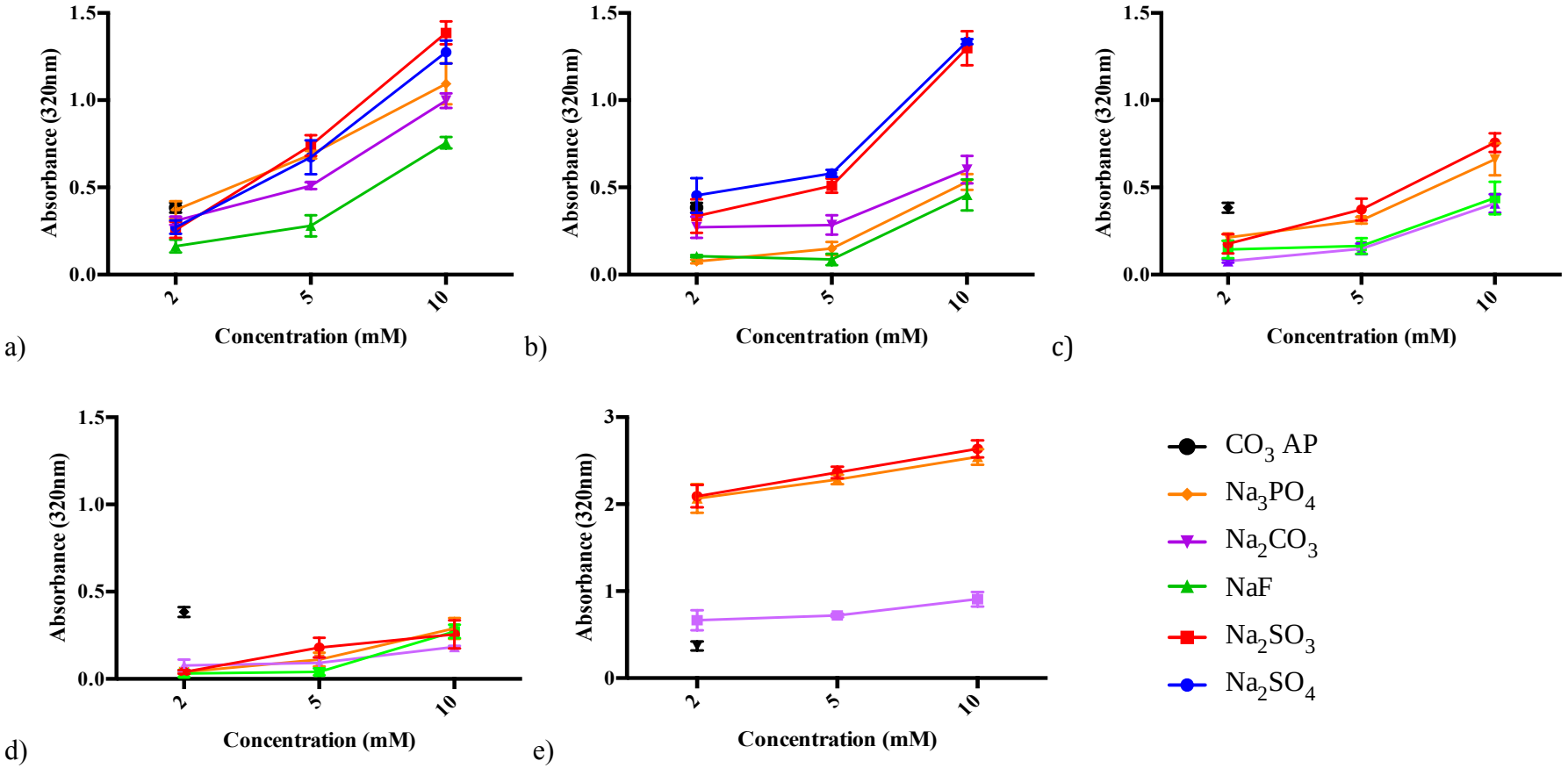

Figure 3.3: Effect of cation-providing salt concentration on NPs formations. Various concentrations of (a) $BaCl_2$, (b) $SrCl_2$, (c) $CaCl_2$, (d) $MgCl_2$) or (e) $FeCl_2$ was introduced (2µl, 5µl and 10µl of 1M) into 10µl HEPES buffered media (pH 7.5), followed by mixing of 5µl of 1M Na_2SO_4, Na_2SO_3, NaF, Na_2CO_3 or Na_3PO_4, generating various salt particles upon 30 minutes incubation at 37°C. Subsequently, FBS containing-DMEM media was added to achieve final volume of 1ml particle suspension. Absorbance at 320nm wavelength was obtained using spectrophotometer with reference to CO_3 AP.

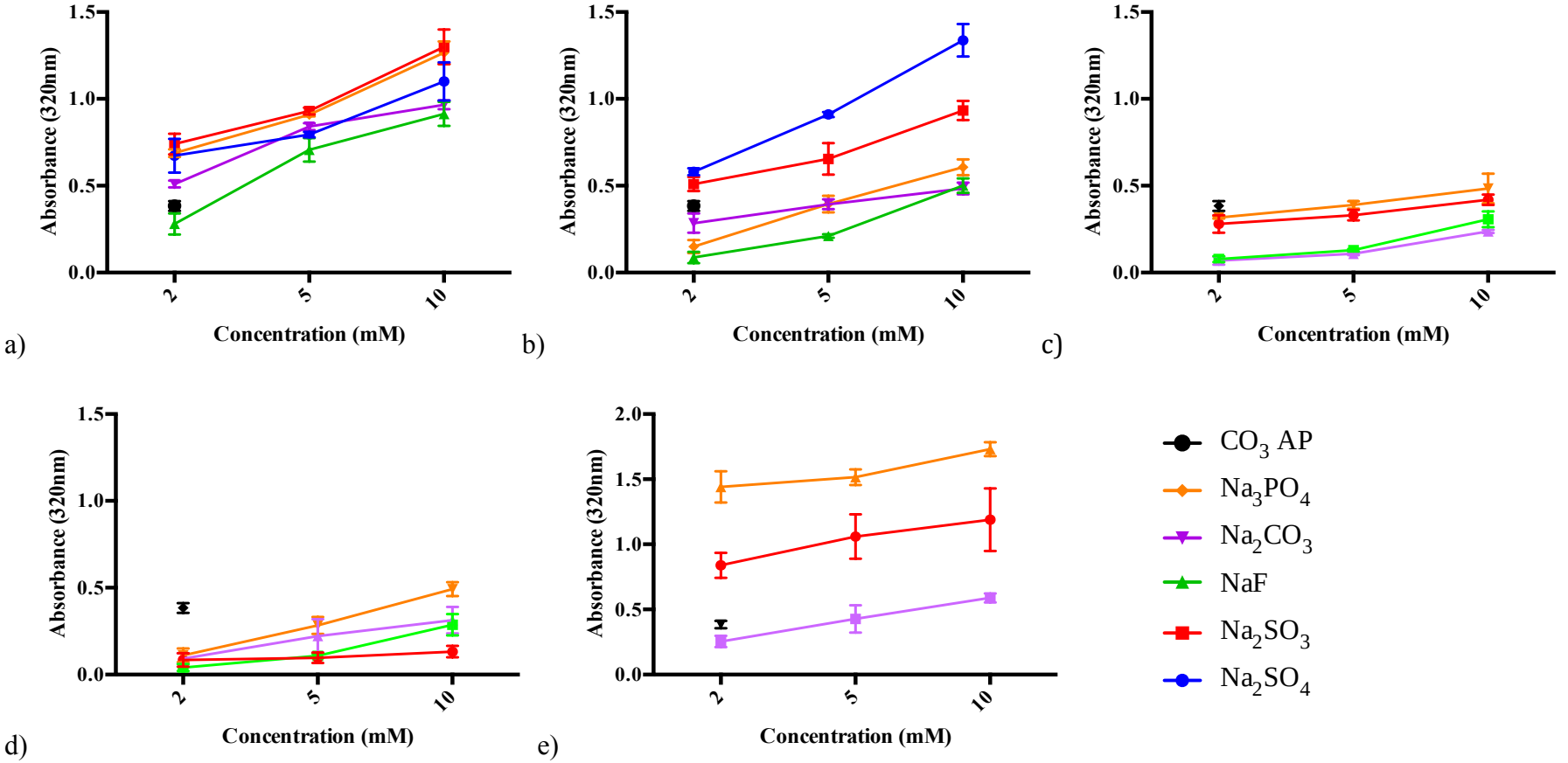

Figure 3.4: Effect of anion-providing salt concentration on NPs formations. 5µl of 1M (a) $BaCl_2$, (b) $SrCl_2$, (c) $CaCl_2$, (d) $MgCl_2$) or (e) $FeCl_2$ was introduced into 10µl HEPES buffered media (pH adjusted to 7.5), followed by mixing of different concentration of Na_2SO_4, NA_2SO_3, NaF, Na_2CO_3 or Na_3PO_4 (2µl, 5µl and 10µl of 1M), generating various salt particles upon 30 minutes incubation at 37ºC. Subsequently, FBS containing-DMEM media was added to achieve final volume of 1ml particle suspension. Absorbance at 320nm was measured for all fabricated NPs using spectrophotometer with reference to CO_3 AP.

Salt fabricated via 30 minutes incubation is emitted absorbance of <0.5, similarly achieved with CO_3 AP, with exception of salts containing sulfate and phosphate ions. Upon 60 minute incubation, superior absorbance level was seen for all the salts tested especially with ferrous and barium salts, of intensity up to 2.5.

Evaluation of pH-dependent analysis was executed through manipulation of HEPES pH upon incorporation of two soluble salts, with fixed incubation time and temperature (30 minutes, 37^{o}C). Acidic pH resulted in overall lower particle number and smaller size reflected by low absorbance level (Figure 3.6). As pH was gradually increased, the absorbance level of NPs intensified almost 3-fold higher than the lowest pH tested, with intensity up to 2.9 demonstrated with $FeSO_3$. Fluoride-based NPs exhibited minimum increment at 320nm wavelength, in comparison with other crystals. At pH 7.5, the absorbance intensity of salt crystals was >0.5, with exception to salts containing sulfate and sulfite, exposing higher intensity upon 30 minutes of incubation.

The importance of temperature on NPs generation was determined through modification of incubation temperature from 4^{o}C to 60^{o}C. Each type of generated salts showed intensified absorbance at 60^{o}C, especially with ferrous salts having the absorbance ranging from 1 to 4, signifying massive particle numbers and sizes, as seen in Figure 3.7. At 4^{o}C, the absorbance of each salt valued at approximately 0.2, except ferrous salts. The fabricated salts presented minimum 3-fold more increment from at 60^{o}C than at 4^{o}C, with 7-times growth anticipated with $BaSO_3$, representing a maximum increase by temperature adjustment. At 37^{o}C, most salts revealed absorbance intensity of <0.5, with exception to sulfate and sulfite-containing salts.

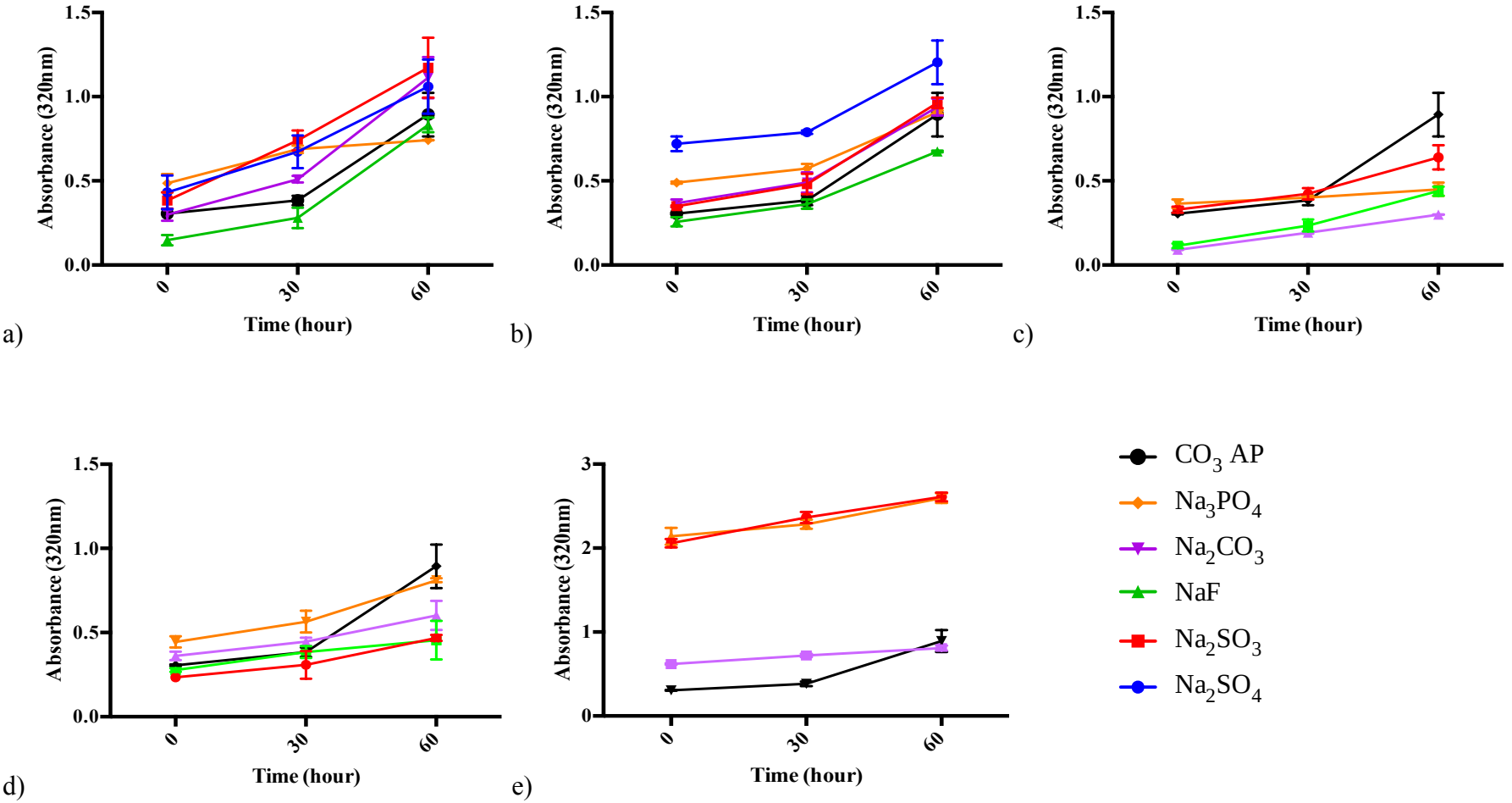

Figure 3.5: Effect of incubation time on NPs formations. 5µl of 1M (a) $BaCl_2$, (b) $SrCl_2$, (c) $CaCl_2$, (d) $MgCl_2$) or (e) $FeCl_2$ was introduced into 10µl HEPES buffered media (pH 7.5), followed by mixing of 2µl of 1M Na_2SO_4, Na_2SO_3, NaF, Na_2CO_3 or Na_3PO_4, generating various salt crystals upon incubation at 37ºC at varying time points (0, 30 and 60 minutes). Subsequently, FBS containing-DMEM media was added to achieve final volume of 1ml particle suspension. Absorbance at 320nm was measured for all fabricated NPs, with reference to CO_3 AP.

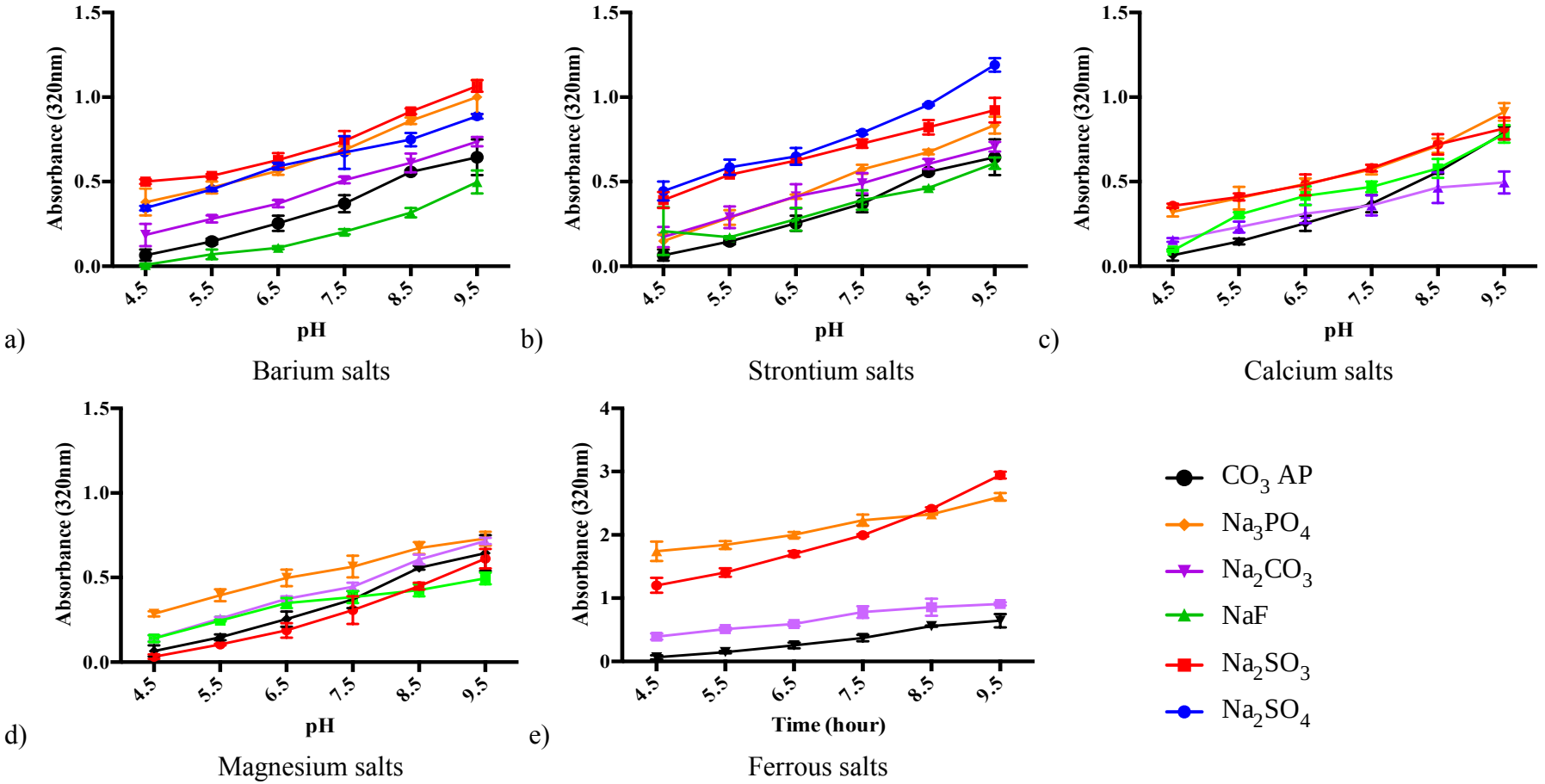

Figure 3.6: Effect of pH adjustment on NPs formations. 5µl of 1M (a) $BaCl_2$, (b) $SrCl_2$, (c) $CaCl_2$, (d) $MgCl_2$) or (e) $FeCl_2$ was introduced into 10µl HEPES buffered media (pH ranging from 4.5-9.5), followed by mixing of 2µl of 1M Na_2SO_4, Na_2SO_3, NaF, Na_2CO_3 or Na_3PO_4, generating various salt crystals upon 30 minutes incubation at 37°C. Subsequently, serum containing-DMEM media was added to achieve final volume of 1ml particle suspension. Absorbance at 320nm was measured for all fabricated NPs, with reference to CO_3 AP.

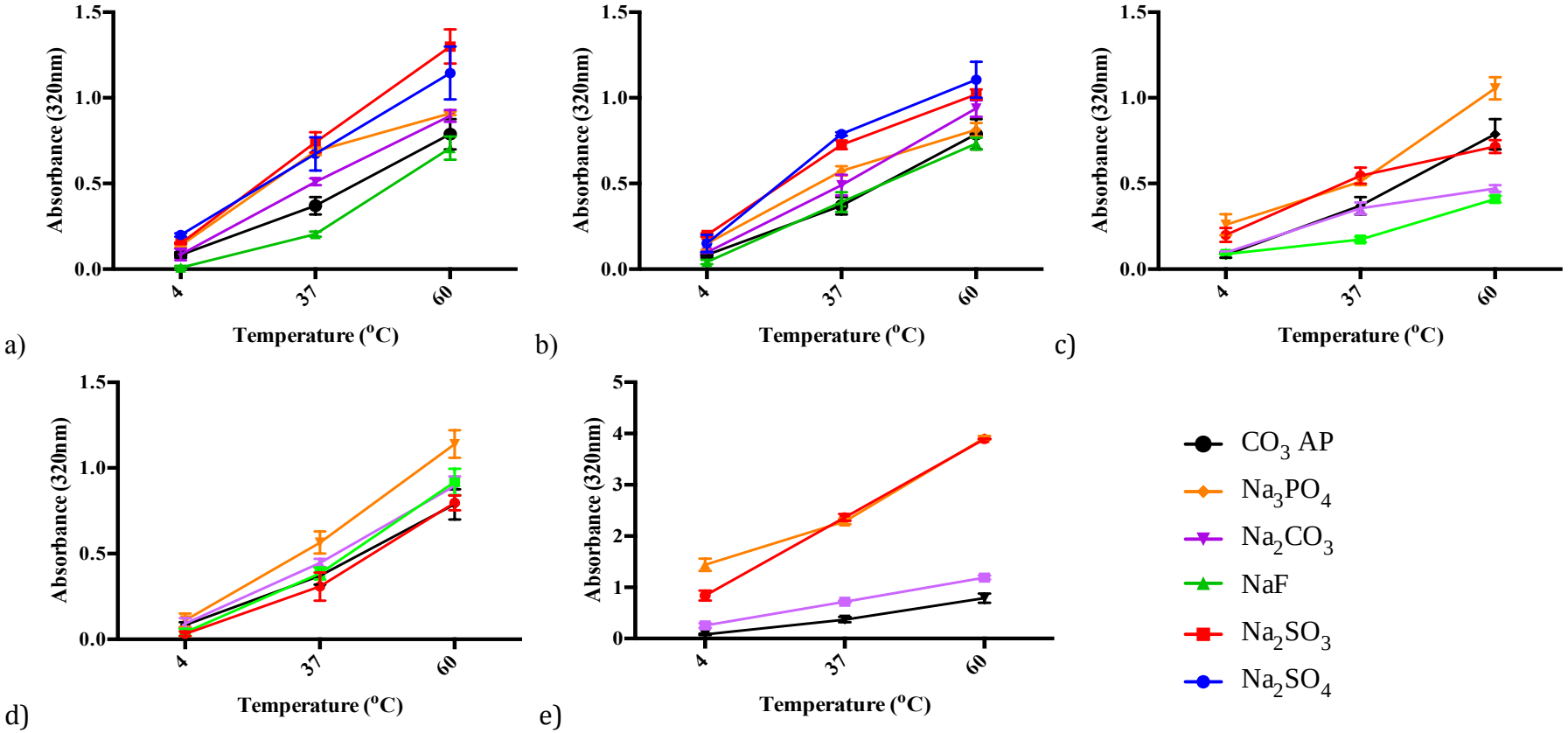

Figure 3.7: Effect of incubation temperature on NPs formations. 5µl of 1M (a) $BaCl_2$, (b) $SrCl_2$, (c) $CaCl_2$, (d) $MgCl_2$) or (e) $FeCl_2$ was introduced into 10µl HEPES buffered media (pH 7.5), followed by mixing of 2µl of 1M Na_2SO_4, Na_2SO_3, NaF, Na_2CO_3 or Na_3PO_4, generating various salt crystals upon 30 minutes incubation at 37°C. Subsequently, FBS containing-DMEM media was added to achieve final volume of 1ml particle suspension. Absorbance at 320nm was measured for all fabricated NPs, with reference to CO_3 AP.

Similarly, CO_3 AP demonstrated higher particle size and number, represented by greater absorbance level with a gradual rise in temperature. The overall modification of pH, temperature, and time analysis enables us to summarize the ideal conditions for subsequent experiments: 37^{o}C for 60 minutes incubation with the pH adjusted to 7.5 and 37^{o}C.

3.3.3 Size estimation and zeta potential measurement of NPs

Determination of average size of each type of NPs was accomplished by introduction of two soluble salts in HEPES media with subsequent incubation for 30 minutes (as performed earlier), followed by particle size and zeta potential characterization via Zeta Sizer system. Salts forming cationic regions of the inorganic compounds; $BaCl_2$, $SrCl_2$, $CaCl_2$, $MgCl_2$ or $FeCl_2$ were fixed at 5µl of 1M, with the intention to observe particle size changes with manipulation of concentrations of anion-providing salts, Na_2SO_4, NA_2SO_3, NaF, Na_2CO_3 or Na_2PO_4, at 2µl and 10µl of 1M, prior to incubation period to generate the desired crystals.

The average size of NPs increased with greater concentration, predominantly noticed with Na_2SO_3. Fluoride salt crystals are associated with smaller salt size, ranging from 7 to 128nm at 2mM and 36 to 491 at 10mM. It was revealed that ferrous and barium NPs groups formed largest structural salts in comparison to others, with dramatical increase upon exposure to greater concentration of anion-providing soluble salts. At 2mM, $BaSO_4$ generated largest diameter of 734nm upon incubation, with size increment of almost three-fold at 10mM. Fabrication of magnesium salts is associated with smaller size, with <100nm at anion-providing salts concentration of 10mM.

Salt Formulation	Concentration of anion-providing salt	Size (d.nm)	Zeta (mV)
$BaSO_4$	2mM	734±41	-8
	10mM	1974±32	-10
$BaSO_3$	2mM	506±19	-11
	10mM	1418±33	-20
BaF_2	2mM	218±29	-6
	10mM	345±28	-15
$BaCO_3$	2mM	243±18	-12
	10mM	315±52	-16
$Ba_3(PO_4)_2$	2mM	345±61	-15
	10mM	344±49	-16
$SrSO_4$	2mM	721±34	-8
	10mM	1455±201	-9
$SrSO_3$	2mM	471±38	-7
	10mM	1586±72	-11
SrF_2	2mM	106±20	-8
	10mM	491±35	-9
$SrCO_3$	2mM	142±30	-6
	10mM	301±27	-7
$Sr_3(PO_4)_2$	2mM	129±39	-7
	10mM	190±31	-8
$CaSO_3$	2mM	15±0.4	-6
	10mM	131±44	-8
CaF_2	2mM	6±0.3	-8
	10mM	129±18	-10
$CaCO_3$	2mM	22±11	-9
	10mM	127±21	-18
$Ca_3(PO_4)_2$	2mM	20±4	-10
	10mM	200±19	-12
$MgSO_3$	2mM	98±13	-7
	10mM	178±31	-8
MgF_2	2mM	7±0.4	-7
	10mM	36±1.9	-7
$MgCO_3$	2mM	5±3.5	-7
	10mM	15±2.3	-9
$Mg_3(PO_4)_2$	2mM	6±1.1	-8
	10mM	40±4	-8
$FeSO_3$	2mM	532±82	-10
	10mM	1232±321	-10
$FeCO_3$	2mM	470±55	-11
	10mM	1572±61	-12
$Fe_3(PO_4)_2$	2mM	313±19	-10
	10mM	1008±210	-12
CO_3 AP	-	321±51	-10

Table 3.4: Particle size and zeta potential of NPs. Fabricated particles were analyzed using Zetasizer to obtain average size and charge of each type of crystals, with reference to CO_3 AP.

At the initial concentration of 2mM, calcium salt also revealed small crystal structures, ranging from 6 to 22nm. Through further increment in concentration, size was increased dramatically to almost ten-fold, with regards to $Ca_3(PO_4)_2$. CO_3 AP as control revealed similarity in size while comparing with sizes of most of the salts at 2mM concentration, with 10mM associated with much greater size. Concurrent Zeta Sizer measurement showed zeta potential of the NPs, with average negative charges. Earlier size characteristic studies showed no correlation with the zeta potential of the NPs. The charge potential demonstrated more negative domains for barium salts particles with increasing in concentration, showing -20mV at 10mM of Na_2SO_3 salts. However, the trend was not equivalent to other NPs, as minute changes in zeta activity observed at higher salt concentration.

FE-SEM images were acquired to assess the morphological features of selected salt crystals. Formation of NPs is associated with the generation of sphere-shaped particles, varying in sizes with the size distribution comparable to that measured by Zeta Sizer. The particles are mostly in aggregated form, possibly due to centrifugation phase to remove the soluble salts. $Fe_3(SO_4)_2$ particles demonstrated large particles size of 3µm, followed by barium salts with sizes ranging from 260nm to 650nm. 90nm of salt diameter was revealed with $MgSO_3$, concurring the small salt size earlier demonstrated with Zeta Sizer. Particle sizes ranging from 100nm to 400nm was seen with strontium salts, with the smallest diameter obtained from SrF_2.

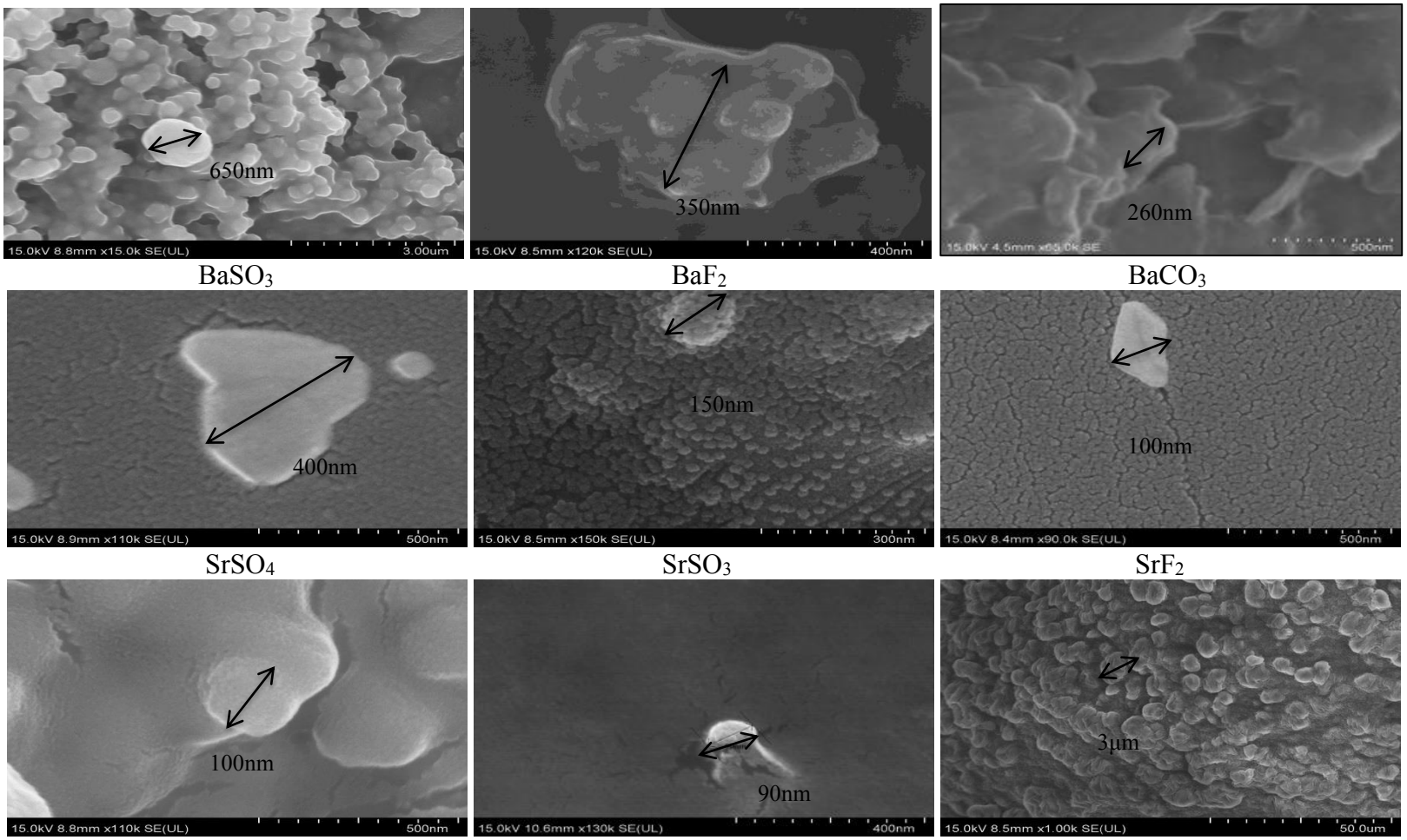

Figure 3.8: SEM visualization of selected NPs. Generation of salts was based on chemical reaction between two soluble components. The salts were incubated for 30 minutes at 37°C and centrifuged at 15,000 RPM for 10 seconds, followed by supernatant removal and resuspension of pelette with 1ml milli-Q water. Fabricated salt crystals were kept on ice prior to microscopic observation. 1µl of resuspeded solution was placed onto carbon tape of sample holder and dried at room temperature, followed by platinum sputtering of each nanocrystals samples for 60 seconds. Sputtered samples were observed at aprroximately 10-15kV.

3.3.4 Binding affinity of pDNA and siRNA with towards NPs

In the second stage of the project, pDNA binding affinity towards the nanocrystals was studied, whereby particles with nano-size dimensions were investigated based on their abilities to adsorb fluorescence-labeled pDNA or siRNA using the fluorescence microscope as well as fluorescence plate reader. Investigation of binding affinity demonstrated efficient adsorption of pDNA towards barium, strontium, calcium and magnesium salt particles through intensity emitted by PI-pDNA bound to the complexes, as seen in Figure 3.9. Ferrous salts had a weak affinity towards pDNA, reflected by low fluorescence-stained pDNA-ferrous complexes. Additionally, all salts containing Na_3PO_4 depicted low intensity, indicating inefficient binding between the genetic material and carriers probably due to the electrostatic repulsion between ions phosphate and nucleic acid. Adsorption of stained pDNA and NPs further revealed greater activity seen with strontium salt groups, predominantly on SrF_2.

The binding affinity of pDNA and siRNA seen via fluorescence microplate reader overall showed similar adsorption trend for all the NPs examined upon 30 minutes of incubation (Figure 10, Figure 11). Quantitative analysis on pDNA-binding activity towards salt particles revealed most efficient gene adsorption towards SrF_2 and BrF_2, with 90% of the pDNA bound corresponded to the fluorescence microscopic images from the earlier studies (Figure 3.10). Approximately >70% of the siRNA confined to both salts, in comparison with CO_3 AP of >80% for both nucleic acids (Figure 3.11). $BaSO_3$ and $SrSO_3$ revealed superior siRNA adsorption than of pDNA, presented with 70% and 90% for respective pDNA and siRNA.

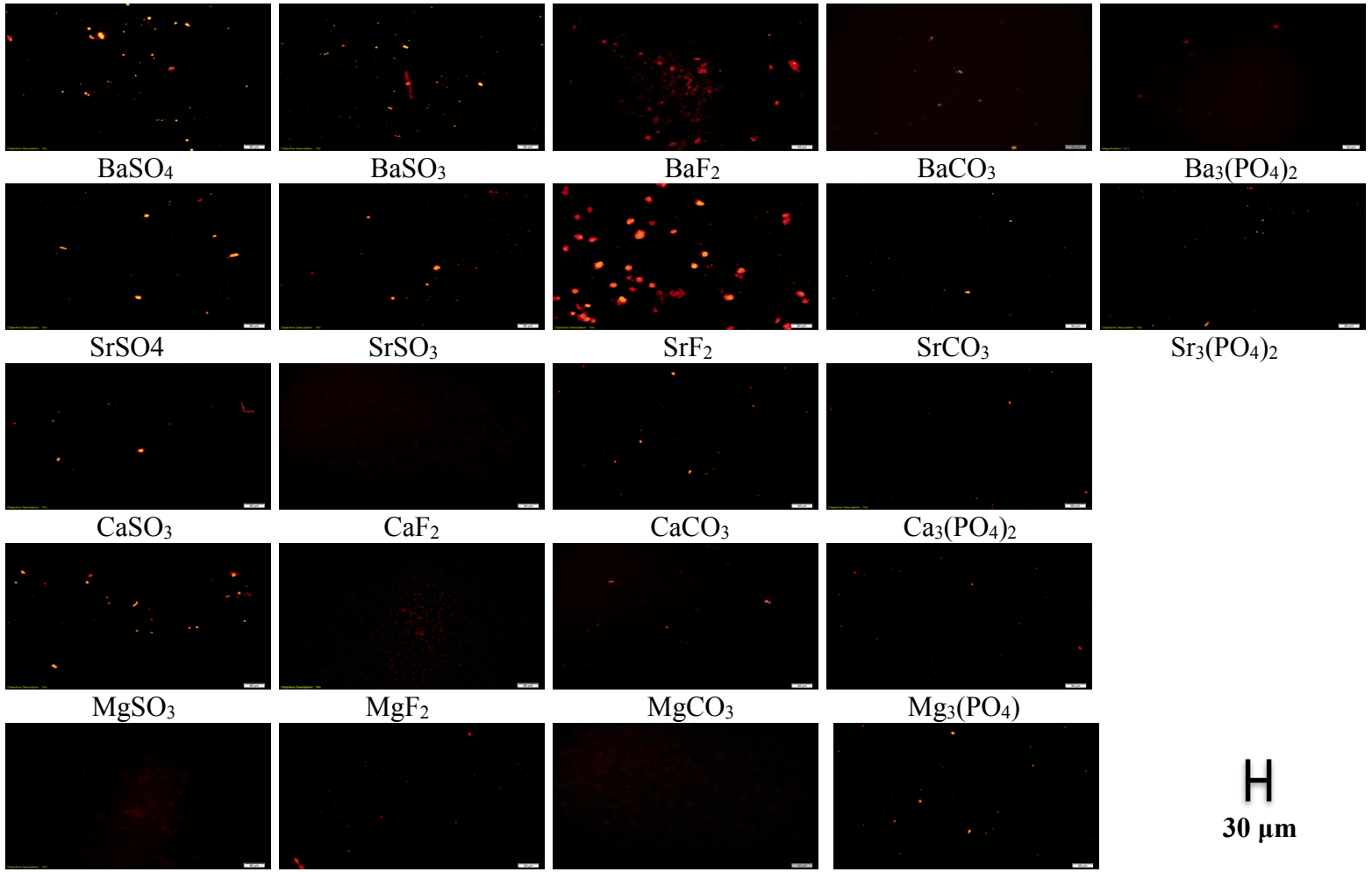

Figure 3.9: Fluorescence microscopic observation for binding affinity of pDNA towards NPs. 5µl of 1M (a) $BaCl_2$, (b) $SrCl_2$, (c) $CaCl_2$, (d) $MgCl_2$) or (e) $FeCl_2$ was introduced along with PI-stained pDNA (1:1 ratio) into 10µl HEPES buffered media, followed by mixing of 2µl of 1M Na_2SO_4, NA_2SO_3, NaF, Na_2CO_3 or Na_2PO_4, generating various salt crystals before 30 minutes incubation at 37°C. FBS containing-DMEM media was added to achieve 1ml solution. Image was captured at 10X resolution under PI filter, with reference to (f) CO_3 AP.

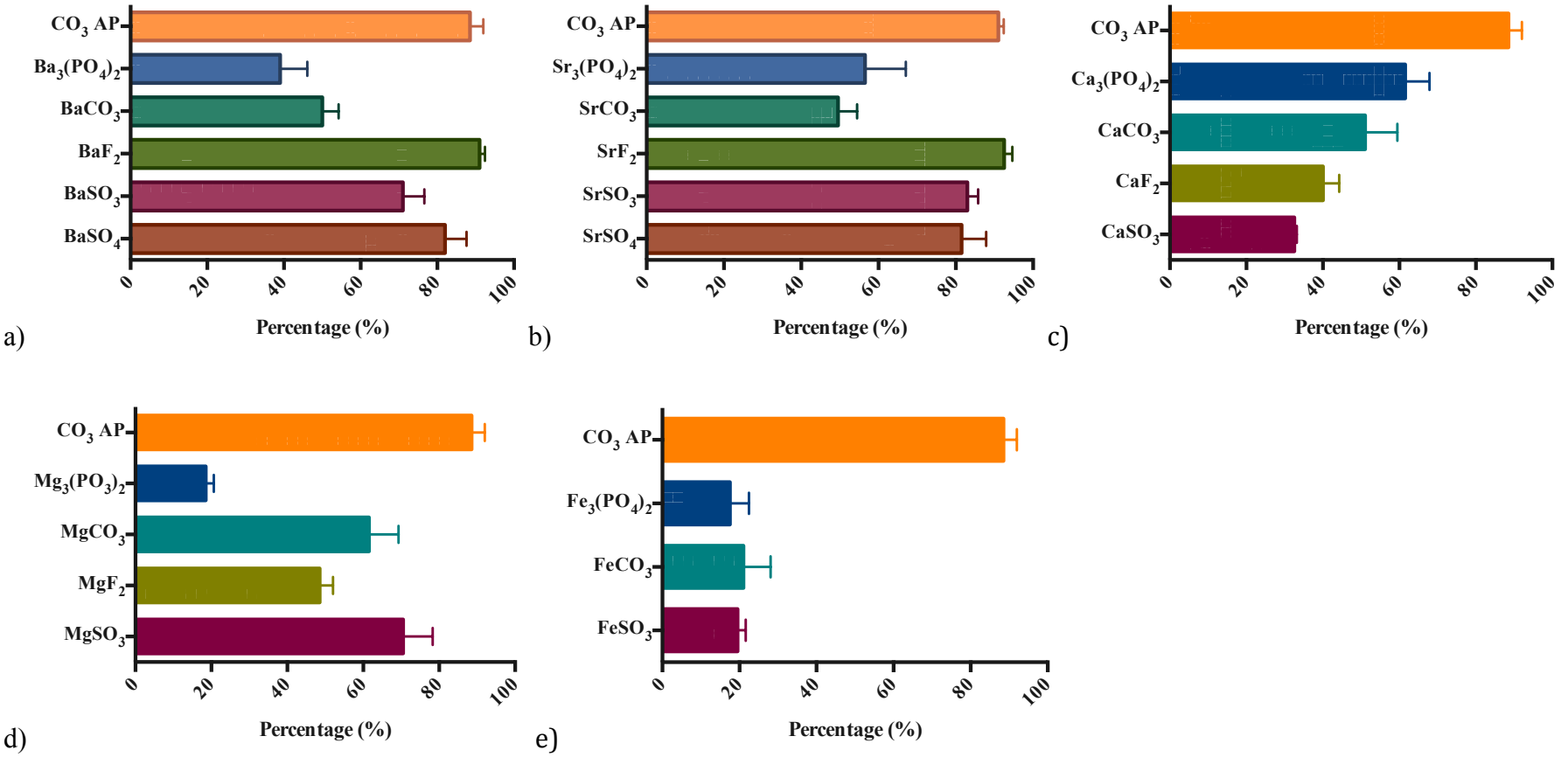

Figure 3.10: Fluorescence analysis for binding affinity of pDNA towards NPs. 5µl of 1M (a) $BaCl_2$, (b) $SrCl_2$, (c) $CaCl_2$, (d) $MgCl_2$) or (e) $FeCl_2$ was introduced along with PI-stained pDNA (1:1 ratio) into 10µl HEPES buffered media, followed by mixing of 2µl of 1M Na_2SO_4, Na_2SO_3, NaF, Na_2CO_3 or Na_3PO_4, generating various salt crystals before 30 minutes incubation at 37°C. FBS containing-DMEM media was added to achieve 1ml solution, with reference to (f) CO_3 AP. Quantitative measurement of NPs-bound pDNA was achieved with multi-label plate reader following centrifugation of fabricated NPs at 15,000 RPM for 5 minutes and aspiration of 100µl into 96 well-plate, prior to fluorescence intensity measurement.

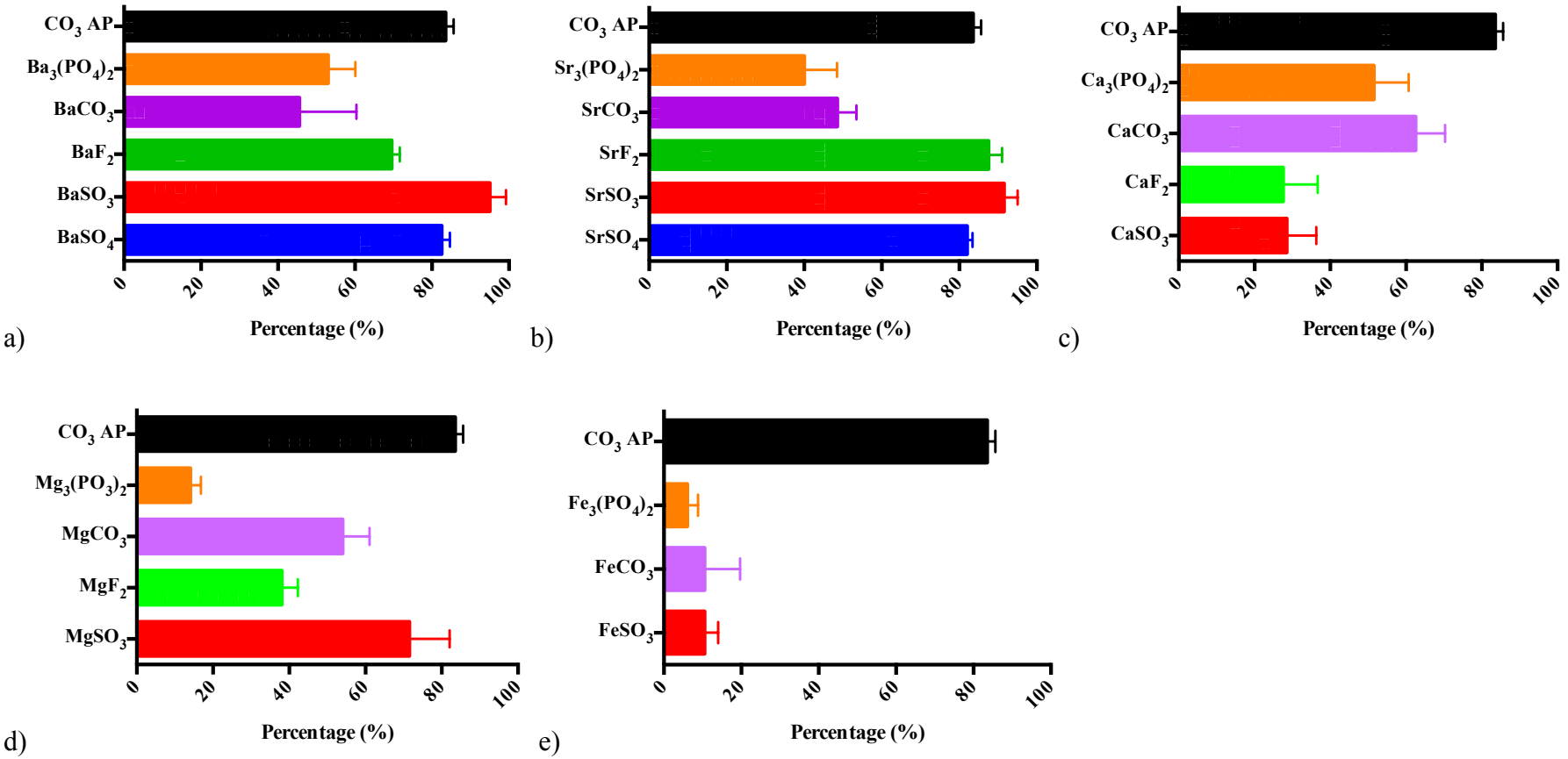

Figure 3.11: Fluorescence analysis for binding affinity of siRNA towards NPs. 5µl of 1M (a) $BaCl_2$, (b) $SrCl_2$, (c) $CaCl_2$, (d) $MgCl_2$) or (e) $FeCl_2$ was introduced along with fluorescence siRNA (AF 488) into 10µl HEPES buffered media, followed by mixing of 2µl of 1M Na_2SO_4, Na_2SO_3, NaF, Na_2CO_3 or Na_3PO_4, generating various salt crystals upon 30 minutes incubation at 37°C. FBS containing-DMEM media was added to achieve 1ml solution, with reference to (f) CO_3 AP. Quantitative measurement of NPs-bound siRNA was achieved with multi-label plate reader following centrifugation of fabricated NPs at 15,000 RPM for 5 minutes and aspiration of 100µl supernatant into 96 well plate, prior to fluorescence intensity measurement.

Similarly following the microscopic images, ferrous salts showed minimum binding affinity with 10-20% adsorption with the genetic loads. Incorporation of Na_3PO_4 to form salt particles is associated with the lowest binding affinity towards both pDNA and siRNA, in comparison to other anion-providing salts. Strontium-forming NPs complexes overall presented high adsorption activity with genes, ranging from 50 to 90% (Figure 3.10 and 3.11). With reference to weak intensified structures seen in the fluorescence microscope, calcium salt crystals displayed 30-60% incorporation of pDNA and siRNA into the salt structures upon 30 minutes of incubation. The consistency of salts demonstrating >70% nucleic acid adsorption affinity was observed for $BaSO_4$, $BaSO_3$, BaF_2, $SrSO_4$, $SrSO_3$, SrF_2, and $MgSO_3$.

3.3.5 Influence of ligand coating on morphology and size of NPs

The study of ligand coating was performed to grasp the impact of coating on the structural changes of NPs, through observation of selected salts coated with transferrin or fibronectin. Upon fabrication of the NPs, transferrin or fibronectin was introduced into the particle solution after formation of salt crystals, forming the outer layer of the crystals, followed by subsequent analysis of size measurement and zeta potential. All NPs demonstrated size reduction and less negative zeta potential with transferrin and fibronectin coating (Table 3.5). The most size reduction was seen with $MgSO_3$ crystals, a third from its original size of 98nm, with similar reduction trend perceived with CO_3 AP nanoparticles. Fibronectin protein adherence to the particle surfaces is associated with smaller salt particles in comparison to transferrin, with exception to $SrSO_4$.

Salt Formulation		Size (d.nm)	Zeta (mV)
$BaSO_3$	Uncoated	506±34	-11
	Transferrin-coated	483±49	-7
	Fibronectin-coated	441±77	-2
BaF_2	Uncoated	218±35	-6
	Transferrin-coated	206±38	0
	Fibronectin-coated	102±29	1
$SrSO_4$	Uncoated	721±94	-8
	Transferrin-coated	518±72	-4
	Fibronectin-coated	623±71	-1
$SrSO_3$	Uncoated	471±30	-7
	Transferrin-coated	348±41	-2
	Fibronectin-coated	331±36	1
SrF_2	Uncoated	106±12	-8
	Transferrin-coated	95±11	-5
	Fibronectin-coated	73±9	-2
$MgSO_3$	Uncoated	98±10	-7
	Transferrin-coated	78±3	1
	Fibronectin-coated	30±4	3
CO_3 AP	Uncoated	321±38	-10
	Transferrin-coated	221±27	-7
	Fibronectin-coated	196±66	-2

Table 3.5: Particle size and zeta potential of NPs with coating of transferrin or fibronectin. Fabricated NPs were observed using zetasizer to obtain average size and surface charge of each type of particles, with reference to CO_3 AP.

Observation of coated salt crystals through SEM analysis shows three selected salts, $SrSO_3$, SrF_2 and $MgSO_3$ with comparable size reduction after adherence of fibronectin protein in reference to uncoated salt particles (Figure 3.12). Observation of size showed minimal declination of salt size up to two-third from the uncoated particles size, concurring the results attained from earlier analysis using Zetasizer. Additionally, the image of NPs revealed appearance of aggregates on the surface of the crystals, suggesting the possible coating of the protein-ligand forming the outer layer of the crystals.

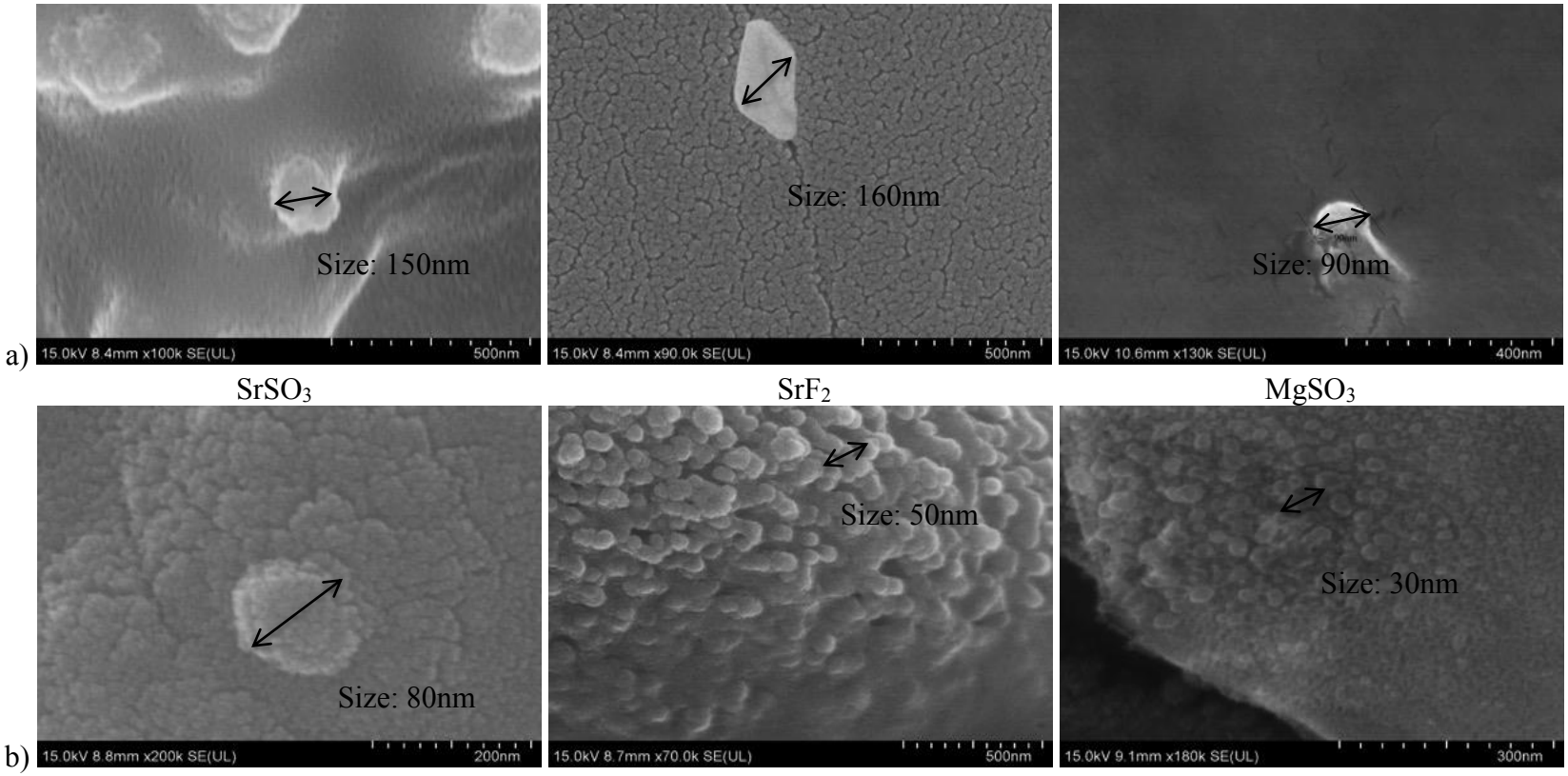

Figure 3.12: SEM visualization of selected NPs (a) uncoated and (b) coated with fibronectin. 1µg fibronectin was incorporated into the fabricated salt particles with additional 10 minutes incubation prior to observation under microscope. The coated salt particles were centrifuged at 15,000 RPM for 10 seconds, followed by supernatant removal and resuspension of pelette with 1ml milli-Q water. Fabricated salt crystals were kept on ice prior to microscopic observation. 1µl of resuspeded solution was placed onto carbon tape of sample holder and dried at room temperature, followed by platinum sputtering of each nanocrystals samples for 60 seconds. Sputtered samples were observed at aprroximately 10-15kV.

3.3.6 Effect of salt combination on morphology and size of NPs

Manipulation of nanocrystals was done through the combination of two types of inorganic salt particles for prospective synergistic effect. The probable augmentation of the effect was addressed by the impression of improving the target structure for superior genetic material binding of the selected particles, which individually showed immense adsorption affinity in the earlier experiments. Qualitative and quantitative experimental studies of salt combinations were accomplished through the generation of two separate forms of inorganic materials, followed by mixing and collectively incubating at 37°C for 30 minutes. The hybrid salt particles were analyzed by the Zeta Sizer alongside their individual salt particles to exercise the size comparison assay in addition to the measurement of zeta potential activity. Ratification of the size modification of salt combinations was done on SEM at 15kV.

Salt Formulations	Size (nm)	Zeta potential (mV)
$BaSO_3$	506±78	-11
$SrSO_3$	471±49	-7
SrF_2	106±21	-8
$MgSO_3$	98±11	-7
BaF_2	218±32	-6
$BaSO_3$+ $SrSO_3$	1525±232	-29.3
$SrSO_3$ + SrF_2	1459±198	-24
$SrSO_3$ + $MgSO_3$	1135±188	-27
SrF_2 + BaF_2	667±89	-17
$BaSO_3$ + $MgSO_3$	773±121	-21
CO_3 AP	321±66	-10

Table 3.6: Particle size and zeta potential analysis of salt combinations. Fabricated NPs were detected using Zetasizer to obtain average size and charge of each particles, with reference to CO_3 AP.

Evaluation of size modification with salt combination demonstrated the generation of larger particles with stronger negative domains, as seen in the average particle size determination and zeta potential analysis than with single counterparts of the earlier experiments. Hybridization of $BaSO_3$ and $SrSO_3$ resulted in largest average sizes, with salt diameter seen approximately 1525nm, in contrast to 506nm and 471nm of individualized $BaSO_3$ and $SrSO_3$ control. Co-mixture of $SrSO_3$ and SrF_2 also demonstrated bigger particle size of 1459nm. Minimal salt diameter of co-precipitated salt particles was seen with SrF_2 + BaF_2 with approximately half of the largest salt combinations, 667nm. Based on this study, it is likely that all possible salt combinations will form large-structured particles with more negative domains existing in the structures. Large particles with greater negative charges may impede with salt efficiency in transporting genetic materials and which were confirmed in vitro studies over the next chapter.

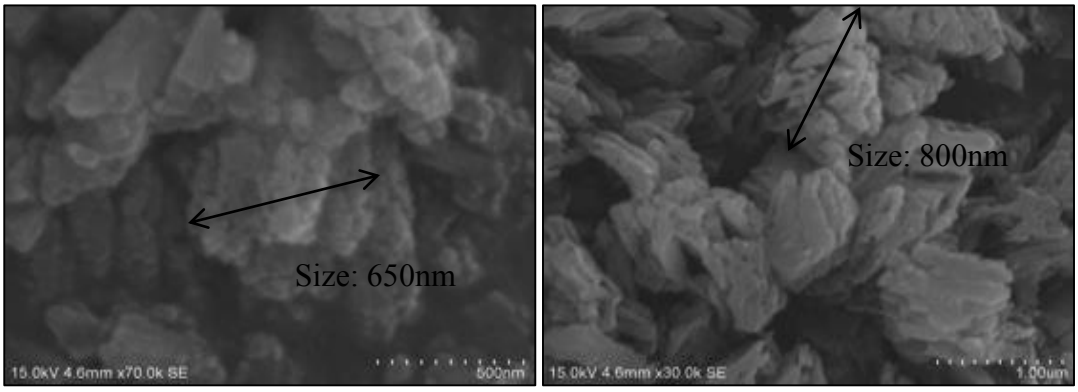

SrF_2 + BaF_2 $BaSO_3$+$MgSO_3$

Figure 3.13: SEM images of salt combinations: SrF_2 + BaF_2 and $BaSO_3$+$MgSO_3$. Formation of salt combinations was based on two separate insoluble salts formed by respective chemical reactions with 30 minutes incubation at 37ºC. The suspensions were centrifuged, followed by removal of supernatant and resuspension of pelette with milli-Q water. 1µl of resuspeded solution was placed onto carbon tape of sample holder and dried at room temperature, followed by platinum sputtering of each nanocrystals samples. Sputtered samples were microscopically observed at aprroximately 10-15kV.

3.4 Discussions

Fabrication of NPs was initially commenced through the incorporation of two soluble salts at 5mM to visualize the proposed precipitation reaction of salt crystals. The solubility properties of NPs are highly critical to prevent premature degradation of the crystals. Hence, the formation insoluble crystals are compulsory to generate stable nanocarriers (1). $CaSO_4$, $MgSO_4$, and $FeSO_4$ were not involved in the salt selection (Figure 3.1) due to their high water solubility features. Additionally, FeF_2 is slightly soluble in water, thus was excluded too from the studies (2). NPs generated from the mixture of soluble components were confirmed based on visualization and absorbance features of individual salt. Superior absorbance intensity, associated with more distinctive precipitates observed through microscopic imaging is related to greater particle number and sizes (3). Multiple nucleation events that occur in the solution mixtures were followed by more significant particle growth to form the larger particles seen as detectable aggregates under the microscope (4).

Particle aggregates are often irreversible, except with introduction of a new environment, hence ultimately preventing the untimely disintegration of salt crystals. Peptization is a reversible process involving dispersion of aggregates to form individual particles, often occurring upon stirring and shearing which allows scattering of salt crystals and may prevent sedimentation of salts at the bottom of the container (5). Barium and ferrous larger salts formation may be resulted from efficient particle nucleation due to practical phase transformation, hence creating more salt aggregates (6). Magnesium and calcium crystals generate small aggregates, hence lowering insolubility features in comparison to their alkaline earth metal counterparts, barium,

and strontium, associated with higher atomic radius down the group. The size of the atom is influenced by the number of layers of the inner electrons which fit around the atom, thus forming larger particles (7). Na_2SO_4, Na_2SO_3, and Na_3PO_4, which are involved in the formation of more precipitates, may also be based on the atomic radius, which consists of a greater number of layers of electrons, resulting in increased generation of salt particles (8). The demonstrated diagram, however, may not determine the actual sizes of NPs, as the optical microscopic images can show the large particles (>50µm). Prediction on actual sizes was elaborated in subsequent Zetasizer and SEM analysis.

Optimization of pH, concentration of reactants, incubation temperature or incubation time, is vital in fabricating ideal nanoparticles. Particle formation is accelerated as the concentration of reactant is escalated, which acts as a driving force for the chemical reaction (9)(10). Turbidity and particle diameter as shown in Figure 3.1 and 3.2 depended on the concentration-dependent response demonstrated between the inorganic salts which are self-assembled in a supersaturated solution, resulting in particle nucleation and formation of nano-sized crystals. Investigation on the effect of concentration showed that particle formulations made increasing concentration of any salts exhibited greater particle growth regardless of cation- or anion-providing salt inclusion (turbidity measurement as seen in Figures 3.3 and 3.4). The study thus suggested the dependency of particle growth on reactant concentrations when the time of incubation, the temperature of incubation, pH, and concentration of the remaining salts remain constant. $FeSO_3$ and $Fe_3(PO_4)_2$ demonstrated higher absorbance intensity, with a greater number and bigger particles sizes than any other salts with increasing soluble ferrous salt concentration. Greater ferrous salts concentrations are associated

with more agglomeration possibly due to attraction by Van der Waals forces, promoting stronger attraction between the crystals' cationic and anionic domains (11). Barium and strontium NPs further demonstrated higher absorbance intensities with increasing of cationic salt concentration than calcium and magnesium NPs, could also be associated with the mass and density characteristics of salts from the alkaline earth metal. The densities of Na_2SO_4 and Na_2SO_3 are greater, reflecting the superior absorbance value with increasing metallic group concentration (12). Carbonate and fluoride-incorporated NPs exhibited overall lower absorbance and thus smaller particles numbers and sizes in comparison with other generated inorganic salts, due low ionization density which enhances as down the non-metal periodic group (13).

Highly basic pH, elevated temperature and prolonged incubation time shift the ionization equilibrium towards the forward direction and hence, the reaction rate is significantly enhanced (14) The time-dependent analysis evaluates the impact of incubation time. Most reactions occur immediately due to a high probability of collisions between reacting ions inside the aqueous solution, generating precipitates. As the time progresses, more reactions can take place to form more number of particles of large size owing to the development of a highly supersaturated solution (16)(17). Accelerated particle growth of NPs at basic pH was signified by high absorbance intensity, as seen from Figure 3.6 (18). The phenomenon may be explained by pH-dependent salt ionization to a greater degree, resulting in faster development of supersaturation and leading to increased particle growth (19). Temperature dependent analysis reveals the proportional increment of salt crystals number and size, explained by higher absorbance intensity as temperature rises. Influence of temperature on the formation of NPs may be explained by the introduction of kinetic energy for stimulating

the chemical reaction between two reactants, resulting in faster nucleation activity and deposition of end product into larger precipitates. Low temperature reduces the rate of nucleation and growth, as shown at 4^{o}C, hence amending the reaction rate to progress at a much slower rate (20). High absorbance intensity visualized throughout external and internal experimental assessment of salt crystals is related to increased number and size of NPs, which may improve their binding affinity for genetic materials while simultaneously obstructing the internalization process through endocytosis and reducing distribution efficiency via passive transport in the biological system (21)(22).

The relationship between absorbance intensity and particle sizes was described by observation of crystals particle diameter via Zeta Sizer analysis. It is proposed that high absorbance intensity is coherent to larger particle diameter and number. Ferrous salts particles are of biggest size diameter amongst the 21 crystals salts, demonstrating size ranges from 500 to 1500nm, which correlates with high absorbance intensity from previous experiments. Augmentation of anion-providing salt concentration resulted in the greater size of NPs, as similarly proven by absorbance determination. Besides ferrous salt particles, barium and strontium crystals generate larger particle sizes, forming precipitates especially from the mixture of Na_2SO_4, Na_2SO_3, and Na_3PO_4. Studies done by Perrault et al. on the effect of nanoparticles sizes ranging from 10 to 100nm on passive tumor targeting reported that particles with 20-100nm diameter stipulated excellent tumor accumulation and could be used for localizing leaky vasculature (23). Also, with smaller sizes, they had longer circulation time and concomitantly higher tumor accumulation (24). Large molecules were readily detected by the reticuloendothelial system (RES) and removed quickly from the circulatory system by the liver sequestration. Hence, size limitation remains helpful parameters to

enable NPs to escape the RES with the size of <500nm, in addition to net charge to be as neutral as possible (25). Although pDNA and siRNA adsorption efficiency of nanocarriers are highly dependent on particle sizes and numbers, too large particle sizes may hinder the cellular uptake activity of NPs hence reducing the amount of internalized crystals (26). Comparative design studies on various salts and CO_3 AP nanoparticles also demonstrated net negative charge of the salt crystals, which could be rapidly opsonized and cleared by macrophages of RES (21,27). However, the net charge of NPs might be transient depending on the surrounding environment of the electrolytes that can unselectively bind to the salts. Optimization of size and zeta charge is a vital strategy to enable the system to be sustained in the circulatory system for an extended period, modulating pharmacokinetics and bioavailability of NPs (28).

Fabrication of nanocrystals was initially commenced with adjusting the concentration of both soluble salts to form salt particles with diameter of less than 500nm. Salts forming the cationic region of particles $BaCl_2$, $SrCl_2$, $CaCl_2$, $MgCl_2$ or $FeCl_2$ and the anionic domains (Na_2SO_4, Na_2SO_3, NaF, Na_2CO_3 or Na_3PO_4) were ideal at 5mM and 2mM, respectively, generating the average size of 50nm to 400nm (using Zetasizer Malvern ZS), based on Table 3.4. Zeta potential measures the net charge on the particle surface and is an influential physical factor, impacting particularly in vivo strategies, including treatment pharmacokinetics and biodistributions. Attachment of nanoparticles to the cell membrane is dominantly affected by the surface charge of particles, which often consists of negatively charged syndecans, influencing the intracellular transportation of NPs complexes of pDNA and siRNA, eventually targeting the gene activity (29)(30). FE-SEM enables visualization of the estimated size of NPs in addition to understanding the morphological structure of crystals, often in semi-

spherical forms. Large particles such as $FeSO_3$ and $BaSO_3$ emerged in the forms of larger clusters of aggregates.

Transferrin and fibronectin adsorption on NPs surfaces was studied to observe the influence of adherence of proteins on the features of the crystals. The alteration in size forming smaller particles of <100nm in diameter with presence of protein ligands improves the functionality of the crystals for greater in vitro and in vivo performance. Protein adsorption helps in the neutralization of charge ion of nanocrystals, hence compacting the salt ionic structure and stabilizing the crystals forms (31). Fibronectin coating enhances further size reduction than transferrin, possibly by high affinity for electrostatic interactions with NPs, associated with improvement of binding site influenced by up-regulation of integrin α5β1 receptor in both carcinoma cells lines (32). Images generated from FE-SEM demonstrated generation of smaller particle clusters with less smooth surface, which may indicate the outer layer of coating. Modification of zeta potential with ligand coating with less negative charges is likely to improve further the biodistribution characteristics of NPs (33). As the particles become more neutral, they will have lower risks of premature degradation in the blood circulation by preventing from binding of scavenging plasma protein onto the crystals surfaces, which otherwise promotes elimination of particles through mononuclear phagocyte system (MPS) (34).

The impact of combining two different particle suspension on the size and zeta potential performed on the resulted hybrid salt particles revealed minimal three-fold increment of size through Zetasizer observation. The hybridized particles are unlikely to execute well in vivo due to enlarged sizes, posing augmented risks of forming larger

clumps of aggregates which may cause capillary blockade and embolism (35). Positive charge domains of coprecipitates often form aggregates with presence of negatively charged serum proteins upon parenteral administration (36).

Adsorption of fluorescence-labeled pDNA and siRNA towards NPs revealed a superior binding affinity with barium, followed by strontium, calcium and magnesium salt crystals in respective orders. The efficient binding activity of NPs, with approximately 95% of maximum binding is coherent with both individual nucleic acids, in comparison to 10-20% of binding affinity to iron NPs. Binding affinity is possibly associated with the ionic strength between positive charge of alkaline earth metal groups and anionic genetic materials increases down the group (37). The degree of binding of nucleic acids with each type of NPs might affect subsequent gene expression or silencing efficacy associated with the lower amount of pDNA or siRNA transported intracellularly (38).

3.5 Conclusion

Our investigation on the formation of insoluble salts from the mixture of two soluble components consisted of $BaCl_2$, $SrCl_2$, $CaCl_2$, $MgCl_2$ or $FeCl_2$, and Na_2SO_4, Na_2SO_3, NaF, Na_2CO_3 or Na_3PO_4 in an aqueous solution. Additionally, we also observed the factors associated the NPs formation, such as salt concentrations, pH, temperature and time of incubation. Greater cation- or anion-providing salt concentration was associated with larger size and number of precipitates, reflected by higher absorbance or turbidity of particle suspension. Basic pH, high temperature and longer incubation time were associated with higher absorbance intensity or enhanced

particle growth. Absorbance intensity was significantly related to NPs size, with larger particles sizes often seen with high absorbance data. Most NPs had net negative charge, which might reflect in lower interactions between negatively charged nucleic acids. Incorporation of protein coating improved the charge to be almost neutral, hence, might help in improving cellular internalization activity by promoting receptor-ligand interactions, on top of diminution of salt diameter. Combination of salts particles however vastly increased the size, enforcing more negative charged structures.

Genetic material adsorption assay demonstrated high efficiency with salt crystals down the alkali earth metal groups. The stronger ionic interactions achieved with barium and strontium was proven to be high, as 95% of pDNA or siRNA was complexed to the designated salts. Subsequent intracellular experiment will show the relationship between adsorption activities and internalization advantage of the complexes. Additionally, exploration of protein coating and hybridization activity in manipulating the cellular activity of target genes in transfected cells will be done in Chapter 4.

3.6 References

1. Xiao RZ, Zeng ZW, Zhou GL, Wang JJ, Li FZ, Wang AM. Recent advances in PEG-PLA block copolymer nanoparticles. Int J Nanomedicine. 2010;5(1):1057–65.
2. Atkins PW. Shriver & Atkins' inorganic chemistry [Internet]. Shriver and Atkin's inorganic chemistry. 2010. 851 p. Available from: http://books.google.com/books?hl=en&lr=&id=tUmcAQAAQBAJ&oi=fnd&pg=PP2&dq=Shriver+%26+Atkins%E2%80%99+Inorganic+Chemistry&ots=i0f_FwEQen&sig=ET7Ct2qnLo_Ucl-wceKNuPUOME4
3. Jain PK, Lee KS, El-Sayed IH, El-Sayed MA. Calculated Absorption and Scattering Properties of Gold Nanoparticles of Different Size, Shape, and Composition: Applications in Biological Imaging and Biomedicine. J Phys Chem B [Internet]. 2006;110(14):7238–48. Available from: http://dx.doi.org/10.1021/jp057170o
4. Thanh NTK, Maclean N, Mahiddine S. Mechanisms of Nucleation and Growth of Nanoparticles in Solution. Chem Rev [Internet]. 2014 Aug 13 [cited 2016 Mar 23];114(15):7610–30. Available from: http://pubs.acs.org/doi/abs/10.1021/cr400544s
5. Mérida F, Chiu-Lam A, Bohórquez AC, Maldonado-Camargo L, Pérez M-E, Pericchi L, et al. Optimization of synthesis and peptization steps to obtain iron oxide nanoparticles with high energy dissipation rates. J Magn Magn Mater [Internet]. 2015;394:361–71. Available from: http://www.sciencedirect.com/science/article/pii/S0304885315302894
6. Farvid SS, Radovanovic P V. Phase transformation of colloidal In2O3 nanocrystals driven by the interface nucleation mechanism: a kinetic study. J Am Chem Soc [Internet]. 2012 Apr 25 [cited 2016 Mar 23];134(16):7015–24. Available from: http://www.ncbi.nlm.nih.gov/pubmed/22448898
7. Kraynov A, Müller TE. Concepts for the Stabilization of Metal Nanoparticles in Ionic Liquids.
8. Issa B, Obaidat IM, Albiss BA, Haik Y. Magnetic nanoparticles: Surface effects and properties related to biomedicine applications. International Journal of Molecular Sciences. 2013. p. 21266–305.
9. Amin S, Barnett G V., Pathak JA, Roberts CJ, Sarangapani PS. Protein aggregation, particle formation, characterization & rheology. Curr Opin Colloid Interface Sci [Internet]. 2014;19(5):438–49. Available from: http://www.sciencedirect.com/science/article/pii/S135902941400096X
10. Mansouri SS, Ghader S. Experimental study on effect of different parameters on size and shape of triangular silver nanoparticles prepared by a simple and rapid method in aqueous solution. Arab J Chem. 2009;2(1):47–53.
11. Nel AE, Mädler L, Velegol D, Xia T, Hoek EM V, Somasundaran P, et al. Understanding biophysicochemical interactions at the nano-bio interface. Nat Mater [Internet]. 2009;8(7):543–57. Available from: http://dx.doi.org/10.1038/nmat2442
12. Luo C-H, Shanmugam V, Yeh C-S. Nanoparticle biosynthesis using unicellular and subcellular supports. NPG Asia Mater [Internet]. 2015;7(8):e209. Available from: http://www.nature.com/doifinder/10.1038/am.2015.90

13. Spencer L. Seager MRS. Chemistry for Today: General, Organic, and Biochemistry. 3rd ed. 2010. 88 p.
14. Destrée C, Debuigne F, Jeunieau L, Nagy JB. Mechanism of formation of inorganic and organic nanoparticles from microemulsions. Adv Colloid Interface Sci [Internet]. 2006;123-126:353–67. Available from: http://www.sciencedirect.com/science/article/pii/S0001868606000777
15. Li Z, Gu L. Effects of mass ratio, pH, temperature, and reaction time on fabrication of partially purified pomegranate ellagitannin-gelatin nanoparticles. J Agric Food Chem. 2011;59(8):4225–31.
16. Na HS, Arnold S, Myerson AS. Cluster formation in highly supersaturated solution droplets. J Cryst Growth. 1994;139(1-2):104–12.
17. Libert S, Gorshkov V, Goia D, Matijevi?? E, Privman V. Model of controlled synthesis of uniform colloid particles: Cadmium sulfide. Langmuir. 2003;19(26):10679–83.
18. Kolasińska M, Krastev R, Gutberlet T, Warszyński P. Surface and Interfacial Forces – From Fundamentals to Applications [Internet]. Progress in Colloid and Polymer Science. 2008. 30-38 p. Available from: http://www.scopus.com/inward/record.url?eid=2-s2.0-54249122913&partnerID=tZOtx3y1
19. Binks BP, Murakami R, Armes SP, Fujii S. Effects of pH and salt concentration on oil-in-water emulsions stabilized solely by nanocomposite microgel particles. Langmuir. 2006;22(5):2050–7.
20. Jiang XC, Chen WM, Chen CY, Xiong SX, Yu a B. Role of Temperature in the Growth of Silver Nanoparticles Through a Synergetic Reduction Approach. Nanoscale Res Lett [Internet]. 2010;6(1):1–9. Available from: http://www.nanoscalereslett.com/content/6/1/32
21. Oh N, Park JH. Endocytosis and exocytosis of nanoparticles in mammalian cells. International Journal of Nanomedicine. 2014. p. 51–63.
22. Zhang S, Li J, Lykotrafitis G, Bao G, Suresh S. Size-dependent endocytosis of nanoparticles. Adv Mater. 2009;21(4):419–24.
23. Perrault SD, Walkey C, Jennings T, Fischer HC, Chan WCW. Mediating tumor targeting efficiency of nanoparticles through design. Nano Lett. 2009;9(5):1909–15.
24. Jain S, Hirst DG, O'Sullivan JM. Gold nanoparticles as novel agents for cancer therapy. Br J Radiol. 2012;85(1010):101–13.
25. Longmire M, Choyke PL, Kobayashi H. Clearance properties of nano-sized particles and molecules as imaging agents: considerations and caveats. Nanomedicine (Lond) [Internet]. 2008;3(5):703–17. Available from: http://www.pubmedcentral.nih.gov/articlerender.fcgi?artid=3407669&tool=pmcentrez&rendertype=abstract
26. De Jong WH, Borm PJ a. Drug delivery and nanoparticles:applications and hazards. Int J Nanomedicine. 2008;3(2):133–49.
27. Huang L, Guo S. Nanoparticles escaping RES and endosome: Challenges for siRNA delivery for cancer therapy. Journal of Nanomaterials. 2011.
28. Sharma D, Maheshwari D, Philip G, Rana R, Bhatia S, Singh M, et al. Formulation and optimization of polymeric nanoparticles for intranasal delivery of lorazepam using Box-Behnken design: In vitro and in vivo evaluation. Biomed Res Int. 2014;2014.
29. Fröhlich E. The role of surface charge in cellular uptake and cytotoxicity of

medical nanoparticles. Int J Nanomedicine [Internet]. 2012 Nov [cited 2016 Mar 24];5577. Available from: http://www.dovepress.com/the-role-of-surface-charge-in-cellular-uptake-and-cytotoxicity-of-medi-peer-reviewed-article-IJN

30. Calatayud MP, Sanz B, Raffa V, Riggio C, Ibarra MR, Goya GF. The effect of surface charge of functionalized Fe3O4 nanoparticles on protein adsorption and cell uptake. Biomaterials [Internet]. 2014 Aug [cited 2016 Mar 24];35(24):6389–99. Available from: http://www.ncbi.nlm.nih.gov/pubmed/24816288
31. Patil S, Sandberg A, Heckert E, Self W, Seal S. Protein adsorption and cellular uptake of cerium oxide nanoparticles as a function of zeta potential. Biomaterials. 2007;28(31):4600–7.
32. McSherry E a, Brennan K, Hudson L, Hill AD, Hopkins AM. Breast cancer cell migration is regulated through junctional adhesion molecule-A-mediated activation of Rap1 GTPase. Breast Cancer Res [Internet]. 2011;13(2):R31. Available from: http://breast-cancer-research.com/content/13/2/R31
33. Kwon D, Park J, Park J, Choi SY, Yoon TH. Effects of surface-modifying ligands on the colloidal stability of ZnO nanoparticle dispersions in in vitro cytotoxicity test media. Int J Nanomedicine. 2014;9:57–65.
34. Prokop A, Davidson JM. Nanovehicular intracellular delivery systems. Journal of Pharmaceutical Sciences. 2008. p. 3518–90.
35. Ernsting MJ, Murakami M, Roy A, Li SD. Factors controlling the pharmacokinetics, biodistribution and intratumoral penetration of nanoparticles. Journal of Controlled Release. 2013. p. 782–94.
36. Balazs D a, Godbey W. Liposomes for use in gene delivery. J Drug Deliv. 2011;2011:326497.
37. Antonio Sgamellotti. Science and Art: The Painted Surface. 3rd ed. 2010. 354 p.
38. Singha K, Namgung R, Kim WJ. Polymers in small-interfering RNA delivery. Nucleic Acid Ther [Internet]. 2011;21(3):133–47. Available from: http://www.pubmedcentral.nih.gov/articlerender.fcgi?artid=3198620&tool=pmcentrez&rendertype=abstract

Chapter 4

In vitro efficacy and safety assessment of NPs

4.1 Introduction

The efficiency of nanocarriers is initially determined by their ability in promoting safe and efficient intracellular activity. A significant barrier to the non-viral delivery is the low uptake of pDNA/siRNA across the plasma membrane of a cell owing to the inappropriate and ineffective interactions of the nucleic acid biological vehicle with the cellular membrane. The ideal carriers should interact electrostatically with anionic heparin sulfate proteoglycans (syndecans) on the cell surface to be endocytosed into the cells in the form of endosomes. Active targeting activity is achieved through attachment of affinity ligands (peptides or antibodies) that only bind to specific receptors on the cellular surface. The utilization of proteins in accomplishing active targeting relied on the over-expression of specific receptors on the tumor cells. Nanocarriers should recognize and bind to the target cells through ligand-receptor interactions, followed by internalization of targeted conjugates via receptor-mediated endocytosis.

The carrier coated inside endosomal pocket should be able to disintegrate and release the entrapped pDNA/siRNA by exploiting the acidic environment of the late endosomes. The disintegration process should commence before the lysosomal activity of the intracellular lysosome, which induces premature degradation or exocytosis of the complexes into the extracellular matrix. Surviving pDNA should be able to initiate transcription process inside the nuclear cavity while siRNA binds to its target mRNA within the cytoplasmic region of carcinoma cells. The safety profile of the NPs should bear no toxicity risk to the cells through the exclusion of genetic loads to evaluate the potential for treatment interference by salts dispositions. The safety features are highly

important to ensure safe gene transporter activity for future biological distributions.

In this study, the salt crystals fabricated based on Chapter 3 were individually evaluated in various intracellular experimentation to observe their carrier activities in improvising cellular uptake, pDNA expression, and siRNA knockdown activity. Additionally, each salt was recognized for its solubility features in the acidic environment, mimicking the late endosomic pH of 3.5. Herein, we demonstrated that selected barium and strontium salts efficiently adsorbed to the cellular surface, promoting better genetic expression of pDNA and silencing activity of siRNA complexes through solubilization of salt crystals in acidic pH. Crystal salts fabricated with Na_2CO_3 and Na_3PO_4 is associated with minimal nucleic activity throughout all observed salts owing to low cellular uptake. Cellular viability assay of salt crystals up to 72 hours presented consistently high cell density treated with selected strontium and magnesium salt particles in comparison with untreated control groups and CO_3 AP. High cytotoxicity was revealed with all barium salts treatment groups, demanding exclusion of the NPs for animal studies despite their effectiveness *in vitro*. Influence of transferrin and fibronectin protein in active targeting effect revealed their importance in further enhancing the cellular uptake and gene expression activity, via coating of protein ligands onto the selected salts, as performed in the earlier studies. Salt combination pursuit based on selected salts discovered almost similar in intracellular gene activity without adjunctive effect in comparison to individual salts.

The selected salts based on the exclusion criteria from various in vitro studies were $SrSO_3$, SrF_2, and $MgSO_3$, which will be applied and further elaborated *in vivo* in Chapter 5.

4.2 Methods and materials

4.2.1 Cellular uptake efficiency of NPs

MCF-7 and 4T1 cells from exponentially growth phase were seeded at 50,000 cells per well into 24-well plates the day before transfection. A total volume of 1ml from each type of NPs loaded with green fluorescence protein plasmid DNA (pGFP) (Addgene, USA) and supplemented with DMEM-powdered medium (Sigma-Aldrich, USA) was introduced into each well. 1µg pGFP was simultaneously added with propidium iodide (PI) (Sigma-Aldrich, USA) at 1:1 ratio, into 5µl of 1M $BaCl_2$, $SrCl_2$, $CaCl_2$, $MgCl_2$ or $FeCl_2$, followed by incorporation of 2µl of 1M Na_2SO_4, Na_2SO_3, NaF, Na_2CO_3 or Na_2PO_4 in 10µl HEPES-buffered solution (Sigma-Aldrich, USA) to generate respective salt precipitates (Table 4.1). The chemical reaction was maintained at 37^{o}C for 30 minutes, followed by mixing of DMEM medium to form a final volume of 1ml particle suspension. Analysis of cellular uptake efficiency with siRNA was performed by introduction of 10nM of AF 488 siRNA (Qiagen, Germany) to 5µl of 1M $BaCl_2$, $SrCl_2$, $CaCl_2$, $MgCl_2$ or $FeCl_2$ followed by incorporation of 2µl of 1M Na_2SO_4, Na_2SO_3, NaF, Na_2CO_3 or Na_2PO_4 in 10µl HEPES media, followed by incubation at 37^{o}C for 30 minutes. DMEM media was mixed into the precipitates to form 1ml final volume of salt suspension.

CO_3 AP, set as positive control for the studies was generated from addition of pGFP:PI and 5mM exogenous $CaCl_2$ sequentially into prepared DMEM medium, followed by incubation for 30 minutes at 37^{o}C and addition of 10% FBS to the suspension. The salt particles were incubated with seeded carcinoma cells for 4 hours,

prior to the salt removal and washing of the cells with 10mM EDTA in 1X PBS. Fluorescence microscopic observation (Olympus, Japan) was performed immediately after washing upon substitution of particulate-containing media with 100µl of serum-supplemented media.

Barium salt	Strontium salt	Calcium salt	Magnesium salt	Ferrous salt
$BaSO_4$	$SrSO_4$	$CaSO_3$	$MgSO_3$	$FeSO_3$
$BaSO_3$	$SrSO_3$	CaF_2	MgF_2	$FeCO_3$
BaF_2	SrF_2	$CaCO_3$	$MgCO_3$	$Fe_3(PO_4)_2$
$BaCO_3$	$SrCO_3$	$Ca_3(PO_4)_2$	$Mg_3(PO_4)_2$	
$Ba_3(PO_4)_2$	$Sr_3(PO_4)_2$			

Table 4.1 Salts experimented for cellular uptake activity of pDNA- and siRNA-loaded NPs

4.2.2 Cytotoxicity profiles of selected NPs

Cytotoxicity of NPs was determined by cell viability assay, following incubation of transfected cells for 24 to 72 hours. Selected salts from earlier studies were individually evaluated for cytotoxicity at different time point, based on the fraction of the viable cells using MTT solution. 5µl of 1M $BaCl_2$, $SrCl_2$ or $MgCl_2$ was incorporated into 2µl of 1M Na_2SO_4, Na_2SO_3 or NaF without nucleic acid. Fabricated NPs, following 30 minutes of incubation at 37^oC were treated onto MCF-7 and 4T1 cells, with CO_3 AP alongside as control. Absorbance of the resulting formazan solution was determined spectrophotometrically at 595 nm wavelength using microplate reader (Beckman Coulter, USA) with reference to 630 nm. Analysis was made using three independent results, expressed in graph as mean±SD of cell viability.

Salt	Regimen for analysis
$BaSO_3$	5µl of 1M $BaCl_2$, 2µl of 1M Na_2SO_3 in 10µl HEPES media, followed by addition of FBS-supplemented DMEM media to attain 1ml particle suspension
BaF_2	5µl of 1M $BaCl_2$, 2µl of 1M NaF in 10µl HEPES media, followed by addition of FBS-supplemented DMEM media to attain 1ml particle suspension
$SrSO_4$	5µl of 1M $SrCl_2$, 2µl of 1M Na_2SO_4 in 10µl HEPES media, followed by addition of FBS-supplemented DMEM media to attain 1ml particle suspension
$SrSO_3$	5µl of 1M $SrCl_2$, 2µl of 1M Na_2SO_3 in 10µl HEPES media, followed by addition of FBS-supplemented DMEM media to attain 1ml particle suspension
SrF_2	5µl of 1M $SrCl_2$, 2µl of 1M NaF in 10µl HEPES media, followed by addition of FBS-supplemented DMEM media to attain 1ml particle suspension
$MgSO_3$	5µl of 1M $MgCl_2$, 2µl of 1M Na_2SO_3 in 10µl HEPES media, followed by addition of FBS-supplemented DMEM media to attain 1ml particle suspension
CO_3 AP	44mM Na_2CO_3 and 5mM $CaCl_2$ added to DMEM media to achieve final volume of 1ml particle suspension with addition of 10% FBS

Table 4.2: Groupings for NPs cytotoxicity and solubility analysis

4.2.3 Gene expression activity of selected NPs

1ml suspension of each type of salt particles loaded with reporter genes, pGFP or luciferase reporter vector (pGL3) pDNA or target genes, p53 and supplemented with DMEM media, was introduced into each well containing approximately 50,000 MCF-7 or 4T1 cells seeded in the previous day. 1µg pGFP, pGL3 or p53 was mixed with 5µl of 1M $BaCl_2$, $SrCl_2$ or $MgCl_2$ before addition of 2µl of 1M Na_2SO_4, Na_2SO_3 or NaF to generate respective salt precipitates in 10µl HEPES media (Table 4.3). The chemical reaction was maintained at 37^{o}C for 30 minutes, followed by addition of serum-

supplemented DMEM media to achieve 1ml of salt suspensions. CO_3 AP as the positive control was prepared with the incorporation of pDNA and 5mM exogenous $CaCl_2$ into prepared DMEM media, and incubated at similar conditions prior to addition of 10% FBS to the suspension.

Each wells containing transfected cells was incubated for 4 hours, before removal of complexed media and brief washing with 10mM EDTA in 1X PBS upon substitution with 1ml serum-containing DMEM media. Subsequent incubation was maintained for 48 hours prior to observation of gene expression through fluorescence microscope (pGFP) and luciferase reporter assay (pGL3) using a commercial kit (Promega, USA) and photon counting (Beckman Coulter, USA). Quantitative luciferase assay was repeated thrice and expressed in a graph as mean±SD of luminescence activity/mg of protein.

For p53 gene expression activity, the addition of 50µl of MTT (5mg/ml in 1X PBS) (Sigma-Aldrich) to each treated wells was performed after 48 hours incubation to form formazan crystals by metabolically active cells. Media containing MTT was aspirated post 4 hours incubation, with formed formazan crystals in each well was dissolved by mixture of 300µl dimethyl sulfoxide (DMSO) (Sigma-Aldrich, USA) solution. Media containing only siRNA (no salt) represented the negative control for the study. Quantitative measurement of formazan crystals, in the form of optical density (OD), was presented at 595nm wavelength with reference to 630nm using microplate spectrophotometer (Biorad, USA).

Salt	Regimen for analysis
$BaSO_3$	5µl of 1M $BaCl_2$, 2µl of 1M Na_2SO_3, reporter pDNA (1µg pGFP or pGL3) or target gene (p53) added to 10µl HEPES media, prior to incubation, followed by addition of serum-supplemented DMEM media to achieve 1ml suspension
BaF_2	5µl of 1M $BaCl_2$, 2µl of 1M NaF, reporter pDNA (1µg pGFP or pGL3) or target gene (p53) added to 10µl HEPES media, prior to incubation, followed by addition of serum-supplemented DMEM media to achieve 1ml suspension
$SrSO_4$	5µl of 1M $SrCl_2$, 2µl of 1M Na_3SO_4, reporter pDNA (1µg pGFP or pGL3) or target gene (p53) added to 10µl HEPES media, prior to incubation, followed by addition of serum-supplemented DMEM media to achieve 1ml suspension
$SrSO_3$	5µl of 1M $SrCl_2$, 2µl of 1M Na_2SO_3, reporter pDNA (1µg pGFP or pGL3) or target gene (p53) added to 10µl HEPES media, prior to incubation, followed by addition of serum-supplemented DMEM media to achieve 1ml suspension
SrF_2	5µl of 1M $SrCl_2$, 2µl of 1M NaF, reporter pDNA (1µg pGFP or pGL3) or target gene (p53) added to 10µl HEPES media, prior to incubation, followed by addition of serum-supplemented DMEM media to achieve 1ml suspension
$MgSO_3$	5µl of 1M $MgCl_2$, 2µl of 1M Na_2SO_3, reporter pDNA (1µg pGFP or pGL3) or target gene (p53) added to 10µl HEPES media, prior to incubation, followed by addition of serum-supplemented DMEM media to achieve 1ml suspension
CO_3 AP	44mM Na_2CO_3, 5mM $CaCl_2$ reporter pDNA (1µg pGFP or pGL3) or target gene (p53), added to DMEM media, final volume of 1ml, addition of 10% FBS to achieve 1ml suspension

Table 4.3: Groupings for intracellular gene expression analysis with salt particles as vectors

4.2.4 siRNA silencing activity of selected NPs

Intracellular siRNA activity via selected salts was further elaborated through siRNA-loaded NC complexes. MAPK siRNA (Qiagen, USA) was incorporated into the proposed vectors to observe siRNA-induced knockdown activity upon treatment, following internalization of siRNA-particles complexes. 10nM MAPK siRNA was introduced to 5µl of 1M $BaCl_2$, $SrCl_2$ or $MgCl_2$ followed by incorporation of 2µl of 1M

Na_2SO_4, Na_2SO_3 or NaF in 10µl HEPES media, followed by incubation at 37°C for 30 minutes. DMEM media was mixed into the precipitates to form 1ml final volume of salt suspension. CO_3 AP as the positive control was prepared addition of MAPK siRNA and 5mM exogenous $CaCl_2$ to the DMEM-powdered media, with similar incubation order and addition of 10% FBS into the suspension. Incubation of transfected cells was maintained for 4 hours, followed by removal of media, cell washing with EDTA in 1X PBS and substitution with 1ml serum- supplemented DMEM media.

Subsequent incubation was performed for 48 hours, before addition of 50µl of MTT (5mg/ml in 1X PBS) (Sigma-Aldrich, USA) to each treated well to form formazan crystals by metabolically active cells. Medium containing MTT was aspirated post 4 hours incubation, with the formed formazan crystals in each well was dissolved by mixing with 300µl dimethyl sulfoxide (DMSO) (Sigma-Aldrich, USA) solution. Media containing only siRNA (no salt) represented the negative control for the study.

Quantitative measurement of formazan crystals, in the form of optical density (OD), was done at 595nm wavelength with reference to 630nm using microplate spectrophotometer (Biorad, USA). The cell viability of siRNA-loaded NCs and naked siRNA (without NCs) was calculated based on the equation:

$$\% \text{ cell viability: } \frac{OD_{\text{loaded NCs}} - OD_{\text{reference}}}{OD_{\text{naked siRNA}} - OD_{\text{reference}}} \times 100$$

Each experiments was done in triplicates and expressed in graph as mean±SD of cell viability.

Salt	Regimen for analysis
$BaSO_3$	5µl of 1M $BaCl_2$, 2µl of 1M Na_2SO_3 with 10nM MAPK siRNA added to 10µl HEPES media, prior to incubation, followed by addition of serum-supplemented DMEM media to achieve 1ml particle suspension
BaF_2	5µl of 1M $BaCl_2$, 2µl of 1M NaF with 10nM MAPK siRNA added to 10µl HEPES media, prior to incubation, followed by addition of serum-supplemented DMEM media to achieve 1ml particle suspension
$SrSO_4$	5µl of 1M $SrCl_2$, 2µl of 1M Na_2SO_4 with 10nM MAPK siRNA added to 10µl HEPES media, prior to incubation, followed by addition of serum-supplemented DMEM media to achieve 1ml particle suspension
$SrSO_3$	5µl of 1M $SrCl_2$, 2µl of 1M Na_2SO_3 with 10nM MAPK siRNA added to 10µl HEPES media, prior to incubation, followed by addition of serum-supplemented DMEM media to achieve 1ml particle suspension
SrF_2	5µl of 1M $SrCl_2$, 2µl of 1M NaF with 10nM MAPK siRNA added to 10µl HEPES media, prior to incubation, followed by addition of serum-supplemented DMEM media to achieve 1ml particle suspension
$MgSO_3$	5µl of 1M $MgCl_2$, 2µl of 1M Na_2SO_3 with 10nM MAPK siRNA added to 10µl HEPES media, prior to incubation, followed by addition of serum-supplemented DMEM media to achieve 1ml particle suspension of serum-supplemented DMEM media to 1ml
CO_3 AP	44mM Na_2CO_3, 5mM $CaCl_2$, 10nM MAPK siRNA added to DMEM media, final volume of 1ml with addition of 10% FBS

Table 4.4: Groupings for intracellular siRNA knockdown analysis with salt particles as vectors

4.2.5 Cell lysis, total protein estimation by Quick-start Bradford assay, SDS-PAGE and Western blot

MAPK-siRNA treated cells (as previous study) were individually lysed with IP lysis buffer (Appendix 1) and subjected to centrifugation process at 13,000 RPM for 20 minutes at 4^{o}C. Supernatant comprising protein sample was collected and 5µl was aspirated to estimate the total amount of proteins through bovine serum albumin (BSA)

assay kit based on the manual. In the initial step, BSA protein was used to create the standard curve, which was used to calculate the total protein concentration of cellular lysates, based on their absorbance intensities. The remaining samples were aliquoted and stored in -80^{o}C upon subsequent SDS-PAGE and Western blot.

The cellular lysates containing 30µg of total protein were mixed with 10µl of 10X loading dye (Appendix 2) and subjected to SDS-PAGE using stain free mini protein SFX gels (15 wells) in 1X running buffer (Appendix 3) at 0.01amp/gel. 7µl precision plus protein standards-dual color was used as molecular weight marker to establish the molecular weight of the sampled proteins. Transfer of protein samples from gel to the 0.2µm PVDF membranes attached to trans-blot turbo transfer pack through trans-blot turbo transfer system was performed for 7 minutes at 1.3 amp, followed by blocking in 5% skimmed milk in 1X TBST (Appendix 4) for 1 hour at room temperature. The membrane was next incubated with primary antibodies (pMAPK, TMAPK, pAKT, TAKT and GAPDH as loading reference) at 4^{o}C overnight with gentle shake followed by washing in 1X TBST for 5 times to remove unbound primary antibodies. HRP-conjugated goat anti-rabbit secondary antibody Ig G (1:3000) was introduced into the membrane for 1 hour with mild agitation, before washing for 5 times in 1X TBST to again eliminate the unbound antibodies.

The membrane was exposed to mixture of ECL (Appendix 5) for 5 minutes before observation of bands through chemiluminescence signals using XRS Chemidoc system (Bio-Rad, USA).

Name	Company	Molecular weight	Clonality	Antibody dilution
P-p44/42 MAPK	Cell signalling	44 kDa 42 kDa	Monoclonal	1:2000
p44/42 MAPK	Cell signalling	44 kDa 42 kDa	Monoclonal	1:1000
P-Akt (Ser473)	Cell signalling	60 kDa	Monoclonal	1:2000
Akt (pan)	Cell signalling	60kDa	Monoclonal	1:1000
GAPDH	Cell signalling	37kDa	Monoclonal	1:3000

Table 4.5: Antibodies used for Western blot analysis

4.2.6 Solubility of NPs in acidic environment

The solubility assessment of selected NPs in the acidic environment was determined over the introduction of hydrochloric acid (HCl) to propose the acidification process the crystal suspensions. HCl was integrated into the fabricated salt crystals (Table 4.2) to attain a gradual acidic pH from 7.5, 6.5, 5.5, 4.5 to 3.5. Each pH adjustment was escorted by absorbance measurement at 320nm wavelength (Spectrophotometer MS).

The experiment was performed in triplicates, expressed as mean±SD of absorbance.

4.2.7 Influence of protein coating on NPs-mediated gene delivery

Analysis on the impact of protein coating on transfection activity of NPs was made performed by incorporation of fibronectin or transferrin protein (Sigma-Aldrich, USA) onto selected fabricated NPs through incubation of 10 minutes, forming a coated layer on the particle surface. 1µg pGL3 was added to 5µl of 1M $BaCl_2$, $SrCl_2$ or $MgCl_2$ followed by incorporation of 2µl of 1M of Na_2SO_4, Na_2SO_3 or NaF in 10µl HEPES-buffered media, generating respective salt precipitates. The chemical reactions were sustained at 37^{o}C for 30 minutes, followed by the introduction of 1µM fibronectin or transferrin protein with incubation prolonged for 10 minutes, before final mixing of DMEM medium. The addition of protein to CO_3 AP particles was done followed by incubation for 10 minutes and subsequent supplementation of 10% FBS into the particle suspension.

Transfected MCF-7 and 4T1 cells with prepared complexes were incubated for 4 hours, followed replacement of treatment media with 1ml serum-supplemented DMEM media after washing with EDTA in 1X PBS. The cells were further cultured for 48 hours prior to luciferase expression by commercial kit and photon counting. The treated cells were lysed and centrifuged, followed by harvesting of supernatant from the lysate to investigate the intracellular luminescence intensity. The analysis was done based on triplicates, expressed in a graph as mean±SD of luminescence activity/mg of protein.

Salt	Regimen for analysis
$BaSO_3$	5µl of 1M $BaCl_2$, 2µl of 1M Na_2SO_3, in 10µl HEPES media, followed b addition of FBS-supplemented DMEM media to achieve 1ml
	5µl of 1M $BaCl_2$, 2µl of 1M Na_2SO_3, in 10µl HEPES media, followed by 1µg fibronectin and FBS-supplemented DMEM media to achieve 1ml
	5µl of 1M $BaCl_2$, 2µl of 1M Na_2SO_3, in 10µl HEPES media, followed by 1µg transferrin and FBS-supplemented DMEM media to achieve 1ml
BaF_2	5µl of 1M $BaCl_2$, 2µl of 1M NaF, in 10µl HEPES media, followed by addition of FBS-supplemented DMEM media to achieve 1ml
	5µl of 1M $BaCl_2$, 2µl of 1M NaF, in 10µl HEPES media, followed by 1µg fibronectin and FBS-supplemented DMEM media to achieve 1ml
	5µl of 1M $BaCl_2$, 2µl of 1M NaF, in 10µl HEPES media, followed by 1µg transferrin and FBS-supplemented DMEM media to achieve 1ml
$SrSO_4$	5µl of 1M $SrCl_2$, 2µl of 1M Na_2SO_4, in 10µl HEPES media, followed by addition of FBS-supplemented DMEM media to achieve 1ml
	5µl of 1M $SrCl_2$, 2µl of 1M Na_2SO_4, in 10µl HEPES media, followed by 1µg fibronectin and FBS-supplemented DMEM media to achieve 1ml
	5µl of 1M $SrCl_2$, 2µl of 1M Na_2SO_4, in 10µl HEPES media, followed by 1µg transferrin and FBS-supplemented DMEM media to achieve 1ml
$SrSO_3$	5µl of 1M $SrCl_2$, 2µl of 1M Na_2SO_3, in 10µl HEPES media, followed by addition of FBS-supplemented DMEM media to achieve 1ml
	5µl of 1M $SrCl_2$, 2µl of 1M Na_2SO_3, in 10µl HEPES media, followed by 1µg fibronectin and FBS-supplemented DMEM media to achieve 1ml
	5µl of 1M $SrCl_2$, 2µl of 1M Na_2SO_3, in 10µl HEPES media, followed by 1µg transferrin and FBS-supplemented DMEM media to achieve 1ml
SrF_2	5µl of 1M $SrCl_2$, 2µl of 1M NaF, in 10µl HEPES media, followed by addition of FBS-supplemented DMEM media to achieve 1ml
	5µl of 1M $SrCl_2$, 2µl of 1M NaF, in 10µl HEPES media, followed by 1µg fibronectin and FBS-supplemented DMEM media to achieve 1ml
	5µl of 1M $SrCl_2$, 2µl of 1M NaF, in 10µl HEPES media, followed by 1µg transferrin and FBS-supplemented DMEM media to achieve 1ml
$MgSO_3$	5µl of 1M $MgCl_2$, 2µl of 1M Na_2SO_3, in 10µl HEPES media, followed by addition of FBS-supplemented DMEM media to achieve 1ml
	5µl of 1M $MgCl_2$, 2µl of 1M Na_2SO_3, in 10µl HEPES media, followed by 1µg fibronectin and FBS-supplemented DMEM media to achieve 1ml
	5µl of 1M $MgCl_2$, 2µl of 1M Na_2SO_3, in 10µl HEPES media, followed by 1µg transferrin and FBS-supplemented DMEM media to achieve 1ml
CO_3 AP	44mM Na_2CO_3, 5mM $CaCl_2$ added to DMEM media to achieve final volume of 1ml with addition of 10% FBS
	44mM Na_2CO_3, 5mM $CaCl_2$ added to DMEM media to achieve final volume of 1ml with 1µg fibronectin addition of 10% FBS
	44mM Na_2CO_3, 5mM $CaCl_2$ added to DMEM media to achieve final volume of 1ml with 1µg transferrin addition of 10% FBS

Table 4.6: Groupings for influence of protein coating on NPs gene carrier activity

4.2.8 Effect of salt combination on NPs gene delivery

Quantitative experimental studies of salt combinations were executed by incorporation of two separate forms of selected inorganic salt particles, mixed and incubated at 37^{o}C for 30 minutes while maintained at pH 7.5. 500ng of pGL3 was incorporated into each selected inorganic salt (Table 4.7), before salt mixing and incubation for 10 minutes, before addition of serum-supplemented DMEM media to form a final volume of 1ml particle suspension for cellular transfection.

Treated MCF-7 and 4T1 cells were incubated for 4 hours, followed by replacement of treatment media with 1ml fresh serum-supplemented DMEM medium upon washing with EDTA in 1X PBS. The cells were further culturing for 48 hours and subsequent luciferase expression activity. Cells were lysed and centrifuged, followed by aspiration of the supernatant from the lysate for intracellular luminescence intensity observation via luminometer.

The analysis was performed in triplicates and expressed in a graph as mean±SD of luminescence activity/mg of proteins.

Group	Combination regimen
$BaSO_3$ + $SrSO_3$	[500ng pGL3 to 5µl of 1M $BaCl_2$ + 2µl of 1M Na_2SO_3 and 500ng pGL3 to 5µl of 1M $SrCl_2$ + 2µl of 1M of 1M Na_2SO_3] in 10µl HEPES buffered media, followed by addition of DMEM to achieve 1ml
$SrSO_3$ + SrF_2	[500ng pGL3 to 5µl of 1M $SrCl_2$ + 2µl of 1M of Na_2SO_3 and 500ng pGL3 to 5µl of 1M $SrCl_2$ + 2µl of 1M NaF] in 10µl HEPES buffered media, followed by addition of DMEM to achieve 1ml
$SrSO_3$ + $MgSO_3$	[500ng pGL3 to 5µl of 1M $SrCl_2$ + 2µl of 1M Na_2SO_3 and 500ng pGL3 to 5µl of 1M $MgCl_2$ + 2µl of 1M Na_2SO_3] in 10µl HEPES buffered media, followed by addition of DMEM to achieve 1ml
SrF_2 + BaF_2	[500ng pGL3 to 5µl of 1M $SrCl_2$ + 2µl of 1M NaF and 500ng pGL3 to 5µl of 1M $BaCl_2$ + 2µl of 1M NaF] in 10µl HEPES buffered media, followed by addition of DMEM to achieve 1ml
$BaSO_3$ + $MgSO_3$	[500ng pGL3 to 5µl of 1M $BaCl_2$ + 2µl of 1M Na_2SO_3 and 500ng pGL3 to 5µl of 1M $MgCl_2$ + 2µl of 1M Na_2SO_3] in 10µl HEPES buffered media, followed by addition of DMEM to achieve 1ml

Table 4.7: Combination salt regimen through mixing of two salt precipitates

4.3 Results

4.3.1 Cellular uptake efficiency of NPs

Cellular uptake activity of pGFP-bound NPs was determined through microscopic observation of pGFP-NPs, with free pGFP and unloaded NPs serving as negative control. MCF-7 cells treated with free pGFP and vacated NPs both showed no fluorescence activity following 4 hours of incubation. Transfected cells with PI-labeled pDNA-NPs demonstrated high fluorescence intensity upon washing with 10mM EDTA in 1X PBS (Figure 4.1). $SrSO_3$-transfected cells are associated with superior fluorescence activity, visualized in MCF-7 cells. Additionally, barium, strontium, and

magnesium salt crystals revealed a better cellular uptake activity, especially with $BaSO_4$, $BaSO_3$, BaF_2, $SrSO_4$, $SrSO_3$, SrF_2 and $MgSO_3$ with comparable fluorescence detection in those of CO_3 AP, in comparison to calcium and ferrous salts. Similarly, AF 488 fluorescence siRNA-particles complexes treated cells (Figure 4.2) revealed enhanced fluorescence activity with barium, strontium and magnesium transporter complexes, highest seen with $SrSO_3$. The cellular uptake efficiency of $SrSO_3$ was comparable with CO_3 AP, known efficient nanocarrier. High cellular uptake of siRNA–transfected NPs studies on human breast carcinoma cells was further seen with $BaSO_4$, $BaSO_3$, BaF_2, $SrSO_4$, $SrSO_3$, SrF_2 and $MgSO_3$ NPs.

Incorporation of Na_2CO_3 and Na_3PO_4 into particle complexes revealed no intracellular fluorescence activity of both pDNA and siRNA, signifying low uptake of nucleic acid salt crystals into MCF-7 cells, excluding $SrCO_3$ particles. Furthermore, no fluorescence intensified cells seen post-ferrous salts treatment suggesting insignificant cellular internalization of nucleic acid salt particles.

Based on the nucleic acid –salt transfection activity, we have concluded the salts which are likely to succeed in *in vitro* studies and hence will be our focus for the subsequent experiments: $BaSO_3$, BaF_2, $SrSO_4$, $SrSO_3$, SrF_2, and $MgSO_3$.

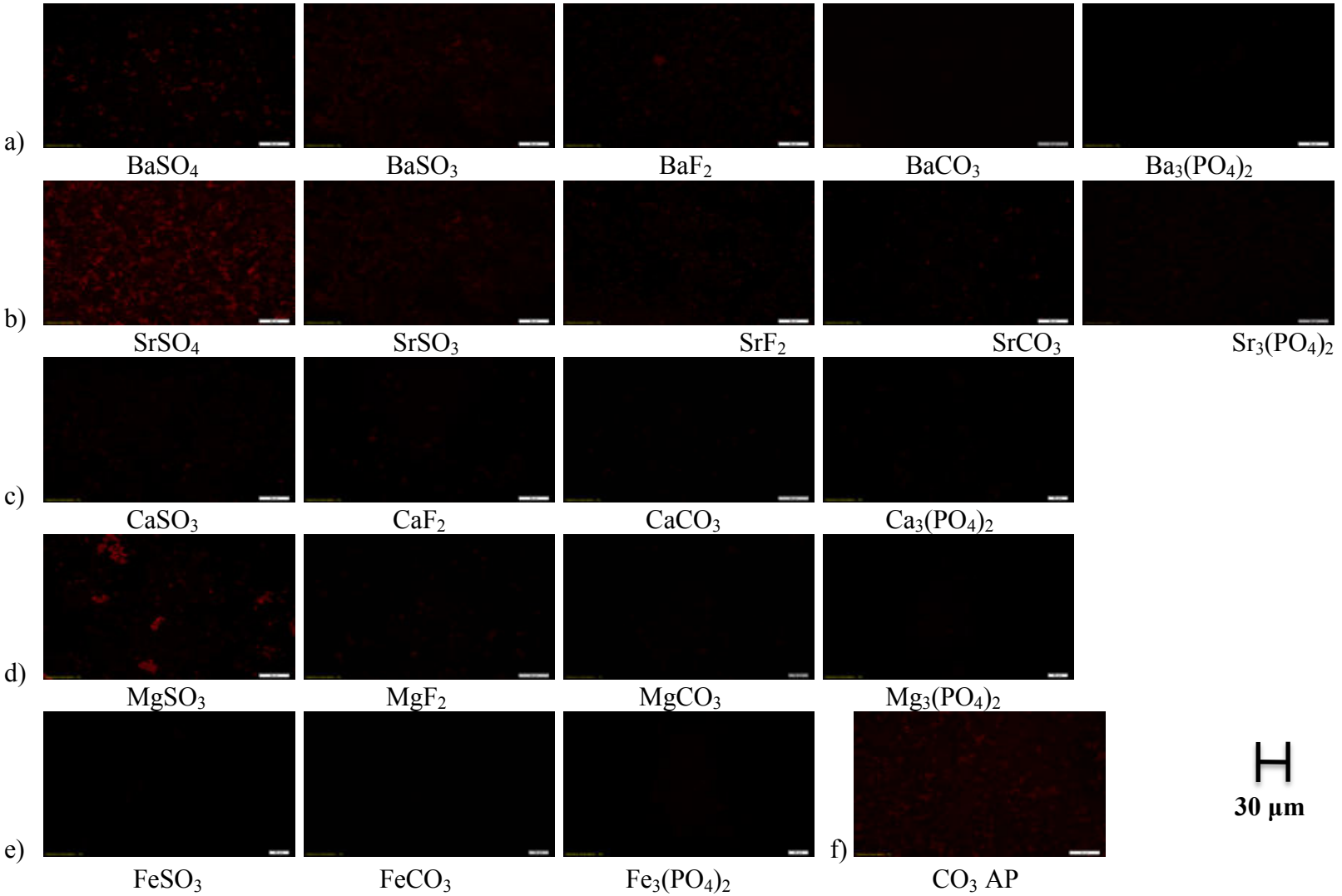

Figure 4.1: Fluorescence microscopic images of cellular uptake with pGFP-loaded NPs by MCF-7 cells. Each type of pGFP-NPs complexes was transferred onto 50,000 seeded cells, followed by incubation for 4 hours. Images were captured upon washing with EDTA in 1X PBS. (a) barium NPs, (b) strontium NPs, (c) calcium NPs, (d) magnesium NPs, (e) ferrous NPs and (f) CO_3 AP NP

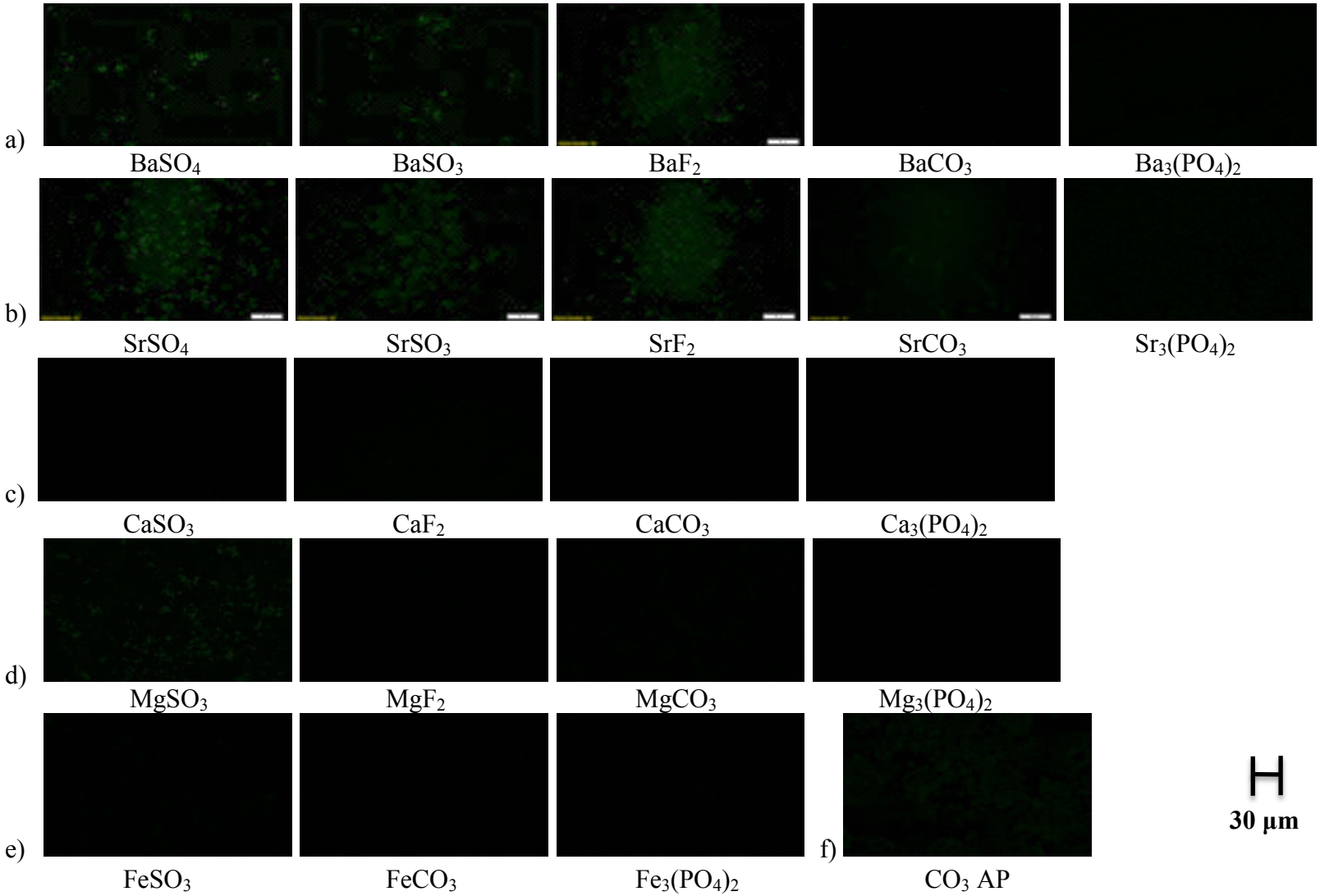

Figure 4.2: Fluorescence microscopic images of cellular uptake with AF 488 siRNA-loaded NPs by MCF-7 cells. Each type of siRNA-NPs complexes was transferred onto 50,000 seeded cells, followed by incubation for 4 hours. Images were captured upon washing with EDTA in 1X PBS. (a) barium NPs, (b) strontium NPs, (c) calcium NPs, (d) magnesium NPs, (e) ferrous NPs and (f) CO_3 AP NP

4.3.2 Cytotoxicity profile of selected NPs

Cytotoxicity studies of NPs were evaluated based on MTT assay, without genetic load incorporation into the complexes. Selected salts based on earlier cellular uptake study were individually used to treat MCf-7 and 4T1 cells for 24 to 72 hours. Untreated cells were set as a control (100% of viability) at each different time point (not included in the graph).

Approximately 50-80% surviving viable cells were seen upon treatment with $BaSO_3$ and BaF_2 for 24 hours, determining high cellular toxicity with salts exposure. Additionally, $BaSO_3$ and BaF_2 on MCF-7 cells were associated with a superior cytotoxicity compared to that in 4T1 cells. The viability of cells, however, rose after 48 to 72 hours of incubation. Strontium salt crystals demonstrated significantly high cell viability in both cells lines at 24 hours, ranging from 110% to 140%, with viability remaining eminent on day 3, ranging from 90% to 95%. $MgSO_3$ treatment showed almost similar cell viability as untreated cells (100%), with low cytotoxicity of 5% to 10% cellular death on day 3, which was comparable to the cells treated with CO_3 AP.

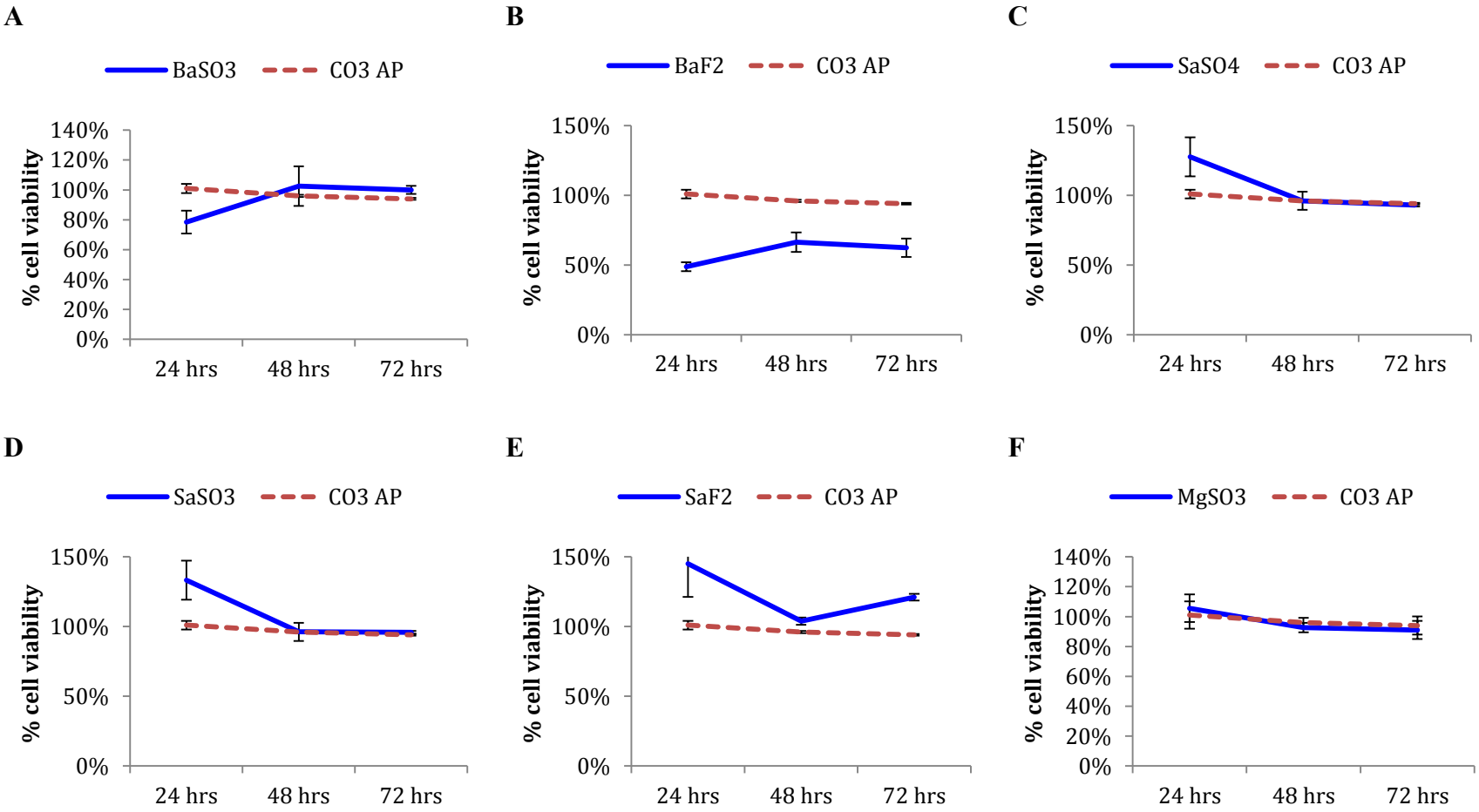

Figure 4.3: Cytotoxicity of selected salts on MCF-7 cells. 50,000 of MCF-7 cells were seeded, treated with NPs and incubated for 24 to 72 hours, with media substitution following first 4 hours of incubation. Subsequently, 50µl of MTT was incorporated into the treated cells, with media containing MTT aspirated after 4 hours incubation and addition of 300µl DMSO. Spectrophotometric reading of viable cells was observed at 595nm wavelength with reference of 630nm. Each type of salts was individually compared with CO_3 AP.

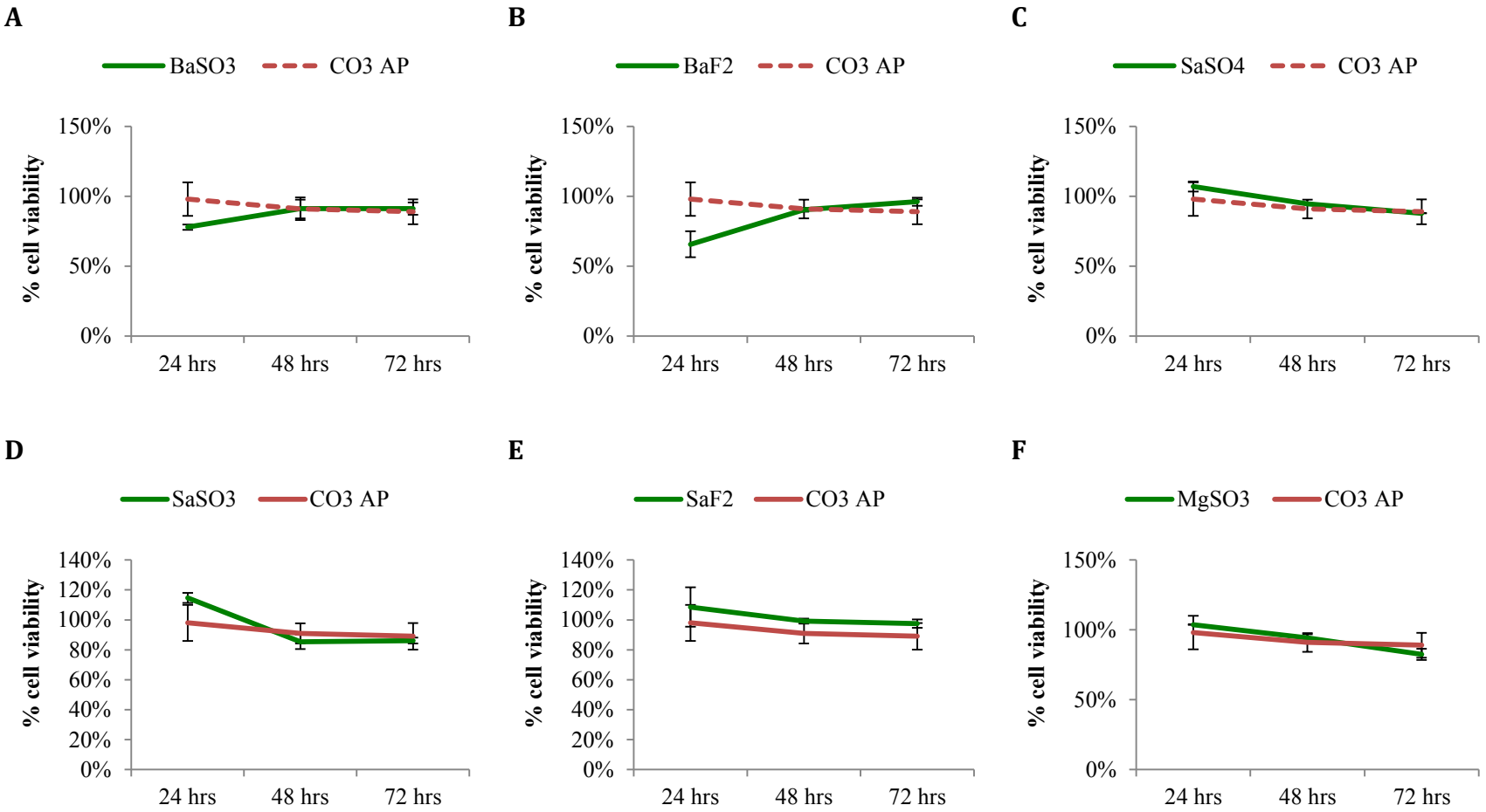

Figure 4.4: Cytotoxicity of selected salts on 4T1 cells. 50,000 of 4T1 cells were seeded, treated with the NPs and incubated from 24 to 72 hours, with media substitution following first 4 hours of incubation. Subsequently, 50µl of MTT was incorporated into the treated cells, with media containing MTT aspirated after 4 hours incubation and addition of 300µl DMSO. Spectrophotometric reading of viable cells was observed at 595nm wavelength with reference of 630nm. Each type of salts was individually compared with CO_3 AP.

4.3.3 Gene expression activity of selected NPs

Qualitative images to observe the impact of gene-loaded particle complexes was microscopically visualized following 48 hours of incubation, via intensity of the fluorescence emitted by pGFP-NPs-transfected cells under fluorescence microscope. Gene expression activity was determined by fluorescence-expressing cells, with reference to naked pGFP and unloaded NPs. It was revealed that cells treated with naked pGFP or unloaded NPs (Appendix 7) did not show any fluorescence activity after 48 hours of incubation. MCF-7 cells were seen GFP-positive following intracellular delivery of pGFP using the NPs of selected salts, $BaSO_3$, BaF_2, $SrSO_4$, $SrSO_3$, SrF_2 and $MgSO_3$, with reference to CO_3 AP (Figure 4.3). Similar observation on the remaining 14 salts from the earlier study revealed null cellular fluorescence intensity with exception of $BaSO_4$, implying the possibility of inefficient gene expression with association to low cellular uptake activity (Appendix 7).

Efficiency of salt crystals was further explored with incorporation of luciferase reporter gene pDNA, pGL3 into the crystals complexes, releasing intracellular luminescence activity upon successful transcription inside the nucleus. High level of bioluminescence intensity was emitted by different mammary carcinoma cells, MCF-7 and 4T1 cells transfected with pGL3-loaded $BaSO_3$, BaF_2, $SrSO_4$, $SrSO_3$, SrF_2 and $MgSO_3$ NPs. 4T1 cells showed slightly higher detection of luciferase expression upon treatment of gene-NP complexes in comparison with MCF-7 cells, similarly seen with CO_3 AP possibly due to inherent variability in light emission (Figure 4.4). Maximum emission of cellular luminescence activity was identified with pGL3-loaded SrF_2, with 2 folds gap in RLU/mg protein with $SrSO_4$ and CO_3 AP. Additionally, strontium salts demonstrated a superior

activity in comparison to barium and magnesium salts. Salts structured by NaF revealed greater luminescence emission in comparison to other anion-providing salts. Further exploration on the remaining 14 salts showed low cellular luciferase activity, with approximately 100 times less than SrF_2, with exception of $BaSO_4$ with comparable luminescence intensity, with selected salts.

Effect of p53 loading in the selected nanocarriers was explained with cell viability assay. Based on Figure 4.5, direct delivery of p53 gene into the cells led to inefficient cytotoxicity in both types of mammary carcinoma cells upon 48 hours of incubation, which might be influenced by low cellular uptake of the naked plasmid via passive diffusion. However, complexed p53 plasmid with selected salts showed variations in percentage of cell viability. Treated MCF-7 and 4T1 cells demonstrated more than 90% of cell death with p53-loaded BaF_2 or $MgSO_3$, which is 5 times greater than CO_3 AP. Cell death was more prominent with barium particles in comparison with strontium particles, possibly owing to the toxicity effect of barium salts. All selected salts conferred greater cytotoxicity effect on both tumor cells in comparison to CO_3 AP, suggesting their potential applications in cancer gene therapy *in vivo*.

All selected salts were found associated with an improved gene system based on various qualitative and quantitative experimentations, as compared to the established delivery system of CO_3 AP. Despite its involvement with excellent gene delivery activity, $BaSO_4$ will not be further investigated for *in vivo* application due to its large particle size (explained in Chapter 3).

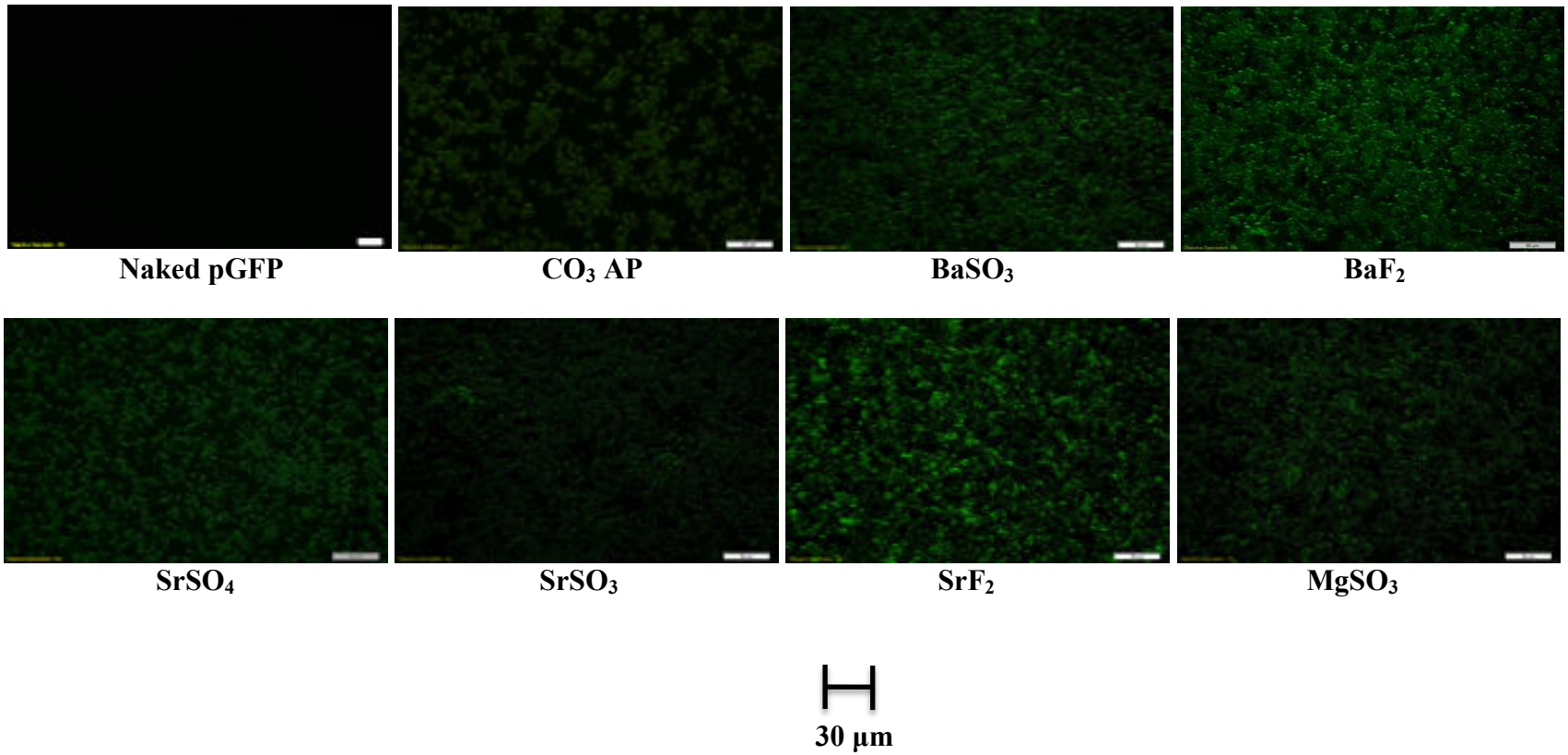

Figure 4.5: Fluorescence microscopic images of gene expression activity of pGFP-NPs in MCF-7 cells. Each type of pGFP-loaded selected NP complexes, $BaSO_3$, BaF_2, $SrSO_4$, $SrSO_3$, SrF_2 and $MgSO_3$, in addition to naked pGFP and CO_3 AP as control, was used to transfect seeded MCF-7 cells, which were subsequently incubated for 4 hours and washed with 10mM EDTA in 1X PBS, followed with 2nd incubation period of 48 hours and observation under FITC-filtered fluorescence microscope.

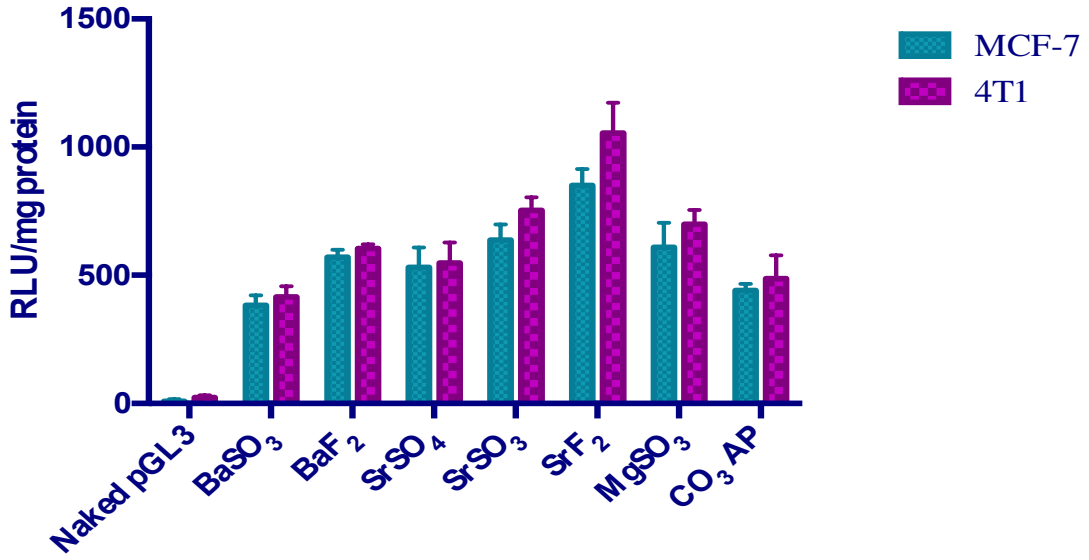

Figure 4.6: Luminescence intensity of pGL3-complexed NPs treated with MCF-7 and 4T1 cells. Each type of pGL3-loaded selected salts, $BaSO_3$, BaF_2, $SrSO_4$, $SrSO_3$, SrF_2 and $MgSO_3$ was transferred into prepared wells containing seeded 50,000 MCF-7 or 4T1 cells and incubated for 48 hours, with serum-supplemented media substitution following first 4 hours of incubation and treatment with 5mM EDTA in 1X PBS. The transfected cells were lysed after the removal of media, followed by lysate centrifugation at 15,000 RPM at 4°C for 10 minutes. 100µl supernatant was aspirated for estimation of relative luminescence activity/mg of protein.

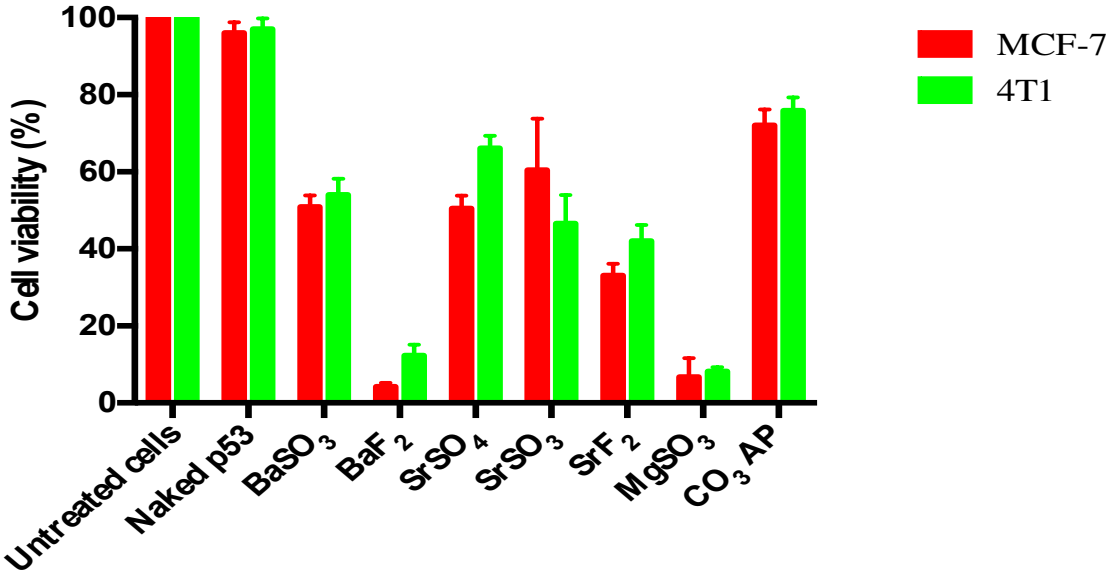

Figure 4.7: MCF-7 and 4T1 cell viability upon treatment with p53-NP complexes. Each type of p53-loaded selected salts, $BaSO_3$, BaF_2, $SrSO_4$, $SrSO_3$, SrF_2 and $MgSO_3$ with reference to CO_3 AP, was transferred into prepared wells containing seeded 50,000 cells and incubated for 48 hours, with serum-supplemented media substitution following first 4 hours of incubation and treatment with 5mM EDTA in 1X PBS. Subsequently, 50µl of MTT was incorporated into the treated cells, with media containing MTT aspirated after 4 hours incubation and addition of 300µl DMSO. Spectrophotometric reading of viable cells was performed at 595nm wavelength with reference of 630nm.

4.3.4 siRNA silencing activity of selected NPs

Knockdown of MAPK gene expression in MCF-7 and 4T1 cells with MAPK siRNA was investigated for 48 hours, revealing a reduction in cell viability. MAPK siRNA loaded with selected salts showed lower cell viability in comparison with naked siRNA, hence proving the selected salts as potential nano-vectors. Effect of siRNA-loaded NP complexes on cytotoxicity was more noticeable with MCF-7 cells, based on higher cellular death in comparison to 4T1 cells, as shown in Figure 4.6. siRNA loaded into $MgSO_3$ demonstrated high efficacy in stimulating cytotoxicity, with <10% of cell viability of both tumor cells lines. $SrSO_4$ revealed minimal cellular toxicity, of approximately 20% in both cell lines, which was lowest amongst the selected experimental salts. Cytotoxicity was more prominent with the salt crystals containing SO_3^{2-} than those having SO_4^{2-} and F^{--}. Most salts are associated with greater cytotoxicity upon treatment with cells than CO_3 AP, with exception to $SrSO_4$.

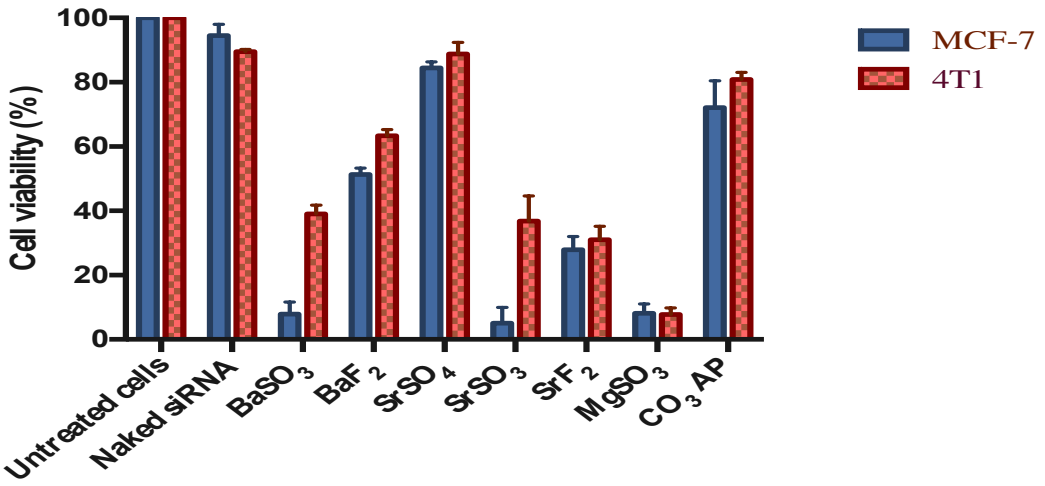

Figure 4.8: MCF-7 and 4T1 cell viability upon treatment of siRNA-loaded NPs. Each MAPK siRNA-loaded selected salts with reference to CO_3 AP was transferred into the cells and incubated for 48 hours, with serum-supplemented media substitution following first 4 hours of incubation and treatment with 5mM EDTA in 1X PBS. Subsequently, 50µl of MTT was incorporated into the cells 4 hours before media removal and addition of 300µl DMSO. Spectrophotometric reading of viable cells was observed at 595nm wavelength with reference of 630nm.

4.3.5 Cell lysis, total protein estimation by Quick-start Bradford assay, SDS-PAGE and Western blot

Assessment of MAPK expression was further observed through Western blot analysis of MAPK-siRNA-treated MCF-7 and 4T1 cells with and without the involvement of nanocarriers. We have selected three salts for this study, $SrSO_3$, SrF_2, and $MgSO_3$ based on earlier experiments involving cytotoxicity and nucleic acid transporting efficacy evaluation. The analysis was performed to detect the endogenous activity of phosphorylated-p44/42 MAPK (phospho-MAPK), p44,42 MAPK (total-MAPK), phosphorylated-Akt (Ser473) and Akt (pan), with reference to GAPDH genes. Based on Figure 4.7, siRNA-loaded SrSO3 and SrF2 demonstrated low band intensity of 44/42kDa of MAPK, which thus interferes with p44/42-MAPK in treated MCF-7 cells. Additionally, $SrSO_3$ and SrF_2 also interfered with expression of p44/42 MAPK, p-Akt and Akt genes, predominantly seen with SrF_2. $MgSO_3$ and CO_3 AP showed lower interruption on protein expression, with a slight reduction in band intensity. Unloaded NPs revealed thick band manifestation throughout the analysis in reference to untreated cells.

Interruption of the expression activity of p44/42 MAPK and Akt genes was detected with MAPK siRNA-loaded $SrSO_3$ and SrF_2 complexes in 4T1 cells. The detection of the endogenous activity of proteins was slightly greater in comparison with MCF-7 cells. Additionally, the band depth was stagnant for p44/42 MAPK, signifying no interruption on the total MAPK expression. Delivery of $MgSO_3$ and CO_3 AP complexed with the siRNA also showed lesser band intensities in comparison with only

salt particles treatments. Investigation on GAPDH protein showed no changes in the thickness of observed bands.

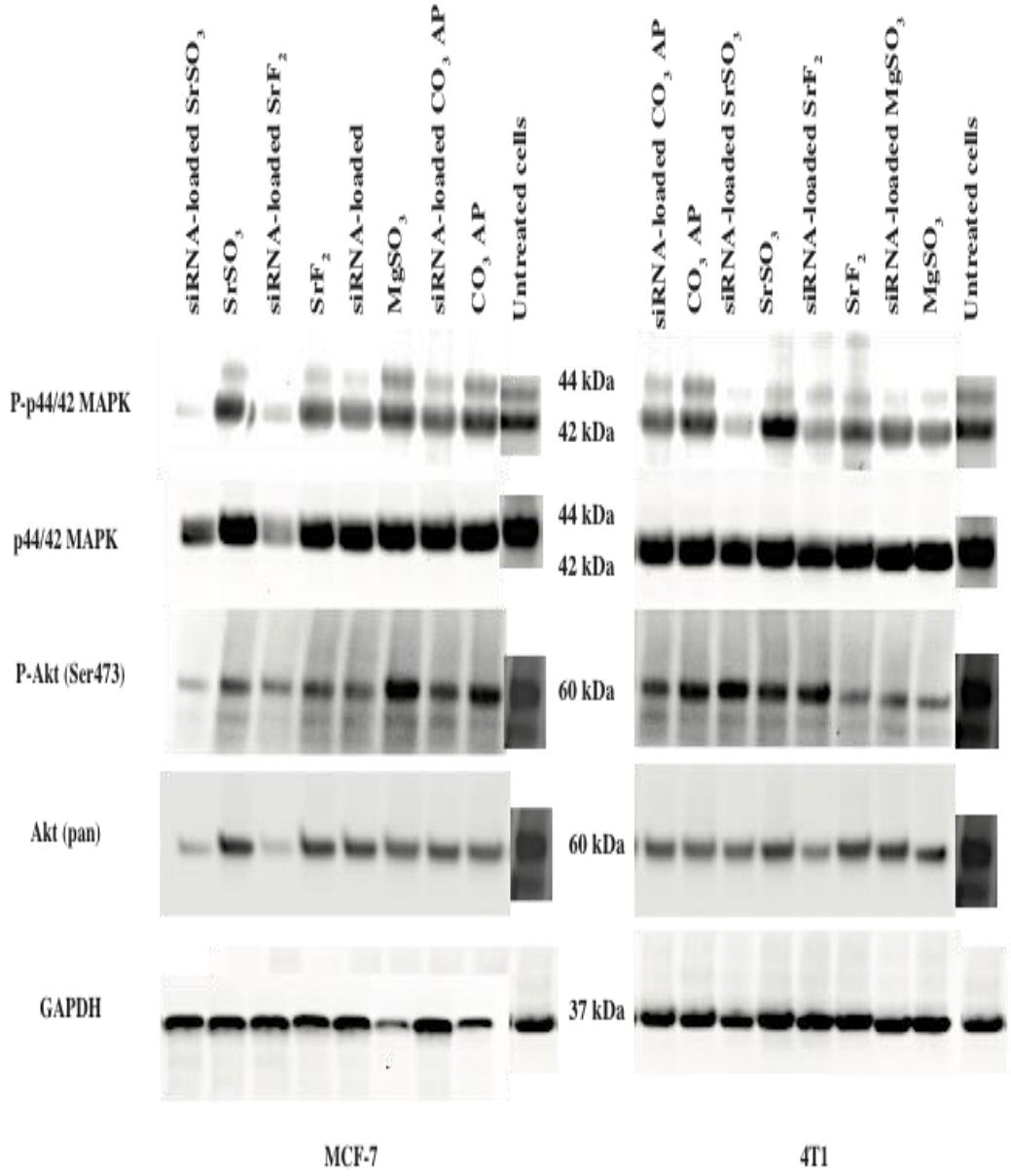

Figure 4.9: MAPK protein expressions following treatment with MAPK-siRNA loaded NPs in MCF-7 and 4T1 cells. Proteins obtained from collected lysates were run in SDS-PAGE and transferred to PVDF membrane, followed by incubation with primary antibodies raised in rabbit against (a) phospho-p44/42 MAPK (b) p42/42 MAPK (c) phospho-Akt (Ser473) and (d) Akt (pan). HRP-conjugated goat anti-rabbit secondary antibody was used to detect the chemiluminescence signals. Predicted bands for pMAPK, TMAPK, pAkt and TAkt are at 44, 42 and 60kDa, respectively. GAPDH was used as loading marker with bands achieved at 37kDa.

4.3.6 Solubility of NPs in acidic environment

Dissolution of salt particles upon exposure to the acidic environment was demonstrated by adjustment of pH in the suspensions of formed NPs complexes, with CO_3 AP representing the positive control. From the initial pH of 7.5 (in which salt crystals were formed), spectrophotometric reading revealed efficient dissolution of BaF_2, $SrSO_3$, SrF_2 and $MgSO_3$, as seen by a gradual decline of the absorbance intensity, followed by total crystals dissolution at pH 4.5, which was demonstrated by null spectrophotometric reading (Figure 4.8). $BaSO_3$ and $SrSO_4$ showed a decrease in solubility upon gradual reduction in pH but were not fully dissolvable, seen with high absorbance data in comparison with other salt crystals and CO_3 AP.

4.3.7 Influence of protein coating on NPs-mediated gene delivery

The outcome of intracellular gene activity as a result of transferrin or fibronectin coating of NPs was demonstrated in both human and mice mammary carcinoma models, based on luminescence intensity/mg of protein after 48 hours of incubation period. Both proteins predominantly fibronectin significantly improved the bioluminescence activity through complexion onto NPs surface (Figure 4.9). Greater cellular luminescence intensity was associated with strontium and magnesium salts, with minimal 10-fold augmentation in both cell lines. Fibronectin-coated salts showed the highest enhancement in RLU/mg of protein with 100X increment seen with $SrSO_4$ and $MgSO_3$ in MCF-7 and 4T1 cells. Protein coating stimulated minimal improvement in $BaSO_3$ particles transfection of both cell lines, as similarly seen with CO_3 AP. The importance of protein binding in improving cellular internalization of particles complexes is thus

realised *in vitro*, which will be further studied in the animal model in Chapter 5 for enhancement of nucleic acid delivery in *in vivo* application.

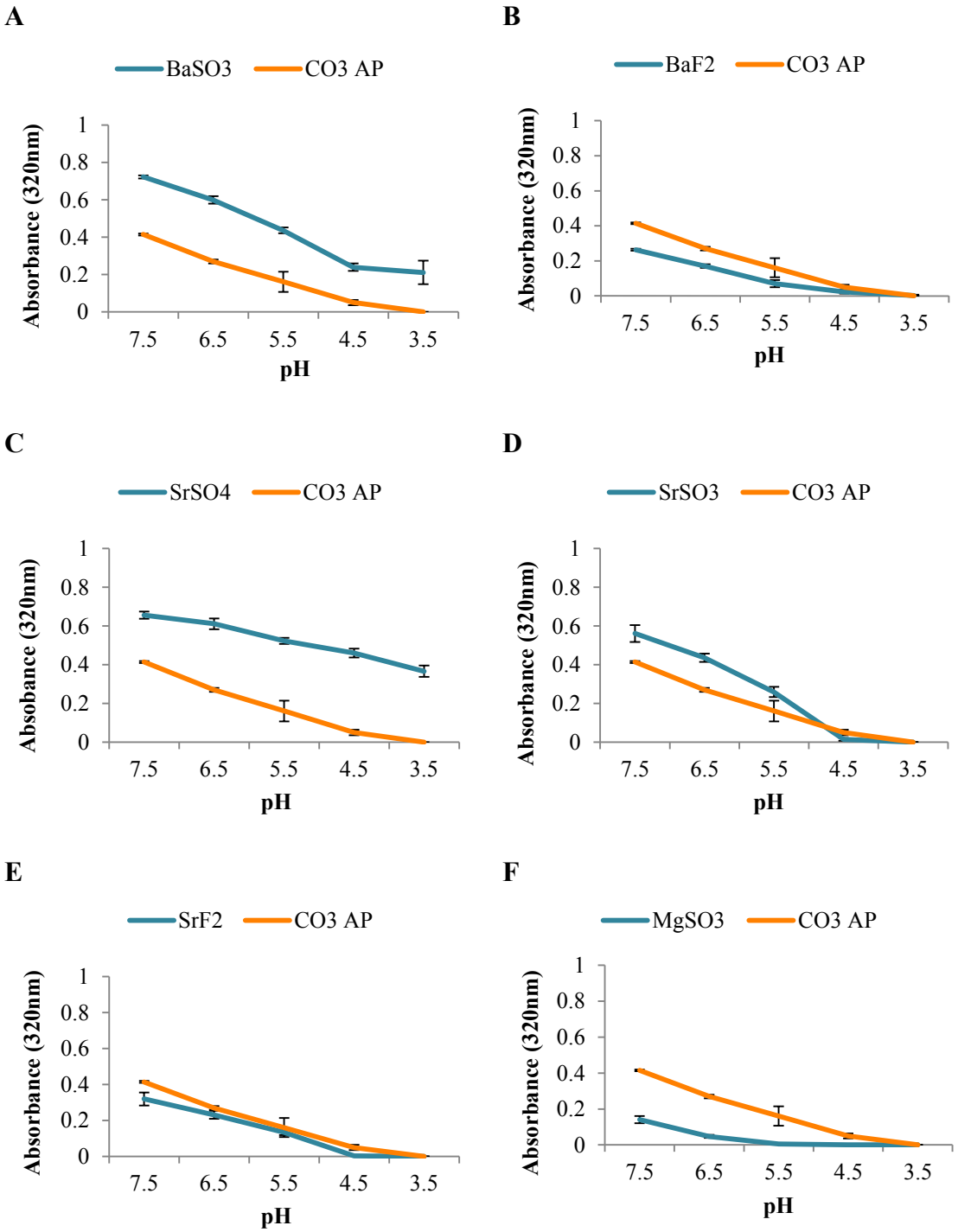

Figure 4.10: Dissolution of selected salt particles at acidic pH. HCl was incorporated into the prepared particle suspension following incubation at 37°C for 30 minutes to achieve pH, of 6.5, 5.5, 4.4 and 3.5. Spectrophotometric reading of suspension was observed at 340nm wavelength.

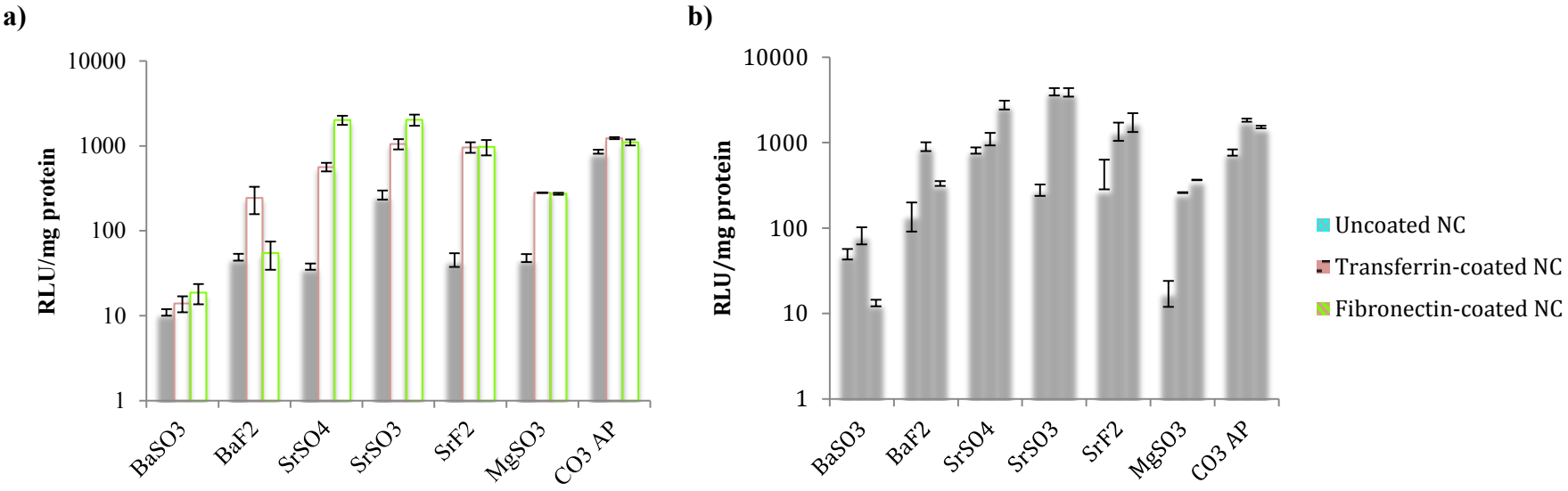

Figure 4.11: Influence of protein coating on luminescence intensity in a) MCF-7 and b) 4T1 cells. 1µg transferrin or fibronectin was introduced into prepared pGL3-loaded selected salt crystals with reference to CO_3 AP after 30 minutes incubation at 37°C. Coated salt particles were subsequently incubated for 10 minutes, followed by inclusion of FBS-containing media to achieve final volume of 1ml particle suspension. The salt complexes were used to transfect into the tumor cells and incubated for 48 hours, with serum-supplemented media substitution following first 4 hours of incubation. Cells were lysed after removal of media, and the remaining lysate was centrifuged to obtain the supernatant, which was used to measure the relative luminescence activity (RLU) of the treated cells.

4.3.8 Effect of salt combination on NPs-mediated gene delivery

The combination of two potential inorganic salts was experimented for possible synergistic effect on gene delivery. Inorganic salts with efficient nucleic acid binding and cellular uptake abilities with minimal cytotoxicity effects were selected for salt combinations studies. According to Figure 4.10, the mixture of potential salt crystals was associated with no synergistic effect on luciferase activity in both MCF-7 and 4T1 cells. SrF_2/BaF_2 salt particles mixture showed similar luminescence activity with BaF_2 in MCF-7 cells but with ten-fold reduction seen in 4T1 cells. Additionally, $SrSO_3$/SrF_2 combination revealed inferior intracellular luminescence intensity in comparison to individual salt, with >10 fold reduction in 4T1 cells. A slight increase of cellular luciferase activity was seen with SrF_2/$MgSO_3$ in 4T1 cells, compared to the individual salts but the activity remained lower than single salt particles in MCF-7 cells.

The salt combination showed overall no beneficial effect on improving luciferase activity and will thus be excluded from the investigation in animal study (Chapter 5).

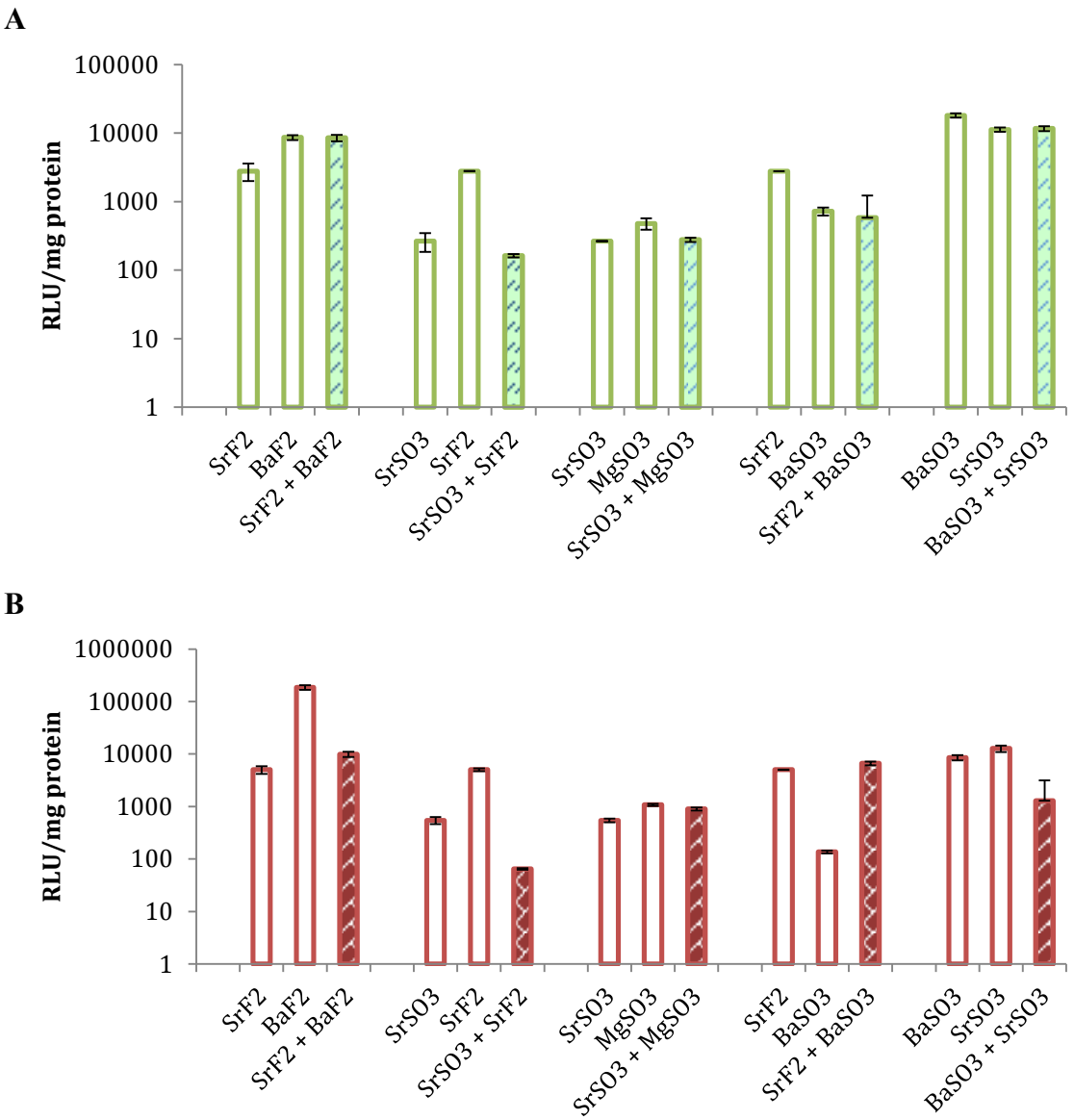

Figure 4.12: Comparison between single and combinations of salt particles on intracellular luminescence activity in (A) MCF-7 and (B) 4T1 cells. Generation of single salt was based on reaction between $BaCl_2$, $SrCl_2$ or $MgCl_2$, and Na_2SO_3 or NaF with incorporation of 1µg pGL3, followed by incubation of 30 minutes at 37°C. Formation of salt combination was based on mixing of two insoluble salts generated with 500ng pGL3 incorporated into each type of insoluble salts prior to mixing, followed by 10 minutes incubation. Serum-supplemented media was added to both NP complexes to achieve final volume of 1ml suspension. Transfected cells were incubated for 48 hours before cellular lysis and centrifugation to obtain the supernatant, followed by measurement of relative luminescence activity (RLU) of treated cells/mg protein.

4.4 Discussions

An ideal salt complex should be associated with efficient cellular uptake, which is dependent on the complex salt size and electrostatic interaction between the negatively charged anionic heparan sulfate proteoglycans (syndecans) of cellular surface and the complex (1). The NP sizes determine the endocytic pathways for transportation into the intracellular matrix. The route of biomaterial internalization is commonly through clathrin- or caveolin-mediated endocytosis, an energy-dependent process (2). Most cell types utilize these pathways to transport nanosize materials, including nanoparticles and viruses (3). Caveolae-dependent endocytosis promotes uptake of molecules ranging from 50 to 80nm in diameter through small invaginations of the plasma membrane. Clathrin-coated vesicles mediate transportation of larger molecules, subsequently followed by formation of early endosomes (4)(5). It is postulated that NPs are commonly engulfed through clathrin-mediated endocytosis in mammalian cells (6).

Efficient cellular uptake activity is therefore associated with small particle sizes (<400nm) and positive zeta charge activity, which is involved in the electrostatic interaction between cellular membranes, prompting effective internalization (7). Barium, strontium and magnesium salt particles revealed efficient cellular uptake, defined by fluorescent cells upon endocytosis of fluorescence pDNA/siRNA-complexes. Washing of cells with EDTA in PBS was vital to remove crystals depositions on the cellular surface and eliminate false positive results. PI-stained pGFP ensures stained pDNA-complexes inside the endosomal cavity as the reporter gene

requires approximately 16 hours to undergo transcription and translation in the transfected cells to emit fluorescence for microscopic visualization (8)(9). $BaSO_3$, BaF_2, $SrSO_4$, $SrSO_3$, SrF_2 and $MgSO_3$ most significantly improved the intracellular delivery of both pDNA and siRNA in comparison to naked pDNA and siRNA based on their efficiency in binding and condensing the genetic material to form a compacted structure (10). Low fluorescence intensity of the cells treated with calcium and ferrous salts was possibly related to low pDNA and siRNA adsorption to the crystals, (11) as described in Chapter 3. Efficient cellular uptake might further regulate the outcome of the subsequent intracellular processing of nucleic acid inside the cytoplasmic or nuclear regions, such as endosomal escape and nuclear translocation (12).

Cytotoxicity profiles of the selected nanocrystals determined by MTT assay revealed a decline in cell viability with barium-fabricated particles at 24 hours post treatment. The role of barium salt as a physiological antagonist of potassium, increases active influx and inhibiting efflux of potassium, by blocking potassium channels of the Na-K pump in the cell membrane, resulting in cell death. Barium-induced cell damage is proportional to the barium salt concentration (13). The cytotoxicity effect of barium proves to be unsafe for the upcoming animal studies, which was prominent during the first 24 hours of incubation, but later masked by cell replication after 27 hours (14). High cell viability of strontium NPs is postulated due to its protective effect on apoptosis. Strontium increases ERK 1/2 phosphorylation to promote cellular proliferation in addition to activation of Akt pro-survival pathway, enhancing the cell viability (15). $MgSO_3$ has minimal intrusion on cellular volume, with minute changes in viability of cells at 72 hours. The ideal NPs should exert minimal influence on cellular

activity to prevent off-target effect (16). In spite of efficaciousness in cellular uptake, dissolution, and expression, the toxicity of barium salt particles might stimulate undesirable cellular death, and hence seem to be dangerous for *in vivo* studies (17). Besides the selected salts, other formulations were also experimented to observe their toxicity ranges, with ferrous-salt particles found to be involved in a very prominent cellular death, causing >60% reduction in cell viability in comparison with non-treated cells (Appendix 14). Higher iron concentration is linked with free radical formation and oxidative damage, hence inducing autophagic cell death (18).

Genetic expression of pDNA and siRNA knockdown activity may occur upon successful internalization of the NPs complexes. Embodied particle complexes, forming endosomes should efficiently disintegrate to release the genetic content from degenerated crystals, followed by subsequent transportation to the areas of interest: nucleus and cytoplasm for respective transcription and translation process (19). To maximize the availability of genes in the cytoplasmic region, NPs should entirely be disintegrated before lysosomal fusion with the endosomes takes place, causing premature degradation of complexes or inducing exocytosis of the complexes into the extracellular matrix (20)(21). pDNA expressional activity measured through analysis of reporter gene expression via cellular fluorescence (pGFP) and luminescence activity (pGL3) with viability assay of target genes through MTT solution (p53) demonstrated by high gene expression in both MCF-7 and 4T1 cells after 48 hours incubation. pGFP encodes for an intracellular protein of 26.9kDa exhibiting green fluorescence upon exposure to light in blue to ultraviolet range, first isolated from jellyfish *Aequorea victoria*. Luciferase reporter pDNA, (also known as pGL3) is an oxidative enzyme

showcasing cellular bioluminescence properties, first derived from firefly *Photinus pyralis*. These reporter genes are transcribed into messenger RNA (mRNA) molecules inside the nuclear cavity before translation into desired protein occurs inside the cytoplasm, releasing respective fluorescence or luminescence light (22)(23). Target gene, p53 is a central regulator of cellular growth, DNA repair, and apoptosis, often down-regulated in cancer patient due to gene missing or malfunction. The introduction of wild-type p53 is hence necessary to normalize the regulatory mechanism of 'guardian of genome' gene (24). p53 genes were introduced just before the formation of NPs to ensure adsorption of the genes into the salt structure. $BaSO_3$, BaF_2, $SrSO_4$, $SrSO_3$, SrF_2, and $MgSO_3$ endorsed efficient gene expression as reflected by intensified fluorescence image and high luminescence activity in both cancerous cells, comparable to established CO_3 AP NPs (25). High cellular uptake and gene expression are the hallmarks of the selected NP, supplemented with biodegradable properties to ensure efficient gene release into the cytoplasm with exposure to acidic pH in late endosome (26)(27). Excellent expression-promoting activities of those NPs might be partly attributed to their high cellular uptake, in addition to being pH-sensing for facilitating endosomal escape and release of the pDNA from the NPs (28).

Investigation on pH-sensitive properties of selected NPs presented in Figure 4.7 was made through exposure of NPs in the acidic environment to mimic the late endosomal stage. Salt particles formation was commenced at pH 7.5, which was reduced with the gradual introduction of hydrochloric acid (HCl) in the order to compare changes in turbidity pH adjustment. Late endosome has pH of approximately 3.5 to 4.5, in which CO_3 AP was able to be successfully dissolved and release pDNA

through proton sponge effect (29). The increment of hydrogen ion (H^+) within endosomes triggers incorporation of chloride ion (Cl^-) into the endosomal cavity, therefore generating high osmotic pressure across the endosomal membrane and finally, swelling and rupturing the endosomes (30). $SrSO_3$, SrF_2 and $MgSO_3$ were dissolved completely at pH 4.5, represented by null absorbance activity. Inefficient escape of pDNA owing to incomplete particle dissolution might limit the transfection efficiency, as experienced with $SrSO_4$, thus slightly lowering pDNA expression (31).

The effectiveness of NPs was further elaborated in the forms of siRNA-mediated gene knockdown in MCF-7 and 4T1 cells. RNA interference (RNAI) process is a post-transcriptional gene regulatory mechanism, which may be modulated by endogenous siRNA. Internalized target siRNA unwinds and is incorporated into RNA-induced silencing complex (RISC), as stable protein-RNA complex, which will be directed to the target mRNA to trigger its degradation, thereby interrupting protein synthesis of the targeted genes (32)(33). Mutation in genes, causing cancer is associated with various triggers such as up-regulation of proto-oncogenes, genes that are involved in cell proliferations, resulting in the formation of oncogenes. These proto-oncogenes include ErbB2, MAPK and PI3K genes, which are overexpressed in malignant cells (34). Up-regulation of anti-apoptotic genes (genes involved in impeding apoptosis) such as Bcl-2 can also lead to cancer (35). The introduction of siRNAs involved in silencing of these genes could result in activation of cellular apoptosis (36).

MAPK siRNA was complexed with each type of selected NPs, followed by transfer into seeded mammary carcinoma cells and incubation for 48 hours to determine

the cytotoxicity effect. With approximately 10% cell viability, $MgSO_3$ NPs was the most successful in transporting siRNA in both cell lines, in addition to efficient pDNA delivery in earlier studies. A high percentage of cell viability was seen with $SrSO_4$ may be explained by lower crystals dissolution rate, therefore impeding the efficient endosomal escape of siRNA into the cytoplasmic region (37). Treatment of human mammary carcinoma was associated with more cellular toxicity in comparison to mice carcinoma (38). MAPK siRNA-loaded complexes endorsed efficient cellular death by inhibition of p44/42 MAP kinase expression in RAS-RAF-MEK-ERK pathway through silencing of ERK1/2 genes (39). Confirmation of MAPK siRNA action was further elaborated through Western blot analysis. It is understood that phospho-MAPK and total-MAPK expression were interrupted by transfection involving MAPK siRNA-loaded $SrSO_3$ and SrF_2, as seen with a reduction in band intensities (40).

Active targeting is achieved by attachment of affinity ligands that bind to specific receptors on cellular surface, enabling the nano-vectors to recognize and bind to target cells through ligand-receptor interactions before being internalized. Receptor should only be highly expressed in specific cells, e.g. tumor to achieve the precise targeting (41). Fibronectin receptor is involved in modulating numerous signaling pathways, including inhibition of ErbB2 signal by inducing proteasome-dependent proteolytic cleavage of ErbB2 cytoplasmic domains through α6β1 integrin. Over-expression of the receptor is also associated with increasing carcinomic aggression (42). It is also suggested to have a critical role in mediating chemotactic and haptotactic migration, thus contributing to spontaneous metastasis of breast tumor to surrounding bone tissues (43). Transferrin receptor, an iron importer, is associated with over-

expression in many malignant cells, including breast tissues up to 100 folds. It is proposed that the increased expression may be due to higher demands of iron to cater rapid growth and proliferation of cancer cells (44)(45).

Influence of intracellular effect with transferrin- or fibronectin-coating of NPs was demonstrated in both human and mice mammary carcinoma models, manipulating the presence of over-expressed transferrin or fibronectin receptors on tumor cells surfaces (45)(46). The introduction of transferrin and fibronectin proteins into the NPs complexes is postulated to involve active transport mechanism into the delivery to pass through the cell membrane. In the earlier studies, integration of 1μg of transferrin/fibronectin protein was shown to assist in the reduction of NPs size diameter with less negatively charged surfaces. The impact of the protein ligands *in vitro* showed improvement in relative luminescence value (RLU/mg protein) in comparison with uncoated NPs. Improvement of gene delivery through the involvement of active targeting was most significant with $MgSO_3$ complexes, almost 100 fold increment of luciferase activity seen with co-delivery of fibronectin and $MgSO_3$ into 4T1 cells. Based on the intracellular experiments, protein coating offered an adjunct effect on improving genetic transportation. It is therefore expected that the additional benefit would be similar in animal studies with the active transport playing a huge role in bioavailability and transtumoral delivery (47).

Selected potential salts were investigated for their ability to magnify the individual gene carrier activity (48). In Chapter 3, we have discussed the generation of hybridized NPs, which showed size increment with more negative charge regions in

overall combinations tested. It is proposed that the positive domains of salt combinations of 5mM of each cation-providing salts may enhance the cellular uptake of the complexes through efficient adsorption with negatively-charged syndecan domains (49). However, the structural changes of the salts, seen with larger sizes in comparison with single salt particles, may also modify the particles stability and disintegration process, therefore, influence the intracellular expression of transported genes (50). Particle stabilization is improved with bigger and more complicated structures, thus requiring a stronger force to induce destabilization process (51).

Qualitative experimental view of co-delivery of salt crystals demonstrated no improvement of cellular uptake for five different crystal combinations, through microscopic observations. Additionally, hybridization of NPs had no further enhancement of luciferase expression, indicating no improvement in the disintegration of the complexes to release the genetic content. Inefficient delivery might have happened due to larger salt sizes, impacting gene expression activity (52). The Large structure of salt combinations could impede the *in vivo* delivery through IV injection as the tendency to form more massive aggregation would be higher with increased risk of clot formation in the blood circulation (53).

4.5 Conclusion

We have investigated NPs for their ability to transport the genetic materials intracellularly, through observation of cellular uptake, salt dissolution properties, gene expression and silencing efficacy. Subsequently, we also studied the viability of NPs to understand their cytotoxicity profiles in human and mice mammary carcinoma cells. The cellular experiments showed the efficiency of $BaSO_3$, BaF_2, $SrSO_4$, $SrSO_3$, $_{SrF2}$ and $MgSO_3$ in intracellular delivery, through microscopic qualitative observation and quantitative luciferase and MTT assay, accomplishing comparative data with established CO_3 AP particles. Co-delivery of pDNA or siRNA with NPs resulted in better cellular internalization and efficient endosomal escape of the nucleic acid. However, naked barium salt particles were associated with high toxicity upon exposure to MCF-7 and 4T1 cells (50-80% viability at 24 hours incubation), therefore raising concern for *in vivo* studies and will be excluded from the subsequent studies (Chapter 5). Additionally, despite being efficacious in cellular studies, the large size of $SrSO_4$ could interfere with intravenous delivery by forming large aggregates and eventually clots, thus, will also be rejected from animal studies.

Based on the exclusion criteria above, in vivo experiments will only be carried out for three NPs, $SrSO_3$, SrF_2, and $MgSO_3$. Incorporation of fibronectin and transferrin protein intensified the gene delivery through the proposed active transport route. Both of the proteins will be further investigated in next chapter to identify the significance of active targeting in biological systems. Co-delivery of individual NPs demonstrated no additional benefit in nanocarrier activity of the salt particles, which was evident from no

further improvement in cellular luminescence intensity, thus was not extensively explored.

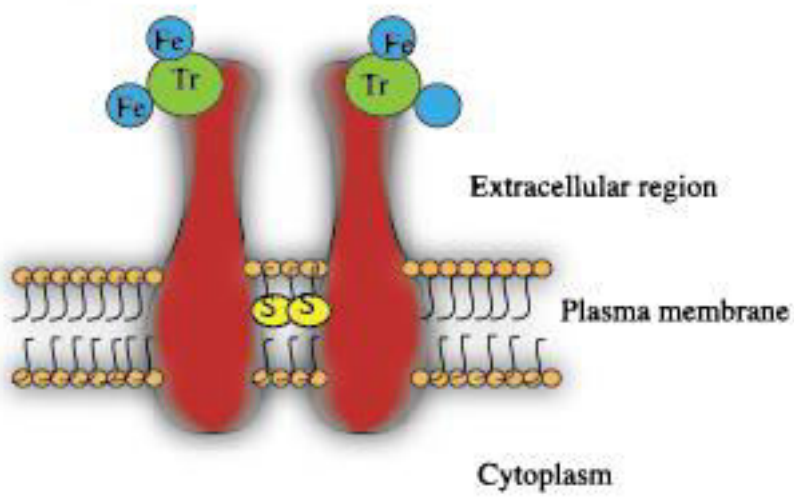

Figure 4.13: Transferrin receptor. Adapter by Z.M. Qian, H. Li, H. Sun, K. Ho Targeted drug delivery via the transferrin receptor-mediated endocytosis pathway. Pharmacol Rev, 54 (2002), p561-587

4.6 References

1. Sarrazin S, Lamanna WC, Esko JD. Heparan sulfate proteoglycans. Cold Spring Harb Perspect Biol. 2011;3(7):1–33.
2. Panariti A, Miserocchi G, Rivolta I. The effect of nanoparticle uptake on cellular behavior: Disrupting or enabling functions? Nanotechnology, Science and Applications. 2012. p. 87–100.
3. Oh N, Park JH. Endocytosis and exocytosis of nanoparticles in mammalian cells. International Journal of Nanomedicine. 2014. p. 51–63.
4. Sahay G, Alakhova DY, Kabanov A V. Endocytosis of nanomedicines. Journal of Controlled Release. 2010. p. 182–95.
5. Pelkmans L, Kartenbeck J, Helenius a. Caveolar endocytosis of simian virus 40 reveals a new two-step vesicular-transport pathway to the ER. Nat Cell Biol. 2001;3(5):473–83.
6. El-Sayed A, Harashima H. Endocytosis of gene delivery vectors: from clathrin-dependent to lipid raft-mediated endocytosis. Mol Ther. 2013;21(6):1118–30.
7. Fröhlich E. The role of surface charge in cellular uptake and cytotoxicity of medical nanoparticles. Int J Nanomedicine [Internet]. 2012 Nov [cited 2016 Mar 24];5577. Available from: http://www.dovepress.com/the-role-of-surface-charge-in-cellular-uptake-and-cytotoxicity-of-medi-peer-reviewed-article-IJN
8. Elliott DJ. Illuminating the transcriptome through the genome. Genes. 2014. p. 235–53.
9. Al-Jamal KT, Kostarelos K. Assessment of Cellular Uptake and Cytotoxicity of Carbon Nanotubes Using Flow Cytometry. In: Carbon Nanotubes: Methods and Protocols, Methods in Molecular Biology [Internet]. 2010. p. 123–34. Available from: http://link.springer.com/10.1007/978-1-60761-579-8
10. Pack DW, Hoffman AS, Pun S, Stayton PS. Design and development of polymers for gene delivery. Nat Rev Drug Discov [Internet]. 2005;4(7):581–93. Available from: http://www.ncbi.nlm.nih.gov/pubmed/16052241
11. Madani F, Lindberg S, Langel Ü, Futaki S, Gräslund A. Mechanisms of Cellular Uptake of Cell-Penetrating Peptides. J Biophys. 2011;2011:1–10.
12. Gujrati M, Malamas A, Shin T, Jin E, Sun Y, Lu ZR. Multifunctional cationic lipid-based nanoparticles facilitate endosomal escape and reduction-triggered cytosolic siRNA release. Mol Pharm. 2014;11(8):2734–44.
13. Ribera a B, Spitzer NC. Both barium and calcium activate neuronal potassium currents. Proc Natl Acad Sci U S A. 1987;84(18):6577–81.
14. Akkari YM, Bateman RL, Reifsteck C a, Olson SB, Grompe M. DNA replication is required To elicit cellular responses to psoralen-induced DNA interstrand cross-links. Mol Cell Biol. 2000;20(21):8283–9.
15. Fromigué O, Haÿ E, Barbara A, Petrel C, Traiffort E, Ruat M, et al. Calcium sensing receptor-dependent and receptor-independent activation of osteoblast replication and survival by strontium ranelate. J Cell Mol Med. 2009;13(8 B):2189–99.
16. Kamaly N, Xiao Z, Valencia PM, Radovic-Moreno AF, Farokhzad OC. Targeted polymeric therapeutic nanoparticles: design, development and clinical translation. Chem Soc Rev [Internet]. 2012;41(7):2971–3010. Available from: http://pubs.rsc.org/en/content/articlehtml/2012/cs/c2cs15344k

17. Wan J, Wang J-H, Liu T, Xie Z, Yu X-F, Li W. Surface chemistry but not aspect ratio mediates the biological toxicity of gold nanorods in vitro and in vivo. Sci Rep [Internet]. 2015;5:11398. Available from: http://www.nature.com/srep/2015/150622/srep11398/full/srep11398.html
18. Perry G, Cash AD, Smith M a. Alzheimer Disease and Oxidative Stress. J Biomed Biotechnol [Internet]. 2002;2(3):120–3. Available from: http://www.pubmedcentral.nih.gov/articlerender.fcgi?artid=161361&tool=pmcentrez&rendertype=abstract
19. Uzman A, Lodish H, Berk A, Zipursky L, Baltimore D. Molecular Cell Biology (4th edition) New York, NY, 2000, ISBN 0-7167-3136-3. Biochem Mol Biol Educ. 2000;29:Section 1.2The Molecules of Life.
20. Schulze H, Kolter T, Sandhoff K. Principles of lysosomal membrane degradation. Cellular topology and biochemistry of lysosomal lipid degradation. Biochimica et Biophysica Acta - Molecular Cell Research. 2009. p. 674–83.
21. Lodish H, Berk A, Matsudaira P, Kaiser CA, Krieger M, Scott MP, et al. Molecular Cell Biology [Internet]. Perspective. 2008. 973 p. Available from: http://www.amazon.ca/exec/obidos/redirect?tag=citeulike09-20&path=ASIN/0716743663
22. Tsien RY. The green fluorescent protein. Annu Rev Biochem [Internet]. 1998;67:509–44. Available from: http://www.ncbi.nlm.nih.gov/pubmed/9759496
23. Gould SJ, Subramani S. Firefly luciferase as a tool in molecular and cell biology. Anal Biochem. 1988;175:5–13.
24. Riley T, Sontag E, Chen P, Levine A. Transcriptional control of human p53-regulated genes. Nat Rev Mol Cell Biol. 2008;9(5):402–12.
25. Chowdhury EH, Akaike T. High performance DNA nano-carriers of carbonate apatite: multiple factors in regulation of particle synthesis and transfection efficiency. Int J Nanomedicine. 2007;2(1):101–6.
26. Sunshine JC, Peng DY, Green JJ. Uptake and transfection with polymeric nanoparticles are dependent on polymer end-group structure, but largely independent of nanoparticle physical and chemical properties. Mol Pharm. 2012;9(11):3375–83.
27. Chowdhury EH, Maruyama A, Kano A, Nagaoka M, Kotaka M, Hirose S, et al. pH-sensing nano-crystals of carbonate apatite: Effects on intracellular delivery and release of DNA for efficient expression into mammalian cells. Gene. 2006;376(1-2):87–94.
28. Hossain S, Stanislaus A, Chua MJ, Tada S, Tagawa Y ichi, Chowdhury EH, et al. Carbonate apatite-facilitated intracellularly delivered siRNA for efficient knockdown of functional genes. J Control Release. 2010;147(1):101–8.
29. Huang L, Guo S. Nanoparticles escaping RES and endosome: Challenges for siRNA delivery for cancer therapy. Journal of Nanomaterials. 2011.
30. Tada S, Chowdhury EH, Cho CS, Akaike T. pH-sensitive carbonate apatite as an intracellular protein transporter. Biomaterials. 2010;31(6):1453–9.
31. Morachis JM, Mahmoud E a., Sankaranarayanan J, Almutairi A. Triggered Rapid Degradation of Nanoparticles for Gene Delivery. J Drug Deliv. 2012;2012:1–7.
32. Agrawal N, Dasaradhi PVN, Mohmmed A, Malhotra P, Bhatnagar RK, Mukherjee SK. RNA interference: biology, mechanism, and applications. Microbiol Mol Biol Rev [Internet]. 2003;67(4):657–85. Available from: http://www.pubmedcentral.nih.gov/articlerender.fcgi?artid=309050&tool=pmcen

trez&rendertype=abstract
33. Wilson RC, Doudna JA. BB42CH10-Doudna Molecular Mechanisms of RNA Interference Argonaute: a protein capable of binding short ssRNAs and, in some cases, cleaving a bound complementary strand. Annu Rev Biophys. 2013;42:217–39.
34. Li J, Dai X, Zhang H, Zhang W, Sun S, Gao T, et al. Up-regulation of human cervical cancer proto-oncogene contributes to hepatitis B virus-induced malignant transformation of hepatocyte by down-regulating E-cadherin. Oncotarget [Internet]. 2015;6(30):29196–208. Available from: http://www.ncbi.nlm.nih.gov/pubmed/26470691
35. Konopleva M, Konoplev S, Hu W, Zaritskey a Y, Afanasiev B V, Andreeff M. Stromal cells prevent apoptosis of AML cells by up-regulation of anti-apoptotic proteins. Leuk Off J Leuk Soc Am Leuk Res Fund, UK. 2002;16(9):1713–24.
36. Reynolds A, Leake D, Boese Q, Scaringe S, Marshall WS, Khvorova A. Rational siRNA design for RNA interference. Nat Biotechnol [Internet]. 2004;22(3):326–30. Available from: http://www.ncbi.nlm.nih.gov/pubmed/14758366
37. Yoshida T, Lai TC, Kwon GS, Sako K. pH- and ion-sensitive polymers for drug delivery. Expert Opin Drug Deliv [Internet]. 2013;10(11):1497–513. Available from: http://www.pubmedcentral.nih.gov/articlerender.fcgi?artid=3912992&tool=pmcentrez&rendertype=abstract
38. Banin Hirata BK, Oda JMM, Losi Guembarovski R, Ariza CB, Oliveira CEC De, Watanabe MAE. Molecular markers for breast cancer: Prediction on tumor behavior. Disease Markers. 2014.
39. Meloche S, Pouysségur J. The ERK1/2 mitogen-activated protein kinase pathway as a master regulator of the G1- to S-phase transition. Oncogene [Internet]. 2007;26(22):3227–39. Available from: http://dx.doi.org/10.1038/sj.onc.1210414
40. Frazier WJ, Xue J, Luce WA, Liu Y. MAPK Signaling Drives Inflammation in LPS-Stimulated Cardiomyocytes: The Route of Crosstalk to G-Protein-Coupled Receptors. Wu GS, editor. PLoS One [Internet]. 2012 Nov 30 [cited 2016 Mar 28];7(11):e50071. Available from: http://dx.plos.org/10.1371/journal.pone.0050071
41. Accardo A, Aloj L, Aurilio M, Morelli G, Tesauro D. Receptor binding peptides for target-selective delivery of nanoparticles encapsulated drugs. International Journal of Nanomedicine. 2014. p. 1537–57.
42. Desgrosellier JS, Cheresh DA. Integrins in cancer: biological implications and therapeutic opportunities. Nat Rev Cancer [Internet]. 2010;10(1):9–22. Available from: http://www.pubmedcentral.nih.gov/articlerender.fcgi?artid=4383089&tool=pmcentrez&rendertype=abstract
43. Sloan EK, Pouliot N, Stanley KL, Chia J, Moseley JM, Hards DK, et al. Tumor-specific expression of alphavbeta3 integrin promotes spontaneous metastasis of breast cancer to bone. Breast Cancer Res [Internet]. 2006;8(2):R20. Available from: http://breast-cancer-research.com/content/8/2/R20
44. Anderson CP, Shen M, Eisenstein RS, Leibold EA. Mammalian iron metabolism and its control by iron regulatory proteins. Biochim Biophys Acta [Internet]. 2012;1823(9):1468–83. Available from: http://www.pubmedcentral.nih.gov/articlerender.fcgi?artid=3675657&tool=pmce

ntrez&rendertype=abstract
45. Högemann-Savellano D, Bos E, Blondet C, Sato F, Abe T, Josephson L, et al. The transferrin receptor: a potential molecular imaging marker for human cancer. Neoplasia [Internet]. 2003;5(6):495–506. Available from: http://www.pubmedcentral.nih.gov/articlerender.fcgi?artid=1502574&tool=pmcentrez&rendertype=abstract
46. McSherry E a, Brennan K, Hudson L, Hill AD, Hopkins AM. Breast cancer cell migration is regulated through junctional adhesion molecule-A-mediated activation of Rap1 GTPase. Breast Cancer Res [Internet]. 2011;13(2):R31. Available from: http://breast-cancer-research.com/content/13/2/R31
47. Steichen SD, Caldorera-Moore M, Peppas NA. A review of current nanoparticle and targeting moieties for the delivery of cancer therapeutics. Eur J Pharm Sci [Internet]. 2013 Feb [cited 2016 Mar 28];48(3):416–27. Available from: http://linkinghub.elsevier.com/retrieve/pii/S0928098712004782
48. Mu Q, Jiang G, Chen L, Zhou H, Fourches D, Tropsha A, et al. Chemical basis of interactions between engineered nanoparticles and biological systems. Chemical Reviews. 2014. p. 7740–81.
49. Åmand HL, Rydberg HA, Fornander LH, Lincoln P, Nordén B, Esbjörner EK. Cell surface binding and uptake of arginine- and lysine-rich penetratin peptides in absence and presence of proteoglycans. Biochim Biophys Acta - Biomembr. 2012;1818(11):2669–78.
50. Khadka P, Ro J, Kim H, Kim I, Kim JT, Kim H, et al. Pharmaceutical particle technologies: An approach to improve drug solubility, dissolution and bioavailability. Asian Journal of Pharmaceutical Sciences. 2014. p. 304–16.
51. Shi J. Steric Stabilization. 2001;
52. Liu G, Li D, Pasumarthy MK, Kowalczyk TH, Gedeon CR, Hyatt SL, et al. Nanoparticles of compacted DNA transfect postmitotic cells. J Biol Chem. 2003;278(35):32578–86.
53. Ho D, Wang C-HK, Chow EK-H. Nanodiamonds: The intersection of nanotechnology, drug development, and personalized medicine. Sci Adv [Internet]. 2015;1(7):e1500439. Available from: http://www.pubmedcentral.nih.gov/articlerender.fcgi?artid=4643796&tool=pmcentrez&rendertype=abstract

Chapter 5

In vivo efficacy of selected NPs

5.1 Introduction

Selected salt crystals determined from various experiments in vitro were introduced in the animal model to appreciate their carrier ability via systemic delivery. Parenteral administration is associated with inefficient gene transportation, due to the presence of circulatory monocyte, which is involved in clearance and elimination of foreign materials by reticuloendothelial systems (RES). Nuclease attack is often associated with premature degradation of genetic materials, which interactions are derived through electrostatically bound nuclease and negatively charged pDNA and siRNA. Scavenging plasma proteins in the circulatory systems tends to bind to uncoated and hydrophobic vectors, inducing elimination signals from the blood distribution. Large carrier sizes may encourage the embolization of blood capillaries, causing a life-threatening blockage in the blood vessel, thus should be omitted from the in vivo studies.

Determination of nanocarriers in promoting efficient transportation of genes in vivo was performed by introduction of intravenous injection comprising of gene-loaded NPs into 4T1 tumor-bearing mice, followed by subsequent observation of gene deposition in various organs upon different time points. Investigation on the influence of salt concentration in the formation of salt particles may demonstrate influence on bioavailability with diverse anionic-providing salt concentration. The internal organ siRNA deposition was further examined via transferrin and fibronectin-coated NPs in hope to determine the potential active transport activity upon 4 hours of incubation. Effect of tumor regression activity of 4T1 cells was reviewed by monitoring tumor volume measurement for two weeks post treatment. The importance of ideal

concentration of p53 and MAPK siRNA was performed on mice studies, alongside protein coating in promoting active transportation and improving biological distributions into desired organs for effective treatment over a period of 2 weeks.

Experimentation *in vivo* demonstrated efficient distributions of salt crystals towards kidney and liver, representing possible involvement of RES uptake for systemic clearance. Deposition of NPs in tumor tissues is approximately four times lower in comparison with kidney and liver. Brain siRNA-NPs accumulation is comparatively high in all salts tested, conceivably passing through blood brain barrier. Adsorption of protein onto the surface of salt particles enhances the targeting specificity towards improving tumor tissues accumulation, hence the likely presence of active transportation. Through biodistribution experimentation, $SrSO_3$ and SrF_2 are associated with greater nanocarrier activity upon complexation with genetic material in comparison to $MgSO_3$ and CO_3 AP.

Tumor regression studies on 4T1 tumor-induced BALB/c mice revealed efficient delivery of each target genes-loaded NPs towards halting tumor growth, upon observation over 28 days. Fibronectin and transferrin coating involve in lowering the carcinogenic growth rate, with tumor size difference of minimal $150mm^3$ throughout all NPs studied. Reduction in cancerous tissues growth rate may be linked to their efficient adsorption towards specific target receptor, hence greater internalization of complexes via receptor-mediated endocytosis. Tumor regression studies of $SrSO_3$, SrF_2, and $MgSO_3$ *in vivo* have proven effectiveness in transporting genetic materials into the targeted site for subsequently greater gene expression activity.

5.2 Methods and materials

5.2.1 Time-dependent biodistribution studies

4T1 tumor cells (50,000 cells/mouse) were subcutaneously inoculated into the mammary gland of 6-8 week old BALB/c mice, before randomly assigned into different groups, consisted of 5 mice/group. Total volume of 100µl from each salt particles loaded with AF 488 siRNA and supplemented with DMEM-powdered media was intravenously administered to each mouse (at right or left caudal tail vein) once the tumors reach the average size of 13.20 ±2.51mm3. 1µM AF 488, fluorescence-labeled siRNA was added to 5µl of 1M $SrCl_2$ or $MgCl_2$, followed by incorporation of 2µl of 1M Na_2SO_3 or NaF in 10µl HEPES-buffered media to generate respective $SrSO_3$, SrF_2 and $MgSO_3$ salt precipitates. The chemical reaction was maintained at 37^oC for 30 minutes, followed by a brief mixture of DMEM-powdered media to form a final volume of 100µl particle suspension. Transfected cells were inoculated for 4 hours period, followed by mice sacrificial. The inclusion of CO_3 AP as the positive control for the treatment was done by incorporation of 1µM AF 488 siRNA and 5µl of 1M exogenous $CaCl_2$ into prepared DMEM-powdered media to form 100µl solution, at similar incubation condition.

All mice were sacrificed by cervical dislocation following 4 hours incubation and organ tissues consisting of brains, kidney, liver, lung, spleen and tumor were harvested immediately and washed with 1X chilled PBS. The tissue culture was maintained on ice throughout the experiment. 1ml chilled lysis buffer per 500gram of tissue mass was added after washing, followed by homogenization of organ tissues using Homogenizer (Eppendorf, Germany), until completely homogenized lysate is

produced. The tissue lysate was next centrifuged for 10 minutes at 15,000 RPM at 4oC. 100µl of centrifuged supernatant was added into 96-well black opti-plate to measure the fluorescence intensity of AF 488-labeled siRNA with 2030 multilabel reader Victor TM X5 (Perkin Elmer, USA), using Perkin Elmer 2030 manager software with λex = 490nm and λem = 535nm.

Studies involving time-dependent influential was performed by adjusting the incubation of $SrSO_3$, SrF_2, $MgSO_3$ and CO_3 AP particles upon intravenous transfection at 1, 2 and 4 hours before mice sacrificial and organ harvestment (Figure 5.1). Untreated mice group represented negative control for the experiment.

Data was expressed as mean±SD of fluorescence intensity /500mg of organ mass (values were blank-corrected using untreated group).

Group	Regimen	No of mice
Untreated	100µl 1X PBS	15
1 hour	5µl of 1M $SrCl_2$, 2µl of 1M Na_2SO_3, 1µM AF 488 siRNA, in 10µl HEPES-buffered media, followed by addition of DMEM to achieve 100µl suspension	5
	5µl of 1M $SrCl_2$, 2µl of 1M NaF, 1µM AF 488 siRNA, in 10µl HEPES-buffered media, followed by addition of DMEM to achieve 100µl suspension	5
	5µl of 1M $MgCl_2$, 2µl of 1M Na_2SO_3, 1µM AF 488 siRNA, in 10µl HEPES buffered media, followed by addition of DMEM to achieve 100µl suspension	5
	44mM Na_2CO_3, 5µl of 1M $CaCl_2$, 1µM AF 488 siRNA, followed by addition of DMEM to achieve 100µl suspension	5
2 hours	5µl of 1M $SrCl_2$, 2µl of 1M Na_2SO_3, 1µM AF 488 siRNA, in 10µl HEPES-buffered media, followed by addition of DMEM to achieve 100µl suspension	5
	5µl of 1M $SrCl_2$, 2µl of 1M NaF, 1µM AF 488 siRNA, in 10µl HEPES-buffered media, followed by addition of DMEM to achieve 100µl suspension	5
	5µl of 1M $MgCl_2$, 2µl of 1M Na_2SO_3, 1µM AF 488 siRNA, in 10µl HEPES-buffered media, followed by addition of DMEM to achieve 100µl suspension	5
	44mM Na_2CO_3, 5µl of 1M $CaCl_2$, 1µM AF 488 siRNA, followed by addition of DMEM to achieve 100µl suspension	5
4 hours	5µl of 1M $SrCl_2$, 2µl of 1M Na_2SO_3, 1µM AF 488 siRNA, in 10µl HEPES-buffered media, followed by addition of DMEM to achieve 100µl suspension	5
	5µl of 1M $SrCl_2$, 2µl of 1M NaF, 1µM AF 488 siRNA, in 10µl HEPES-buffered media, followed by addition of DMEM to achieve 100µl suspension	5
	5µl of 1M $MgCl_2$, 2µl of 1M Na_2SO_3, 1µM AF 488 siRNA, in 10µl HEPES-buffered media, followed by addition of DMEM to achieve 100µl suspension	5
	44mM Na_2CO_3, 5µl of 1M $CaCl_2$, 1µM AF 488 siRNA, followed by addition of DMEM to achieve 100µl suspension	5

Table 5.1 Mice grouping for time-dependent biodistribution studies.

5.2.2 Concentration-dependent biodistribution studies

The concentration-dependent analysis was performed by manipulation of anion-providing salts, Na_2SO_3 and NaF concentration to form the particle complexes, to demonstrate the influence on nano-vector activity upon increasing in salt concentration. 5µl of 1M $SrCl_2$ or $MgCl_2$ was mixed with 1µM AF 488 siRNA, followed by incorporation of 2µl or 5µl of 1M Na_2SO_3 or NaF in 10µl HEPES-buffered media, followed by addition of DMEM to achieve final volume of 100µl salt suspension (Figure 5.2). Incubation of fabricated salt particles were similarly held at 37^oC for 30 minutes, prior to transfection into the mice systemic circulation via intravenous injection. Mice were sacrificed and organ tissues including brain, kidney, liver, lung, spleen and tumour were harvested to perform biodistribution analysis, as of 5.2.1. Data was represented as mean±SD of fluorescence intensity /500mg of organ mass (values were blank-corrected using untreated group).

Figure 5.1: 4T1 tumor injection site on mammary gland of BALB/c mouse via subcutaneous delivery

Group	Regimen	No of mice
Untreated	100µl 1X PBS	5
$SrSO_3$	5µl of 1M $SrCl_2$, 2µl of 1M Na_2SO_3, 1µM AF 488 siRNA, in 10µl HEPES-buffered media, followed by addition of DMEM to achieve 100µl suspension	5
	5µl of 1M $SrCl_2$, 5µl of 1M Na_2SO_3, 1µM AF 488 siRNA, in 10µl HEPES-buffered media, followed by addition of DMEM to achieve 100µl suspension	5
SrF_2	5µl of 1M $SrCl_2$, 2µl of 1M NaF, 1µM AF 488 siRNA, in 10µl HEPES-buffered media, followed by addition of DMEM to achieve 100µl suspension	5
	5µl of 1M $SrCl_2$, 5µl of 1M NaF, 1µM AF 488 siRNA, in 10µl HEPES-buffered media, followed by addition of DMEM to achieve 100µl suspension	5
$MgSO_3$	5µl of 1M $MgCl_2$, 2µl of 1M Na_2SO_3, 1µM AF 488 siRNA, in 10µl HEPES-buffered media, followed by addition of DMEM to achieve 100µl suspension	5
	5µl of 1M $MgCl_2$, 5µl of 1M Na_2SO_3, 1µM AF 488 siRNA, in 10µl HEPES-buffered media, followed by addition of DMEM to achieve 100µl suspension	5
CO_3 AP	44mM Na_2CO_3, 5µl of 1M $CaCl_2$, 1µM AF 488 siRNA, followed by addition of DMEM to achieve 100µl suspension	5

Table 5.2: Mice grouping for concentration-dependent biodistribution studies

5.2.3 Influence of protein coating on biodistribution studies

Influence of protein binding on particle surface was initiated by incorporation of protein coating on NPs complexes to determine the effect of active targeting *in vivo*. 5µl of 1M $SrCl_2$ or $MgCl_2$ was mixed with 1µM AF 488 siRNA, followed by incorporation of 2µl Na_2SO_3 or NaF in 10µl HEPES-buffered media, followed by addition of DMEM to achieve final volume of 100µl salt suspension. 1µM transferrin or Fibronectin was incorporated into the generated NPs and incubated for 10 minutes at 37^{o}C. Subsequent coated, complexed salts were introduced intravenously into the mice tail vein and incubated similarly at 4 hours. Mice were sacrificed and organ tissues including brain, kidney, liver, lung, spleen and tumor were harvested to

perform biodistribution analysis, as of 5.2.1. Data was represented as mean±SD of fluorescence intensity /500mg of organ mass.

Group	Regimen	No of mice
$SrSO_3$	5µl of 1M $SrCl_2$, 2µl of 1M Na_2SO_3, 1µM AF 488 siRNA, in 10µl HEPES-buffered media, followed by addition of DMEM to achieve 100µl suspension	5
	5µl of 1M $SrCl_2$, 2µl of 1M Na_2SO_3, 1µM AF 488 siRNA, in 10µl HEPES-buffered media, followed by 1µg fibronectin and DMEM to achieve volume of 100µl	5
	5µl of 1M $SrCl_2$, 2µl of 1M Na_2SO_3, 1µM AF 488 siRNA, in 10µl HEPES-buffered media, followed by 1µg transferrin and DMEM to achieve volume of 100µl	5
SrF_2	5µl of 1M $SrCl_2$, 2µl of 1M NaF, 1µM AF 488 siRNA, in 10µl HEPES-buffered media, followed by addition of DMEM to achieve 100µl suspension	5
	5µl of 1M $SrCl_2$, 2µl of 1M NaF, 1µM AF 488 siRNA, in 10µl HEPES-buffered media, followed by 1µg fibronectin and DMEM to achieve volume of 100µl	5
	5µl of 1M $SrCl_2$, 2µl of 1M NaF, 1µM AF 488 siRNA, in 10µl HEPES-buffered media, followed by 1µg transferrin and DMEM to achieve volume of 100µl	5
$MgSO_3$	5µl of 1M $MgCl_2$, 2µl of 1M Na_2SO_3, 1µM AF 488 siRNA, in 10µl HEPES-buffered media, followed by addition of DMEM to achieve 100µl suspension	5
	5µl of 1M $MgCl_2$, 2µl of 1M Na_2SO_3, 1µM AF 488 siRNA, in 10µl HEPES-buffered media, followed by 1µg fibronectin and DMEM to achieve volume of 100µl	5
	5µl of 1M $MgCl_2$, 2µl of 1M Na_2SO_3, 1µM AF 488 siRNA, in 10µl HEPES-buffered media, followed by 1µg transferrin and DMEM to achieve volume of 100µl	5
CO_3 AP	44mM Na_2CO_3, 5µl of 1M $CaCl_2$, 1µM AF 488 siRNA, followed by addition of DMEM to obtain 100µl suspension	5
	44mM Na_2CO_3, 5µl of 1M $CaCl_2$, 1µM AF 488 siRNA, followed by addition of DMEM to obtain 100µl suspension and 1µg fibronectin	5
	44mM Na_2CO_3, 5µl of 1M $CaCl_2$, 1µM AF 488 siRNA, followed by addition of DMEM to obtain 100µl suspension and 1µg transferrin	5

Table 5.3: Mice grouping for impact of protein coating on biodistribution studies

5.2.4 Tumor regression studies involving p53-loaded NPs

Approximately 50,000 4T1 cells were inoculated to the mammary gland of each 6-8 week old BALB/c mice through subcutaneous injection, before randomly assigned into different groups, consisting of 5 mice/group. Once the tumor growth reached 13.20±2.51mm^3, 100µl of total suspension by various preparations of salt crystals with p53 gene, supplemented with DMEM was intravenously administered into each mouse (at right or left caudal tail vein). The salts solutions, formed by the mixture of 20µg of p53 gene with 5µl of 1M $SrCl_2$ or $MgCl_2$ was added to 2µl of 1M Na_2SO_3 or NaF in 10µl HEPES-buffered media to fabricate respective $SrSO_3$, SrF_2 and $MgSO_3$ particles, with CO_3 AP as control, as specified in Table 5.4. Subsequent experiment determining the influence of p53 concentration through observation of 10 and 20µg p53 gene on tumor volume was examined via similar NPs regimen. The chemical reaction was sustained for 30 minutes at 37^{o}C, followed by a brief mixture of DMEM-powdered media to form final volume of 100µl particle suspension.

Each treatment was repeated two days after the initial treatment regimen. Tumor growth was supervised every two days, measuring width and length of tumor lump using Vernier caliper (mm scale) from the treatment day (day 14), and continuously monitored for two consecutive weeks. Weight of each mouse was observed for any significant changes. The mice were sacrificed by cervical dislocation at the end of the study (day 28), followed by postmortem of selected mouse to see any changes in organ morphology and any potential metastasis.

The volume of the tumor was calculated using the following formula.

$$\textbf{Tumor volume } (mm^3) = \textbf{Length x } (width^2) / 2$$

The data were presented as mean±SD of tumor volume from each group.

Group	Regimen	Number of mice
Untreated	10µg p53 in 100µl DMEM	10
$SrSO_3$	5µl of 1M $SrCl_2$, 2µl of 1M Na_2SO_3, 20µg p53, in 10µl HEPES-buffered media, followed by addition of DMEM to achieve 100µl suspension	5
	5µl of 1M $SrCl_2$, 2µl of 1M Na_2SO_3, 10µg p53, in 10µl HEPES-buffered media, followed by addition of DMEM to achieve 100µl suspension	10
SrF_2	5µl of 1M $SrCl_2$, 2µl of 1M NaF, 20µg p53, in 10µl HEPES-buffered media, followed by addition of DMEM to achieve 100µl suspension	5
	5µl of 1M $SrCl_2$, 2µl of 1M NaF, 10µg p53, in 10µl HEPES-buffered media, followed by addition of DMEM to achieve 100µl suspension	10
$MgSO_3$	5µl of 1M $MgCl_2$, 2µl of 1M Na_2SO_3, 20µg p53, in 10µl HEPES-buffered media, followed by addition of DMEM to achieve 100µl suspension	5
	5µl of 1M $MgCl_2$, 2µl of 1M Na_2SO_3, 10µg p53, in 10µl HEPES-buffered media, followed by addition of DMEM to achieve 100µl suspension	10
CO_3 AP	44mM Na_2CO_3, 5µl of 1M $CaCl_2$, 20µg p53, followed by addition of DMEM to obtain 100µl suspension	5
	44mM Na_2CO_3, 5µl of 1M $CaCl_2$, 10µg p53, followed by addition of DMEM to obtain 100µl suspension	10

Table 5.4: Mice grouping of p53-loaded NPs for tumour regression studies.

5.2.5 Tumor regression studies involving MAPK siRNA-loaded NPs

In a separate study, MAPK siRNA was incorporated into the complexes with the similar manner as p53 gene. 50nM MAPK siRNA was integrated to 5µl of 1M $SrCl_2$ or $MgCl_2$ with 2µl of 1M Na_2SO_3 or NaF in 10µl HEPES-buffered media. The chemical reaction was maintained for 30 minutes at 37^oC, followed by a brief mixture of DMEM-powdered media to form the final volume of 100µl particle suspension. CO_3 AP and naked MAPK were used as respective positive and negative control. Effect of MAPK siRNA concentration on tumor regression was subsequently studied, with 50nM and 100nM MAPK siRNA transfected to each mouse via complexation into various salt crystals, as shown in Table 5.5.

Each treatment was repeated two days after the initial treatment regimen. Tumor growth was supervised every two days, measuring width and length of tumor lump using Vernier caliper (mm scale) from the treatment day (day 14), for two consecutive weeks. The mice were sacrificed by cervical dislocation at the end of the study (day 28).

Group	Regimen	Number of mice
Untreated	50nM MAPK siRNA in 100µl DMEM	10
$SrSO_3$	5µl of 1M $SrCl_2$, 2µl of 1M Na_2SO_3, 50nM MAPK siRNA in 10µl HEPES-buffered media, followed by addition of DMEM to achieve 100µl suspension	10
	5µl of 1M $SrCl_2$, 2µl of 1M Na_2SO_3, 100nM MAPK siRNA in 10µl HEPES-buffered media, followed by addition of DMEM to achieve 100µl suspension	5
SrF_2	5µl of 1M $SrCl_2$, 2µl of 1M NaF, 50nM MAPK siRNA in 10µl HEPES-buffered media, followed by addition of DMEM to achieve 100µl suspension	10
	5µl of 1M $SrCl_2$, 2µl of 1M NaF, 100nM MAPK siRNA in 10µl HEPES-buffered media, followed by addition of DMEM to achieve 100µl suspension	5
$MgSO_3$	5µl of 1M $MgCl_2$, 2µl of 1M Na_2SO_3, 50nM MAPK siRNA in 10µl HEPES-buffered media, followed by addition of DMEM to achieve 100µl suspension	10
	5µl of 1M $MgCl_2$, 2µl of 1M Na_2SO_3, 100nM MAPK siRNA in 10µl HEPES-buffered media, followed by addition of DMEM to achieve 100µl suspension	5
CO_3 AP	44mM Na_2CO_3, 5µl of 1M $CaCl_2$, 50nM MAPK siRNA, followed by addition of DMEM to obtain 100µl suspension	10
	44mM Na_2CO_3, 5µl of 1M $CaCl_2$, 100nM MAPK siRNA, followed by addition of DMEM to obtain 100µl suspension	5

Table 5.5: Mice grouping of MAPK siRNA-loaded NPs for tumor regression studies.

5.2.6 Tumor regression studies involving ligand-coated NPs

Effect of ligand binding on improving nanocarrier activity was performed by incorporating 100µl of total suspension by various preparations of salt crystals with p53 gene, supplemented with DMEM for intravenous administration into each mouse (at right or left caudal tail vein). The ligand-bound NPs, formed by a mixture of 20µg of p53 gene with 5µl of 1M $SrCl_2$ or $MgCl_2$ was added to 2µl of 1M Na_2SO_3 or NaF in 10µl HEPES-buffered media to fabricate respective $SrSO_3$, SrF_2, and $MgSO_3$ particles, with CO_3 AP as control, as specified in Table 5.6. The chemical reaction was sustained for 30 minutes at 37^oC, followed by subsequent incorporation of 1µg Fibronectin or transferrin into the fabricated salt crystals and incubated for 10 minutes, before addition of DMEM-powdered media to form a final volume of 100µl particle suspension.

Treatment involving complexed solution was transfected into mice and repeated two days following the initial treatment regimen. Tumor growth was supervised every two days, measuring width and length of tumor lump using Vernier caliper (mm scale) from the treatment day (day 14), for two consecutive weeks. The weight of each mouse was observed for any significant changes. The mice were sacrificed by cervical dislocation at the end of the study (day 28), followed by postmortem of selected mouse to see any changes in organ morphology and any potential metastasis.

Group	Regimen	Number of mice
$SrSO_3$	5µl of 1M $SrCl_2$, 2µl of 1M Na_2SO_3, 20µg p53, in 10µl HEPES-buffered media, followed by addition of DMEM to achieve 100µl suspension	5
	5µl of 1M $SrCl_2$, 2µl of 1M Na_2SO_3, 20µg p53, in 10µl HEPES-buffered media, followed by addition of 1µg fibronectin and final volume of DMEM to achieve 100µl suspension	5
	5µl of 1M $SrCl_2$, 2µl of 1M Na_2SO_3, 20µg p53, in 10µl HEPES-buffered media, followed by addition of 1µg transferrin and final volume of DMEM to achieve 100µl suspension	5
SrF_2	5µl of 1M $SrCl_2$, 2µl of 1M NaF, 20µg p53, in 10µl HEPES-buffered media, followed by addition of DMEM to achieve 100µl suspension	5
	5µl of 1M $SrCl_2$, 2µl of 1M NaF, 20µg p53, in 10µl HEPES-buffered media, followed by addition of 1µg fibronectin and final volume of DMEM to achieve 100µl suspension	5
	5µl of 1M $SrCl_2$, 2µl of 1M NaF, 20µg p53, in 10µl HEPES-buffered media, followed by addition of 1µg transferrin and final volume of DMEM to achieve 100µl suspension	5
$MgSO_3$	5µl of 1M $MgCl_2$, 2µl of 1M Na_2SO_3, 20µg p53, in 10µl HEPES-buffered media, followed by addition of DMEM to achieve 100µl suspension	5
	5µl of 1M $MgCl_2$, 2µl of 1M Na_2SO_3, 20µg p53, in 10µl HEPES-buffered media, followed by addition of 1µg fibronectin and final volume of DMEM to achieve 100µl suspension	5
	5µl of 1M $MgCl_2$, 2µl of 1M Na_2SO_3, 20µg p53, in 10µl HEPES-buffered media, followed by addition of 1µg transferrin and final volume of DMEM to achieve 100µl suspension	5
CO_3 AP	44mM Na_2CO_3, 5µl of 1M $CaCl_2$, 20µg p53, followed by addition of DMEM to obtain 100µl suspension	5
	44mM Na_2CO_3, 5µl of 1M $CaCl_2$, 20µg p53, followed by addition of DMEM to obtain 100µl and 1µg fibronectin into the suspension	5
	44mM Na_2CO_3, 5µl of 1M $CaCl_2$, 20µg p53, followed by addition of DMEM to obtain 100µl and 1µg transferrin into the suspension	5

Table 5.6: Mice grouping for influence of protein coating on tumor regression studies

5.3 Results

5.3.1 Time-dependent biodistribution studies

Biodistribution characteristic of selected salt particles was investigated upon 1, 2 and 4 hours after intravenous administration into randomly assigned tumor-bearing mice. The injections were well tolerated, and mice did not exhibit any alteration in behavior. Tissue size, color, and morphology remained unchanged, as compared to PBS-treated mice. High overall accumulation of fluorescence activity was found in the liver and kidney, followed by brain, lung, spleen and tumor 1-hour post intravenous delivery.

The kidney was the preferential site for accumulation of siRNA-nanocrystals with values as high as 2200/mg protein, seen in $SrSO_3$ (Figure 5.2). Highest detection of fluorescence activity in organ tissues was observed at 2 hours, with up to 3-fold increment detected in respective liver, kidney, brain and tumor tissues. Subsequently, intensity reduction was observed at 4 hours post treatment, with an approximate reduction of 50% seen with brain and tumor throughout all nanocarrier tested. Fluorescence activity remained low for lung and spleen, throughout various hours of experimental studies. Trans-tumoral delivery in each organ was comparable between all NPs, including CO_3 AP particles (studied and showed proven benefit in vivo). $SrSO_3$ has higher siRNA deposition in all organs, particularly lung and spleen, as compared to all salts tested, with stagnant level throughout 4 hours. $MgSO_3$ is associated with less efficient siRNA carrier, demonstrating slightly lower fluorescence intensity per tissue mass.

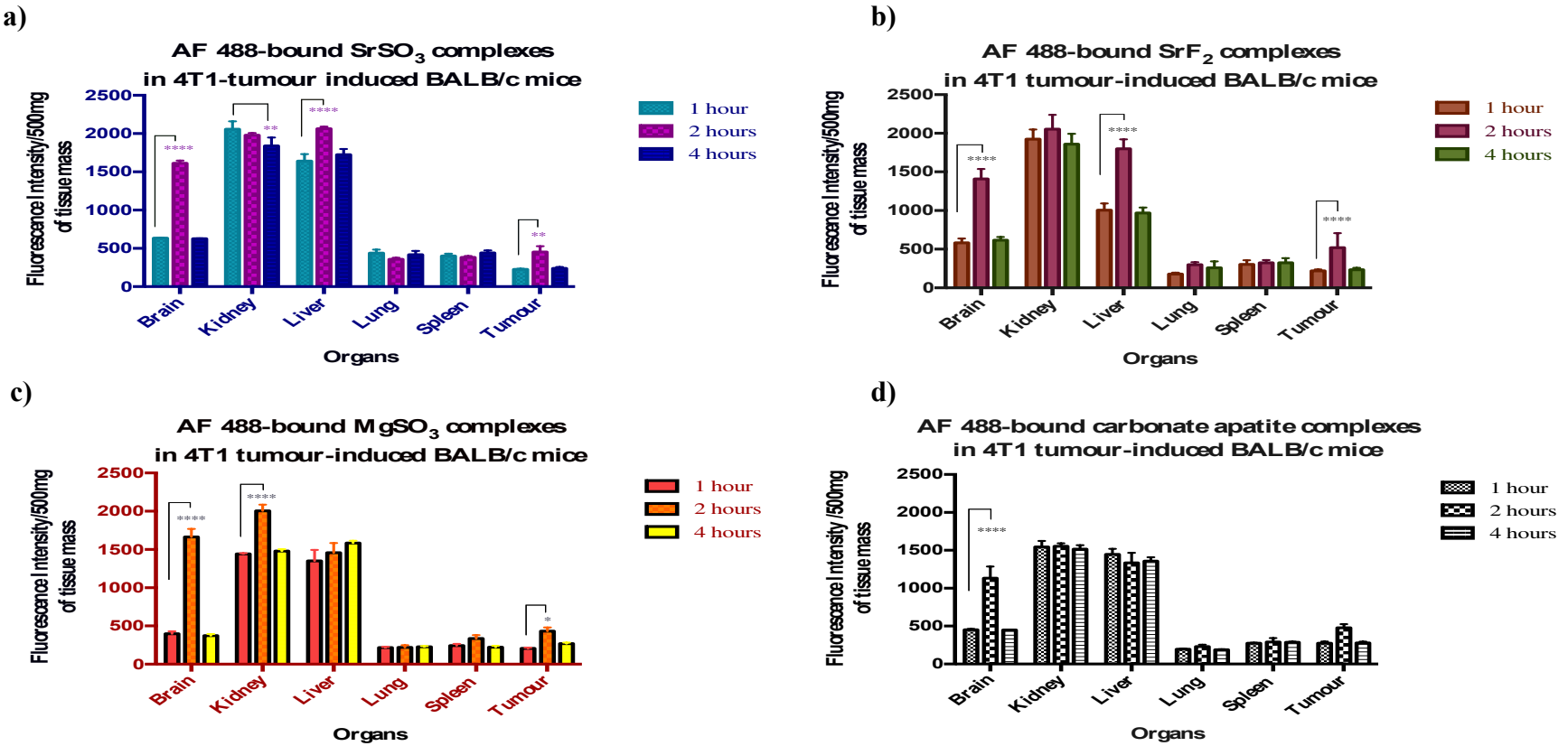

Figure 5.2: Biodistribution of AF 488 siRNA-loaded NPs on various organs at different time points. 4T1 tumor induced BALB/c mice were treated intravenously through tail-vein injection. 100µl suspension formed by mixture of 5µl 1M $SrCl_2$/ $MgCl_2$ and 2µl 1M Na_2SO_3/NaF with 1µM fluorescence-labeled negative siRNA was administered as the tumor volume reached approximately 13.20 ±2.51mm^3. Mice were sacrificed 1, 2 or 4 hours post intravenous treatment, followed by organ harvestment and organ tissues lysis. The homogenized tissue lysates were next centrifuged at 15,000 RPM for 30 minutes at 4^o C; with 100µl supernatants taken for analysis for each organs' fluorescence intensity. Mice were randomly selected and separate at 5 mice/group, data was represented as mean±SD of the fluorescence intensity/500mg of tissue mass. 1, 2 and 4 hours of incubation time for organ distributions of (a) $SrSO_3$, (b) SrF_2, (c) $MgSO_3$ and (d) CO_3 AP. ****p<0.0001 and **p<0.01 as compared to CO_3 AP of each respective organs.

Figure 5.3: Harvested organs upon treatment and BALB/c mice sacrificial. From top left to right, tumor tissue, kidneys, liver, lung, spleen. Bottom left: brain.

5.3.2 Concentration-dependent biodistribution studies

Effect of salts concentration on biodistribution profile was independently observed via intravenous injection of NPs complexed with various concentration of Na_2SO_3 and NaF (20mM and 50mM, respectively). The treatment was well tolerated, and mice did not exhibit any alteration in behavior. Tissue size, color, and morphology remained unchanged, as compared to CO_3 AP-treated mice.

Effect on sulfite and fluoride concentration modification showed no additional benefit on trans-tumoural deposition. No vast difference was seen for other organs, except for lung and spleen of AF 488-loaded $SrSO_3$ complexes. $SrSO_3$ has higher tissue fluorescence intensity of each organ in comparison to SrF_2, $MgSO_3$ and CO_3 AP. Fluorescence intensity expressed from magnesium sulfite-treated groups showed data similarity with CO_3 AP, with lower liver activity throughout the studies.

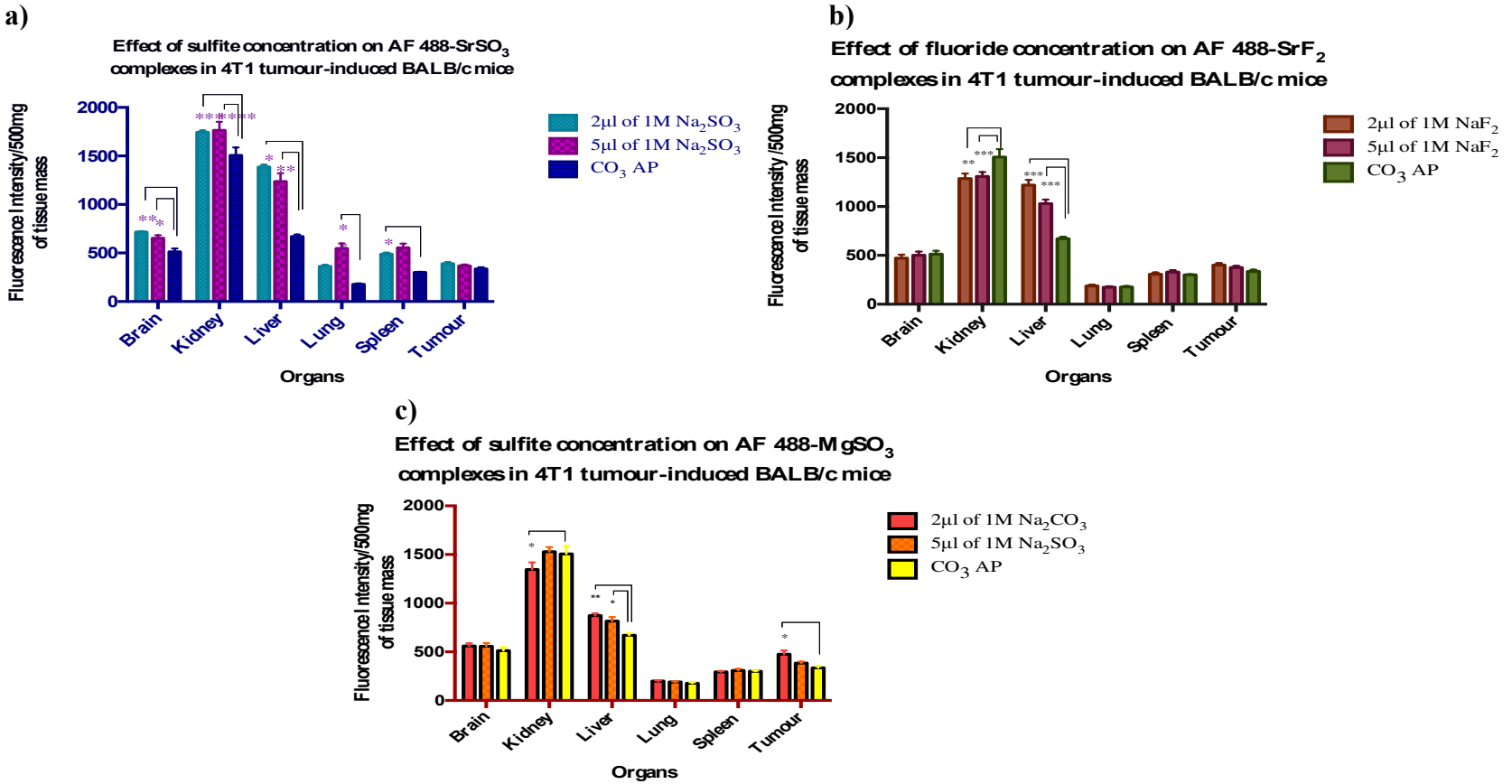

Figure 5.4: Biodistribution of AF 488 siRNA-loaded NPs on various organs with different Na_2SO_3 or NaF concentrations. 4T1 tumor-induced BALB/c mice were intravenously treated through tail-vein injection. 100µl treatment suspensions, formed with 5µl 1M $SrCl_2$/ $MgCl_2$ and 2µl 1M Na_2SO_3/NaF with 1µM fluorescence-labeled negative siRNA was administered as the tumor size reached approximately 13.20 ±2.51mm^3. Mice were sacrificed 4 hours post-intravenous treatment, followed by organ harvesting and tissue lysis. Tissue lysates were centrifuged at 15,000 RPM for 30 minutes at 4^o C; with 100µl of supernatants were observed for fluorescence intensity of each tissues. 5 mice/group were randomly assigned after tumor induction, and data was represented as mean±SD of the fluorescence intensity/500mg of tissue mass. 20mM and 50mM of sulfite and fluoride concentration incorporated into (a) $SrSO_3$, (b) SrF_2 and (c) $MgSO_3$. ****p<0.0001, ***p<0.001, **p<0.01 and *p<0.05 for each respective salts, as compared with CO_3 AP.

5.3.3 Influence of protein coating on biodistribution studies

Study on biodistribution activity influenced by ligand coating *in vivo* was explained through the incorporation of fibronectin and transferrin protein upon formation of siRNA-loaded particle complexes, generating ligand-coated gene-NPs. To achieve active targeting manner, 1µg of selected proteins was incorporated into fabricated salts for 10 minutes incubation prior to the mixture of DMEM media to form complexes suspension for intravenous delivery into tumor-bearing BALB/c mice, with fixed salt concentrations and incubation time (4 hours). Ligand-coated NPs consisted of $SrSO_3$, SrF_2 and $MgSO_3$ were compared with uncoated ones, with reference to CO_3 AP particles. The injections were well tolerated, and mice did not exhibit any alteration in behavior. Tissue size, color, and morphology remained unchanged, as compared to CO_3 AP-treated mice. Fibronectin protein increasing in fluorescence activity of all organs studied, with a greater proportional rise at the tumor site, as seen in Figure 5.3. Fibronectin-coated AF 488-NPs complexes enhanced the trans-tumoral activity with up to three-fold increment. Transferrin protein is also associated with greater improvement in organ tissue accumulation. Brain and kidney have more fluorescence detection upon transferrin-coated NPs treatment, in comparison to uncoated ones. Additionally, transferrin protein improved tumor fluorescence deposition for both $SrSO_3$ and CO_3 AP. Transferrin has lesser intra-tumoral integration than fibronectin-coated particle complexes. Liver tissue accumulation was reduced upon transfection with protein-complexed NPs, with exception to SrF_2. Lung and spleen did not show any vast changes in fluorescence activity from both transferrin or fibronectin-coated in reference to uncoated salts particles. $SrSO_3$ showed greater detection of fluorescence intensity of most organs in comparison to SrF_2, $MgSO_3$ and CO_3 AP.

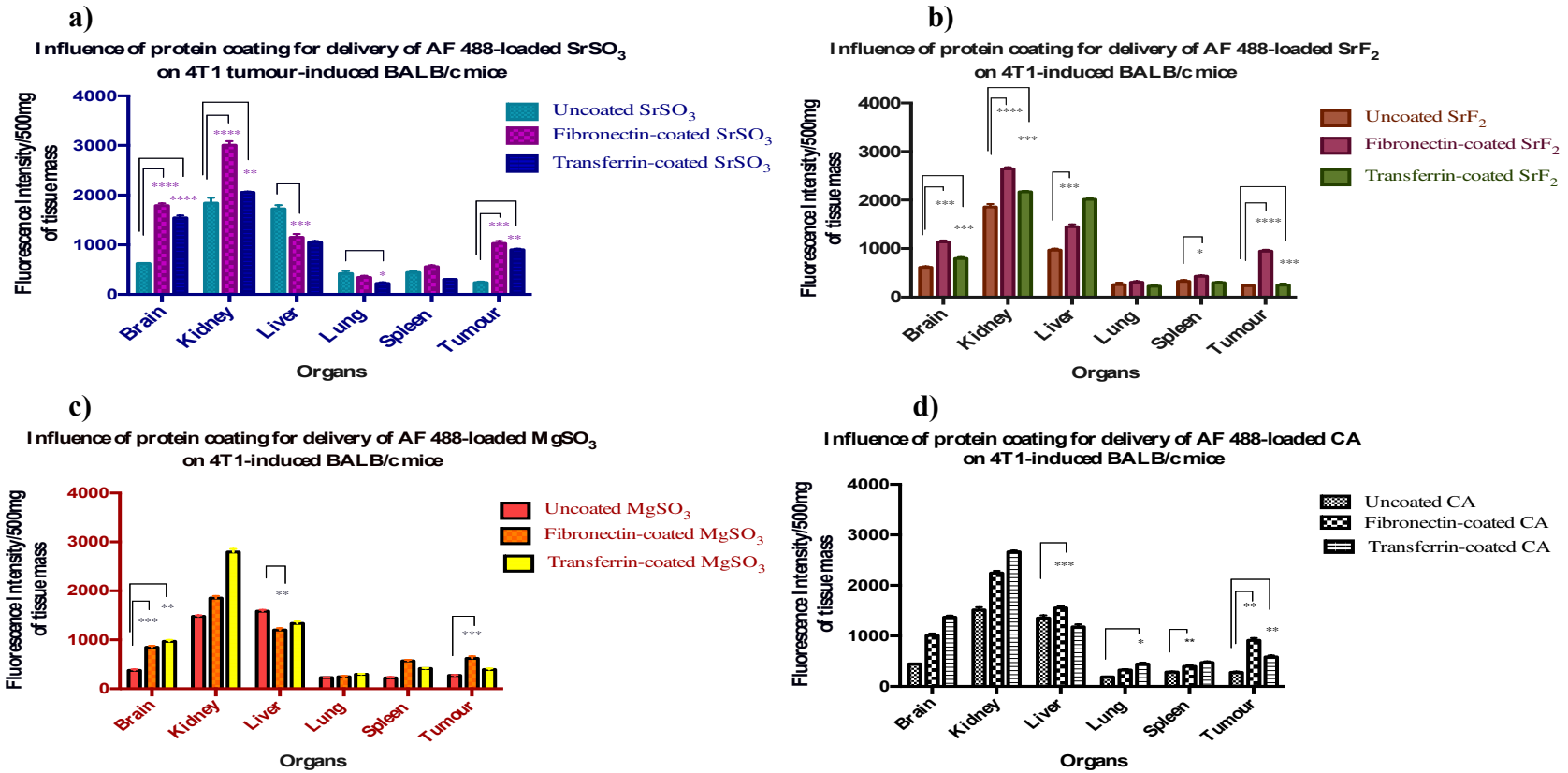

Figure 5.5: Biodistribution of AF 488 siRNA-NP complexes on various organs with involvement of fibronectin and transferrin coating. 4T1 tumor-induced BALB/c mice were treated intravenously through tail-vein injection. 100µl suspection formed by mixture of 5µl 1M $SrCl_2$/ $MgCl_2$ and 2µl 1M Na_2SO_3/NaF with 1µM fluorescence-labeled negative siRNA was administered as the tumor volume reached approximately 13.20 ±2.51mm^3. Mice were sacrificed 4 hours post treatment, followed by organs harvesting and lysis. Tissue lysates were centrifuged at 15,000 RPM for 30 minutes at 4^o C; with 100µl supernatants taken for observation to detect fluorescence activity in each organs. 5 mice/group were randomly assigned after tumor induction, and data was represented as mean±SD of the fluorescence intensity/500mg of tissue mass. Fibronectin and transferrin-coated (a) SrSO3, (b) SrF2, (c) MgSO3 and (d) CO_3 AP (control). ****p<0.0001, ***p<0.001, **p<0.01 and *p<0.05 as compared to uncoated salts for each respective organs.

5.3.4 Tumor regression studies involving p53-loaded NPs

Experiment on tumor regression studies was developed to review the path beyond internalization of target genes, which consisted of disintegration process to release genetic materials and for transcription process to occur inside the nuclear cavity. Integrated target genes, p53 with NP complexes were administered intravenously, followed by tumor size measurement every two days for any changes in tumor volume throughout four weeks from initial tumor induction. The injections were well tolerated, and mice did not exhibit any alteration in behavior. Tumor tissue mass and morphology differed based on types of treatment, as compared to CO_3 AP-treated mice. The spleen was seen enlarged, with minimal 2-fold size increment for all mice, including control group on day 28 upon mice sacrificial. No metastasis was visibly observed in lung and liver.

Comparative study on tumor changes with p53-loaded salt particles transfection showed a reduction in tumor progression over 28 days post tumor induction based on all salts experimented. In general, all transfected mice showed a decrease in tumor size until day 18, followed by gradual increase in tumor volume up to day 28. SrF_2 showed a lower rate of tumor growth than CO_3 AP, exhibiting size of 400mm^3, followed by $SrSO_3$ and $MgSO_3$ as seen in Figure 5.4. The tumor size of naked p53 was consistently high, similarly seen with untreated mice group. $SrSO_3$ and $MgSO_3$ have higher growth rate in comparison with CO_3 AP, indicating less ability in suspending the tumor growth, regarded with respective 600mm^3 and 700mm^3 upon day 28. The effect of p53 concentration on tumor regression activity was subsequently performed, inclusive of naked p53 and untreated mice as the experimental control. According to Figure 5.5, there was no significant alteration in tumor volume of mice treated with SrF_2 and $MgSO_3$ particles, with respect to the increased amount of the apoptotic

plasmid involved. The rate of tumor growth, however, decelerated with 20µl p53-$SrSO_3$ complexes in comparison to 10µl p53, with an approximately 100mm^3 difference in tumor volume on day 28. The tumor size of mice transfected with naked p53 or of untreated groups remained high throughout the study.

5.3.5 Tumor regression studies involving MAPK siRNA-loaded NPs

Studies on tumor volume were comparably done with MAPK siRNA, which selectively silence MAP Kinase pathway. MAPK siRNA-complexed with $SrSO_3$, SrF_2 and $MgSO_3$ NPs were administered intravenously, followed by tumor size measurement every two days for any changes in tumor mass throughout four weeks from initial tumor induction. The injections were well tolerated, and mice did not exhibit any alteration in behavior. Tumor tissue size and morphology differed based on types of treatment, as compared to CO_3 AP-treated mice. The spleen was seen enlarged, with minimal 2-fold size increment for all mice, including control group on day 28 upon mice sacrificial. No metastasis was visibly observed in lung and liver.

MAPK-loaded NPs displayed slower growth rate through $SrSO_3$, SrF_2, and MgSO3, with comparison to CO_3 AP particles, based on Figure 5.8. Tumor volumes of salt crystals were, at least, 100mm^3 smaller compared to control group, with the largest size differential was seen $SrSO_3$, followed by SrF_2 and $MgSO_3$. Tumor development in BALB/c mice reduced up to 200mm^3 in size (in comparison with naked siRNA treatment) with incorporation of MAPK siRNA into the complexes. Treatment involving naked siRNA showed minor changes with untreated group, representing no effect of siRNA on potentially silencing the MAP kinase pathway.

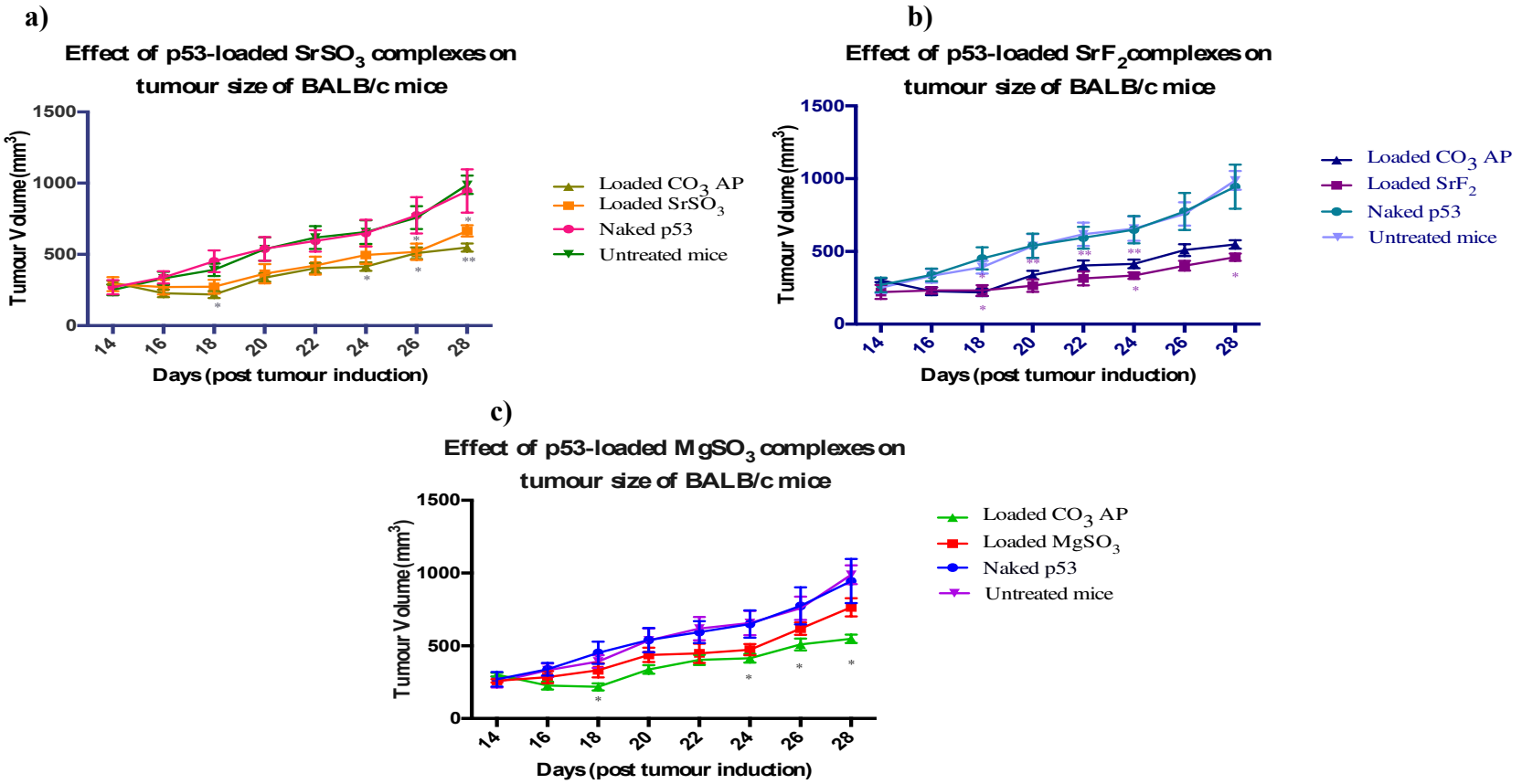

Figure 5.6: Tumor regression studies of p53-loaded NPs on BALB/c mice. 4T1 tumor induced BALB/c mice were treated intravenously through tail-vein injection with 100µl solution fabricated by 5µl 1M $SrCl_2$/ $MgCl_2$ and 2µl 1M Na_2SO_3/NaF with 20µg p53 in 10µl HEPES media, as the tumor volume reached approximately 13.20 ±2.51mm^3 (estimation on day 14). Naked p53 and CO_3 AP groups represented positive and negative control, in addition to untreated group as experimental control. 2nd dose was administered after 2 days of 1st treatment (day 17). Tumor growth was monitored every two days, constantly for two weeks. 5 mice/group were randomly selected after tumor induction and data was represented as mean±SD. p53-loaded (a) $SrSO_3$, (b) SrF_2 and (c) $MgSO_3$. **p<0.01 and *p<0.05 as compared to naked p53 group throughout the experiment.

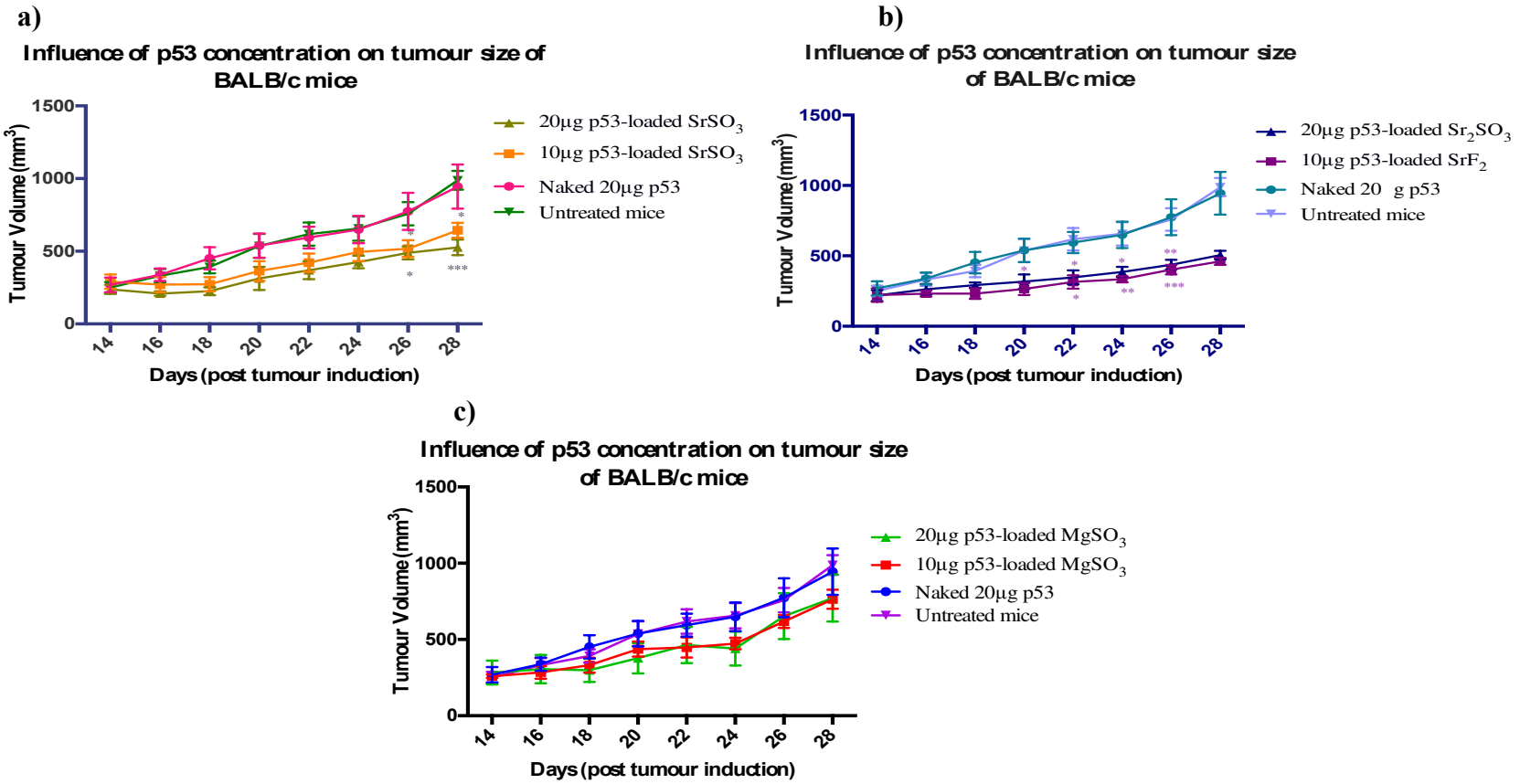

Figure 5.7: Tumor regression studies of p53 concentration effect on BALB/c mice. 4T1 tumor induced BALB/c mice were treated intravenously through tail-vein injection with 100µl solution fabricated by 5µl 1M $SrCl_2$/ $MgCl_2$ and 2µl 1M Na_2SO_3/NaF with 10 and 20µg p53 in 10µl HEPES as the tumor volume reached approximately 13.20 ±2.51mm^3 (estimation on day 14). Naked p53 group and untreated mice represented experimental negative control. 2nd dose was administered after 2 days of 1st treatment (day 17). Tumor growth was monitored every two days, constantly for two weeks. 5 mice/group were randomly selected after tumor induction and data was represented as mean±SD. 10 and 20µg p53 generated with (a) $SrSO_3$, (b) SrF_2 and (c) $MgSO_3$. **$p<0.01$ and *$p<0.05$ as compared to naked p53 group throughout the experiment.

Additionally, all salt particles improved the siRNA activity greater than established CO_3 AP particles.

Subsequent experiments following the effect of MAPK siRNA concentration on tumor volume of BALB/c mice revealed that with 100nM MAPK concentration, tumor growth rate was superior to 50nM concentration, as seen by siRNA-loaded $SrSO_3$ and SrF_2 (Figure 5.7). However, tumor volume of $MgSO_3$ is smaller upon increasing in siRNA concentration, with around 100mm^3 difference. The mass of tumor remained less with siRNA-loaded with vector than the naked counterpart. Treatment involving naked siRNA showed minor changes with untreated group, representing no effect of siRNA on potentially silencing the MAP kinase pathway.

5.3.6 Tumor regression studies involving ligand-coated NPs

The impact of fibronectin and transferrin coating on tumor size on BALB/c mice was studied with the incorporation of 1µg of protein into p53-loaded particle complexes, followed by intravenous injection into tumor-bearing BALB/c mice and tumor size measurement every two days for any changes in tumor volume throughout four weeks from initial tumor induction. The treatment was well tolerated, and mice did not exhibit any alteration in behavior. Tumor tissue size and morphology differed based on types of treatment, as compared to CO_3 AP-treated mice. The spleen was seen enlarged, with minimal 2-fold size increment for all mice, including control group on day 28 upon mice sacrificial. No metastasis was visibly observed in lung and liver.

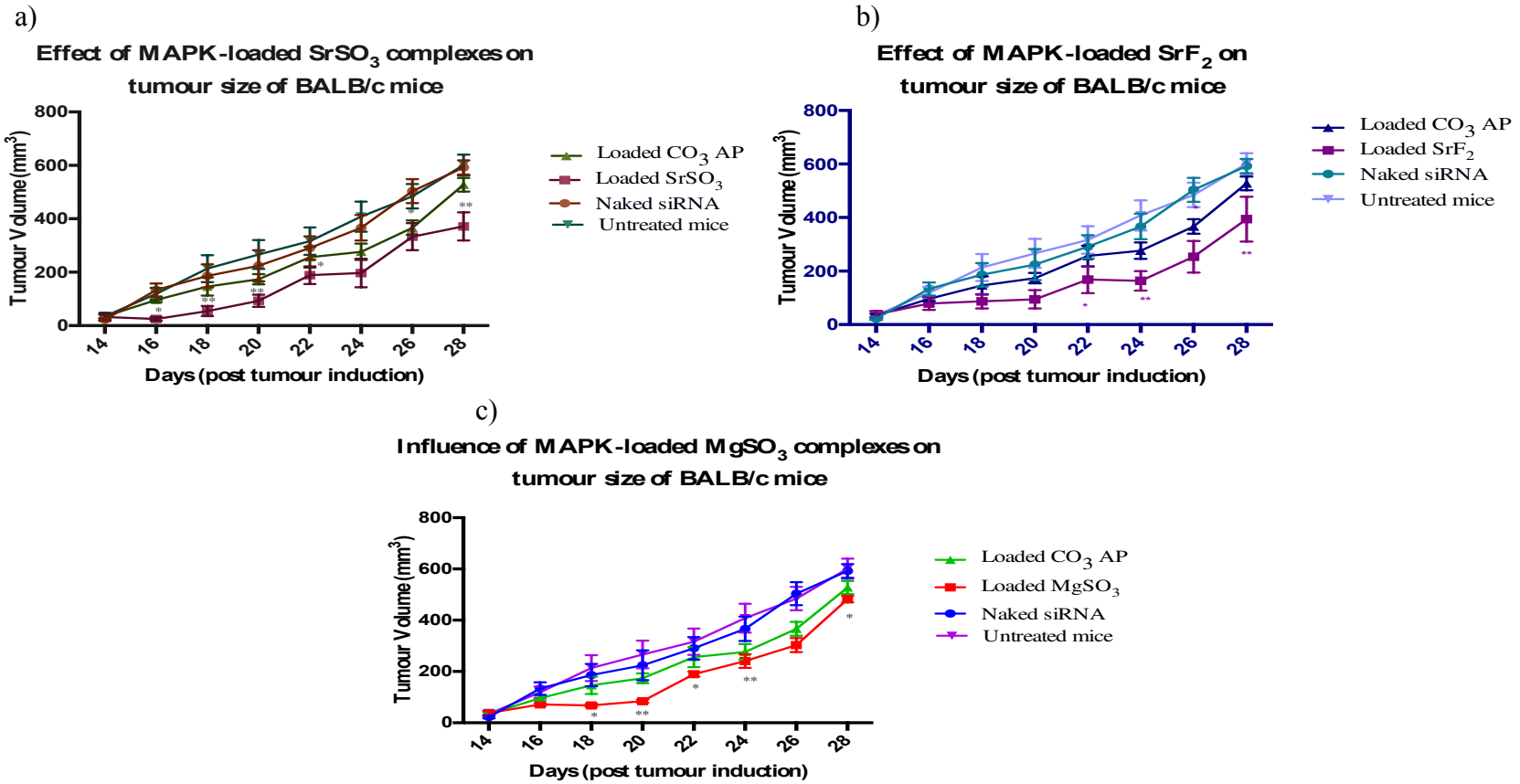

Figure 5.8: Tumor regression studies of MAPK siRNA-loaded NPs on BALB/c mice. 4T1 tumor induced BALB/c mice were treated intravenously through tail-vein injection with 100µl solution fabricated by by 5µl 1M $SrCl_2$/ $MgCl_2$ and 2µl 1M Na_2SO_3/NaF with 50mM MAPK in 10µl HEPES as the tumor volume reached approximately 13.20 ±2.51mm^3 (estimation on day 14). Untreated, naked siRNA and CO_3 AP groups represented positive and negative control. 2nd dose was administered after 2 days of 1st treatment (day 17). Tumor growth was monitored every two days, constantly for two weeks. 5 mice/group were randomly selected after tumor induction and data was represented as mean±SD. MAPK-loaded (a) $SrSO_3$, (b) SrF_2 and (c) $MgSO_3$. **p<0.01 and *p<0.05 as compared to naked MAPK siRNA throughout the experiment.

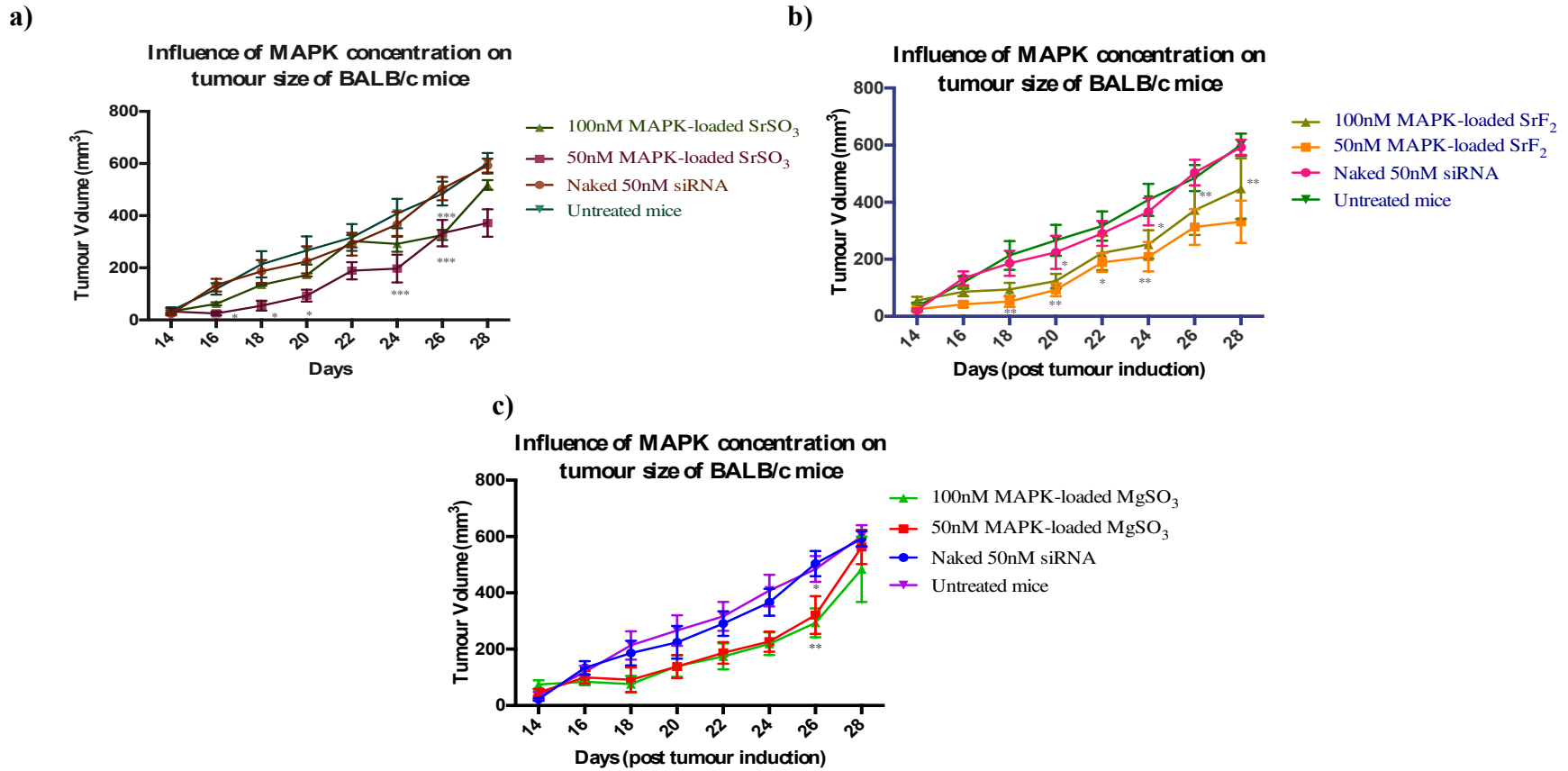

Figure 5.9: Tumor regression studies of MAPK concentration effect on BALB/c mice. 4T1 tumor induced BALB/c mice were treated intravenously through tail-vein injection with 100µl solution fabricated by 5µl 1M $SrCl_2$/ $MgCl_2$ and 2µl 1M Na_2SO_3/NaF with 50mM and 100nM MAPK in 10µl HEPES as the tumor volume reached approximately 13.20 ±2.51mm^3 (estimation on day 14). Uncoated and naked siRNA represented the negative control group. 2nd dose was administered after 2 days of 1st treatment (day 17). Tumor growth was monitored every two days, constantly for two weeks. 5 mice/group were randomly selected after tumor induction and data was represented as mean±SD. MAPK-loaded (a) $SrSO_3$, (b) SrF_2 and (c) $MgSO_3$. **p<0.01 and *p<0.05 as compared to naked MAPK siRNA throughout the experiment.

Figure 5.10: Tumor mass seen from excision biopsy of sacrificed BALB/c mouse on day 28. The enlarged spleen was seen next to the carcinoma tissue.

Transferrin and fibronectin protein incorporation are associated with the reduction in tumor progression, through coating onto all salts. In comparison to uncoated p53-NP complexes, the tumor mass decreased up to 300mm^3 upon 28 days post tumor induction. Fibronectin showed superiority in assisting tumor shrinkage of p53-loaded $SrSO_3$ and SrF_2 than by transferrin coating. Nonetheless, transferrin improves the tumor reduction rate for $MgSO_3$ greater than fibronectin-complexed particles. The changes in tumor growth rate vary between salts and proteins used, with fibronectin-coated, p53-loaded SrF_2 showed smallest tumor size of 100mm^3 on day 28, in comparison to 180mm^3 and 200mm^3 of respective $SrSO_3$ and $MgSO_3$, further indicating that the size reduction assisted by fibronectin is almost 70% from uncoated SrF_2, followed by 40% and 50% on $SrSO_3$ and $MgSO_3$. The tumor size of transferrin-coated, p53-bound $MgSO_3$ was 140mm^3 on day 28, followed by 190mm^3 and 200mm^3

with respect to $SrSO_3$ and SrF_2, revealing size reduction in association to transferrin is approximately 70% with $MgSO_3$, followed by 40% of both $SrSO_3$ and SrF_2.

The size differential from naked p53 delivery in comparison to various treatments hence verified the vast improvement in genetic delivery *in vivo* via potential vectors, in association to ligand coating. Through comparison on different types of p53 delivery, the highest reduction of tumor growth seen with approximately 90% with fibronectin-coated p53-SrF_2 complexes, determined on day 28 from 950mm^3 of tumor size treated with naked p53, followed by 85% reduction by transferrin-coated p53-$MgSO_3$ complexes.

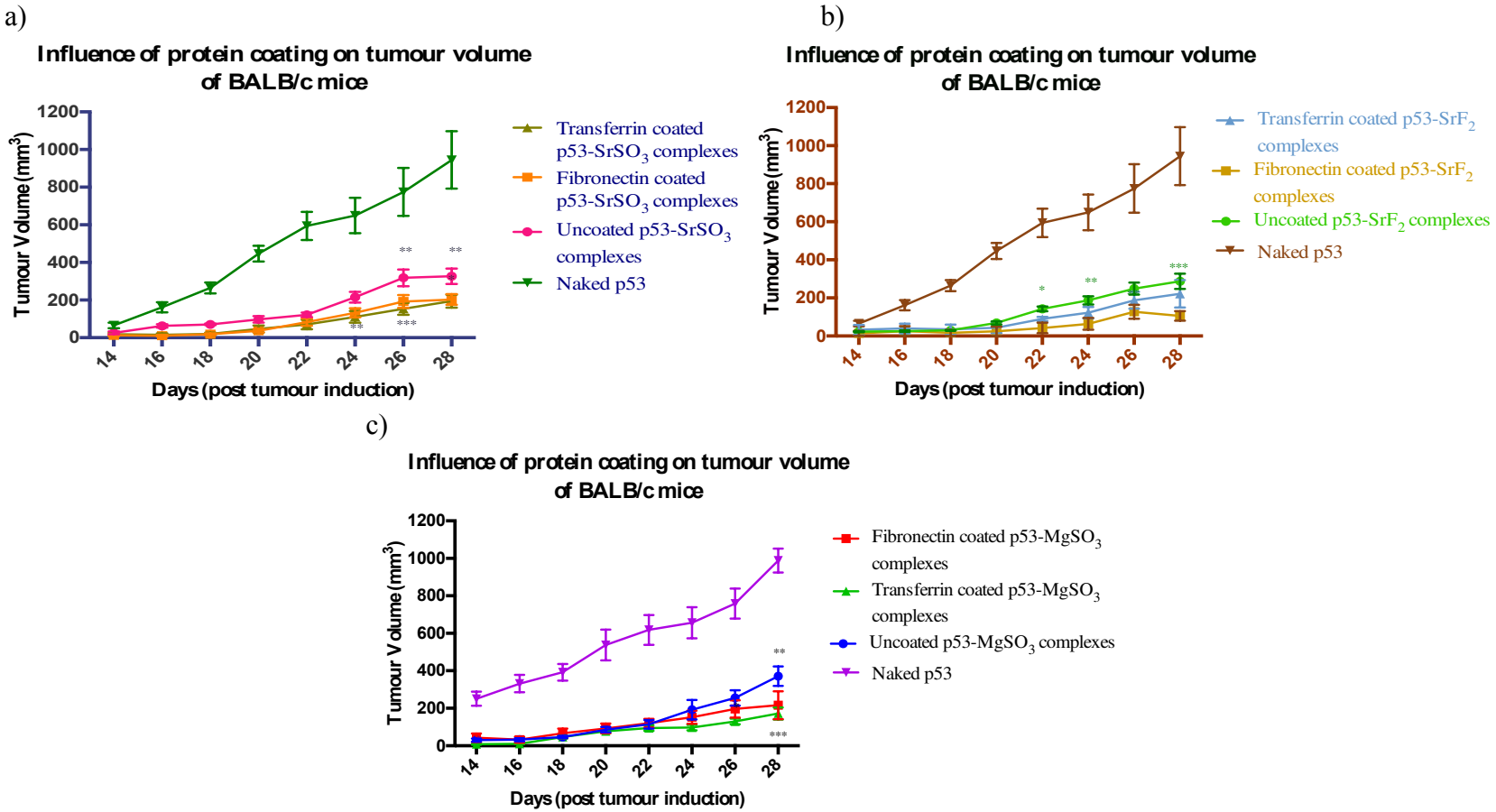

Figure 5.11: Tumor regression studies for impact of protein coating on BALB/c mice. 4T1 tumor induced BALB/c mice were treated intravenously through tail-vein injection with 100µl solution fabricated by 5µl 1M $SrCl_2$/ $MgCl_2$ and 2µl 1M Na_2SO_3/NaF with 20µg p53 in 10µl HEPES, followed by addition of 1µg fibronectin or transferrin as the tumor volume reached approximately 13.20 ±2.51mm^3 (estimation on day 14). Uncoated NP complexes represented negative control. 2nd dose was administered after 2 days of 1st treatment (day 17). Tumor growth was monitored every two days, constantly for two weeks. 5 mice/group were randomly selected after tumor induction and data was represented as mean±SD. p53-loaded (a) $SrSO_3$, (b) SrF_2 and (c) $MgSO_3$. **$p<0.01$ and *$p<0.05$ as compared to uncoated NPs.

5.4 Discussions

The influence of selected nano-vectors in efficiently transporting genetic material in vivo was explored in this chapter. Each salt particle with the ability to improve transportation of the nucleic acid *in vitro*, in addition to low cellular toxicity was further studied to understand the impact of each potential nanocarriers in the biological system. The efficient utilization of genetic material both in vitro and in vivo are often hindered by their high molecular weight and negative charge, which is associated with instability in the blood circulation (1). Both pDNA and siRNA are double-stranded nucleic acids with anionic phosphodiester backbones. Distinctive size, structure and chemistry of pDNA and siRNA impose particular requirements for fabricating ideal nanocarriers. The size differential of pDNA in relation to siRNA results in the different level of electrostatic interactions with vectors. siRNA has lower ability to generate stable complexes compared to pDNA duplexes. siRNA is more degradable due to RNA backbone consisting ribose with a hydroxyl group at the 2' position of the pentose ring in comparison to a more stabilized structure of pDNA via deoxyribose. Both types of nucleic acids vary in their site of action, in which cytoplasmic delivery of siRNA is only required to perform a silencing activity, in comparison to pDNA, which requires a nuclear transfer for transgenic expression (2)(3). The inclusion of both pDNA and siRNA was hence fundamental to appreciate the vector potential of selected salt crystals.

Efficient systemic distribution of gene therapy is impeded by various extracellular barriers, involving serum endonuclease attack causing premature degradation of gene and active removal by glomerular filtration, associated with the plasma half-life of <10 minutes (4). Fundamental problems related to potential carriers may further worsen the inefficiency of gene delivery, including opsonization of nanoparticles with non-specific

plasma proteins, enabling it to become more visible towards the phagocytic cells (e.g., macrophages, monocyte or phagocyte). Following opsonization, phagocytosis may occur, depending on their surface characteristics, including Zeta charge and hydrophilicity. Opsonization happened within minutes after intravenous delivery, removes the particles from the circulatory via mononuclear and polymorphonuclear phagocytic system (5). Reticuloendothelial system (RES), which is part of the immune response system, is located in the liver (Kupffer cells), spleen and lung. RES consists of phagocytic cells including circulatory monocytes and macrophages, binding to the opsonized particles, which are readily coated with serum protein to trigger the mechanism for RES detection in the blood circulation (6). The uptake via RES organs depends on particle sizes and surface characteristics, which hydrophobic particles are preferred 'objects' to be taken up mostly by the liver and spleen (7).

Transportation of particles passing through cancer endothelium region is more efficient than normal endothelium, associated with leaky vasculature (permeation) and inefficient lymphatic drainage (retention) of the tumor microenvironment, often referred to 'enhanced permeability and retention' (EPR) effect (8). Nonetheless, EPR effect may efficiently occur for particles that are not rapidly cleared from the circulatory system for the opportunity to encounter the leaky vasculature (6).

Biodistribution analysis supports the notion that $SrSO_3$, SrF_2, and $MgSO_3$ have little ability to escape RES, according to high fluorescence intensity primarily in liver and kidney. The rapid translocation into organs was suggested by clearance from the bloodstream by circulating macrophages, proven as early as 1-hour post injection. As time progress, the fluorescence kidney saturation remains almost stagnant, implying

possible little kidney elimination properties. Kidney efficiently excretes particles with hydrodynamic diameter <35nm via renal filtration and urinary excretion, but larger particles are often eliminated by the liver (9). It is proposed that the particles with neutral surface charge have longer circulation time and little accumulation in RES organs (10). Blood circulatory time may be prolonged by coating with polyethylene glycol (PEG), the most efficient method to reduce scavenging protein adsorption, hence are likely to avoid the RES system (11). However, PEG coating may prevent the essential non-bilayer intermediate formation, thus inhibit the fusion with the cellular and the endosomal membrane, associated with cellular internalization and endosomal escape, decreasing the gene activity (12).

Increased fluorescence activity in the brain at 2 hours implies the ability if salt particles to assist in transportation across the blood-brain barrier (BBB), showing possible hydrophobic properties of treatment complexes. $SrSO_3$ has higher lung and spleen siRNA deposition of all salts tested, indicating more diverged distribution of the salt throughout the body. BBB prevents the uptake of most particles, with exception to small hydrophilic compounds with less than 150Da or highly hydrophobic compounds with less than 600Da via passive diffusion (13). However, NPs phagocytosis by monocyte approach may assist in the delivery of gene-loaded NPs into the brain, like Trojan horses. A BBB-impermeable drug, serotonin embedded into negatively charged particles showed a greater concentration of serotonin in the brain, up to two-fold than the free drug (14). Hence, it is also likely that the salt particles are transported via Trojan horse mechanism, increasing the availability of fluorescence siRNA activity in the brain tissues.

Following 4 hours of IV injection, the RES organ is associated with the majority of NPs uptake with low tumor tissue saturation (Figure 5.1). Upon parenteral delivery, the availability of siRNA inside the organ tissues, demonstrated by fluorescence intensity was observed as minimal time as 1 hour to various organs, including tumor site. Angiogenesis, which promotes the development of irregular blood vessels with discontinuous epithelium and lack the basal membrane of normal vascular structures, results in fenestrations inside the capillaries ranging from 200 to 2000nm (15). The loosely packed endothelial cells facilitate in the diffusion, associated with the enhanced permeation portion of EPR effect, seen with fluoresced cancer cells.

With the addition of Na_2SO_3 and NaF concentrations, the particle size becomes larger with zeta potential becomes more negative, due to anionic domains from the sulfite and fluoride. Concentration increment is related to higher crystal number and greater volume, which may not have an added benefit to the transfection efficacy due to efficient clearance of large particles by circulating macrophages. Larger particles are more efficiently captured by the RES and sequestered by the liver due to opsonization and protein association on the particle surface (16). The circulatory plasma proteins tend to bind to larger particulate matter and trigger macrophages response, causing inefficiency in circulatory transportation (17). Higher concentration is also related increased risk of salt toxicity, attributed to reduced kidney elimination. Renal excretion would not be expected for large particles (18), hence, will be highly dependent the liver metabolism with fecal clearance (19).

Fibronectin receptor, which modulates numerous signaling pathway, are over-expressed in many tumors, associated with increased carcinoma aggression (20).

Transferrin receptor, which acts as an iron importer, is also over-expressed in many malignant cells (100 folds) due to high demands for iron. Additionally, transferrin receptor is widely studied in BBB targeting, regulates the uptake of iron intracellularly via transferrin (21), which explains the enhanced bioavailability of fluorescence siRNA upon coating with transferrin protein. Enhancement in tumor bioavailability was likely associated with incorporation of active targeting, which specifically transported $SrSO_3$, SrF_2 and $MgSO_3$ into the tumor tissues. Modification of nanocarriers with active targeting moieties (including transferrin and fibronectin) can significantly enhance the accumulation in cancer tissues and improve the complexes uptake by tumor cells, hence the anticancer effect. Additionally, with smaller size, transferrin and fibronectin-coated nanocrystals complexes has better retention activity at the tumor site, therefore, improve chances for internalization (22)(23).

Tumor regression study on target genes was performed to identify the effect of the carrier in improving the delivery of genes and subsequently increasing the targeted effect. p53 is a gene that codes for a protein which regulates the cell cycle, playing a prominent role in conserving stability of cells by preventing genome mutations. DNA damage and other stress signals may trigger the increased of p53 proteins, with three primary functions: growth arrest, DNA repair and apoptosis (24). p53-loaded NPs demonstrated a reduction in tumor progress, as seen in Figure 5.4 with the comparison to naked p53. Naked p53 are readily degraded by many endogenous enzymes, therefore, brings to the importance of nanocarriers in improving the bioavailability in the circulatory system (25). $SrSO_3$, SrF_2 and $MgSO_3$ particles loaded with the p53 were able to protect the gene from early degradation, comparable to CO_3 AP NPs to improve the amount of salt particles transported intracellularly and subsequent escape of p53 for transcription inside the

nuclear cavity to activate the apoptotic mechanism, as referred to tumor size reduction (26). However, with increasing p53 concentrations, tumor tissue growth remained stagnant, possibly due to the insufficiency of p53 concentration to further enhance the p53-associated cell death (27), hence, a larger concentration of p53 may be needed to promote greater tumor reduction effect. It is also proposed that saturation of excess p53 intracellularly may bring to exocytosis of the genes from the cancer cells (28).

Mitogen-activated protein kinase (MAP kinase) initiate the transmission and amplification of signals linked to cell proliferation and death. Recent studies have shown that breast cancers frequently contain an increased proportion of cells with activated form of MAP kinase (29). p44/42 MAPK siRNA brings to inhibition of MAP kinase expression via RNA interference (RNAi), which expression were selectively silenced through the delivery of double stranded RNA molecules (30). The activation of siRNA with RNA-induced silencing complex (RISC) via cleaving of dsRNA resulted in an activated-RISC that targets the specific mRNA for recognition. Argonaute 2, from RISC, cleaves the mRNA, hence inducing mRNA degradation and gene silencing (31).

Tumor development in BALB/c mice decelerated with the incorporation of MAPK siRNA into the complexes due to the ability of the complexes to protect naked siRNA from disintegration by circulating nuclease (32). Without vector, naked siRNA will be eliminated from the blood within 5 minutes post injection (33). Lower tumor volume of salt particles in comparison with CO_3 AP implies better and longer protection of the RNA for therapeutic applications. Raising siRNA concentration quicken the tumor growth activity, as seen with larger tumor mass of 100nM than of 50nM. The divergence between the concentration and intended effect is caused by off-target mechanism,

resulted from unintended gene interaction of different gene pathway. The integration of passenger strand into the RISC induces the off-target activity, which may be prevented by modifying the seed region, such as 2'-O-methyl ribosyl substitution, hence enhancing the specificity of siRNA and lessening the off-target effect (34). Additionally, pooling siRNA with the different region of target mRNA may further reduce the effect and subsequently improve the silencing activity (35). Prolonged existence of siRNA inside the cells may also activate the lysosomal activity to degrade or exocytose the nucleic acid extracellularly (36).

SrF_2 and $SrSO_3$ improve the delivery of p53 and MAPK siRNA more than $MgSO_3$ and CO_3 AP, demonstrated by greater carcinoma size reduction on day 28. Improved carrier activity is possibly related to stronger binding with nucleic acid (Figure 3.10 and 3.11), enhancing the transportation of genetic materials into the targeted areas (37). The high binding affinity of salt particles may also transport more pDNA and siRNA into the cells, increasing the availability of the nucleic acids for transcription and translation activity in the nucleus and cytoplasmic region (31).

Transferrin and fibronectin protein coating may protect the salt particles from non-specific binding with plasma proteins, causing non-specific delivery and uptake into various organs (38). Additionally, transferrin- or fibronectin-coated NPs is associated with the reduction in particle structure due to the covalent bond between proteins to the NPs surface, hence causing shrinkage in salts' morphology (39)(40). NPs size affects the accessibility of target organs, the mode of cellular uptake, and efficiency of endocytic pathway thus is one of the most important parameters to establish the ideal gene vector (22). Synergistic effect of active transport with the presence of transferrin and

fibronectin; and the size reduction activity was proven in both tumor fluorescence activity of biodistribution studies (Figure 5.3) and reduction in tumor growth (Figure 5.8). Size reduction of NPs also shifted the zeta potential into less negatively-charged particles. Stronger electrostatic interactions from the cation-providing domains of NPs to the negatively-charged cellular membrane, in addition to ligand-receptor binding, improves the gene delivery system (41), as shown with higher cancer distribution and lower tumor tissue growth.

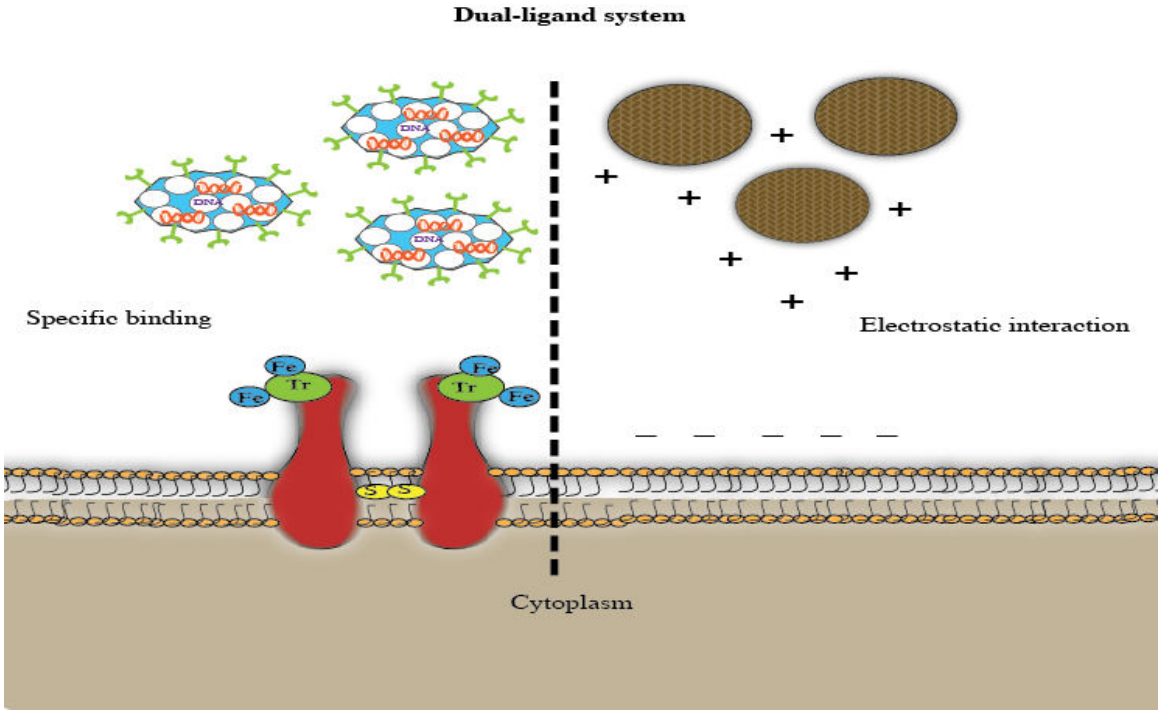

Figure 5.12: Proposed dual-ligand system of protein binding and electrostatic interactions on improving intracellular delivery of genetic material

5.5 Conclusion

Here we have studied the ability of selected NPs to transport the genetic materials in the animal model, as proven in vitro backgrounds. The animal study shows improvement of gene-transporting ability of NPs, especially with $SrSO_3$ and SrF_2, in comparison to established CO_3 AP. Higher concentration of Na_2SO_3 and NaF did not improve the carrier ability of salts, probably size-related. Intravenous delivery of p53-NPs involving $SrSO_3$, SrF_2, and $MgSO_3$, of smaller size (<100nm in diameter), had better anti-tumoral effect in mice when coated with transferrin or fibronectin. The significant tumor growth reduction suggests the potential characteristics of salt particles in improvising the therapeutic gene efficacy of both pDNA and siRNA. The increment of genetic material concentration may not be beneficial to enhance the silencing efficiency, related to the off-target effect of siRNA.

Further investigations concerning toxicity profile on salt particles may be advantageous to extend the existing knowledge of the safety manners of prospective carrier salts in the animal model.

5.6 References

1. Huang L, Guo S. Nanoparticles escaping RES and endosome: Challenges for siRNA delivery for cancer therapy. Journal of Nanomaterials. 2011.
2. Nancy S Templeton. Gene and Cell Therapy: Therapeutic Mechanisms and Strategies. 4th ed. 2011. 322 p.
3. Scholz C, Wagner E. Therapeutic plasmid DNA versus siRNA delivery: Common and different tasks for synthetic carriers. Journal of Controlled Release. 2012. p. 554–65.
4. Van De Water FM, Boerman OC, Wouterse AC, Peters JGP, Russel FGM, Masereeuw R. Intravenously administered short interfering RNA accumulates in the kidney and selectively suppresses gene function in renal proximal tubules. Drug Metab Dispos. 2006;34(8):1393–7.
5. Moghimi SM, Szebeni J. Stealth liposomes and long circulating nanoparticles: Critical issues in pharmacokinetics, opsonization and protein-binding properties. Progress in Lipid Research. 2003. p. 463–78.
6. Li SD, Huang L. Stealth nanoparticles: High density but sheddable PEG is a key for tumor targeting. Journal of Controlled Release. 2010;145(3):178–81.
7. Brannon-Peppas L, Blanchette JO. Nanoparticle and targeted systems for cancer therapy. Advanced Drug Delivery Reviews. 2012. p. 206–12.
8. Seymour LW. Passive tumor targeting of soluble macromolecules and drug conjugates. Crit Rev Ther Drug Carrier Syst [Internet]. 1992;9(2):135–87. Available from: http://www.ncbi.nlm.nih.gov/pubmed/1386002
9. Choi HS, Liu W, Misra P, Tanaka E, Zimmer JP, Itty Ipe B, et al. Renal clearance of nanoparticles. Nat Biotechnol [Internet]. 2007;25(10):1165–70. Available from: http://dx.doi.org/10.1038/nbt1340
10. Blanco E, Shen H, Ferrari M. Principles of nanoparticle design for overcoming biological barriers to drug delivery. Nat Biotechnol [Internet]. 2015;33(9):941–51. Available from: http://www.nature.com/doifinder/10.1038/nbt.3330\nhttp://www.ncbi.nlm.nih.gov/pubmed/26348965
11. Allen TM, Hansen C, Rutledge J. Liposomes with prolonged circulation times: factors affecting uptake by reticuloendothelial and other tissues. BBA - Biomembr. 1989;981(1):27–35.
12. Drummond DC, Zignani M, Leroux J-C. Current status of pH-sensitive liposomes in drug delivery. Prog Lipid Res. 2000;39(5):409–60.
13. Santaguida S, Janigro D, Hossain M, Oby E, Rapp E, Cucullo L. Side by side comparison between dynamic versus static models of blood-brain barrier in vitro: A permeability study. Brain Res. 2006;1109(1):1–13.
14. Afergan E, Epstein H, Dahan R, Koroukhov N, Rohekar K, Danenberg HD, et al. Delivery of serotonin to the brain by monocytes following phagocytosis of liposomes. J Control Release. 2008;132(2):84–90.
15. Jain RK. The next frontier of molecular medicine: delivery of therapeutics. Nat Med. 1998;4(6):655–7.
16. Longmire M, Choyke PL, Kobayashi H. Clearance properties of nano-sized particles and molecules as imaging agents: considerations and caveats. Nanomedicine (Lond) [Internet]. 2008;3(5):703–17. Available from: http://www.pubmedcentral.nih.gov/articlerender.fcgi?artid=3407669&tool=pm

centrez&rendertype=abstract
17. Ernsting MJ, Murakami M, Roy A, Li SD. Factors controlling the pharmacokinetics, biodistribution and intratumoral penetration of nanoparticles. Journal of Controlled Release. 2013. p. 782–94.
18. Xu ZP, Zeng QH, Lu GQ, Yu AB. Inorganic nanoparticles as carriers for efficient cellular delivery. Chemical Engineering Science. 2006. p. 1027–40.
19. Choi S, Choy J. Effect of physico-chemical parameters on the toxicity of inorganic nanoparticles. Journal of Materials Chemistry. 2011. p. 5547.
20. Ranka R, Petrovskis I, Sominskaya I, Bogans J, Bruvere R, Akopjana I, et al. Fibronectin-binding nanoparticles for intracellular targeting addressed by B. burgdorferi BBK32 protein fragments. Nanomedicine Nanotechnology, Biol Med. 2013;9(1):65–73.
21. Moos T, Nielsen TR, Skjørringe T, Morgan EH. Iron trafficking inside the brain. Journal of Neurochemistry. 2007. p. 1730–40.
22. Oh N, Park JH. Endocytosis and exocytosis of nanoparticles in mammalian cells. International Journal of Nanomedicine. 2014. p. 51–63.
23. Shang L, Nienhaus K, Nienhaus GU. Engineered nanoparticles interacting with cells: size matters. J Nanobiotechnology [Internet]. 2014;12(1):5. Available from: http://www.jnanobiotechnology.com/content/12/1/5
24. Tseng S-J, Liao Z-X, Kao S-H, Zeng Y-F, Huang K-Y, Li H-J, et al. Highly specific in vivo gene delivery for p53-mediated apoptosis and genetic photodynamic therapies of tumour. Nat Commun [Internet]. 2015;6:6456. Available from: http://www.ncbi.nlm.nih.gov/pubmed/25739372
25. Li D, Marchenko ND, Schulz R, Fischer V, Velasco-Hernandez T, Talos F, et al. Functional inactivation of endogenous MDM2 and CHIP by HSP90 causes aberrant stabilization of mutant p53 in human cancer cells. Mol Cancer Res. 2011;9(5):577–88.
26. Freed-Pastor WA, Prives C. Mutant p53: One name, many proteins. Genes Dev. 2012;26(12):1268–86.
27. Rodier F, Campisi J, Bhaumik D. Two faces of p53: Aging and tumor suppression. Nucleic Acids Res. 2007;35(22):7475–84.
28. Sharma B, Ma W, Adjei IM, Panyam J, Dimitrijevic S, Labhasetwar V. Nanoparticle-mediated p53 gene therapy for tumor inhibition. Drug Deliv Transl Res. 2011;1(1):43–52.
29. Santen RJ, Song RX, McPherson R, Kumar R, Adam L, Jeng M-H, et al. The role of mitogen-activated protein (MAP) kinase in breast cancer. J Steroid Biochem Mol Biol [Internet]. 2002;80(2):239–56. Available from: http://www.ncbi.nlm.nih.gov/pubmed/15056731
30. Zhang W, Liu HT, Tu LIU H. MAPK signal pathways in the regulation of cell proliferation in mammalian cells. Cell Res [Internet]. 2002;12(1):9–18. Available from: http://www.cell-research.com
31. Agrawal N, Dasaradhi PVN, Mohmmed A, Malhotra P, Bhatnagar RK, Mukherjee SK. RNA interference: biology, mechanism, and applications. Microbiol Mol Biol Rev [Internet]. 2003;67(4):657–85. Available from: http://www.pubmedcentral.nih.gov/articlerender.fcgi?artid=309050&tool=pmcentrez&rendertype=abstract
32. Jhaveri AM, Torchilin VP. Multifunctional polymeric micelles for delivery of drugs and siRNA. Frontiers in Pharmacology. 2014.
33. Wang J, Lu Z, Wientjes MG, Au JL-S. Delivery of siRNA Therapeutics: Barriers and Carriers. AAPS J [Internet]. 2010 Dec 11 [cited 2016 Mar

5];12(4):492–503. Available from: http://www.springerlink.com/index/10.1208/s12248-010-9210-4

34. Jackson AL, Bartz SR, Schelter J, Kobayashi S V, Burchard J, Mao M, et al. Expression profiling reveals off-target gene regulation by RNAi. Nat Biotechnol. 2003;21(6):635–7.
35. Kittler R, Surendranath V, Heninger A-K, Slabicki M, Theis M, Putz G, et al. Genome-wide resources of endoribonuclease-prepared short interfering RNAs for specific loss-of-function studies. Nat Methods. 2007;4(4):337–44.
36. Shukla RS, Jain A, Zhao Z, Cheng K. Intracellular trafficking and exocytosis of a multi-component siRNA nanocomplex. Nanomedicine Nanotechnology, Biol Med. 2016;
37. Fröhlich E. The role of surface charge in cellular uptake and cytotoxicity of medical nanoparticles. Int J Nanomedicine [Internet]. 2012 Nov [cited 2016 Mar 24];5577. Available from: http://www.dovepress.com/the-role-of-surface-charge-in-cellular-uptake-and-cytotoxicity-of-medi-peer-reviewed-article-IJN
38. Chen H, Wang L, Yeh J, Wu X, Cao Z, Wang YA, et al. Reducing non-specific binding and uptake of nanoparticles and improving cell targeting with an antifouling PEO-b-PγMPS copolymer coating. Biomaterials. 2010;31(20):5397–407.
39. Pitek AS, O'Connell D, Mahon E, Monopoli MP, Francesca Baldelli F, Dawson KA. Transferrin coated nanoparticles: Study of the bionano interface in human plasma. PLoS One. 2012;7(7).
40. Saptarshi SR, Duschl A, Lopata AL, Duschl A, Lopata AL. Interaction of nanoparticles with proteins: relation to bio-reactivity of the nanoparticle. J Nanobiotechnology [Internet]. 2013;11:26. Available from: http://eutils.ncbi.nlm.nih.gov/entrez/eutils/elink.fcgi?dbfrom=pubmed&id=23870291&retmode=ref&cmd=prlinks\npapers2://publication/doi/10.1186/1477-3155-11-26
41. Honary S, Zahir F. Effect of Zeta Potential on the Properties of Nano-Drug Delivery Systems -A Review (Part 1). Trop J Pharm Res April J Cit ReportsScience Ed [Internet]. 2013 [cited 2016 Mar 31];12(122):255–255. Available from: http://www.tjpr.org

Chapter 6

General Conclusion

6.1 Conclusion

Our studies have explored various potential insoluble NPs fabricated from the different mixture of soluble components in improving the readily available nucleic acid carriers. We have revealed the association between several external factors such as salt concentration, pH, temperature and time of incubation in forming various sizes and numbers of particles, in which we have selected 5:2 ratio of cation-providing salt and anion-providing salt concentration to form 21 different types of salt particles. Based on the studies, the ideal condition to fabricate salt crystals is adapted at pH 7.5 with incubation set at 37^{o}C for 30 minutes and simultaneously compared to an established CO_3 AP NPs. Further observation revealed the correlation between absorbance intensity with particle size. Additionally, the NP size determination demonstrated the significant association of protein coating and co-precipitation of NPs in modifying the diameter of salt particles.

The efficiency in adsorbing negatively charged pDNA and siRNA is interrelated to NPs competency in promoting cellular internalization, followed by subsequent gene expression and siRNA silencing efficacy. Gene expression and silencing activity commence upon proficient disintegration of $BaSO_3$, BaF_2, $SrSO_4$, $SrSO_3$, SrF_2 and $MgSO_3$ NPs complexes via exposure of acidic environment in the late endosome, enabling the escape of pDNA and siRNA from particle structures as well as from endosomes. Reduced cellular viability upon transfection with $BaSO_4$, $BaSO_3$, and BaF_2, in the cytotoxicity assay, affected the selection of barium crystals despite high efficacy in conveying the genetic materials into the targeted areas in vitro. Analysis of MAPK siRNA delivery via cellular viability assay and Western blotting proved $SrSO_3$, SrF_2, and $MgSO_3$ NPs as the superior nucleic acid carrier in comparison to CO_3 AP, hence, they were further investigated *in vivo*. Gene transportation

was enhanced with the coating of NPs with ligands involving transferrin and fibronectin via involvement of active targeting through ligand-receptor interaction, thus stimulating ligand-mediated endocytosis.

Transportation of the genetic materials in vivo observed via biodistribution studies on 4T1-tumour induced female BALB/c mice demonstrated high fluorescence siRNA accumulation in the liver and kidney, followed by brain and tumor tissues upon parenteral administration of siRNA-loaded $SrSO_3$, SrF_2, and $MgSO_3$ particles. We also discovered high fluorescence intensity in tumor with protein coating, indicating more deposition of siRNA in the tumor region. The selected particles seemingly improved the targeted delivery of p53 and MAPK siRNA based on tumor regression studies, seen with reduction of cancer cells growth following observation over 28 days. Transferrin and fibronectin coating further enhanced the vector-associated anti-tumoral activity seen with further reduction of tumor lump throughout the studies.

As the conclusion, $SrSO_3$, SrF_2, and $MgSO_3$ salt particles are proven as excellent vectors with the ability to adsorb negatively charged nucleic acids, assisting in cellular internalization and ultimately, improving transportation of various genetic materials into mammary carcinoma cells, both *in vitro* and *in vivo*.

6.2 Future recommendation

The selected NPs may be further experimented *in vivo* to investigate the pharmacokinetic and pharmacodynamic characteristics of the salt particles, which may determine the dosing range for optimal transfection efficiency with the understanding of the salts absorption, distribution, metabolism and elimination process. Determination of short- and long-term toxicity of individual salts may also be beneficial for application in future clinical studies. Incorporation of PEG into the particle complexes may improve the availability of salt particles inside the circulatory system, hence, should ideally be explored in the future. The use of different types of ligand coating could have further augmentation in active targeting towards tumor cells, or even can enable the targeting of various types of carcinoma based on their receptor specificity.

We also hoped that the selected NPs could be elaborately investigated as a carrier for various carcinogenic therapies such as cytotoxic drugs, which are often associated with many life-threatening side effects (e.g. drug-induced cardiotoxicity, renal toxicity). Accumulation of drugs in the targeted tumor region may be elevated via efficient nanocarriers, hence reducing the scavenging drugs in the biological circulation. In different approaches, NPs may equally enhance other therapeutic treatments of various types of diseases, with issues in drug stability and toxicity, such as oral delivery of hypoglycemic agents and insulin for management of diabetes mellitus.

Appendices

Appendix 1

IP Lysis Buffer (pH 7.4)

0.025M Tris
0.15M NaCl
0.001M EDTA
1% NP-40
5% glycerol
1X protease inhibitor

Appendix 2

10X gel loading dye

500mM Tris (pH 7.6)
40% Glycerol
20% SDS
1% Bromophenol blue
5% β-mercaptoethanol (added before use)
50% Glycerol (added before use)

Appendix 3

10X running buffer

250mM Tris
19.2M Glycine
35mM SDS

Appendix 4

10X TBST buffer (300ml)

7.3g Tris

26.3g NaCl

Appendix 5

5% skimmed milk in 1X TBST

2.5g skim milk

50ml 1X TBST

Appendix 6

Enhanced chemiluminescence (ECL) substrate

10ml Clarity western peroxide reagent

10ml Clarity wastern luminol/enhancer reagent

Appendix 7

Fluorescence images of gene expression activity of pGFP-NPs on MCF-7 cells

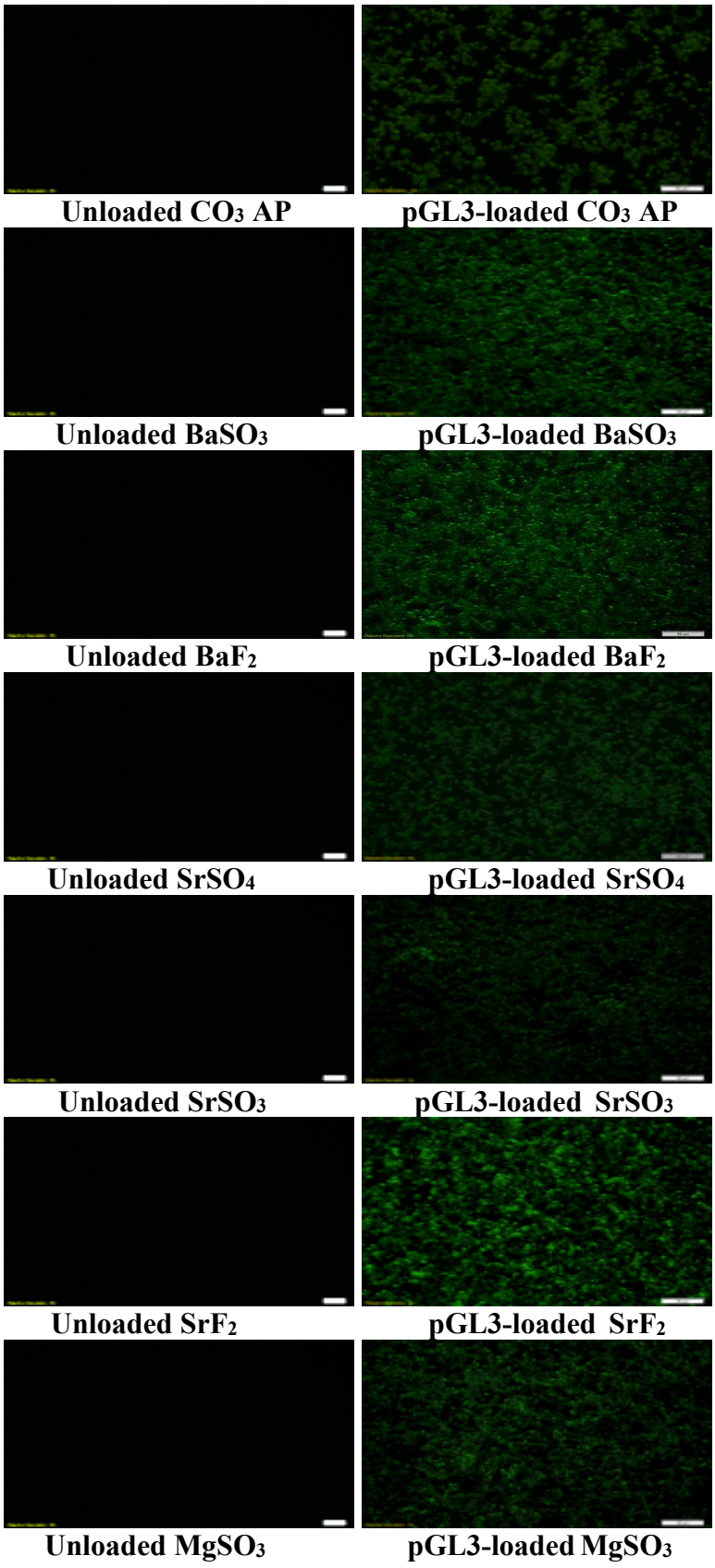

Appendix 8

Fluorescence microscopic images of gene expression activity of pGFP-complexed NPs on MCF-7 cells

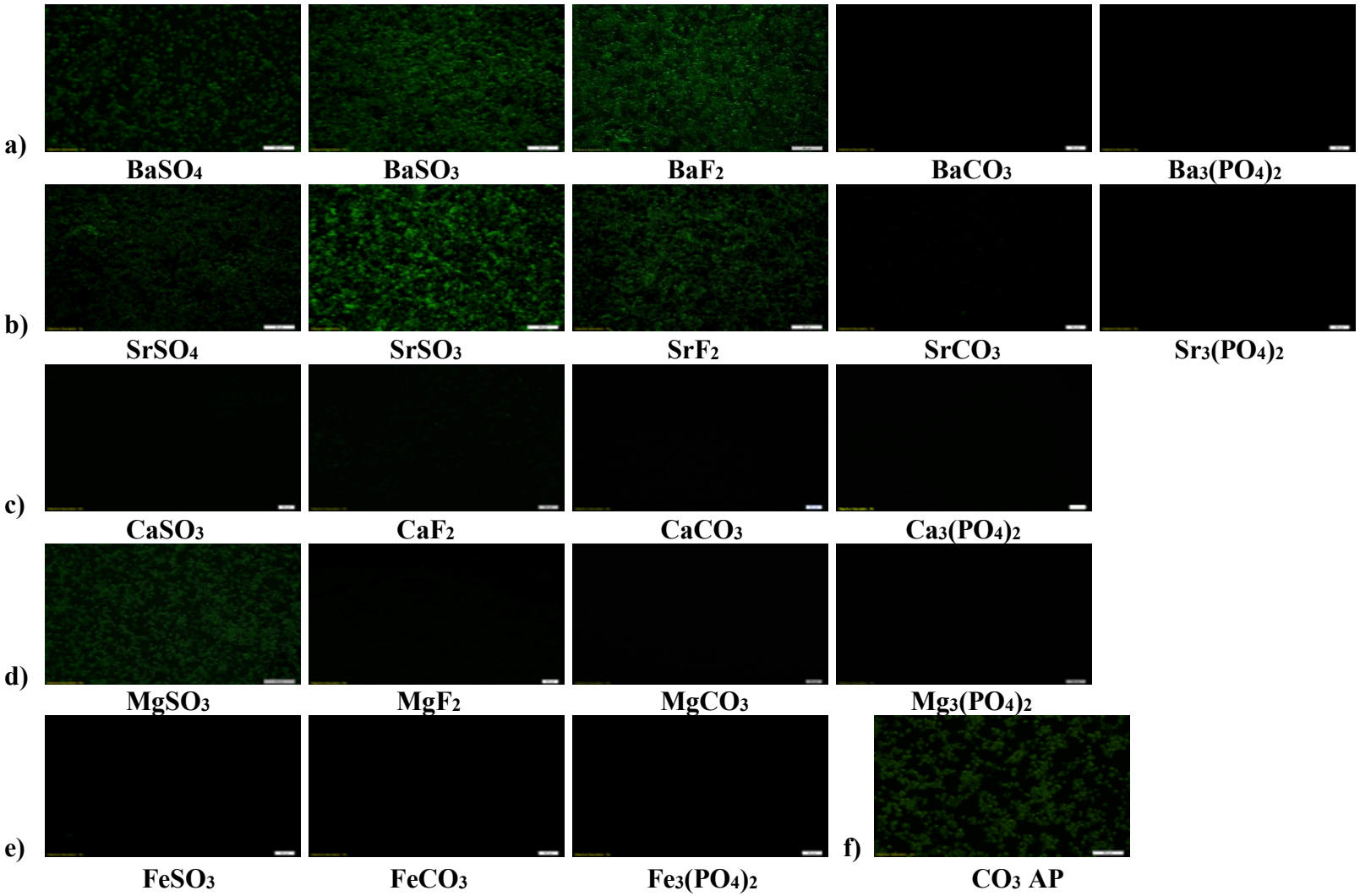

Appendix 9

Luminescence intensity of pGL3-complexed NPs on MCF-7 and 4T1 cells

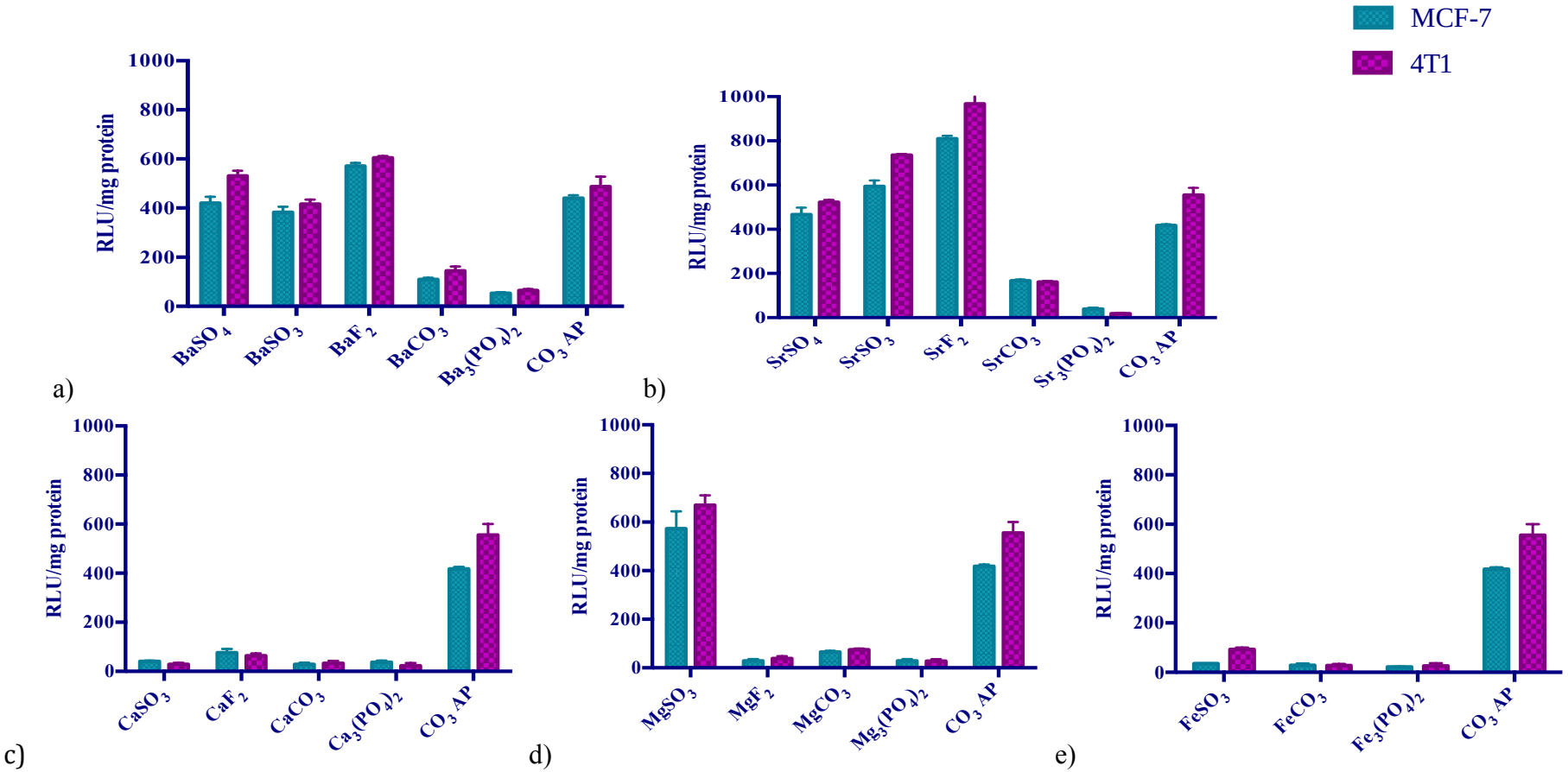

Appendix 10

Cell viability of MAPK siRNA-loaded NPs on a) MCF-7 and b) 4T1

a)

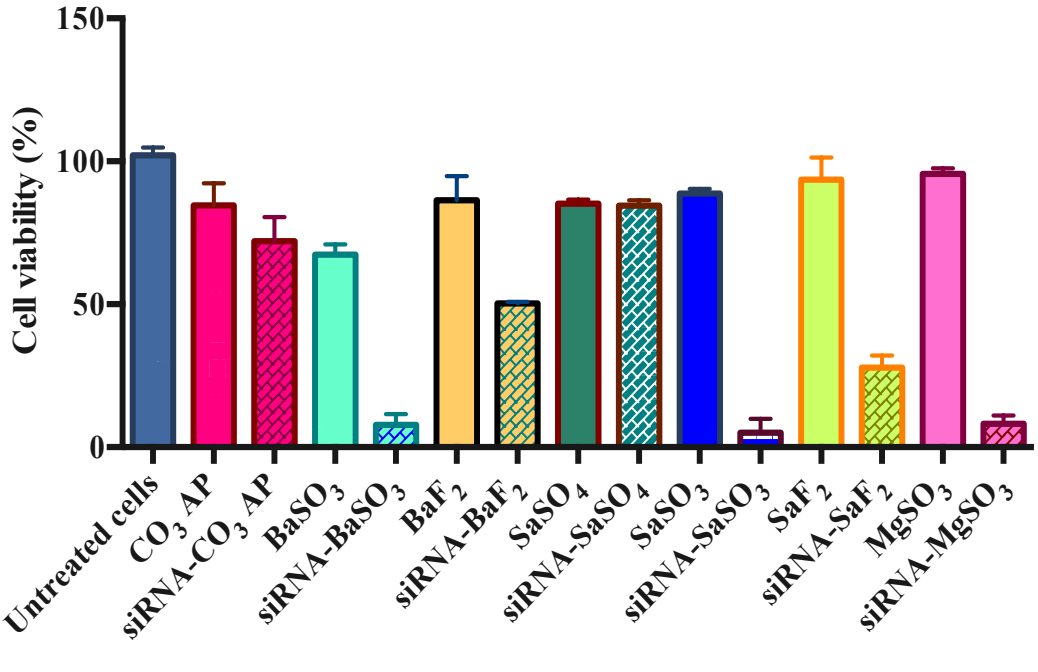

b)

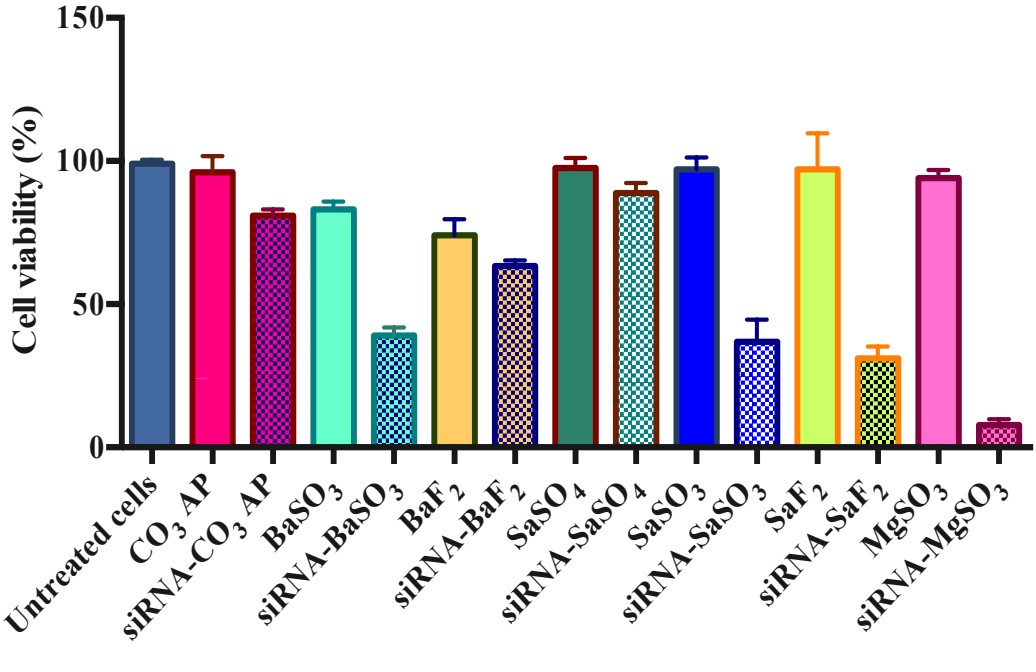

Appendix 11

MCF-7 and 4T1 cell viability of Bcl-2, ErbB2, MAPK, PI3K and ROS1 siRNA-loaded NPs

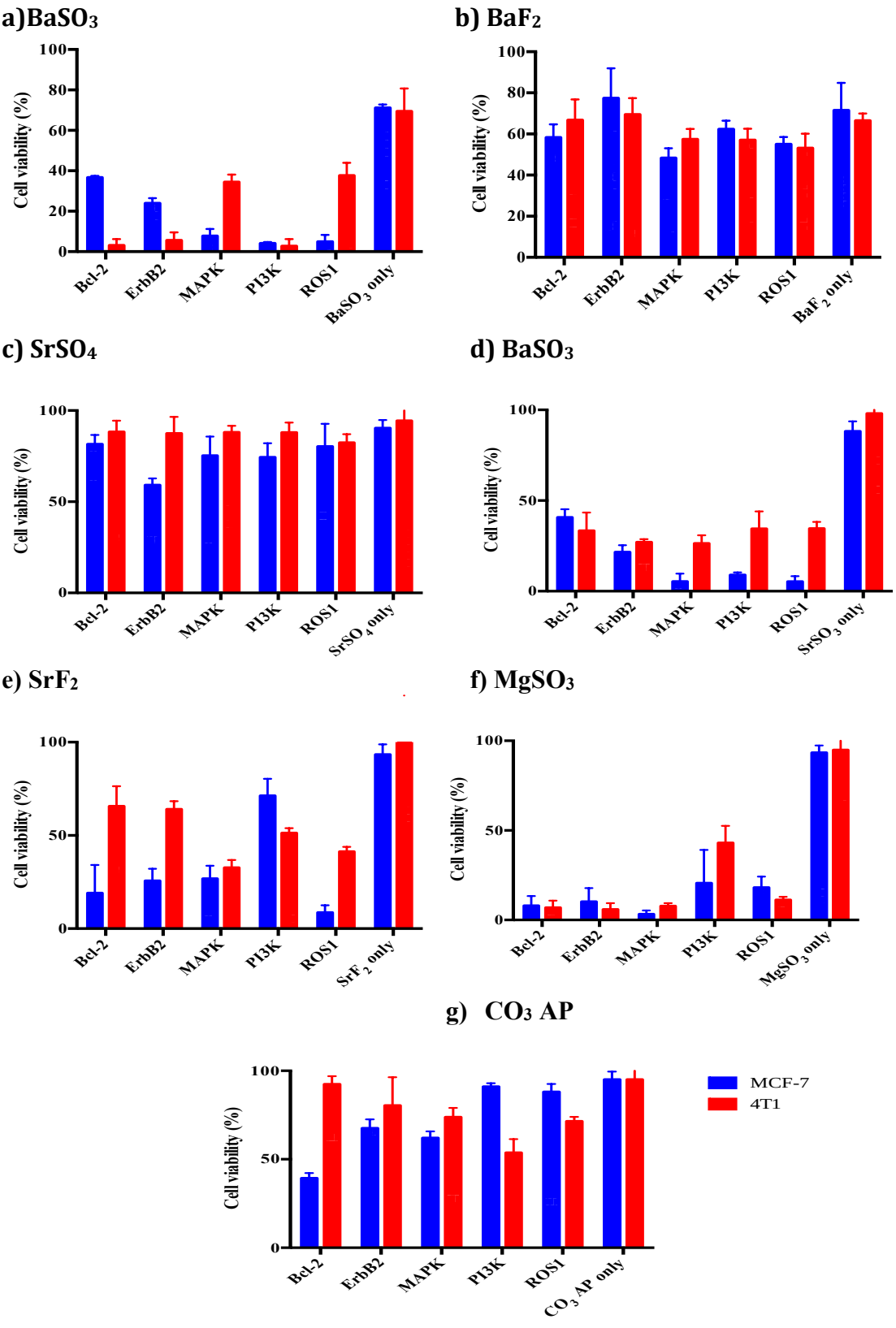

Appendix 12

Percentage of Cell Viability with Salt Combination on a) MCF-7 and b) 4T1 cells for 24 to 72 hours

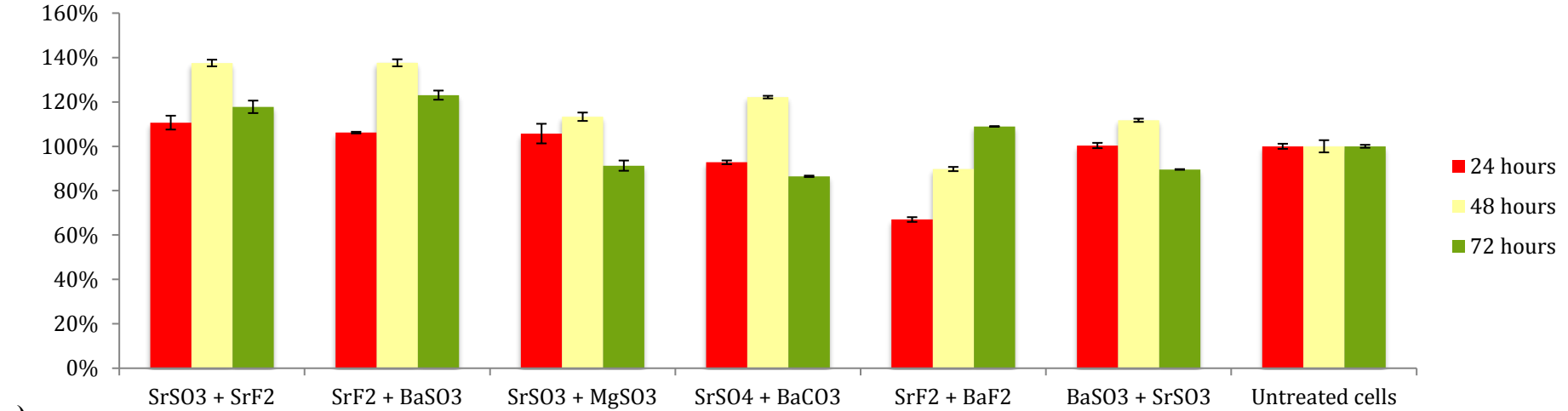

a)

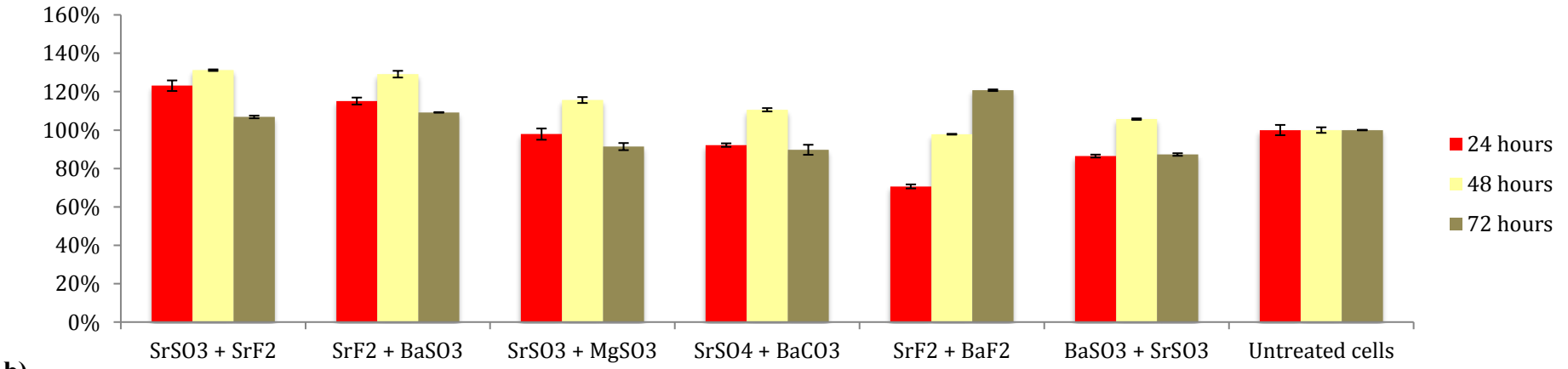

b)

Appendix 13

Effect of different pGL3 concentrations on luciferase activity in MCF-7 and 4T1 cells (Log Scale)

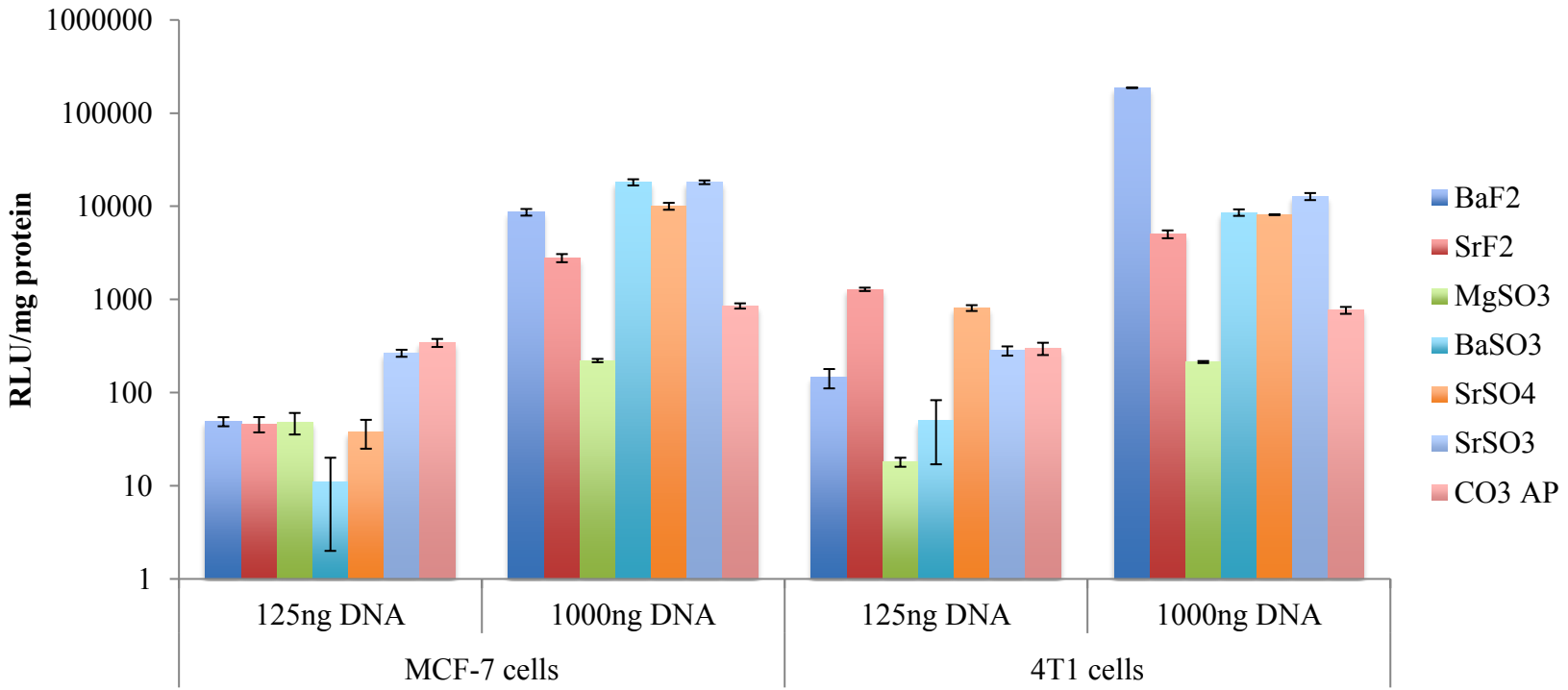

Appendix 14

Percentage of Cell Viability with salt particles on MCF-7 cells for 24 to 48 hours

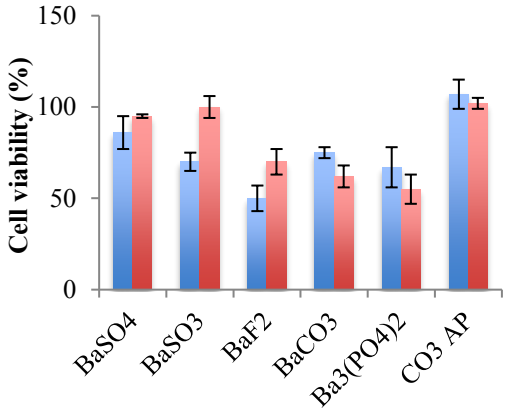

a) Barium salts

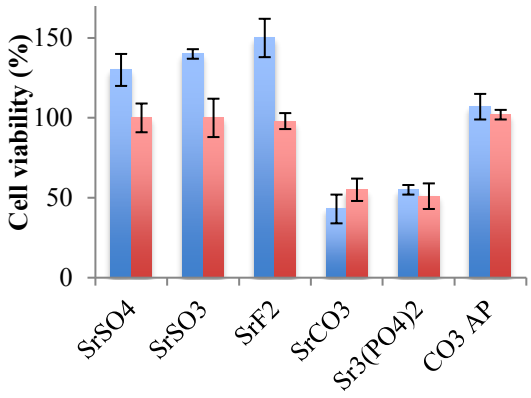

b) Strontium salts

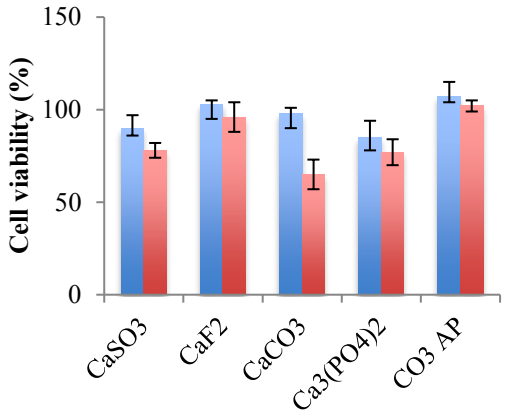

c) Calcium salts

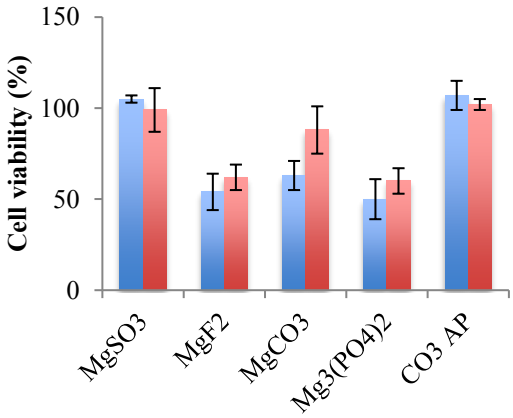

d) Magnesium salts

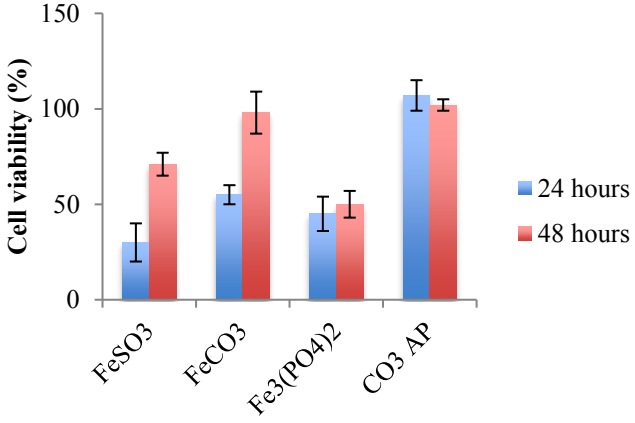

e) Ferrous salts

Appendix 15

Bakhtiar A, *et al*. Intracellular delivery of potential therapeutic genes: Prospects in cancer gene therapy. Current gene therapy. 2014, 14: 247-257.

Send Orders for Reprints to reprints@benthamscience.net

Current Gene Therapy, 2014, *14*, 247-257

Intracellular Delivery of Potential Therapeutic Genes: Prospects in Cancer Gene Therapy

Athirah Bakhtiar[1,#], Mustak Sayyad[2,#], Rozita Rosli[2], Atsushi Maruyama[3] and Ezharul H. Chowdhury[1,*]

[1]*Advanced Engineering Platform and Jeffrey Cheah School of Medicine and Health Sciences, Faculty of Medicine, Nursing and Health Sciences, Monash University, Malaysia;* [2]*Genetics Unit, Department of Obstetrics and Gynecology, Faculty of medicine and health Sciences, UPM, Malaysia;* [3]*Department of Biomolecular Engineering, Graduate School of Bioscience and Biotechnology, Tokyo Institute of Technology, 4259 Nagatsuta-cho, Midori-ku, Yokohama 226-8501, Japan*

Abstract: Conventional therapies for malignant cancer such as chemotherapy and radiotherapy are associated with poor survival rates owing to the development of cellular resistance to cancer drugs and the lack of targetability, resulting in unwanted adverse effects on healthy cells and necessitating the lowering of therapeutic dose with consequential lower efficacy of the treatment. Gene therapy employing different types of viral and non-viral carriers to transport gene(s) of interest and facilitating production of the desirable therapeutic protein(s) has tremendous prospects in cancer treatments due to the high-level of specificity in therapeutic action of the expressed protein(s) with diminished off-target effects, although cancer cell-specific delivery of transgene(s) still poses some challenges to be addressed. Depending on the potential therapeutic target genes, cancer gene therapy could be categorized into tumor suppressor gene replacement therapy, immune gene therapy and enzyme- or prodrug-based therapy. This review would shed light on the current progress of delivery of potentially therapeutic genes into various cancer cells *in vitro* and animal models utilizing a variety of viral and non-viral vectors.

Keywords: Gene therapy, cancer, nanoparticles, liposomes, polymer, adenovirus, p53, p21, thymidine kinase, TRAIL, cytokine, angiotensin, interleukin, interferon.

INTRODUCTION

Cancer belongs to a group of diseases characterized by uncontrolled cell division along with inactivation of apoptotic processes and subsequent spread of malignant cells to various organs of the body. Abnormal cell proliferation is the results of mutations in proto-oncogenes, anti-apoptotic genes and tumor suppressor genes while acquisition of metastatic properties is due to the down-regulation of cell adhesion receptors, up-regulation of cell motility-enhancing receptors and activation of membrane metalloproteases. Different types of cancers are diagnosed depending on the organs involved like breast, lung, colon, urinary bladder, ovary, kidney and prostate cancer. In majority of cases, by the time it is diagnosed, the patients have already developed secondary tumors (metastases) and if the spread is not controlled, cancer can lead to mortality [1]. Cancer is thus one of the major causes of deaths in the world with about 7.8 million people deaths owing to cancer in 2008. According to the American Cancer Society, in the United States alone approximately 1,638,910 new cases have been reported in the year 2012. Different factors that have been identified contributing to the development of cancer include genetic factors including family history, environmental factors, such as, exposure to radiations, intense sun exposure and chemicals (carcinogens), lifestyle and diet related factors such as, cigarette smoking, heavy alcohol intake, obesity and poor nutrition. Some types of specific cancers are known to be caused by infectious agents, such as, human papilloma virus (HPV), hepatitis B virus (HBV), human immunodeficiency virus (HIV), *Helicobacter Pyroli* and others. Various treatment approaches are available for cancer depending on the type and stage of cancer, which include chemotherapy, radiation therapy, targeted therapy, hormonal therapy, surgery and gene therapy. For breast cancer the treatment options involve breast-conserving surgery, mastectomy along with chemotherapy or radiation alone or in combination. Lymphedema of the arms is one of the most common side effects associated with these methods; others are numbness or tightness and pulling or stretching in the chest wall, arms, or shoulder. Treatment strategies available for cancer of colon and rectum depend on tumor location and stage. For early stage surgery is considered to be the primary option with chemotherapy alone or in combination with radiation being opted for the late stage disease before or after surgery and the side effects associated with these methods are bowel dysfunction and recurrence. Lung cancer is classified as small cell or non-small cell type for selection of the treatment. For small cell lung cancer radiation therapy alone or in combination with chemotherapy whereas for early stage non-small cell lung cancer, surgery as well as

*Address correspondence to this author at the Advanced Engineering Platform and Jeffrey Cheah School of Medicine and Health Sciences, Faculty of Medicine, Nursing and Health Sciences, Monash University, Malaysia; Tel: +603-5514-4978; Fax: +603-5514-6323; E-mail: md.ezharul.hoque@monash.edu

#*These authors equally contributed to the work.*

1875-5631/14 $58.00+.00

chemotherapy or radiation are used and advanced stage cancer is treated with chemotherapy alone, radiation alone or in combination [2]. Conventional therapies available for cancer such as chemotherapy, surgery and radiotherapy are associated with risks of poor survival rates due to multiple factors including development of resistance to drugs and also lack in target specificity, resulting in unwanted side effects on surrounding healthy cells and thus demanding a reduction in the therapeutic dose [3]. Gene therapy involves employing different types of viral and non-viral carriers to transport therapeutic gene(s) of interest and facilitate the production of the desirable therapeutic protein(s) overcoming multiple biological barriers and thereby increasing the efficacy and target specificity of genetic materials while decreasing the side-effects. If the current major hurdle of target specificity could be overcome, gene therapy would be a promising approach considering the safety issue conferring significantly less side effects as compared to other currently available strategies [4]. Depending on the therapeutic target gene therapy could be classified into three major categories including tumor suppressor gene replacement therapy, immune gene therapy and enzyme- or prodrug-based therapy [5]. This review is particularly focused on the current progress of delivery of emerging cancer therapeutic genes potentially capable of inducing apoptosis in cancer cells both in cell culture (*in vitro*) and animal models *(in vivo)* using a variety of potent viral and non-viral carriers.

DELIVERY AND EXPRESSION OF p53 GENE

The p53 gene belongs to the class of tumor suppressor genes and is considered to be one of the most important genes playing roles in defending mechanism of tumor development [6]. In majority of human cancer cases it is found to be mutated leading to activate the underlying mechanism which triggers tumorigenesis [7]. p53 is therapeutically important gene for cancer treatment as it is responsible for cell cycle progression, DNA repair and induction of apoptosis against cellular stress and damage, and therefore more often referred to as "guardian of genome" [8]. In addition, p53 has a pivotal role in increasing the therapeutic effects of chemotherapy, radiotherapy and anti-angiogenesis therapy [9]. The mechanisms by which p53 plays critical roles in a cell are depicted in (Fig. 1).

p53 gene was delivered using a number of viral and non-viral carriers into different types of cancer cells *in vitro* and *in vivo*. Liposomes are among those vectors used very efficiently for the delivery purpose. Systemic administration of the liposome-p53 complex consisting of *N*[1-(2,3-dioleyloxy)propyl]-*N,N,N*-trimethylammonium chloride (DOTMA) and dioleoylphosphatidylethanolamine (DOPE) together with β-actin promoter-containing p53 plasmid, was reported to reduce not only the size of the primary tumors but also prevented the relapse and metastases of a malignant human breast cancer in nude mice [10]. Liposome-mediated delivery of CMV-p53 plasmid DNA alone was proved ineffective in promoting cell death in MDA-MB231 breast cancer cells, but when incubated with estradiol, the liposomal p53 complex was shown to increase cell killing activity by two fold as compared to the cells transfected with the corresponding mock vector [11]. The cell killing was found to be due to apoptosis involving apoptotic body formation, cell shrinkage and increase in fluorescence after terminal end-labeling, whereas the mechanism for action of estradiol is speculated to be redistribution of the gene from cytoplasm to the nucleus which could occur during both the uptake and post-uptake phases. Anti-transferrin receptor single-chain antibody Fv fragment (ScFv)-directed delivery of immunoliposome/p53 gene complex in various tumor models resulted in an improvement of transfection efficiency and penetration into tumor cells in comparison with the whole antibody immunoliposome complex or transferrin molecule itself as demonstrated in previous studies, because scFv is smaller in size with better penetrating ability [12]. To enhance the transfection efficiency and target specific delivery of wild-type p53 gene, liposomal nanoparticles targeted by a single-chain antibody fragment to the transferrin receptor (TfRscFv) were investigated in combination with gemcitabine in metastatic pancreatic model, demonstrating a prolonged median survival and also decreased tumor burden compared with single drug therapy [13]. In a recent study, targeted lipid microbubbles were synthesized to enhance the transfection efficiency of wild-type (wt) p53 gene to ovarian cancer cells through ultrasound targeted microbubble destruction (UTMD) technique [14]. Lipid microbubbles conjugated with luteinizing hormone-releasing hormone analog (LHRHa) and mixed with the pEGFP-N1-wt p53 plasmid significantly enhanced transfection efficiency of wt p53 gene with higher apoptosis rate in comparison with other treatment groups [14]. In a similar attempt to increase the transfection efficiency of p53 gene, dextran graft-poly (2-dimethyl amino) ethyl methacrylate) (DPD) vector was developed and used to transfect MCF7 breast cancer cell lines, leading to significantly higher transfection efficiency compared to Lipofectamine 2K (commercial vector) [15]. In addition, the DPD/pEGFP-c1-p53 complex successfully minimized the tumor growth in MCF7 xenograft tumor models [15]. Breast cancer cells transfected with wt p53 DNA (*Wt*-p53-DNA)-loaded poly(D,L-lactide-co-glycoside) nanoparticles promoted sustained and significantly greater antiproliferative activity compared to those with naked wt p53-DNA or wt p53-DNA complexed with Lipofectamine (commercially available vector) suggesting that the slow release of DNA from the nanoparticles in the cells might have contributed to the better effect [16]. Intracellular delivery of p53 gene using epidermal growth factor receptor (EGFR) targeting peptide-modified thiolated gelatin nanoparticles significantly decreased survival of pancreatic cancer cells when compared with the positive control using lipofectin-DNA complex and other treatments using commercially available carriers of p53 gene [17]. Again in a novel approach exploiting changes in lipid metabolism and cell membrane biophysics usually observed during malignancy, surface modified nanoparticles formulated with surfactant didodecyldimethylammoniumbromide (DMAB) and p53 plasmid DNA resulted in greater interaction with the membrane lipid of human prostate carcinoma cells than with unmodified nanoparticles *in vitro* and increased uptake by endothelial cells & increased tumor accumulation, which could be correlated to improved efficacy of p53 gene *in vivo* [18]. In another study, supercoiled plasmid DNA isolated with arginine-based chromatographic matrix was encapsulated within chitosan nanoparticles with the use of ionotropic gelatin. The *in vitro* transfection results confirmed the highest p53 expression

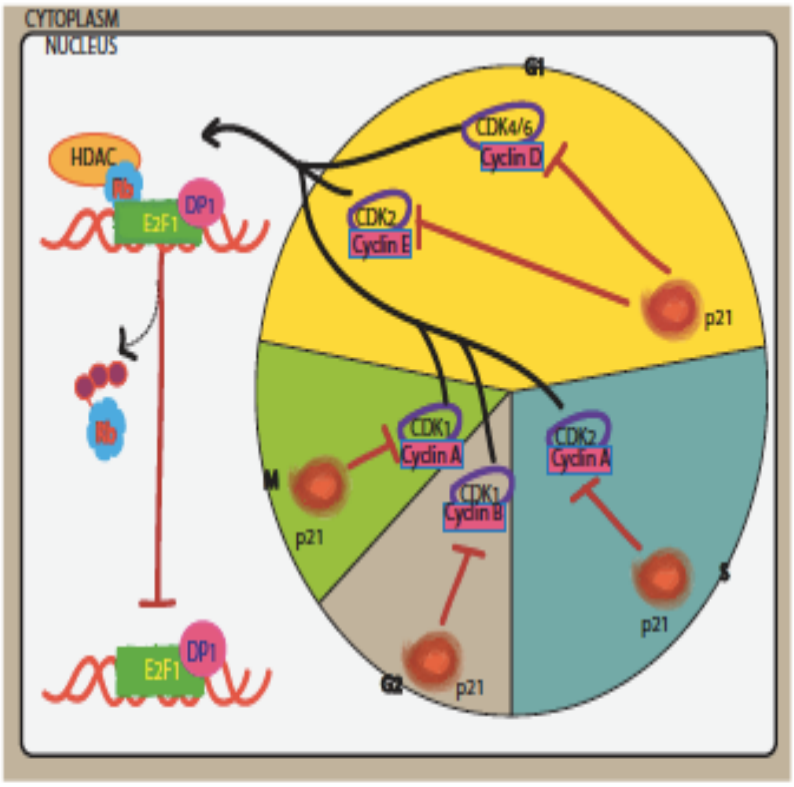

Fig. (1). p53 is activated by different stress signals such as DNA damage and various oncogenic chances and induces various mechanisms in response to such signals, which include growth arrest, apoptosis or DNA repair. Growth arrest is mainly mediated through activation of CDK inhibitor p21 gene, suppressing wide range of CDKs. Apoptosis is facilitated through activation of many genes including BAX and NOXA, destabilizing mitochondrial membrane to assist cytochrome C release and thus triggering apoptotic cascade of caspase activation. One of p53 transcriptional target genes, p53R2, encodes ribonucleotide reductase, which is essential for both DNA replication and repair. The expression of p53 is controlled by rapid ubiquitin/proteasome-dependent degradation, mainly caused by Mdm2, often over-expressed in many cancers. Mdm2 binds directly to p53 to promote p53 degradation and forms a negative feedback loop to control the level of p53. Mdm2-mediated p53 suppression is inhibited by the action of ARF tumor suppressor. ARF blocks interaction between p53 and Mdm2 by binding to Mdm2 and therefore stabilizes and activates p53. ARF expression is dependent on the transcription factor E2F-1, regulated by the retinoblastoma (Rb) tumor-suppressor and by the action of oncogenes. DNA damage activates protein kinase including ATM and ATR to phosphorylate p53 at the residues, causing p53 increment. Mdm2 has no effect on phosphorylated p53, promoting more expression of p53. Protein kinase will be inactive as DNA damage is repaired. P53 is thus dephosphorylated and destroyed by the accumulated Mdm2.

with the supercoiled DNA as compared to other formulations, establishing a potential sustained nucleic acid-based approach for cancer therapy [19]. The p53 plasmid complex of ethylenediamine-functionalized single-walled carbon nanotubes (f-SWCNTs) was successfully tested *in vitro* in MCF-7 breast cancer cell lines with highly enhanced activity of caspase-3, thus strongly supporting the action of induced apoptosis [20]. Very recently, delivery of p53 gene using biodegradable poly(β-amino ester) (PBAE) polymers in small cell lung cancer (SCLC) cells was shown to induce apoptosis and accumulate the cells in sub-G1 phase with functional p53 activity while intratumoral injection of polymer-carrying p53 gene in xenograft model of SCLC led to marked tumor growth inhibition [21]. Gendicine™, the first gene therapy virus approved for clinical use in China, is a p53 adenovirus for the treatment of head- and neck squamous cell cancer in combination with radiotherapy [22]. A similar product, Advexin™ is currently under Phase III clinical trials [23].

DELIVERY AND EXPRESSION OF THYMIDINE KINASE GENE

Herpes simplex virus thymidine kinase (HSV*tk*) is the most commonly used thymidine kinase gene for cancer gene therapy. It was delivered individually as well as in combination with gancyclovir (GCV) (a prodrug) as the most successful enzyme/prodrug combination used both *in vitro* and *in vivo* [24]. Fig. (2) illustrates the pro-drug activation process by the expressed HSV*tk*. Thymidine kinase gene was subjected to cellular delivery using a varying number of delivering agents with liposomes being one of them. In a way to introduce a noninvasive molecular imaging technique for monitoring gene delivery and its expression, liposomal nanoparticles were used for the delivery of HSV*tk* and molecular imaging of gene expression to probe breast cancer processes [25]. BALB/c mice were injected with a triple fusion gene containing the herpes simplex virus truncated thymidine kinase (HSV-ttk) and renilla luciferase (Rluc) and

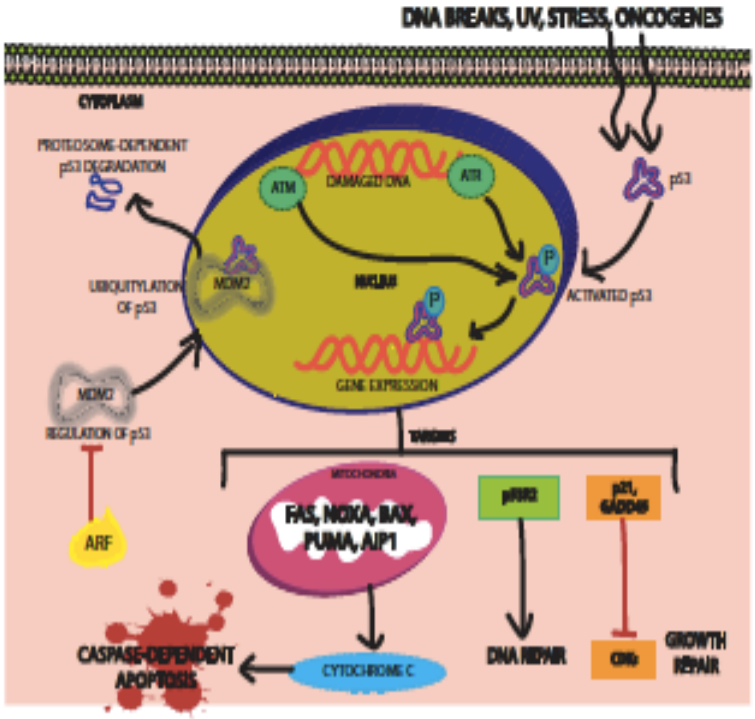

Fig. (2). Thymidine kinase (TK) gene from Herpes simplex virus (HSV) is delivered to the tumor cells by a viral vector (genetically-altered adeno-virus). The HSV-tk gene will undergo transcription and translation to an enzyme, HSV-TK. As potential prodrug passes through the cell, HSV-TK phosphorylates the prodrug to the monophosphate form. Cellular phosphorylation process further changes the drug to the triphosphate form which is later incorporated into cellular DNA, resulting in DNA chain termination, DNA fragmentation and ultimately cell death. Bystander effect helps in facilitating cytotoxicity in cells with no HSV-TK genes through the metabolic product movement across the gap junction.

red fluorescent protein (RFP) and subsequently treated with ganciclovir, paving a potentially useful way for gene delivery, monitoring its expression and patient's response to gene therapy treatment. In another study, recombinant adeno-associated virus-2 mediated HSV*tk* gene transfer along with ganciclovir for the treatment of MCF-7 breast cancer cells was analyzed for the antitumor effect with and without doxycycline induction [26]. The antitumor effect of rAAV-mediated HStk/GCV gene therapy under the Dox induction following direct intratumoral injection was found to be useful method for the treatment of breast cancer [26]. In a study using ultrasound targeted microbubble destruction for the delivery of KDRP-CD thymidine kinase gene to MCF-7 and LS174T cell lines, the recombinant plasmid pEGFP-KDRP-CD/TK was successfully transfected into MCF-7 and LS174T cells with the CD/TK fusion gene being found to be expressed in MCF-7 cells but not expressed in LS174T cells [27]. The cells were also treated with the pro-drugs 5-FC and GCV for producing cytotoxic effect. However, transgenic LS174T cells were not shown sensitivity to any of the pro-drugs demonstrating that the KDR promoter could augment the expression of CD/TK gene target in MCF-7 cells, and the targeted killing effect of the KDP-CD/Tk gene on MCF-7 cells *in vitro* had good synergy with expression of the CD/TK fusion gene. Electroporation technique was used to deliver the herplex simplex virus 1 thymidine kinase (HSV*tk*) gene and gancyclovir prodrug system against BJMC3879 mammary carcinoma cells with consequential increased apoptosis (about 80% cell death) after the transfection [28]. *In vivo* results indicated a significant decrease in tumor size, increase in apoptosis, and a decrease in DNA synthesis in the pHSVtk/GCV treatment group with suppression of metastasis to lymph nodes and lungs in comparison with other groups. In order to enhance the therapeutic efficacy of HSV-1*tk*/ gancyclovir prodrug system, baby hamster kidney (BHK) tumors growing as xenografts in severe combined immunodeficiency disease (SCID) mice were used as a model for assessing the anti-tumor activity after delivery of sindbis viral vector [29]. The results were proven to be positive in expressing HSV*tk* enzyme in infected cells both *in vitro* and *in vivo*, which in turn enhanced the process of prodrug GCV conversion for bystander effects responsible for killing of surrounding untransducted tumor cells. In an interesting move to enhance the antitumor effects of HSV*tk*/GCV recombinant adenoviral delivery system, monocyte chemoattractant protein (MCP)-1 was co-delivered in hepatocellular carcinoma cells (HCC) with resultant adjuvant effect for adenovirally delivered MCP-1, as there was an increased anti-tumor effect of the HSV-*tk*/ GCV system synergistically by recruitment/activation of macrophages in tumor tissues, suggesting an effective immunotherapy for HCC and other tumors [30]. In a similar approach, repeated delivery of HSVtk gene under alpha-fetoprotein (AFP) promoter (AFPTK1) using hemagglutinating virus of Japan (HVJ)-

liposomes in the tumors induced by using AFP-producing (HUH7) and AFP-nonproducing (LS180) liver cancer cells, followed by GCV treatment significantly inhibited the growth of tumors in the liver and markedly improved the survival of animals [31]. The combined delivery of HSV*tk* and hrTNF-α fusion genes using recombinant retroviral expression vector PLXSN in SGC7901 gastric cancer cells resulted in no significant difference of cell survival between the groups after maintaining the transfected cells in the GCV-containing medium [32]. Whereas, in the *in vivo* study tk/GCV, tk-TNF-α/GCV and TNF-α were shown to inhibit the tumor growth with an obvious enhanced anti-tumor activity of tk-TNF-α/GCV and TNF-α groups [32]. In a different study, the cytostatic activity of **ganciclovir elaidic acid** ester (E-GCV) and **ganciclovir** (GCV) was compared in HSV*tk*-1 gene-transfected FM3A mammary carcinoma cells revealing that E-GCV was more effective and cytostatic than HSV*tk*-1 gene-transfected mammary carcinoma cells as E-GCV was found to have longer retention time than GCV metabolites [33]. This effect could be due to E-GCV's marked stability in human plasma and much higher lipophilicity than GCV [33]. Although retroviral HSV-tk gene therapy was not efficient enough in human clinical trials due to the lack of efficacy with higher rate of side effects, adenoviral HSV-tk/GCV therapy was found to be well tolerated without significant safety issues with an overall mean survival of 70.6 weeks compared to 39.0 weeks for the standard therapy group in glioblastoma multiforme (GBM), following intratumoral injection of virus-associated HSV-tk gene and subsequent intravenous administration of GCV [34].

DELIVERY AND EXPRESSION OF TNF-RELATED APOPTOSIS INDUCING LIGAND (TRAIL) GENE

The tumor necrosis factor (TNF) related apoptosis-inducing ligand (TRAIL) belongs to the family of tumor necrosis family and is a type-II transmembrane protein which includes a tumor necrosis factor and a Fas ligand [35]. Upon binding to its receptors, R1 and R2, the death-inducing signaling complex (DISC) is assembled, which in turn, directs cleavage and activation of caspases, leading to apoptosis. TRAIL is considered to be one of the most promising gene therapeutics in cancer treatment especially for its specificity in inducing apoptosis and toxicity in cancer cells in comparison with normal tissue [36]. TRAIL is reported to be delivered using both viral and nonviral gene carriers. Salmonella typhimurium was designed as a non-pathogenic vector to secrete murine TRIAL under the control of the prokaryotic radiation-inducible RecA promoter [37]. *In vitro*, after irradiation the secreted TRAIL was found to cause caspase-3-mediated apoptosis and death of cancer cells. *In vivo*, TRAIL was responsible for causing significant delay in mammary tumor growth and also reduced risk of death, as well as improved the survival as compared to irradiated controls. A new delivering agent using mesenchymal stem cells (MSCs) was developed for the delivery of TRIAL in lung cancer cells [38]. A nonviral vector, PEI_{600}-Cyd prepared by linking low molecular weight polyethylenimine (PEI) with β-cyclodextrin (β-CD) was used to introduce the TRIAL gene to MSCs [38]. Both *in vitro* and *in vivo* studies were found to be supportive for cellular uptake and significant reduction in the tumor size [38]. In another study, synthesized poly (amino-co-ester) terpolymers were used for delivery of TRAIL gene supporting the evidence for significant inhibition of tumor growth, with minimal toxicity both *in vitro* and *in vivo* [39]. In order for gene delivery to the brain, a low molecular weight polyethylenimine ($PEI_{10\ k}$) modified with myristic acid (MC) was complexed with TRAIL gene to prepare MC- $PE_{10\ k}$/DNA nano particles [40]. The results were proven to be effective with gene expression being higher both *in vitro* (glioblastoma cells) and *in vivo* for MC- $PE_{10\ k}$/DNA nanoparticles as compared to unmodified $PE_{10\ k}$/DNA nanoparticles and there was an improvement in median survival time of the MC- $PE_{10\ k}$/pORF-hTRAIL as compared to other groups [40]. In a way to improve the transfection efficiency, the surface of TRAIL and/or endostatin delivering agent was modified by applying TIPS-*b*-(PCL-ran-PGA) nanoparticles along with polyethylenimine and delivered into human cervical cancer cells (HeLa) [41]. The *in vivo* data showed that the nanoparticles could efficiently deliver plasmids into the cells with significantly higher cytotoxicity by TRIAL/endostatin-loaded nanoparticles in comparison with other control groups [41]. Some studies have reported to deliver TRAIL in combination with conventional chemotherapeutic agents. Mesenchymal stem cells TRAIL (MSCsTRAIL) were delivered along with 5-flourouracil in HCT116 colon cancer cells leading to significantly increased apoptosis both *in vitro* and *in vivo* as compared to the single-agent treatment [42]. Interestingly, the HCT116 xenografts treated with 5-FU and systemically delivered with MSCsTRAIL went into remission. This effect was p53 independent and mediated by TRAIL-receptor2 upregulation, supporting the applicability of this approach in p53-defective tumors [42]. The combination of doxorubicin and pTRAIL gene used for delivery into human ovarian cancer cells *in vivo* was proved to be efficient with higher retention time of drugs achieving good therapeutic effects in inhibiting the tumor growth and resulting in significantly prolonged survival of tumor bearing mice [43]. In an interesting approach to target brain glioma cells, the combination of pEGFP-hTRAIL and paclitaxel was delivered using angiosp-2 modified cationic liposome (ANG-CLP) as a carrier with an improved cellular uptake and gene expression both in U87 MG cells and BCEs [44]. The apoptosis induced by ANG-CLP/PTX/pEGFP-hTRAIL was more efficient than single medication system and unmodified co-delivery system contributing to significantly longer median survival time of brain tumor-bearing and animals treated with ANG-CLP/PTX/pEGFP-hTRAIL as compared to the other groups including commercial temozolomide group [44]. In a similar way to improve the transfection efficiency of TRAIL and paclitaxel through blood-brain barrier (BBB) and blood-tumor barrier (BTB), c(RGDyK)-poly(ethylene glycol)-polyethylenimine (RGD-PEG-PEI) nanoparticles were prepared for the co-delivery of TRAIL gene and paclitaxel, thereby producing better anti-glioblastoma effects both *in vitro* and *in vivo* [45].

DELIVERY AND EXPRESSION OF p21 GENE

p21 is a vital regulator of cell cycle progression and it can block cell-cycle progression from the G1 to S phase [46] through inactivation of cyclin/CDK activity (Fig. 3). p21 gene was delivered using retroviral vector in breast cancer cells which is mutated in p53 gene with the results showing

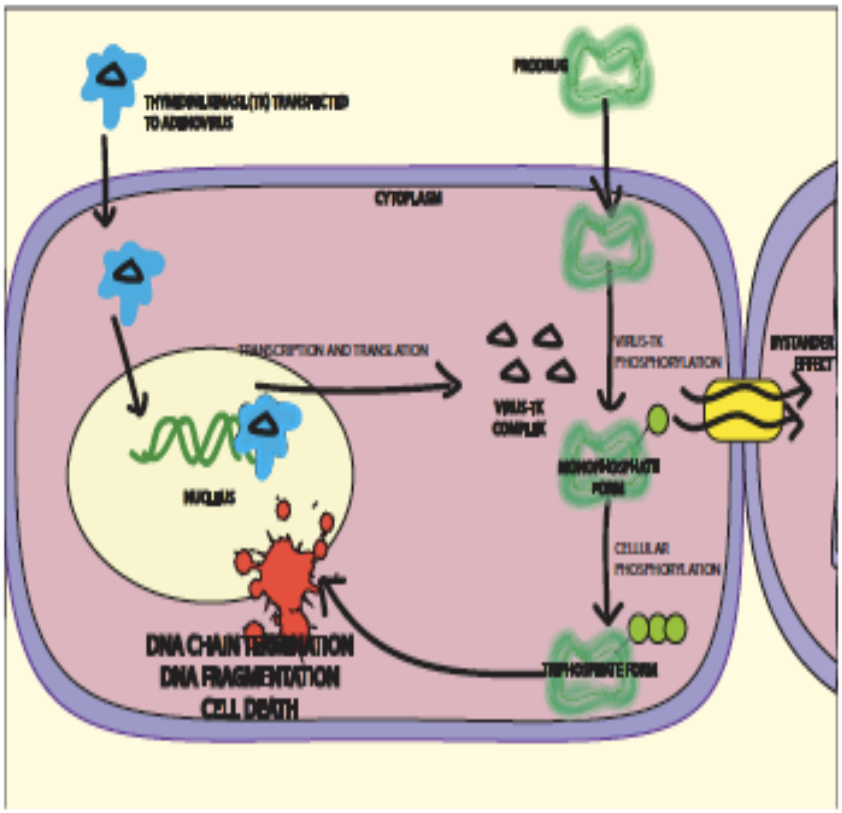

Fig. (3). Different Cyclin-CDK complexes are involved in regulating different cell cycle transitions: Cyclin-D/CDK4 or CDK6 for G1 progression, Cyclin-E/CDK2 for the G1-S transition, Cyclin-A/CDK2 for S-phase progression, Cyclin-B/CDK1 for G2 progression and Cyclin-A/CDK1 for entry into M phase. Cyclins associate with CDKs to regulate their activity and the progression of the cell cycle. CDK/Cyclin and the transcription complex that includes Rb and E2F are pivotal in controlling cell cycle checkpoint. The Rb-HDAC repressor complex binds to the E2F-DP1 transcription factors, inhibiting the downstream transcription. E2F activity consists of a heterodimeric complex of an E2F polypeptide and a DP1 protein. Phosphorylation of Rb by CDK dissociates the Rb-repressor complex, permitting transcription of phase genes encoding for proteins that amplify phase switch, required for replication. Under non-stressed conditions, p21 is expressed at low levels, thus enabling cell cycle progression. Under stress condition, p21 expression is increased through p53 dependent and independent pathways. Increased p21 binds and inactivates Cyclin/CDK activity, thus halting cell cycle activity.

that the overexpression of p21 in C3(1)/Tag mammary tumor cells resulted in increased apoptosis, reduced cell proliferation *in vitro* and reduced tumor growth *in vivo* due to the reduced expression of cyclins D1 and E, and Cdks 2, 4, and 6 mediated by p21 [47]. In a different approach, the response of p21 gene promoter to radiation was demonstrated in MCF-7 breast cancer cells using adeno-associated virus (rAAV) vectors [48]. The results showed that the response of p21 gene promoter transduced by rAAv vector was higher than that transiently transfected by electroporation even with the low dose of radiation, indicating that p21 gene promoter in combination with a rAAV vector is highly potential for development of a low-dose radiation-inducible vector in cancer gene therapy [48].

DELIVERY AND EXPRESSION OF PRO-INFLAMMATORY CYTOKINES

The lack of expression of recognizable tumor antigens, the inability of the expressed tumor antigens to adequately stimulate the immune system or the down-regulation of the immune response by the tumors themselves might contribute to their survival and sustainable growth [49]. Tumor expression of the genes encoding pro-inflammatory cytokine, such as granulocyte macrophage colony stimulating factor (GM-CSF) or fms-like tyrosine kinase 3 receptor ligand (Flt3L) and subsequent immunization using the tumor lysate as the source of tumor-associated antigens, could dramatically increase in blood the number of the most potent antigen-presenting dendritic cells (DCs). In one study, vaccination with the CT26 colon carcinoma cell lysate and the Flt3L-encoding adenoviral vector (pAdFlt3L) that were injected subcutaneously prevented the tumor growth in a BALB/c mouse model due to significant expansion of DCs [50]. Irradiated tumor cells expressing human granulocyte-macrophage colony-stimulating factor (GM-CSF) was found to stimulate potent, long-lasting, and specific anti-tumor immunity in patients with metastatic melanoma [51].

DELIVERY AND EXPRESSION OF ANGIOTENSINS

Angiotensin II is an octapeptide hormone with a key role in the rennin-angiotensin system by binding with angiotensin II type 1 or type 2 receptors [52]. Angiotensin II type 2 (AT2R) is an important factor in tumor growth as it is known to inhibit cell proliferation and stimulate apoptosis [53]. In a

recent study, a nonviral vector dTAT NP was synthesized using dimerized HIV-1 TAT peptide for the intratracheal delivery of angiotensin II type-2 receptor gene in Lewis lung cancer cells (LLC) [54]. The results demonstrated that the AT2R gene was successfully transfected into the cells both *in vitro* and *in vivo* in orthotopic tumor grafts with a marked reduction in tumor growth following bolus administration of dTAT NP-encapsulated AT2R or TNF-related apoptosis-inducing ligand (TRAIL) pDNA [54].

A defective adenovirus expressing a secretable angiostatin K3 molecule from the cytomegalovirus promoter (AdK3) was shown to be effective to deliver the angiostatin gene as AdK3 selectively inhibited endothelial cell proliferation and disrupted the G2/M transition induced by M-phase-promoting factors. A single intratumoral injection of AdK3 into rat C6 glioma or human MDA-MB-231 breast carcinoma established in athymic mice resulted in a significant arrest of tumor growth with suppression of neovascularization within and at the vicinity of the tumors [55].

DELIVERY AND EXPRESSION OF INTERLEUKINS

Intratumoral coinjection of adenoviral vectors expressing cytokines, interleukin-2 (IL-2) and IL-12 in mice bearing subcutaneous mammary tumors resulted in effective regression of injected and untreated distal tumors indicating that the combination of IL-2 and IL-12 is a potent inducer of antitumor immune responses with the hope in the treatment of metastatic cancer [56].

Intratumoral injection with adenovirus vectors expressing human interleukin-2 gene and wild-type human p53 gene driven by the human cytomegalovirus immediate early promoter led to the regression of 65% of the treated tumors without toxicity and demonstrated specific antitumor cytolytic T lymphocyte (CTL) activity, in a transgenic mouse mammary adenocarcinoma model [57].

DELIVERY AND EXPRESSION OF INTERFERONS

Injection of recombinant hamster interferon-α (IFN-α)-carrying adenovirus into syngeneic subcutaneous tumors of hamster pancreatic cancer (PGHAM-1) cells led to the suppression of tumor growth as a result of both cell death and T cell- and natural killer cell-mediated antitumor immunity without demonstration of any significant systemic toxicity [58]. Direct intratumoral delivery of murine adenoviral IFN-β (Ad-mIFN-β) and human adenoviral IFN-β (Ad-hIFN-β) inhibited the growth of human bladder cancer in athymic mice by activating tumoricidal host effector cells with mIFN-β and by suppressing tumor-induced angiogenesis with hIFN-β [59]. Intravenous delivery of recombinant adenovirus containing the human IFN-beta (hIFN) in nude mouse xenograft model of human colorectal cancer liver metastases significantly produced hIFN-beta in the liver, inducing apoptosis in the tumors with significant regression of tumor volume [60]. Similarly, systemic delivery of the murine IFN-beta (mIFN-beta) cDNA also resulted in improved survival in syngeneic mouse models of colorectal cancer liver metastases [60]. Adenovirus-mediated delivery of interferon-γ gene was shown to inhibit the proliferation of nasopharyngeal carcinoma (NPC) cell lines by inducing G1 phase arrest and cell apoptosis while intratumoral administration of Ad-IFNγ suppressed the growth of NPC xenografts in nude mice [61].

OTHER GENES DELIVERY AND EXPRESSION

Esophageal cancer-related gene 2 (ECRG2) known to regulate urokinase-type plasmin activator receptor and extracellular matrix function with its polymorphism in exon 4 being associated with cancer relapse, was delivered using adenoviral vector (Ad-ECRG2) into hepatic cancer cells [62], thus altering the expression of nuclear factor-kB, matrix metalloproteinase 2 and E-cadherin and contributing to reverse malignancy phenotype of cancer cells. The intratumoral Ad-ECRG2 administration led to a significant inhibition of tumor growth without any evidence of toxicity in treated animals [62].

Fas ligand (FasL) is a cytokine that triggers apoptosis of Fas-positive target cells, such as, human glioma cells. Transduction with recombinant adenovirus (rAd) expressing FasL cDNA under control of the cytomegalovirus promoter (rAd-CMV-FasL) induced significant cytotoxicity in Fas-positive glioma cell lines whereas intratumoral delivery of rAd-CMV-FasL improved the survival of rats bearing intracranial glioblastoma (GBM) [63, 64].

Adenoviral delivery of inducible Caspase-9 (iCaspase-9) under transcriptional control of endothelial cell-specific vascular endothelial growth factor receptor-2 (VEGFR2) promoter (Ad-hVEGFR2-iCaspase-9) induced apoptosis of proliferating human dermal microvascular endothelial cells (HDMECs), but not human tumor cells, UM-SCC-17B (head and neck squamous cell carcinoma), HepG2 (hepatocellular carcinoma), PC-3 (prostate adenocarcinoma), SLK (Kaposi's sarcoma), MCF-7 (breast adenocarcinoma) [65]. Moreover, local delivery of Ad-hVEGFR2-iCaspase-9 followed by intraperitoneal injection of AP20187, a dimerizer drug for activation of iCaspase-9, removed tumor microvessels and inhibited xenografted tumor growth in all tumor models [65].

In order to develop efficacious therapy for resistant prostate cancer, ultrasound (US) contrast agents (microbubbles) were employed for direct intratumoral (IT) injection of adenoviral vectors carrying *p53* and *RB genes* under external beam radiation resulting in profound tumor reduction in DU-145 (human prostate cancer cells) xenografted nude mice compared to radiation alone [66]. In a similar approach, the antitumor effects of tumor necrosis factor (TNF-α) were evaluated following intratumoral injection of TNF-α plasmid DNA into murine solid breast carcinoma induced [67].

CONCLUSION

Gene therapy holds a great potential in cancer treatment with a number of genes having been explored alone or in combination with conventional chemotherapeutic agents for enhancement of their therapeutic efficacy in treating cancer. The most critical factor in gene delivery is to ensure high level of transgene expression with greater specificity reducing the off-target effects on the normal cells. Although viral vectors, particularly adenovirus have been extensively used owing to the degree of efficacy for the pre-clinical trials of gene therapy, their severe side-effects in the context of the

Table 1.

Types of Cancer Cells/Tumor Models	Delivered Genes	Gene Carriers	References
Female athymic nude mice with MDA-MB-435 (human breast cancer cells) carcinoma	p53	Polymeric Nanoparticles	[6, 16]
Female athymic nude mice with MDA-MB-435 carcinoma	p53	Liposome	[10]
MDA-MB231 (human breast cancer cells)	p53	Liposome with estradiol	[11]
Mouse model of metastatic pancreatic cancer (Panc02 cells)	p53	Liposome	[13]
A2780/DDP (Human ovarian cancer cells)	p53	Ultrasound-targeted microbubble destruction (UTMD)	[14]
MCF-7 (human breast cancer cells)	p53	DPD(dextran-graft-poly((2-methyl amino) ethyl methacrylate)	[15]
PANC-1 (human pancreatic adenocarcinoma cells)	p53	Peptide modified thiolated gelatin	[17]
PC-3 prostate carcinoma mouse model	p53	Didodecyl dimethylammonium bromide (DMAB) NPs	[18]
A549 (Human lung adenocarcinoma epithelial cells), HeLa (human cervical epithelial carcinoma)	p53	chitosan nanoparticles	[19]
MCF-7	p53	Single-walled carbon nanotubes (f-SWCNTs)	[20]
Athymic female nude mice with tumors of small cell lung cancer (SCLC) cells	p53	Poly(β-amino ester) (PBAE) polymers	[21]
Patients with head and neck squamous cell cancer	p53	Adenoviral vector	[22]
BALB/c mice with tumor of 4T1 (mouse breast cancer cells)	HSVtk	Liposomal nanoparticles	[25]
BALB/c nude mice with tumor of MCF-7	HSVtk	Recombinant adeno-associated virus-2 (rAAV)	[26]
MCF-7	HSVtk	Ultrasound targeted microbubble destruction (UTMD)	[27]
BALB/c mice with BJMC3879 metastatic mammary carcinoma	HSVtk	Electroporation	[28]
SCID (severe combined immunodeficiency disease) mice with baby hamster kidney (BHK) tumors	HSVtk	Sindbis viral vector	[29]
Athymic mice with hepatocellular carcinoma (HCC)	HSVtk	Recombinant adenovirus	[30]
SCID mice with hepatic tumor of HUH7 cells	HSVtk	Hemagglutinating virus of Japan (HVJ)-liposomes	[31]
Nude mice with tumors of SGC7901 gastric cancer cells	HSVtk /TNF-alpha gene	Liposome	[32]
Patients with GBM	HSVtk	adenoviral vector	[34]
BALB/c mice with tumor of 4T1	TRAIL	Salmonella typhimurium	[37]
C57BL/6 mice with lung metastases	TRAIL	Mesenchymal stem cells (MSCs)	[38]
Mice bearing A549 (human lung adenocarcinoma epithelial cell line)-derived tumour xenografts	TRAIL	Biodegradable poly(amine-co-ester) terpolymers	[39]
Intracranial U87 glioblastoma-bearing mice	TRAIL	Myristic acid (MC)-modified polyethylenimine (PEI)	[40]
Nude mice with subcutaneously implanted tumor xenografts (HeLa)	TRAIL	TPGS-*b*-(PCL-*ran*-PGA) copolymer	[41]
Female nude mice with induced tumors of human colorectal cancer HCT116 cells	TRAIL	MSCs	[42]
BALB/c nude mice bearing SKOV-3 ovarian tumors	TRAIL	PEI-cyclodextrin (CD)	[43]

(Table 1) contd.....

Types of Cancer Cells/Tumor Models	Delivered Genes	Gene Carriers	References
U87 MG glioma-bearing mice	TRAIL	Angiopep-2 modified cationic liposome (ANG-CLP)	[44]
Intracranial glioblastoma-bearing model mice	TRAIL	Cyclic RGD peptide-containing poly(ethylene glycol)-polyethyleneimine (RGD-PEG-PEI)	[45]
C3(1)/Tag mammary tumor cells	p21	Retroviral vector	[47]
Female BALB/c mice with CT26 colon cancer	Flt3L	Adenoviral vector	[50]
Patients with metastatic melanoma	GM-CSF	Irradiated autologous melanoma	[51]
Wild-type female C57BL/6 mice with Lewis lung carcinoma (LLC)	Angiotensin II type 2 receptor gene	HIV-1 TAT peptides in tandem (dTAT)	[54]
Nude mice with C6 glioma cells or MDA-MB-231 cells	angiostatin K3 gene	Recombinant adenovirus	[55]
Transgenic mouse model of mammary adenocarcinoma	IL-2 and IL-12 genes	Recombinant adenovirus	[56]
Transgenic mouse mammary adenocarcinoma model	IL-2 and p53	Recombinant adenovirus	[57]
Syrian hamster with subcutaneous tumors of hamster pancreatic cancer (PGHAM-1) cells	IFN-α	Recombinant adenovirus	[58]
Nude mice with 253J B-V(R) human bladder transitional cell carcinoma (TCC) and human colorectal cancer liver metastases	IFN-β	Recombinant adenovirus	[59, 60]
Nasopharyngeal carcinoma (NPC) xenografts in nude mice	IFN-γ	Recombinant adenovirus	[61]
Mouse xenograft of BEL-7402 (human hepatoma cell)	ECR02	Recombinant adenovirus	[62]
Rats with intracranial glioblastoma (GBM)	Fasl.	Recombinant adenovirus	[63, 64]
Immunodeficient (SCID) mice with xenografted tumors (Hep02, UM-SCC-17B, or SLK)	iCaspase-9	Recombinant adenovirus	[65]
Nude mice with DU-145 (human prostate cancer cells) xenograft	p53, pRB, and p130	US cavitation of microbubbles	[66]
SCID mice with murine breast carcinoma (EMT6)	TNF-α	Nanobubbles and ultrasound	[67]

immune response of human body to the viral proteins pose a major concern to the clinical implementation. On the other hand, non-viral counterparts are still inefficient in transgene delivery and expression predominantly due to the obstacles in endosomal escape and nuclear translocation of the associated genetic materials.

CONFLICT OF INTEREST

The authors confirm that this article content has no conflict of interest.

ACKNOWLEDGEMENTS

This work has financially been supported by a research grant (Project ID 02-02-10-SF0083) of the Ministry of Science, Technology and Innovation (MOSTI), Malaysia.

PATIENT CONSENT

Declared none.

REFERENCES

[1] Bahan CK, Cronin M, Hanlon DO, Sullivan GCO, Tangney M. Bacteria as vectors for gene therapy of cancer. Bioengin Bugs 2010; 1(6): 385-94.

[2] Siegel R, Naishadham D, Jemal A. Cancer Statistics, 2012. CA Cancer J Clin 2012; 62(1): 10-29.

[3] Ryan RM, Green J, Lewis CE. Use of bacteria in anti-cancer therapies. Bioessays 2006; 28(1): 84-94.

[4] Li YT, Chua MJ, Kunrath AP, Chowdhury EH. Reversing multidrug resistance in breast cancer cells by silencing *ABC* transporter genes with nanoparticle-facilitated delivery of target siRNAs. Int J Nanomedicine 2012; 7: 2473-81.

[5] Sakai Y, Kaneko S, Nakamoto Y, Kagaya T, Makaida N, Kobayashi K. Enhanced anti-tumor effects of herpes simplex virus thymidinekinase/ganciclovir system by codelivering monocyte chemoattractant protein-1 in hepatocellular carcinoma. Cancer Gene Ther 2001; 8: 695-704.

[6] Prabha S, Sharma B, Labhasetwar V. Inhibition of tumor angiogenesis and growth by nanoparticle-mediated p53 gene therapy in mice. Cancer Gene Ther 2012; 19(8): 530-7.

[7] Junttila MR, Evan GI. p53-a Jack of all trades but master of none. Nat Rev Cancer 2009; 9: 821-9.

[8] Vogelstein B, Lane D, Levine AJ. Surfing the p53 network. Nature 2000; 408: 307-10.

[9] Roth JA, Nguyen D, Lawrence DD, *et al.* Retrovirus-mediated wild-type p53 gene transfer to tumors of patients with lung cancer. Nat Med 1996; 2(9): 985-91.

[10] Lesoon-Wood LA, Kim WH, Kleinman HK, Weintraub BD, Mixson AJ. Systemic gene therapy with p53 reduces growth and metastases of a malignant human breast cancer in nude mice. Hum Gene Ther 1995; 6(4): 395-405.

[11] Jain PT, Seth P, Gewirtz DA. Estradiol enhance liposome-mediated uptake, preferential nuclear accumulation and functional expression of exogenous genes in MDA-MB231 breast tumor cells. Biochim Biophys Acta 1999; 1451: 224-32.

[12] Xu L, Huang C, Huang W, *et al.* Systemic Tumor-targeted Gene Delivery by Anti-Transferrin Receptor scFv-Immunoliposomes. Mol Cancer Ther 2002; 1: 337-46.

[13] Camp ER, Wang C, Little EC, *et al.* Transferrin receptor targeting nanomedicine delivering wild-type p53 gene sensitizes pancreatic cancer to gemcitabine therapy. Cancer Gene Ther 2013; 20: 222-8.

[14] Chang S, Guo J, Sun J, *et al.* Targeted microbubbles for ultrasound mediated gene transfection and apoptosis induction in ovarian cancer cells. Ultrason Sonochem 2013; 20: 171-9.

[15] Li W B, Yuan W, Xu F J, Zhao C, Ma J, Zhan QM. Functional study of dextran-graft-poly((2-dimethyl amino)ethyl methacrylate) gene delivery vector for tumor therapy. J Biomater Appl 2013; 28(1): 125-35.

[16] Prabha S, Labhasetwar V. Nanoparticle-Mediated Wild-Type p53 Gene Delivery Results in Sustained Antiproliferative Activity in Breast Cancer Cells. Mol Pharm 2004; 3: 211-9.

[17] Xu J, Amiji M. Therapeutic Gene Delivery and Transfection in Human Pancreatic Cancer Cells using Epidermal Growth Factor Receptor-targeted Gelatin Nanoparticles. J Vis Exp 2012; 59: 1-9.

[18] Sharma B, Peetla C, Adjei SM, Labhasetwar V. Selective biophysical interactions of surface modified nanoparticles with cancer cell lipids improve tumor targeting and gene therapy. Cancer Lett 2013; 334(2): 228-36.

[19] Gaspar VM, Correia IJ, Sousa A, *et al.* Nanoparticle mediated delivery of pure P53 supercoiled plasmid DNA for gene therapy. J Control Release 2011; 156: 212-22.

[20] Karmakar A, Bratton SM, Dervishi E, *et al.* Ethylenediamine functionalized-single-walled nanotube (f-SWNT)-assisted *in vitro* delivery of the oncogene suppressor p53 gene to breast cancer MCF-7 cells. Int J Nanomedicine 2011; 6: 1045-55.

[21] Kamat CD, Shmueli RB, Connis N, Rudin CM, Green JJ, Hann CL. Poly(β-amino ester) nanoparticle delivery of TP53 has activity against small cell lung cancer *in vitro* and *in vivo*. Mol Cancer Ther 2013; 12(4): 405-15.

[22] Wilson JM. Gendicine: the first commercial gene therapy product. Hum. Gene Ther 2005; 16(9): 1014-5.

[23] Merritt JA, Roth JA, Logothetis CJ. Clinical evaluation of adenoviral-mediated p53 gene transfer: review of INGN 201 studies. Semin Oncol 2001; 28(5 Suppl 16), 105-14.

[24] Mesnil M, Yamasaki H. Bystander effect in herpes simplex virus-thymidine kinase/ganciclovir cancer gene therapy: role of gap-junctional intercellular communication. Cancer Res 2000; 60(15): 3989-99.

[25] Zhou M, Wang L, Su W, *et al.* Assessment of Therapeutic Efficacy of Liposomal Nanoparticles Mediated Gene Delivery by Molecular Imaging for Cancer Therapy. J Biomed Nanotechnol 2012; 8: 742-50.

[26] Li ZB, Zeng ZJ, Chen Q, Luo SQ, Hu WX. Recombinant AAV-mediated HSVtk gene transfer with direct intratumoral injections and Tet-On regulation for implanted human breast cancer. BMC Cancer 2006; 6: 66.

[27] Li XH, Zhou P, Wang LH, *et al.* The targeted gene (KDRP-CD/TK) therapy of breast cancer mediated by SonoVue and ultrasound irradiation *in vitro*. Ultrasonics 2012; 52(1): 186-91.

[28] Shibata MA, Morimoto J, Otsuki Y. Suppression of murine mammary carcinoma growth and metastasis by HSVtk/GCV gene therapy using *in vivo* electroporation. Cancer Gene Ther 2002; 9: 16-27.

[29] Tseng JC, Zanzonico PB, Levin B, Finn R, Larson SM, Meruelo D. Tumor-specific *in vivo* transfection with HSV-1 thymidine kinase gene using a Sindbis viral vector as a basis for prodrug ganciclovir activation and PET. J Nucl Med 2006; 47(7): 1136-43.

[30] Sakai Y, Kaneko S, Nakamoto Y, Kagaya T, Makaida N, Kobayashi K. Enhanced anti-tumor effects of herpes simplex virus thymidine kinase/ganciclovir system by codelivering monocyte chemoattractant protein-1 in hepatocellular carcinoma. Cancer Gene Ther 2001; 8(10): 695-704.

[31] Hirano T, Kaneko S, Kaneda Y, *et al.* HVJ-liposome-mediated transfection of HSVtk gene driven by AFP promoter inhibits hepatic tumor growth of hepatocellular carcinoma in SCID mice. Gene Ther 2001; 8(1): 80-3.

[32] Zhang JH, Wan MX, Pan BR, Yu B. Cytotoxicity of HSVtk and hrTNF-alpha fusion genes with IRES in treatment of gastric cancer. Cancer Lett 2006; 235(2): 191-201.

[33] Balzarini J, Degreve B, Andrei G, *et al.* Superior cytostatic activity of the ganciclovir elaidic acid ester due to the prolonged intracellular retention of ganciclovir anabolites in herpes simplex virus type 1 thymidine kinase gene-transfected tumor cells. Gene Ther 1998; 5: 419-26.

[34] Määttä AM, Samaranayake H, Pikkarainen J, Wirth T, Ylä-Herttuala S. Adenovirus mediated herpes simplex virus-thymidine kinase/ganciclovir gene therapy for resectable malignant glioma. Curr Gene Ther 2009; 9(5): 356-67.

[35] Takeda K, Smyth MJ, Cretney E, *et al.* Critical role for tumor necrosis factor-related apoptosis-inducing ligand in immune surveillance against tumor development. J Exp Med 2002; 195: 161-9.

[36] Yagita H, Takeda K, Hayakawa Y, Smyth MJ, Okumura K. TRAIL and its receptors as targets for cancer therapy. Cancer Sci 2004; 95(10): 777-83.

[37] Garai S, Arenas RB, Forbes NS. Tumour-targeted delivery of TRAIL using Salmonella typhimurium enhances breast cancer survival in mice. British J Cancer 2009; 101: 1683-91.

[38] Hu YL, Huang B, Zhang TY, *et al.* Mesenchymal Stem Cells as a Novel Carrier for Targeted Delivery of Gene in Cancer Therapy Based on Nonviral Transfection. Mol Pharm 2012; 9: 2698-709.

[39] Zhou J, Liu J, Cheng CJ, *et al.* Biodegradable poly(amine-co-ester) terpolymers for targeted gene delivery. Nat Mater 2011; 11(1): 82-90.

[40] Li J, Gu B, Meng Q, *et al.* The use of myristic acid as a ligand of polyethylenimine/DNA nanoparticles fortargeted gene therapy of glioblastoma. Nanotechnology 2011; 22 (43): 435101.

[41] Zheng Y, Chen H, Zeng X, *et al.* Surface modification of TPGS-b-(PCL-ran-PGA) nanoparticles with polyethyleneimine as a co-delivery system of TRAIL and endostatin for cervical cancer gene therapy. Nanoscale Res Lett 2013; 8(1): 161.

[42] Yu R, Deedigan L, Albarenque SM, Mohr A, Zwacka RM. Delivery of sTRAIL variants by MSCs in combination with cytotoxic drug treatment leads to p53-independent enhanced antitumor effects. Cell Death Dis 2013; 4: e505.

[43] Fan H, Hu QD, Xu FJ, Liang WQ, Tang GP, Yang WT. *In vivo* treatment of tumors using host-guest conjugated nanoparticles functionalized with doxorubicin nag therapeutic gene pTRAIL. Biomaterials 2012; 33: 1428-36.

[44] Sun X, Pang Z, Ye H, *et al.* Codelivery of pEGFP-hTRAIL and paclitaxel to brain glioma mediated by an angiopep-conjugated liposome. Biomaterials 2012; 33: 916-24.

[45] Zhan C, Wei X, Qian J, Feng L, Zhu J, Lu W. Co-delivery of TRAIL gene enhances the anti-glioblastoma effect of paclitaxel *in vitro* and *in vivo*. J Control Release 2012; 160: 630-6.

[46] Dash BC, El-Deiry WS. Phosphorylation of p21 in G2/M promotes cyclin B-Cdc2 kinase activity. Mol Cell Biol 2005; 25(8): 3364-87.

[47] Shibata MA, Yoshidome K, Shibata E, Jorcyk CL, Green J E. Suppression of mammary carcinoma growth *in vitro* and *in vivo* by inducible expression of the Cdk inhibitor p21. Cancer Gene Ther 2001; 8(1): 23-35.

[48] Nenoi M, Daino K, Ichimura S, Takahashi S I, Akuta T. Low-dose radiation response of the *p21WAF1/CIP1* gene promoter transduced by adeno-associated virus vector. Exp Mol Med 2006; 38(5): 553-64.

[49] Gabrilovich DI, Nadaf S, Corak J, Berzofsky JA, Carbone DP. Dendritic cells in antitumor immune responses. II. Dendritic cells grown from bone marrow precursors, but not mature DC from tumor-bearing mice, are effective antigen carriers in the therapy of established tumors. Cell Immunol 1996; 170:111–9.

[50] Riedinger C, Wingender G, Knolle P, Aulmann S, Stremmel W, Encke J. Fms-like tyrosine kinase 3 receptor ligand (Flt3L)-based vaccination administered with an adenoviral vector prevents tumor

growth of colorectal cancer in a BALB/c mouse model. J Cancer Res Clin Oncol 2013; 139(12): 2097-110.

[51] Soiffer R, Lynch T, Mihm M, *et al.* Vaccination with irradiated autologous melanoma cells engineered to secrete human granulocyte-macrophage colony-stimulating factor generates potent anti-tumor immunity in patients with metastatic Melanoma. Proc Natl Acad Sci USA 1998; 95: 13141-6.

[52] Timmermans PB, Wong PC, Chiu AT, *et al.* Angiotensin II receptors and angiotensin II receptor antagonists. Pharmacol Rev 1993; 45: 205-51.

[53] Grady EF, Sechi LA, Griffin CA, Schambelan M, Kalinyak JE. Expression of AT2 receptors in the developing rat fetus. J Clin Invest 1991; 88: 921-33.

[54] Kawabata A, Baoum A, Ohta N, *et al.* Intratracheal administration of a nanoparticle-based therapy with the angiotensin II type 2 receptor gene attenuates lung cancer growth. Cancer Res 2012; 72(8): 2057-67.

[55] Oriscelli F, Li h, Oriscelli AB, *et al.* Angiostatin gene transfer. Inhibition of tumor growth *in vivo* by blockage of endothelial cell proliferation associated with a mitosis arrest. Proc Natl Acad Sci USA 1998; 95: 6367-72.

[56] Addison CL, Bramson JL, Hitt MM, Muller WJ, Gauldie J, Graham FL. Intratumoral coinjection of adenoviral vectors expressing IL-2 and IL-12 results in enhanced frequency of regression of injected and untreated distal tumors. Gene Ther 1998; 5(10): 1400-9.

[57] Pittner BM, Bramson JL, Addison CL, *et al.* Combination therapy with interleukin-2 and wild-type p53 expressed by adenoviral vectors potentiates tumor regression in a murine model of breast cancer. Hum Gene Ther 1998; 9(5): 707-18.

[58] Hara H, Kobayashi A, Yoshida K, *et al.* Local interferon-alpha gene therapy elicits systemic immunity in a syngeneic pancreatic cancer model in hamster. Cancer Sci 2007; 98(3): 455-63.

[59] Izawa JI, Sweeney P, Perrotte P, *et al.* Inhibition of tumorigenicity and metastasis of human bladder cancer growing in athymic mice by interferon-beta gene therapy results partially from various antiangiogenic effects including endothelial cell apoptosis. Clin Cancer Res 2002; 8(4): 1258-70.

[60] Liu RY, Zhu YH, Zhou L, *et al.* Adenovirus-mediated delivery of interferon-γ gene inhibits the growth of nasopharyngeal carcinoma. J Transl Med 2012; 10: 256.

[61] Tada H, Maron DJ, Choi EA, *et al.* Systemic IFN-beta gene therapy results in long-term survival in mice with established colorectal liver metastases. J Clin Invest 2001; 108(1): 83-95.

[62] Song H, Song C, Wang H, *et al.* Suppression of hepatocarcinoma model *in vitro* and *in vivo* by BCR02 delivery using adenoviral vector. Cancer Gene Ther 2012; 19(12): 875-9.

[63] Amber BB, Frei K, Malipiero U, Morelli AE, Castro MO, Lowenstein PR, Fontana A. Treatment of experimental glioma by administration of adenoviral vectors expressing Fas ligand. Hum Gene Ther 1999; 10(10): 1641-8.

[64] Villa-Morales M, Fernández-Piqueras J. Targeting the Fas/FasL signaling pathway in cancer therapy. Expert Opin Ther Targets 2012; 16(1): 85-101.

[65] Song W, Dong Z, Jin T, Mantellini MG, Nunez G, Nor JE. Cancer gene therapy with iCaspase-9 transcriptionally targeted to tumor endothelial cells. Cancer Gene Ther 2008; 15: 667-75.

[66] Nande R, Greco A, Grossman MS, *et al.* Microbubble-assisted p53, RB, and p130 gene transfer in combination with radiation therapy in prostate cancer. Curr Gene Ther 2013; 13(3): 163-74.

[67] Horie S, Watanabe Y, Ono M, Mori S, Kodama T. Evaluation of antitumor effects following tumor necrosis factor-α gene delivery using nanobubbles and ultrasound. Cancer Sci 2011; 102(11): 2082-9.

Received: January 30, 2014 **Revised: May 12, 2014** **Accepted: May 13, 2014**

Appendix 16

Bakhtiar A, *et al*. 2015 Nano Today Conference, Dubai, UAE.